Tuning Interfacial Properties in Perovskite Solar Cells through Defined Molecular Assemblies

Dissertation

zur Erlangung des akademischen Grades
doctor rerum naturalium (Dr. rer. nat.)
in der Wissenschaftsdisziplin Physik

eingereicht an der
Mathematisch-Naturwissenschaftlichen Fakultät
Institut für Physik und Astronomie
der Universität Potsdam
und durchgeführt am
Helmholtz-Zentrum Berlin für Materialen und Energie
von:

Laura Canil

Potsdam, August 2021

Published online on the
Publication Server of the University of Potsdam:
https://doi.org/10.25932/publishup-54633
https://nbn-resolving.org/urn:nbn:de:kobv:517-opus4-546333

Supervisors:
Prof. Dr. Antonio Abate
Prof. Dr. Dieter Neher

Examination Committee:
Prof. Dr. Antonio Abate
Prof. Dr. Dieter Neher
Prof. Dr. Jovana Milić
Prof. Dr. Andreas Taubert

Chair:
Prof. Dr. Regina Hoffmann-Vogel

ABSTRACT

In the frame of a world fighting a dramatic global warming caused by human-related activities, research towards the development of renewable energies plays a crucial role. Solar energy is one of the most important clean energy sources and its role in the satisfaction of the global energy demand is set to increase. In this context, a particular class of materials captured the attention of the scientific community for its attractive properties: halide perovskites. Devices with perovskite as light-absorber saw an impressive development within the last decade, reaching nowadays efficiencies comparable to mature photovoltaic technologies like silicon solar cells. Yet, there are still several roadblocks to overcome before a wide-spread commercialization of this kind of devices is enabled. One of the critical points lies at the interfaces: perovskite solar cells (PSCs) are made of several layers with different chemical and physical features. In order for the device to function properly, these properties have to be well-matched.

This dissertation deals with some of the challenges related to interfaces in PSCs, with a focus on the interface between the perovskite material itself and the subsequent charge transport layer. In particular, molecular assemblies with specific properties are deposited on the perovskite surface to functionalize it. The functionalization results in energy level alignment adjustment, interfacial losses reduction, and stability improvement.

First, a strategy to tune the perovskite's energy levels is introduced: self-assembled monolayers of dipolar molecules are used to functionalize the surface, obtaining simultaneously a shift in the vacuum level position and a saturation of the dangling bonds at the surface. A shift in the vacuum level corresponds to an equal change in work function, ionization energy, and electron affinity. The direction of the shift depends on the direction of the collective interfacial dipole. The magnitude of the shift can be tailored by controlling the deposition parameters, such as the concentration of the solution used for the deposition. The shift for different molecules is characterized by several non-invasive techniques, including in particular Kelvin probe. Overall, it is shown that it is possible to shift the perovskite energy levels in both directions by several hundreds of meV. Moreover, interesting insights on the molecules deposition dynamics are revealed.

Secondly, the application of this strategy in perovskite solar cells is explored. Devices with different perovskite compositions ("triple cation perovskite" and $MAPbBr_3$) are prepared. The two resulting model systems present different energetic offsets at the perovskite/hole-transport layer interface. Upon tailored perovskite surface functionalization, the devices show a stabilized open circuit voltage (V_{oc}) enhancement of approximately 60 meV on average for devices with $MAPbBr_3$, while the impact is limited on triple-cation solar cells. This suggests that the proposed energy level tuning method is valid, but its effectiveness depends on factors such as the significance of the energetic offset compared to the other losses in the devices.

Finally, the above presented method is further developed by incorporating the ability to interact with the perovskite surface directly into a novel hole-transport material (HTM), named PFI. The HTM can anchor to the perovskite halide ions via halogen bonding (XB). Its behaviour is compared to that of another HTM (PF) with same chemical structure and properties, except for the ability of forming XB.

The interaction of perovskite with PFI and PF is characterized through UV-Vis, atomic force microscopy and Kelvin probe measurements combined with simulations. Compared to PF, PFI exhibits enhanced resilience against solvent exposure and improved energy level alignment with the perovskite layer. As a consequence, devices comprising PFI show enhanced V_{oc} and operational stability during maximum-power-point tracking, in addition to hysteresis reduction. XB promotes the formation of a high-quality interface by anchoring to the halide ions and forming a stable and ordered interfacial layer, showing to be a particularly interesting candidate for the development of tailored charge transport materials in PSCs.

Overall, the results exposed in this dissertation introduce and discuss a versatile tool to functionalize the perovskite surface and tune its energy levels. The application of this method in devices is explored and insights on its challenges and advantages are given. Within this frame, the results shed light on XB as ideal interaction for enhancing stability and efficiency in perovskite-based devices.

KURZFASSUNG

Im Kampf gegen den menschengemachten Klimawandel spielt die Forschung und Entwicklung von erneuerbaren Energien eine tragende Rolle. Solarenergie ist eine der wichtigsten grünen Energiequellen und von steigender Bedeutung für die Deckung des globalen Energiebedarfs. In diesem Kontext hat eine bestimme Materialklasse aufgrund ihrer attraktiven Eigenschaften die Aufmerksamkeit der Wissenschaft erregt: Halogenid-Perowskit. Perowskit-Solarzellen haben im letzten Jahrzehnt eine beeindruckende Entwicklung durchgemacht und erreichen heutzutage Effizienzen, die mit weit entwickelten Photovoltaik-Technologien wie Silizium-Solarzellen vergleichbar sind. Jedoch existieren immer noch mehrere Hürden, die einer marktweiten Kommerzialisierung dieser jungen Technologie im Wege stehen. Eines der kritischen Probleme befindet sich an den Grenzflächen. Perowskit-Solarzellen bestehen aus mehreren Schichten mit unterschiedlichen chemischen und physikalischen Eigenschaften. Damit die Solarzelle bestmöglich funktioniert, müssen diese Eigenschaften aufeinander abgestimmt sein.

Diese Dissertation beschäftigt sich mit einigen Herausforderungen im Zusammenhang mit Grenzflächen in Perowskit-Solarzellen, dabei liegt der Fokus auf der Grenzfläche zwischen Perowskit-Absorber und der angrenzenden Ladungstransportschicht. Insbesondere werden organische Moleküle mit spezifischen Eigenschaften verwendet um die Oberfläche des Perowskiten zu funktionalisieren. Dadurch wird eine Bandanpassung erreicht, Grenzflächenverluste reduziert und die Stabilität der Solarzellen erhöht.

Zunächst wird eine Strategie zum Anpassen der Bandenergien vorgestellt: Selbst-organisierende Monoschichten dipolarer Moleküle werden auf die Perowskit-Oberfläche abgeschieden, um diese zu funktionalisieren. Dadurch wird eine Anpassung des Energie-Levels im Perowskiten und die Sättigung von ungebundenen Elektronenbindungen (engl. *dangling bonds*) an der Oberfläche erreicht. Die Richtung der Energielevel-Verschiebung hängt von der Richtung des kollektiven Grenzflächen-Dipols ab. Der Betrag der Energielevel-Verschiebung kann über die Depositionsparameter während der Schichtherstellung eingestellt werden. Die Energielevel-Verschiebung bei der Verwendung verschiedener Moleküle wird mit Hilfe verschiedener non-invasiver Charakterisierungsmethoden untersucht, insbesondere mit der Hilfe von Kelvin-Sonde Messungen. Diese Messungen ermöglichen interessante Erkenntnisse über die Dynamik der Deposition der Moleküle. Es ist möglich die Energielevel in beide Richtungen um mehrere hundert meV zu verschieben.

Als Zweites wird die Anwendung dieser Stategie in Perowskit-Solarzellen erforscht. Solarzellen mit Perowskit-Absorbern unterschiedlicher Zusammensetzung (“Dreifach-Kationen-Perowskit” und MAPbBr3) werden präpariert; die beiden Modellsysteme besitzen dann unterschiedliche energetische Offsets an der Perowskit-Lochleiter Grenzfläche. Mit einer maßgeschneiderter Funktionalisierung der Perowskit-Oberfläche zeigen die $MAPbBr_3$ Solarzellen eine permanente Verbesserung der offene-Klemmen-Spannung (engl. *open circuit voltage*, V_{oc}) um durchschnittlich 60 meV, während der Einfluss auf die Solarzellen mit Dreifach-Kationen-Perowskit gering ist. Dies zeigt, dass die vorgestellte Methode zur Bandanpassung funktioniert, aber ihre Effektivität zudem von weiteren Faktoren

abhängt: Die Relevanz des energetischen Offsets im Vergleich zu anderen Verlustmechanismen beeinflusst unter anderem die Effektivität der Funktionalisierung.

Abschließend wird beschrieben, wie die präsentierte Methode zur Bandanpassung weiterentwickelt wird, indem das Vermögen, mit der Perowskit-Oberfläche zu interagieren, direkt in einen neuartigen Lochleiter („PFI“) integriert wird. Der Lochleiter kann sich über Halogenbindungen an den Perowskiten anlagern. Das Verhalten von PFI wird verglichen mit dem eines anderen Lochleiters („PF“), welcher die fast gleiche chemische Struktur und sehr ähnliche Eigenschaften aufweist, ausgenommen der Fähigkeit eine Halogenbindung zu formen. Die PFI-Perowskit und PF-Perowskit Interaktion wird durch UV-Vis Spektroskopie, Rasterkraftmikroskopie und Kelvin-Sonde Messungen, kombiniert mit Simulationen, charakterisiert. Beim direkten Vergleich von PFI und PF zeigt sich die Bildung der Halogenbindung in einer bei PFI verbesserten Widerstandskraft gegen Lösungsmittel und Bandanpassung zum Perowskiten. Beim Folgerichtig zeigen Solarzellen mit PFI zusätzlich zu einer verringerten Hysterese einen höheren V_{oc} und eine erhöhte Stabilität während des Betriebs unter Maximum-Power-Point Tracking

Zusammenfassend stellt diese Dissertation somit ein vielseitiges Werkzeug zur Funktionalisierung von Perowskit-Oberflächen und der dadurch erreichten Bandanpassung vor. Die Anwendung dieses Werkzeugs an Solarzellen wird erprobt und Einsichten in seine Vorteile und Nachteile erlangt. Die Halogenbindung wird als spezifische Interaktion identifiziert, die sich ideal zur Steigerung von Effizienz und Stabilität von Perowskit-basierten optoelektronischen Bauteilen erweisen könnte.

LIST OF ABBREVIATIONS

PSC	Perovskite solar cell
PCE	Power conversion efficiency
V_{oc}	Open circuit voltage
FF	Fill factor
J_{sc}	Short circuit current
JV	Current density-voltage
MPP	Maximum power point
V_{bi}	Built-in potential
QFLS	Quasi-Fermi level splitting
PV	Photovoltaic
HTM	Hole transport material
HTL	Hole transport layer
ETL	Electron transport layer
CTL	Charge transport layer
WF	Work function
E_G	Bandgap
E_{VAC}	Vacuum level
E_F	Fermi level
QFLS	Quasi-fermi level splitting
EA	Electron affinity
IE	Ionization energy
VB	Valence band
VBM	Valence band maximum
CB	Conduction band
CBM	Conduction band minimum
HOMO	Highest occupied molecular orbital
LUMO	Lowest occupied molecular orbital
ELA	Energy level alignment
PLQY	Photoluminescence quantum yield
CPD	Contact potential difference
KP	Kelvin probe
KPFM	Kelvin probe force microscopy
AFM	Atomic force microscopy
APS	Ambient-pressure photoemission spectroscopy
UV-Vis	Ultraviolet and visible absorption spectroscopy
PL	Photoluminescence spectroscopy
CV	Cyclic-voltammetry
SEM	Scanning electron microscope
TCO	Transparent conductive oxide
FTO	Fluorine-doped tin oxide
ITO	Indium-doped tin oxide
Spiro-OMeTAD	2,2',7,7'-Tetrakis[N,N-di(4-methoxyphenyl)amino]-9,9'-spirobifluorene
PTAA	Poly(triaryl amine)
MA	Methylammonium
FA	Formamidinium
IPA	Isopropanol
csc5	Amyl sulfide
TOPO	Trioctylphosphine oxide
IPFC10	Perfluorodecyl iodide
IPFC12	Perfluorododecyl iodide
SAM	Self-assembled monolayer

TABLE OF CONTENTS

PART I

BACKGROUND & FUNDAMENTALS

1 INTRODUCTION

THE BIG PICTURE - fighting global warming

Venice, November 13th 2019[1]

During the night between the 12th and the 13th of November 2019 an exceptional *acqua alta* (the local term for the periodical extraordinary high tide, i.e. sea level rise > 110 cm) hit Venice in combination with a violent storm. The sea level rose to 187 cm: San Marco Square, the lowest part of the city, was under more than 1 m of water, 80 % of the city was submerged, the water combined with the strong wind brought severe damages to homes, businesses and landmarks, boats (like the Gondola in the picture above) were stranded. It was the second highest tide in the recorded history[1] and the worst of the last 50 years. However, what is worrying is not the single exceptional event, but the fact that until ~ 1950 in average 2-3 events of *acqua alta* were recorded every 10 years, after that the numbers started to increase almost exponentially, reaching 95 events between 2010 and 2020 with a peak of 26 only in 2019.[2] It is true that Venice is slowly sinking because of subsidence (~ 1 mm/year),[3] however the extraordinary increase in frequency of particularly high tide events is linked to a less

[1] Official recording started in 1872.

natural factor: the global warming induced by human activities since the industrial revolution.[4] According to predictions, in 100 year Venice will be at high risk of floods covering 97 % of its territory, and in a similar situation will be several other costal sites in the Mediterranean sea.[5]

The case of Venice is just a small example of the effects of the ongoing climate change and much more drastic events are currently taking place all over the world. Glaciers are melting, forests are burning, ocean currents are collapsing. On the 9th of August this year (2021) the Intergovernmental Panel on Climate Change (IPCC), which is the United Nations body for evaluating climate change, published the new assessment report.[6] The results are not a surprise yet they are scary, and the message is clear: the human influence has warmed the atmosphere leading to unprecedented climate changes. It is still possible to limit global warming to 1.5 °C, but rapid and large scale reductions of greenhouse gas emissions have to start now. The next UN Climate Change Conference will take place in November in Glasgow. Based on the new IPCC report, the objectives of the Paris Agreement[7] will be re-discussed with the aim of enhancing the efforts in the fight against global warming and ensure the goal of reaching net-zero[2] by 2050.

It is clear that in the current situation the research towards the development of renewable energies is more important than ever. Currently hydroelectric, wind, photovoltaic and bioenergy are the main sources of clean power, but they produce only the 25% of electricity generation. To keep the global temperature below 1.5 °C it is necessary to reach an almost complete decarbonisation of the electricity sector by 2050. The aim is to expand the installed generation capacity of renewable power from 2800 GW to over 27700 GW in the next 30 years, with the renewable energies producing the 90% of the required electricity and the remaining 10% divided between natural gas and nuclear power. In this context, wind and solar energy are supposed to lead the way, providing 63% of the total electricity requirements.[8]

At the moment 95% of photovoltaic energy is produced by crystalline Si solar modules, which can provide efficiencies up to 24.4%[3] and 25+ years certified stability.[9] However, despite its success, Si is not an ideal candidate as light absorber, indeed it has low absorption coefficient, indirect bandgap and it requires high temperatures manufacturing processes. Therefore, research is currently shifting towards other semiconductors, especially the so-called *thin-film solar cells*. The name already highlights one feature of these solar cells: the reduced thickness compared to Si (few µm instead of hundreds of µm). This is an interesting characteristic because it allows to expand the applications of these kinds of devices, for example producing flexible and light modules that can be integrated in buildings or used in IoT. Thin-film solar cells include cadmium telluride (CdTe), copper indium gallium selenide (CIGS), organic semiconductors or dyes and halide perovskites. The latter in particular attracted the attention of the scientific community in the last decade, quickly becoming one of the most promising alternative to Si solar cells.[10]

[2] Net-zero refers to the target of reaching a complete balance between the amount of emitted and absorbed greenhouse gasses.

[3] The value refer to the modules on the market. The record lab monocrystalline Si cell reached 26.7% efficiency.

HALIDE PEROVSKITE SOLAR CELLS - a brief introduction

Halide perovskites are a class of materials with composition ABX_3, where A is monovalent cation, B a divalent metal and X a monovalent anion. The sites can be occupied by different atoms and molecules, as long as the structure remains stable. This depends on the dimensions of the ions and it is determined by a quantity called *Goldschmidt tolerance factor*.[11] For example, A is often methylammonium (MA^+), formamidinium (FA^+) or Cs^+, B is primarily Pb^{2+} or Sn^{2+}, and X is an halide, mainly I^-, Br^- or Cl^-. The electronic structure is determined by the choice of ions forming the ABX_3 structure and it is mainly dependant on the energy levels of the metal and halides ions, while the A cation has orbitals with energies more deep within the bands.[12] The variety of possible combinations for A, B and X leads to a broad range of possible bandgaps, going approximately from 1.2 eV to 3.5 eV.[13] Therefore, perovskites are a particularly versatile class of materials, with tunable optoelectronic properties and stoichiometry.[14]

Halide perovskites were first used in solar cells in 2009 as development of dye-sensitized solar cells.[15] Indeed, in these first devices, the perovskite was deposited on a TiO_2 scaffold and it was covered with a liquid electrolyte. The solar cells had low efficiency and stability, but proved the possibility of using perovskite as light absorber. A major breakthrough happened in 2012, when the substitution of the liquid electrolyte with the solid hole-transport layer 2,2',7,7'-tetrakis-(N,N-di-p-methoxyphenyl-amine)-9,9'-spirobifluorene (spiro-OMeTAD) pushed the efficiency of the devices up to around 10%.[16,17] From this moment the interest of the scientific community drastically increased, triggering an exceptionally fast development that lead to a record efficiency of 25.5% by 2020.[18] Nowadays, perovskite solar cells are an established technology at the lab level, able to produce efficient devices with different structures and features.[19,20]

The reason behind the success of perovskite-based devices lies in the combination of cheap and easy fabrication methods with appealing properties such as direct (and tunable) bandgap, high absorption coefficient and long diffusion length.[21] These properties are per se not unprecedented in semiconductors, however their combination within one kind of material is unique.[22] The source of these features is in the perovskite ionic nature, the large lattice constant and the anti-bonding coupling between Pb s orbitals and I p orbitals. This results in unique defects properties.[23] A large part of the perovskite defects have shallow energy levels, i.e. their energy is close to the energy of the bands edges. In this case, the defects are basically harmless, indeed trapped charges can easily escape if thermally or optically excited.[24] Perovskite is thus generally defined as *defect-tolerant* and, because of this characteristic, devices can reach high efficiency, in spite of the presence of a high density of defects in the material. On the other hand, the perovskite ionic nature is also responsible for one of the main sources of losses in perovskite solar cells: ion migration.[25] Ions in the perovskite material are highly mobile and, upon light and bias, they migrate through the device, leaving behind defects and accumulating at interfaces. This increases non-radiative recombination and results in phenomena like hysteresis.[26]

Thanks to their exceptional properties, perovskites can be a valid alternative to Si or can be used in combination with it in so-called tandem solar cells.[27] However, despite their success, perovskite solar cells are still a young technology and require further research before being ready for a full-scale commercialization. For example, one of the main limitations, and probably the most relevant, is the operational stability. Perovskite solar cells degradation can indeed be induced by several factors. These can be extrinsic, such as humidity, heat, and UV-light, or intrinsic, like ion migration and charge accumulation.[28] In this regard, an important role is played by *interfaces*. The properties of interfaces not only affect the stability of perovskite-based devices, but they are also an additional source of non-radiative recombination and they determine the efficiency of the charge transfer.[29]

MOTIVATION AND OUTLINE

"*God made the bulk; surfaces were invented by the devil.*" – Wolfgang Pauli

The surface is the most vulnerable part of a material. Within the bulk every atom is surrounded by other similar atoms. On the surface, however, the material is abruptly interrupted, leaving the atoms undercoordinated and free to interact with what surrounds them. This affects the physical and chemical properties of the material, determining its behaviour.

A more general term for surface is *interface*, indeed a surface is nothing else than an interface where the second layer is air or the vacuum. In devices like solar cells interfaces play a crucial role and their careful optimization with respect to the adjacent layer is responsible for important improvements in efficiency and stability.[29] In fact, as the Nobel prize winner Herbert Krömer stated, "in many cases, the interface *is* the actual device".[30]

Perovskite solar cells are generally formed by an absorber (the perovskite itself), two charge transport layers and two external contacts. Each of these layers has interfaces, which need to be optimized so that their physical and chemical properties match. As per definition of interface, between the different layers there will be defects related to structural imperfections and dangling bonds.[24] Additionally, perovskite is typically a polycrystalline material. As a result, the film presents grains, whose boundaries are areas of high concentration of defects.[31] The interfacial defects are an important source of recombination, moreover they are responsible for phenomena like the aforementioned hysteresis and ion migration, which hinder stability and performance in devices.[32] This is in particular true for the interface between the perovskite and the subsequent layer, because of the complicated perovskite surface stoichiometry arising from the varied nature of the ABX_3 structure. A common method to mitigate the negative impacts of interfacial defects is by surface passivation, of which coordinate bonding via Lewis bases or acids is a common approach.[33]

From the energetic point of view, the different layers of a perovskite solar cell need to be aligned in order to efficiently extract charge carriers, meaning they need to be disposed as a "staircase", thus allowing electrons to flow towards lower energies and holes towards higher energies. Every interface between layers correspond to a step in this energetic staircase. The importance and effect of the dimension of this step is a heavily debated topic and will be discussed in Section 3.2, however, in general, a too big or misaligned step is source of non-radiative recombination and it poses a barrier to charge transport. This can cause severe losses in devices, especially a reduction of the open circuit voltage (V_{oc}).[34] Indeed, under illumination, the Fermi level within the perovskite semiconductor and the solar cell splits into a hole and an electron quasi-Fermi levels. The energetic difference between these two levels, denoted as quasi-Fermi level splitting, determines the V_{oc} of the device.[35] In presence of large interfacial offsets the quasi-Fermi levels cannot completely extend from the perovskite to the external contacts without bending, and thus reducing V_{oc}. Moreover, energy level offsets cause an exponential increase in charge carriers density in the transport layers, which results in enhanced recombination.[36]

In light of this, it is clear that interfaces are a critical part of semiconductor-based devices, and especially of perovskite solar cells. They are source of losses and require particular optimization. However, at the same time, the interfacial properties can be adjusted, becoming a tool to enhance the performance and stability of perovskite-based devices.

This work studies and discusses the tuning of the interfacial properties of halide perovskite with the adjacent hole-transport layer. The focus is in particular on the energetic alignment, with the objective of giving some guidelines to systematically adjust the energy levels depending on the requirements of the stack in the device.

The dissertation is structured as follows:

Part I gives the background information relevant for the understanding of the studies here presented. In particular, Chapter 2 presents the fundamentals of semiconductor physics from the point of view of photovoltaic and solar cells, followed by an introduction to the properties of halide perovskites and related devices. Chapter 3 dives deeper into the role of interfaces in perovskite solar cells, reviewing properties, challenges and different surface functionalization strategies. Chapter 4 briefly describes samples and devices preparation processes, together with the main characterization techniques used throughout this dissertation.

Part II shows the main results obtained during the course of my doctoral studies. Specifically:

Chapter 5 shows how to tune the perovskite energy levels by functionalizing its surface through assemblies of dipolar molecules. This method is known in organic and inorganic semiconductor physics, but it was never systematically applied to the perovskite layer. The study shows that it is possible to control direction and magnitude of the energy levels shift, obtaining a variation up to approximately 600 meV in both directions. In particular, the direction depends on the direction of the dipole, while the magnitude depends on the molecules' deposition parameters, such as the solution's concentration. The energetic shifts are characterized through different techniques and for different molecules, revealing insights on the relation between the deposition dynamics, and the molecules' and surface's features.

Chapter 6 explores the application in perovskite solar cells of the method exposed in Chapter 5. Devices are prepared using the same overall stack but different perovskite compositions, namely the so called triple-cation (with a bandgap of 1.6 eV) and $MAPbBr_3$ (with a bandgap of 2.3 eV). Because of the difference in bandgap, the two systems present different offsets at the perovskite/hole-transport layer interface. Specifically, approximately 300 meV in the first case and 800 meV in the second. The perovskite is functionalized in order to reduce this offset. For this purpose, different molecules are chosen depending on the requirements of the system. The functionalization is performed for different solution concentrations in order to evaluate the relation between measured energy levels shift and effect on the solar cells. In both cases a correlation between open-circuit voltage (V_{oc}) enhancement and measured energy levels shifts is noted. The improvement is limited to 10 mV in the case of triple-cation devices, therefore drift-diffusion simulations are performed to further support its relation to an energy level alignment adjustment. Solar cells with $MAPbBr_3$ show, instead, a clear trend in V_{oc}, culminating with an enhancement of approximately 60 meV for a solution concentration of 20 mM. Based on these results, consideration on the effectiveness of the energy level tuning method

depending on the systems are presented. Moreover, the relation between the measured energetic shifts and the actual V_{oc} improvement is commented.

Chapter 7 investigates the advantages of using a novel hole-transport material (HTM) that can interact with the halide ions on the perovskite surface via halogen bonding. In this case, the functionalization ability is incorporated directly within the HTM, without the need of an additional molecular interlayer. The behaviour of the material, named PFI, is compared with a reference HTM (PF) with same structure and optoelectronic properties, but without the ability of forming halogen bonding. Thanks to halogen bonding PFI can form a more ordered layer compared to PFI, improving the interface with the perovskite. The interaction of the two materials with the perovskite is explored through density functional theory simulations, Kelvin probe, ultraviolet-visible spectroscopy (UV-Vis) and atomic force microscopy (AFM). By comparing PFI and PF, the simulations support the presence of halogen bonding for PFI, Kelvin probe measurements indicate an improved energy level alignment, UV-Vis and AFM show increased resilience to solvent exposure. Devices are prepared with both HTMs, and their performance and operational stability assessed. Solar cells with PFI present reduced hysteresis and a V_{oc} enhancement of about 20 meV. The results are compatible with a reduction of recombination due to the improved energy level alignment and a limited ion migration due to the interaction between PFI and the I^- ions on the perovskite. This is also reflected in improved operational stability, determined through ageing measurements performed for 500 h under continuous maximum power point tracking.

Chapter 8 summarizes the findings from Chapters 5, 6 and 7 and comments on the results. Based on this some considerations to take into account when employing the presented energy level tuning method are given. Finally, some remaining unclear aspects are discussed and research questions for future works are proposed.

2 FUNDAMENTALS OF SEMICONDUCTORS AND SOLAR CELLS

This section presents the basic scientific concepts relevant to this dissertation. The backbone of this work lies in semiconductor physics, with a focus on the role of the materials' energetics. The relevant quantities are here presented and shortly discussed, followed by a description of semiconductor junctions and their role in solar cells. The physics of photovoltaics and the working principles of solar cells are discussed. Finally, halide perovskite solar cells and their most relevant characteristics are introduced. For a more detailed description it is possible to find several comprehensive books,[37–42] which were used as reference in addition to the works cited throughout the chapter.

2.1 Relevant energetic quantities

The energetic properties of a solid define its optoelectronic and electronic responses. This is particularly relevant in devices, where the parameters characterizing the energetics govern the overall electronic transport. Therefore, before going into details, it is important to present the most relevant quantitates underpinning the behaviours examined throughout this dissertation.[43,44] A simplistic representation of the fundamental energetics of a semiconductor is reported in Figure 2.1a.

Bands and band edges. In a solid material the electron energy states broaden into electronic bands. The valence band (VB) is the highest energetic band filled with electrons, while the conduction band (CB) is the lowest energetic band, which becomes occupied only when electrons are excited. In the CB the electrons can move freely. The energy states with highest energy in the VB form the valence band maximum (VBM) and the states in the CB with lowest energy form conduction band minimum (CBM). VBM and CBM are generally referred to as *transport levels* or *band edges*, and are the parts of the electronic bands relevant to charge transport. Based on the molecular orbital theory, their equivalent in organic semiconductors are the highest occupied molecular orbital (HOMO) and the lowest unoccupied molecular orbital (LUMO).

Bandgap. The bandgap (E_G) is the energetic difference between VBM and CBM. In other words, E_G is the energy that an electron needs to obtain in order to jump from VBM to CBM. For semiconductors

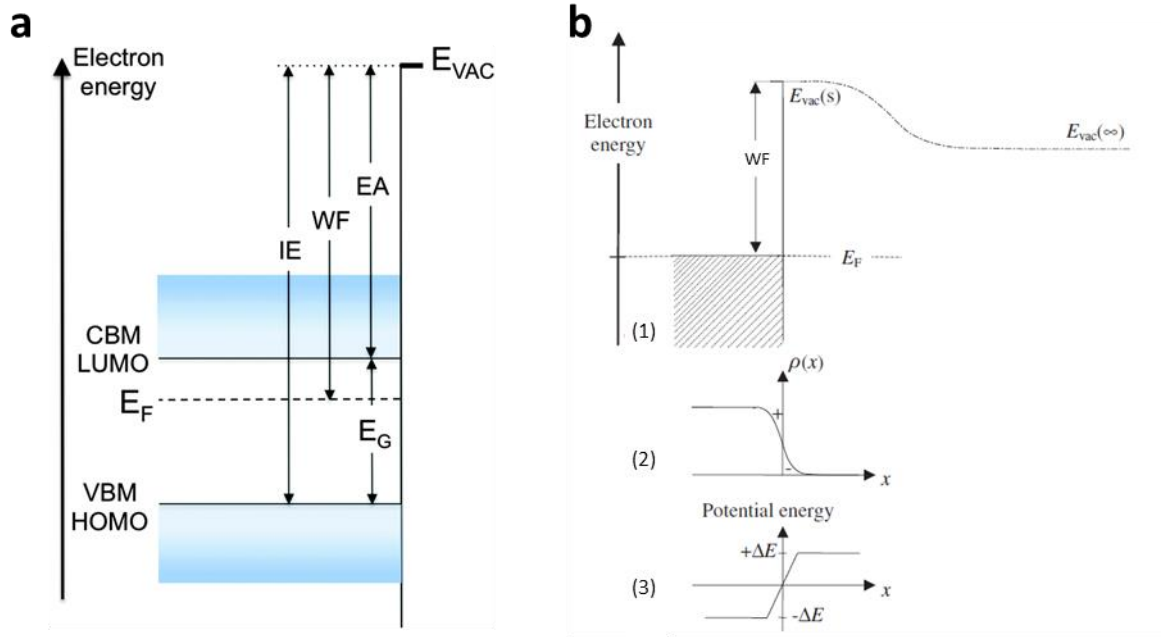

Figure 2.1. (a) Simplistic representation of an energy diagram of a semiconductor with the main energetic quantities: band edges (CBM/LUMO and VBM/HOMO), Fermi level (E_F), bandgap (E_G), work function (WF) and vacuum level (E_{VAC}). Adapted from Kahn A., Mater. Horiz. 3 (2016). Copyright © 2016 Royal Society of Chemistry. (b) Representation E_{VAC} at the surface ($E_{VAC}(s)$) and at infinity ($E_{VAC}(\infty)$). In (1) change of E_{VAC} from close to the surface ($E_{VAC}(s)$) to infinity ($E_{VAC}(\infty)$). (2) Variation of electron density ρ(x) inside and outside a solid: the electrons "spill out" and form an interfacial dipole. (3) Step in the electron potential energy induce by the interfacial dipole. Adapted from Cahen *et al*., Adv. Mat. 15 (2003). Copyright © 2003 Wiley.

the bandgap generally ranges from 0.5 eV to 4 eV.[42] It can be direct or indirect, depending on the momentum of VBM and CBM. If their momentum is different, an electron needs a phonon (lattice vibration) in addition to a photon to reach the CBM. This makes the general photon absorption probability lower and therefore, when used in solar cells, indirect bandgap semiconductors (such as Si) need a thicker absorber layer compared to direct bandgap semiconductors (like GaAs and halide perovskites).

Fermi level. The Fermi level (E_F) is the hypothetical energy level that has a 50% probability of getting occupied by an electron. In semiconductors, E_F is located within the bandgap and its position is crucial for the electrical properties of the solid. Indeed, if E_F is close to CB, the transport of electrons is facilitated. Conversely, if E_F is close to VB, the transport of holes is favoured. E_F can be influenced by the doping concentration in the material.

Vacuum level. The vacuum level (E_{VAC}) is generally defined as the energy of an electron at rest outside a solid. It is important to distinguish between surface (or local) vacuum level ($E_{VAC}(s)$) and vacuum level at infinity ($E_{VAC}(\infty)$). $E_{VAC}(\infty)$ is a theoretical concept and cannot be determined experimentally. It represents the energy on an electron at rest at infinite distance from the solid and it is common to all materials in a system. $E_{VAC}(s)$, instead, is the energy of an electron at rest right outside the surface of the solid and it is the actual reference for the experimental measurement of a material's energetic levels. The local vacuum level is affected by surface dipoles and, in crystals, it depends on the exposed facet.[45] The change in E_{VAC} from the surface to infinite distance is represented in Figure 2.1b: at the surface the solid is abruptly interrupted, resulting in electrons spill out (Figure 2.1b(2)), which creates

an interfacial dipole. The electrons potential energy is increased (Figure 2.1b(3)) and thus E_{VAC}, which then slowly decays until $E_{VAC}(\infty)$. A detailed discussion on the distinction between $E_{VAC}(s)$ and $E_{VAC}(\infty)$ is provided by Cahen *et al*.[44]. If not differently specified, in this dissertation the term E_{VAC} refers to $E_{VAC}(s)$.

Work function. The work function (WF) of a material is directly connected to the concepts of E_{VAC} and E_F. It is described as the energy necessary to remove an electron from the solid, i.e. the energetic difference between the E_F and E_{VAC}. Theoretically, there is a WF referred to $E_{VAC}(\infty)$ and a WF referred to $E_{VAC}(s)$, however also in this case the relevant quantity is the local one. WF is composed of a bulk and a surface component, which are challenging to separate experimentally. The bulk WF is the dominant one, while the surface WF takes into account interfacial charges redistribution and dipoles, resulting in an additional positive or negative potential step. The surface WF determines the behaviour at the interface.

Ionization energy and *electron affinity*. The ionization energy (IE) is the energy difference between E_{VAC} and VBM, therefore IE represents the energy necessary to remove an electron from the VBM. The electron affinity (EA), complementarily to IE, is the energy difference between E_{VAC} and CBM, therefore it represents the energy gained by dropping an electron from E_{VAC} to the CBM. The experimental determination of IE and EA corresponds to the identification of the position of VBM and CBM, respectively.

2.2 p-n junction

When two or more semiconductors are put into contact they form a junction. The above described energetic quantities adjust their reciprocal position according to specific requirements and form what is called a band diagram. In particular, upon contact, E_F has to be aligned, while keeping E_{VAC} continuous and preserving the energetics.

Junctions between semiconductors with different doping are at the base of semiconductor electronic devices and are called p-n junctions. Specifically they comprise a p- and n-doped material. They are referred to as *homojunctions* if the two semiconductors are the same material and *heterojunctions* if the semiconductors are different. The behaviour is similar in the two cases, with the main difference arising from discontinuities between the transport bands due to the different bandgaps. These discontinuities can be described as “cliffs” or “spikes” (Figure 2.2b) and form potential steps that could act as barriers.

The behaviour of p-n heterojunction is schematically represented in Figure 2.2, together with the band diagrams corresponding to the condition before and after contact. A p-type material has a high concentration of holes, while an n-type material has a high concentration of electrons. As a

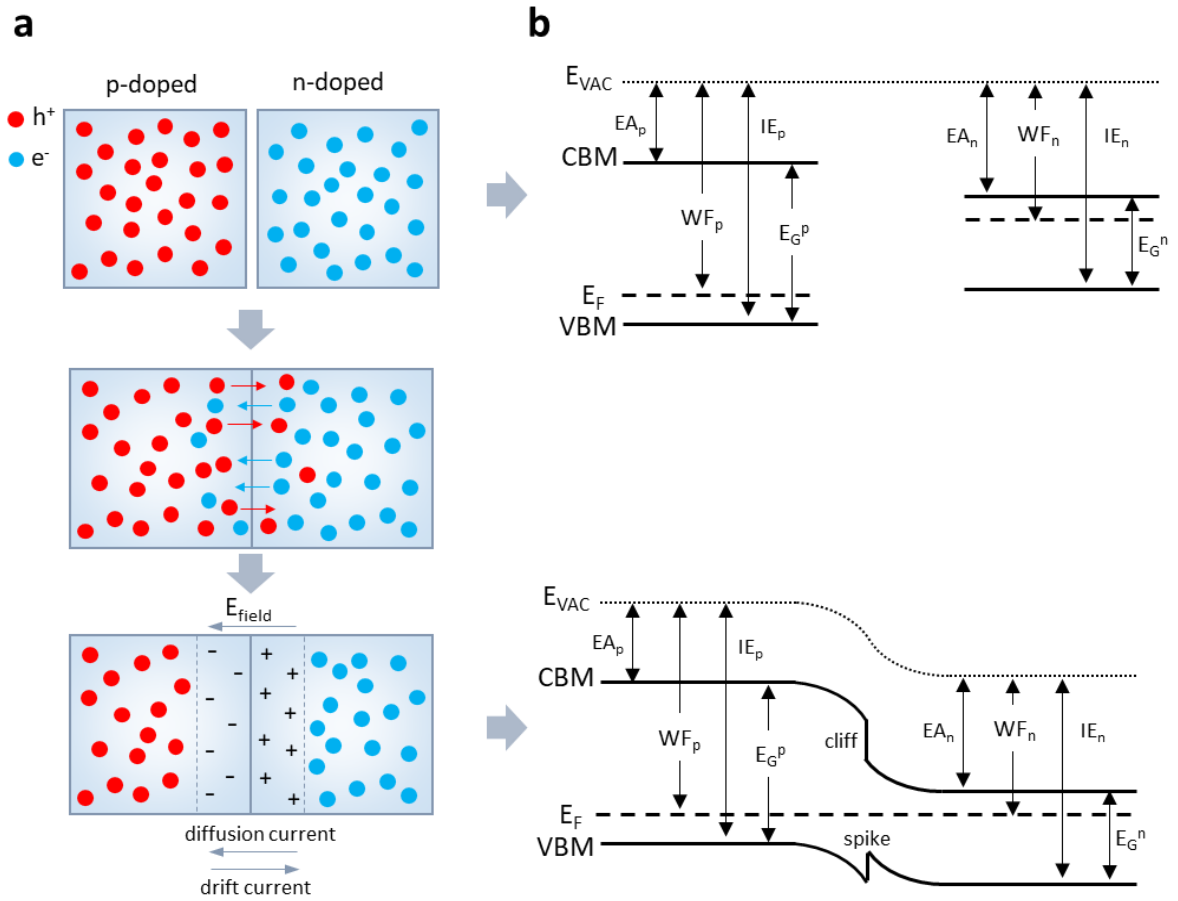

Figure 2.2. (a) Schematic representation of a p-n heterojunction in dark. From top to bottom: p- and n-doped semiconductors before contact, materials after contact with electrons and holes diffusion, formation of depletion region with electric field (E_{field}), diffusion current and drift current. (b) Band diagrams related to the corresponding situations on the left side. Before contact the materials are aligned according to the vacuum level (E_{VAC}), after contact the Fermi levels (E_F) align. CBM and VBM are conduction band minimum and valence band maximum, WF is the work function, E_G is the bandgap, EA and IE are electron affinity and ionization energy.

consequence, when a p-n junction is formed, electrons and holes start to diffuse towards the region with opposite charge until reaching equilibrium (Figure 2.2a – middle). This results in an area at the interface called *depletion region*, which is depleted of electronic charges and contains the charged defects (dopants) left behind by the diffused carriers, i.e. positive impurities in the n-type semiconductor and negative impurities in the p-type semiconductor. The depletion region creates an electric field which opposes the diffusion process and generates a current in opposite direction called *drift current*. In absence of external bias, an equilibrium is reached when the diffusion current equals the drift current, and a potential is present across the junction (Figure 2.2a – bottom). This potential, called built-in potential (V_{bi}), corresponds to the voltage that can be measured from a solar cell with that junction and it is given by the difference in WF of the two semiconductors. V_{bi} can also be expressed in terms of carrier concentration:

$$V_{bi} = \frac{k_B T}{e} ln\left(\frac{n \cdot p}{n_i^2}\right) \qquad 2.1$$

Where n is the electron concentration in the n-type material, p is the hole concentration in the p-type material, n_i is the intrinsic carrier concentration, e the elementary charge, k_B is the Boltzmann constant and T is the temperature.

If a p-n junction is illuminated photogenerated electron-hole pairs are created and, thanks to the electric field, holes move towards the p-type contact and electrons towards the n-type contact. If an external load is connected to the contacts a current can be extracted.

2.3 p-i-n junction

It is also possible to form a junction with an intrinsic semiconductor sandwiched between the two doped layers. In this case, the junction is referred to as *p-i-n junction*. An energy diagram is sketched in Figure 2.3 in equilibrium (Figure 2.3a) and upon illumination, in the case open circuit voltage condition (Figure 2.3b). In a p-i-n junction the potential is fixed by the doped layers and varies linearly between them. If the system is not in equilibrium, for example under illumination, the carrier population cannot be represented by a single Fermi level. To describe a situation of deviation from equilibrium it is necessary to introduce the concept of quasi-Fermi levels, which represents the electrochemical potentials of electrons and holes separately (E^F_n and E^F_p in Figure 2.3b). The separation of E_F under illumination is called quasi-Fermi level splitting (QFLS) and it is directly related to the voltage obtained from a solar cell at open circuit conditions.[35] In a solar cell the intrinsic semiconductor acts as absorber and photo-generates charges, which are then transported through the doped layers.

2.4 Solar spectrum and photovoltaic effect

The energy generated by the sun thanks to nuclear fusion is emitted in form of radiation and reaches earth with an intensity of 1353 W/m^2 in free space.[42] However, the atmosphere is attenuating the solar irradiance because of scattering from dust particles and absorption from air molecules. Therefore, the actual energy flux reaching the surface depends on the distance that the photons need to travel through the atmosphere. The parameter to account for the spectrum attenuation is referred to as optical air mass (AM) and the standard value for the evaluation of solar cells is AM1.5, corresponding to the spectrum on the surface at a tilt of 48° compared to the equator and giving an

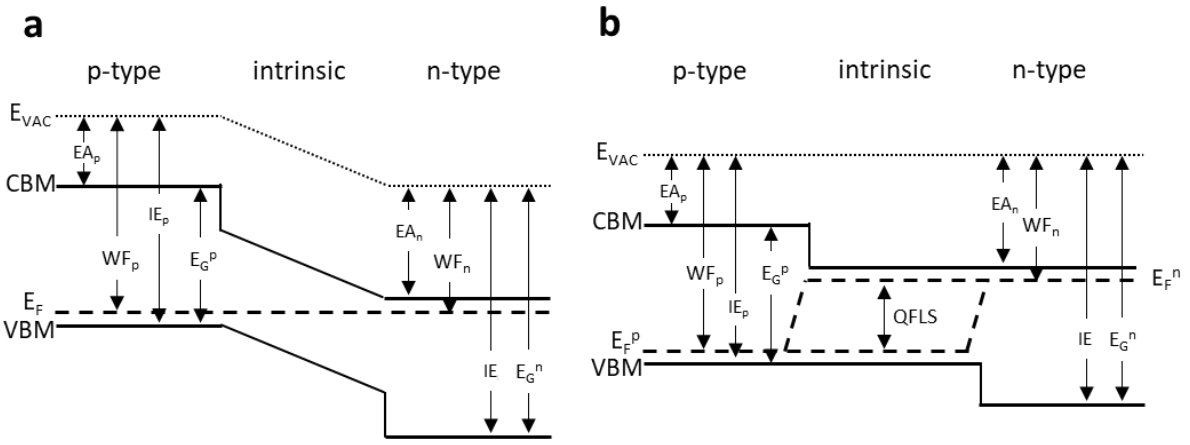

Figure 2.3. Sketch of the band diagram of a p-i-n junction in equilibrium (a) and at open circuit voltage (b), with electron and hole quasi-Fermi levels (E_F^n and E_F^p, respectively), and quasi-Fermi level splitting (QFLS).

energy flux of about 1000 W/m^2. Figure 2.4 displays the spectra corresponding to AM0 and AM1.5, where AM0 refers to the solar spectrum outside the atmosphere.

Light can be converted into electricity thanks to the photovoltaic effect. A photon absorbed by a material generates an electron-hole pair. Normally, these charges would recombine. However, in presence of an electric field such as the one created in a p-n or p-i-n junction, they can be collected and extracted to generate current. Photons can be absorbed only if their energy ($h\nu$) is larger than the material's bandgap E_G. If $h\nu < E_G$ the photons will be transmitted through the material. On the other hand, if $h\nu > E_G$, the photons will be absorbed, but the excited electrons will lose their excess energy by thermalisation and relax to the conduction band.

2.5 Solar cells parameters

Characterization of the performance of solar cells is commonly performed by applying a voltage sweep to the device in light or dark conditions and measuring the resulting current density. The analysis of the curve obtained by plotting voltage and current density as y- and x-axis respectively (*JV curve*) can give significant information on the photovoltaic behaviour of the solar cell. A standard JV curve and the main parameters of a device measured in light or dark are represented in Figure 2.5. The most important photovoltaic parameters are *open circuit voltage* (V_{oc}), *short circuit current* (J_{sc}), *maximum power point* (MPP), and *fill factor* (FF). The V_{oc} is the voltage of the device at open circuit, i.e. with no current flowing, thus it is the maximum voltage achievable by the solar cell. J_{sc} is the current density when the device is short circuited, i.e. when the voltage is 0 V. MPP represents the combination of current and voltage that gives the maximum power output of the device.

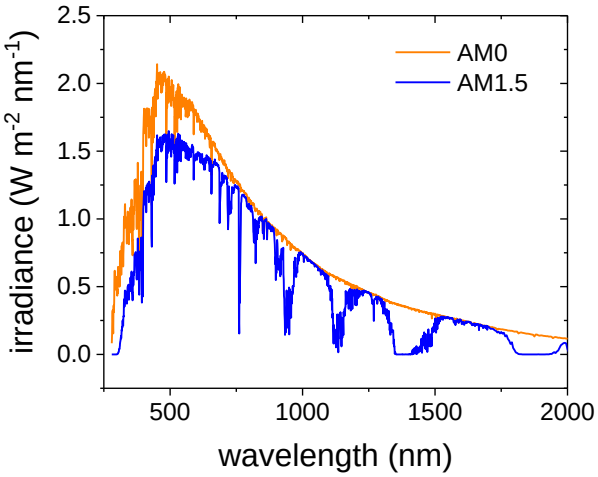

Figure 2.4. Solar irradiance spectrum outside the atmosphere (AM0) and from earth's surface with a tilt angle of 48° (AM1.5). Plotted using ASTM G173-03 reference spectra provided by NREL.[46]

FF is given by the following formula:

$$FF = \frac{V_{MPP}\, J_{MPP}}{V_{oc}\, J_{sc}} \qquad 2.2$$

Where V_{MPP} and J_{MPP} are voltage and current at MPP. This parameter gives the proportion between the ideal behaviour (i.e. if the JV curve would be a rectangle with J_{sc} and V_{oc} as sides - dashed lines in Figure 2.5), and the real behaviour (where J_{MPP} and V_{MPP} define the rectangle). Therefore, it is a measurement of the quality of the device. A perfect solar cell would have a FF of 1, but generally a real (and good) device has a FF of 0.80-0.85. FF is often expressed as percentage.

The ratio of the power output (P_{out}) and the input power (P_{in}) provides the power conversion efficiency (PCE) of the device:

$$PCE = \frac{P_{out}}{P_{in}} \cdot 100 = \frac{V_{oc}\, J_{sc}\, FF}{P_{in}} \cdot 100 = \frac{J_{MPP}\, V_{MPP}}{P_{in}} \cdot 100 \qquad 2.3$$

Where generally P_{in} is 1000 W/m^2, since the measurements are performed in sun simulators that can reproduce the AM1.5 spectrum.

The maximum theoretical efficiency of a single junction solar cell is given by the Shockley-Queisser limit and depends on the bandgap and the incident spectrum.[47] However, since the spectrum is standardized at AM1.5, the relevant parameter is the bandgap. The maximum efficiency for a single junction solar cell (33.7%) can be achieved with a bandgap of 1.4 eV.

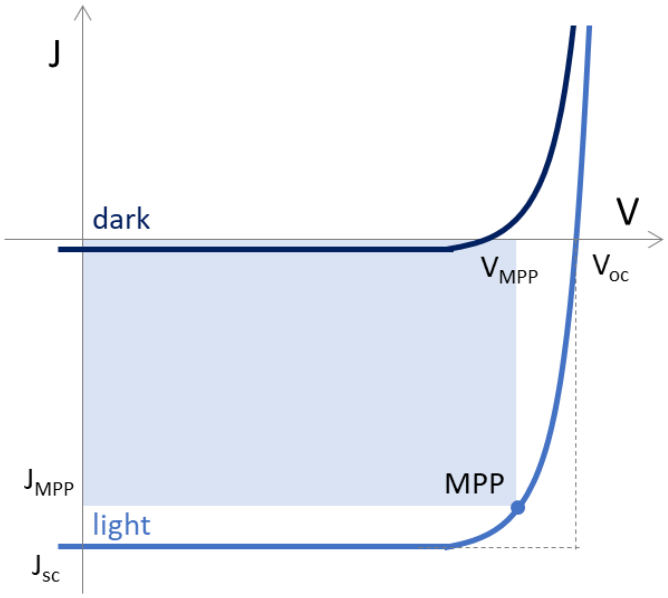

Figure 2.5. Example of standard JV curves in light (light blue) and dark (dark blue) with the different photovoltaic parameters: maximum power point (MPP) with relative current (J_{MPP}) and voltage (V_{MPP}), open circuit voltage (V_{OC}) and short circuit current (J_{SC}).

2.6 Halide perovskite solar cells

Perovskite is a material with a wide range of applications, especially in the field of optoelectronics.[48–53] This section will focus on introducing this compound and its properties from the perspective of its use in photovoltaics. In view of the next chapters, special attention is posed to the electronic structure.

2.6.1 Properties of halide perovskites

The name *perovskite* refers to all the materials with a structure related to $CaTiO_3$, a mineral that was discovered in 1839 by Gustav Rose and that was named after the mineralogist Lew Alexejewitsch Perowski.[54] This structure is described as ABX_3, where A is a monovalent cation, B a divalent cation and X an anion.[55] The most common perovskites can be classified as metal oxides (X=O), metal sulfides (X=S) or as metal halide perovskites (X=F/Cl/Br/I). The latter is the case relevant to this dissertation. The ABX_3 structure is displayed in Figure 2.6a for the cubic aristotype. On the left the single unit cell, on the right a different common representation showing the characteristic corner-sharing octahedra. The structure can tilt and form orthorhombic or tetragonal structures depending on temperature and/or pressure.[56–58] In the case of metal halide perovskites, the cation A can be either organic or

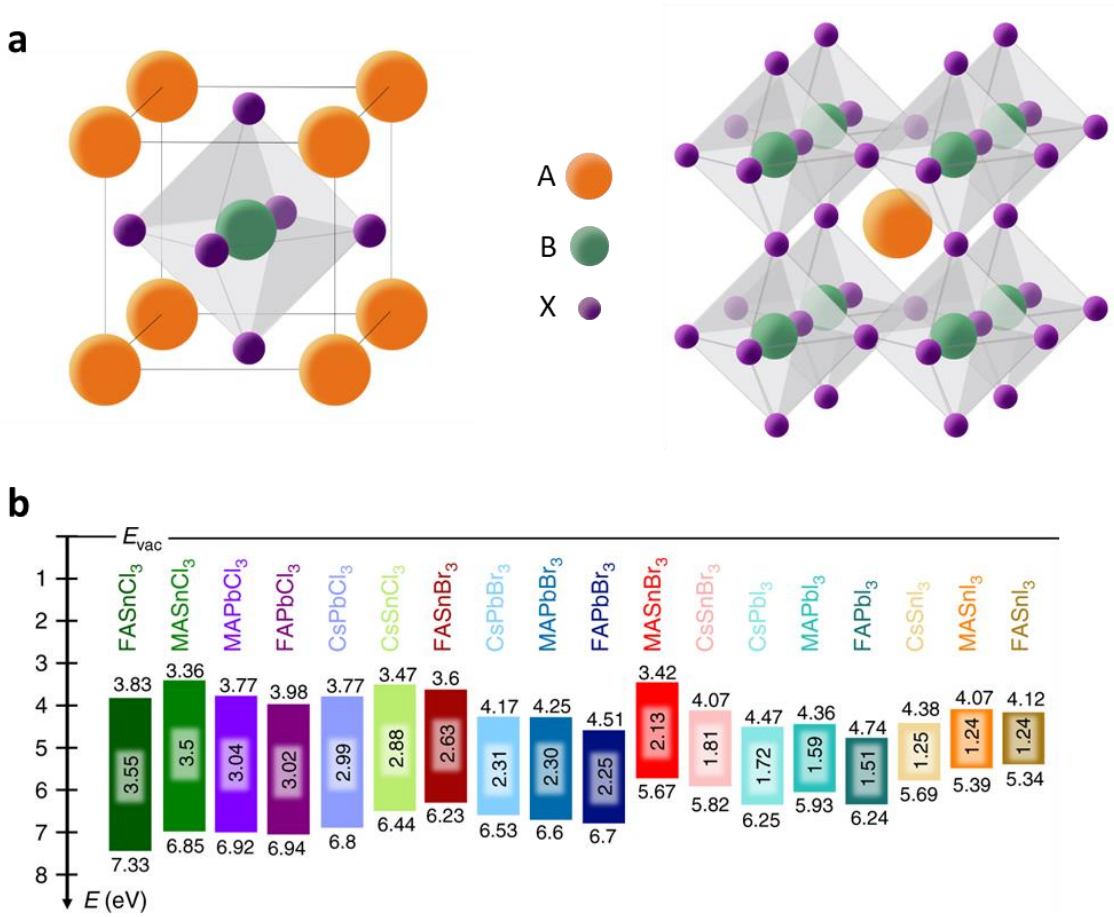

Figure 2.6. (a) Representations of the ABX_3 lattice structure. Specifically, on the left the unit cell in cubic aristotype structure with a sixfold coordinated metal B. The octahedron is surrounded by eight monovalent cations A. On the right, an alternative representation with corner-sharing octahedra caging the A cation. A are the cations (for example methylammonium – MA^+, and formamidinium – FA^+), B smaller divalent cations (generally Pb^{2+} or Sn^{2+}), and X anions (halides in the case of this dissertation). (b) Energy levels of the most common perovskite compositions. (b) Reproduced from Tao *et al*., Nat. Com. 10 (2019). Copyright © 2019 Nature.

inorganic, thus including a wide range of possibilities, from MA^+ (methylammonium - $CH_3NH_3^+$) and FA^+ (formamidinium - $(NH_2)_2CH_2^+$) to Cs^+ or Rb^+. The divalent metal B is often Pb^{2+}, although now the scientific community is trying to shift to the less toxic Sn^{2+}.[59–61] The halide X is generally I^-, Br^- or Cl^-.

The choice of ions for A, B, and X directly affects the electronic structure of perovskite, indeed E_G can be tuned by changing the composition. For example, mixing or substituting I^- with Br^- or Cl^- leads to an increase of E_G, while changing Pb^{2+} with Sn^{2+} can reduce E_G. Moreover, the dimension of A can affect the lattice size and thus E_G as well. Overall, it is possible to tune E_G approximately from 1.2 eV to 3.5 eV.[13,62] An overview of the variations of the energetics depending on the composition is displayed in Figure 2.6b. In general, the metal and the halides are the atoms contributing to the energy of the band edges, while the orbitals related to the A cation lie deeper within the bands. In particular, the VBM is mainly determined by Pb(6s) and I(5p) orbitals, while the CBM by Pb(6p) and I(5p) orbitals, therefore VBM and CBM possess s-orbitals and p-orbital character, respectively.[12,62,63]

The elements that can form the ABX_3 structure are determined by a parameter called *Goldschmidt tolerance factor* and defined as follows:[11]

$$t = \frac{R_A + R_x}{\sqrt{2}(R_B + R_x)} \qquad 2.4$$

Where R_A, R_B and R_X are the ionic radii of A, B, and X respectively. The tolerance factor can predict which combination of materials can give a stable ABX_3 structure depending on their ionic radius. Specifically, stable 3D perovskites are obtained if $0.8 < t < 1$.[64] According to the tolerance factor, perovskite can be formed with a variety of ions, resulting in a system characterized by optoelectronic tunability, but also complex stoichiometry. The impact of these factors will be discussed in Section 3.1.

The first milestone for the use of perovskite in solar cells was set by Miyasaka's group in 2009, obtaining perovskite-based dye-sensitized devices with a PCE of 3.8 %.[15] A second important step was taken in 2012 when 2,2',7,7'-Tetrakis[N,N-di(4-methoxyphenyl)amino]-9,9'-spirobifluorene (spiro-OMeTAD) was introduced as solid hole-transport layer in two works submitted separately but almost simultaneously by the groups of Miyasaka and Snaith[17] on one side, and Park and Grätzel[16] on the other, both obtaining more than 9 % efficiency. From that moment the interest of the scientific community in perovskite solar cells (PSCs) increased rapidly, leading to a fast improvement, which in less than 10 years resulted in a record efficiency of 25.5 %.[18]

The reason for the success of the perovskite material in photovoltaic applications lies in its unique combination of desirable optoelectronic and structural properties,[14,20,21] some of which have been described above. In particular, perovskites possess a *direct (and tunable) bandgap*[65] with a *high absorption coefficient*[66] and good absorption in the solar spectrum. Moreover, *long diffusion length*[67,68] leads to relatively low recombination, in spite of the high defect density. The reason behind this is the soft and polar character of perovskite, and the nature of the defects, which are not all harmful, as will be discussed in Section 3.1.1. This characteristic leads directly to another advantage, i.e. the opportunity of depositing perovskite through different - fairly easy and cheap - *low temperature fabrication processes*.[69]

These properties are not unprecedented and were already observed in other semiconductors. However, what is unique is their combination within one class of materials.[22] Indeed for example high efficiency, stability and long lifetimes are characteristics of the so-called 1st generation solar cells (for example crystalline Si devices), but they also require expensive and energetically demanding fabrication processes. On the other hand, 2nd generation devices (for example cadmium telluride – CdTe – or copper indium gallium selenide – CIGS – solar cells) are cheap and easy to produce, but generally possess low efficiency and stability. PSCs include many of these desirable characteristics, making them a particularly attractive alternative photovoltaic technology.

Nevertheless, PSCs have also some disadvantages, which so far limited the commercialization of this kind of solar cells. In particular, one of the main challenges arises from stability.[70] The factors affecting PSCs stability can be divided into extrinsic and intrinsic. Extrinsic factors are related to the external environment, like humidity, heat and UV light, while intrinsic factors depend on processes within the

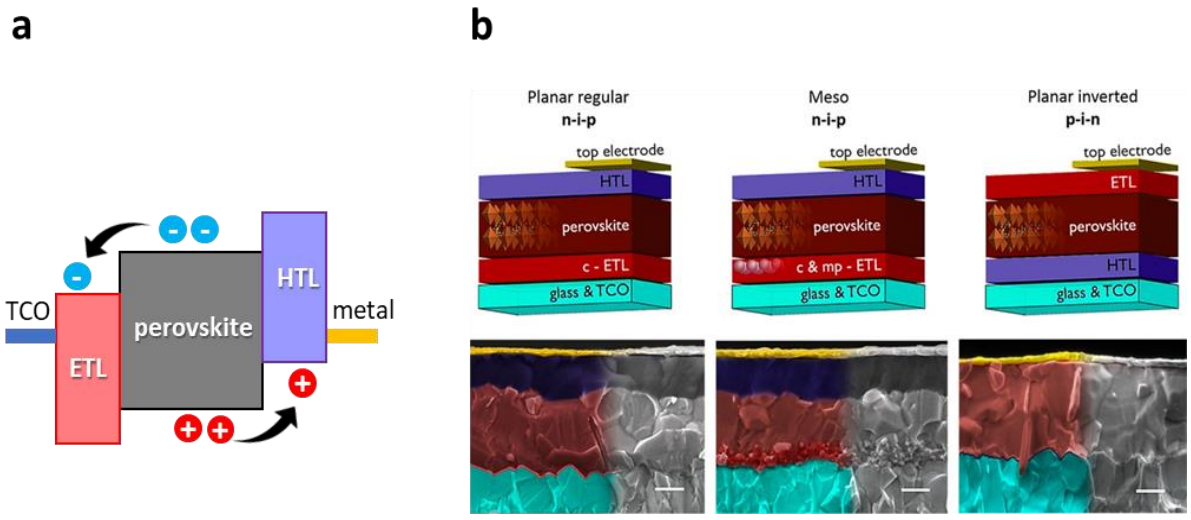

Figure 2.7. (a) Schematic of standard energy level alignment of a n-i-p PSC, with the perovskite absorber sandwiched between an electron transport layer (ETL), a hole transport layer (HTL) and two electrodes (TCO is a transparent conductive oxide), showing the direction of the charges flow. (b) Different architectures of perovskite solar cells (PSCs). Reproduced from Saliba *et al*., Chem. Mater. 30 (2018). Copyright © American Chemical Society.

material, such as ion migration or charge accumulation.[28,71] Moisture, for example, can have relevant effects depending on the composition, in particular water degrades PbI_2 and MAI. Moreover, water ingress is enhanced by spiro-OMeTAD.[72] Heat can induce layer instabilities (for example spiro-OMeTAD crystallizes at temperatures over 80°C, which leads to device degradation[73,74]) and the migration of atoms across the layers (especially Au migration is detrimental for devices).[75] UV-light is mainly a problem for metal oxide layers, for example it activates deep levels traps in the widely used TiO_2, and this is a source of recombination.[76] Some of these issues can be solved through proper encapsulation. However, intrinsic factors are more difficult to eradicate. Nevertheless, it has been shown that in some cases degradation is reversible.[71] This is leading to a re-valuation of the standard parameters and tests to assess stability, in order to tailor them according to the characteristics of PSCs[4].[77,78]

2.6.2 Device structure

Perovskite solar cells generally consist of an absorber layer (the perovskite itself), sandwiched between two charge transport layers (CTLs) and two contact layers (Figure 2.7). Upon illumination, the perovskite absorbs the photons, which produce photo-generated charges. These charges are then extracted through the (often doped) electron- and hole-transport layers (ETLs and HTLs, respectively) and finally collected by the external contacts. Generally, one of the contacts is a metal with suitable WF, the other one is a transparent conductive oxide (TCO) and it allows the transmission of light to the absorber. In order to have efficient charge extraction and low recombination, the different layers

[4] The current testing conditions and requirements are optimized for Si solar cells.

should have a favourable energy level alignment (ELA),[34,79] i.e. they should be arranged like a "staircase" (Figure 2.7a), with descending energetic steps for the electrons and increasing energetic steps for the holes. The energetic step is referred to as *offset* and it is particularly relevant in terms of recombination and V_{oc}. For example, the presence of a big offset between perovskite and HTL in the case of wide bandgap perovskites greatly limits the potential of these kinds of devices.[80,81] The importance and impact of the offset will be discussed more in detail in Section 3.2.1, which is specifically dedicate to ELA.

The first PSCs had a n-i-p structure with TiO_2 as ETL (*n*) and spiro-OMeTAD as HTL (*p*), but within the years new materials started to be synthesized or "borrowed" from organic or dye-sensitized solar cells. Nowadays, both n-i-p and p-i-n architectures[5] (see Figure 2.7b) are widely employed and can reach high efficiencies.[19] In devices with n-i-p structure the TCO is generally FTO (fluorine tin oxide), typical ETLs are TiO_2 (compact or a combination of mesoporous and compact) and SnO_2, and HTLs are often spiro-OMeTAD or PTAA (Poly(triaryl amine)). On the other hand, p-i-n devices commonly use ITO (indium tin oxide) as substrate, PTAA or PEDOT:PSS (poly(3,4-ethylenedioxythiophene) polystyrene sulfonate) as HTLs, and BCP (bathocuproine) or fullerenes, such as C60, as ETLs. However, research towards finding novel more stable and efficient CTLs is constantly in progress, as testified by the many examples reported in reviews for either HTLs[82–85] or ETLs[86–88]. At the same time, some works show working PSCs without HTL[89,90] or ETL[91,92], although in this case one of the challenges to overcome is indeed the energetic misalignment between perovskite and electrodes.

[5] It is worth noting that there is evidence that perovskite is actually not intrinsic, but more p or n doped depending on the substrate.[153,337] Therefore, it would be more correct to talk about p-n-n or p-p-n junction. However, for the sake of simplicity, in this dissertation devices will be still referred to as p-i-n or n-i-p.

3 THE ROLE OF INTERFACES

Interfaces are of utmost importance in any solid-state device. Since the birth of semiconductor devices in the late 19th century, scientists noticed deviations from Ohm's law in presence of junctions between different materials.[93] Soon it was recognized that these anomalies were related to the contact itself, even though a physical understanding of the phenomena took another 50 years to be developed.[40]

The problems rise from the nature of surfaces themselves: the abrupt termination of a material results in an irregular layer with dangling bonds, leading for example to the formation of surface states, possible chemical reactions, and changes in the energetics and the material structure. It is therefore clear that interfaces play a primary role in the determination of a material's properties and in the device functionality.[94,95]

This is particularly true in the case of hybrid organic-inorganic perovskite solar cells (PSCs). As described in Section 2.6.1, the perovskite absorber is formed by several elements and molecules arranged with a fairly complex stoichiometry. This is reflected at the interface with the adjacent layer, resulting in diversified surface terminations, comprising both organic and inorganic elements. Moreover, perovskite films are deposited through many different processes, which result in films with different features and defects.[96,97]

Standard PSCs are a stack of five layers, namely a transparent conductive oxide (TCO) substrate, an electron transport layer (ETL), the perovskite absorber, a hole transport layer (HTL) and a conductive contact, generally a metal (Figure 2.7), which correspond to as many interfaces, either between the materials or with the external environment. However, often there are even more interfaces due to the presence of interlayers.[98] Additionally, the perovskite layer is generally polycrystalline, thus further interfaces can be found in the form of grain boundaries, and grains are likely to have different exposed facets, meaning different surface terminations.[99] It is therefore clear that within a PSC, and especially between perovskite and the adjacent layers, there are many and complex interfaces. This has a great impact on performance and stability of the solar cells, indeed exposed surfaces and metal-semiconductor or semiconductor-semiconductor junctions determine the electronic and transport properties of devices.[29]

The next sections will focus on a more detailed description of such interfaces, especially that between the perovskite and the subsequent layer, and on the related effects on charge transport.

3.1 Features of perovskite and its surface

This section will discuss the characteristic of the perovskite layer and surface in terms of different terminations and defects. First, the different kind of imperfections will be presented, then the related effects will be explored.

3.1.1 Defects and recombination

The variety of different techniques[100] for the deposition of perovskite films inevitably leads to surfaces with different morphologies, chemical composition and electronic properties.[96] Traditionally, the most common method is spin-coating,[19,101] which already produces a high degree of variation on the final result depending only on spinning program, annealing conditions, and eventual vacuum-drying[102] or hot-casting.[103] However, several other techniques are widely used and offer the possibility to tune the surface properties in different ways. For example common methods include co-evaporation,[104] vapour deposition,[105] slot-die coating[106] and inkjet printing.[107]

All these methods allow obtaining state-of-the-art devices, nevertheless little is known about the characteristics of the surface. Many theoretical studies have been devoted to the understanding and prediction of the surface termination. For example, the surface could be MAI-terminated or PbI_2-terminated, and different facets seem to be favoured depending on the structure (i.e. tetragonal, orthorhombic and cubic).[108–110] However, these studies are generally restricted to ideal stoichiometric surfaces and are limited by the finite set of parameters needed for the simulations. Experimental investigation of the "real" surface structure is in principle possible through techniques like LEED (Low Energy Electron Diffraction) or STM (Scanning Tunneling Microscopy), but the requirement for these experiments make the application on perovskite challenging, therefore it is possible to find only a few related studies.[111]

What is clear from experimental and theoretical investigations is that the nature of the processes employed to form the perovskite layer leads to polycrystalline films with non-stoichiometric surfaces, grain boundaries and imperfections in the crystal structure.[24,32,112] Nevertheless, it is known that one of the benefits of perovskite as absorber is to be defects tolerant,[113] allowing the devices to reach high performances in spite of a high concentration of defects. This is an advantage compared to other semiconductor-based devices, such as Si solar cells, that require high purity materials in order to be efficient.[114] However, defects are still one of the main causes of energy loss in perovskite solar cells, being related to phenomena like ion migration and hysteresis, and thereby affecting fundamental parameters such as recombination and charge transport.

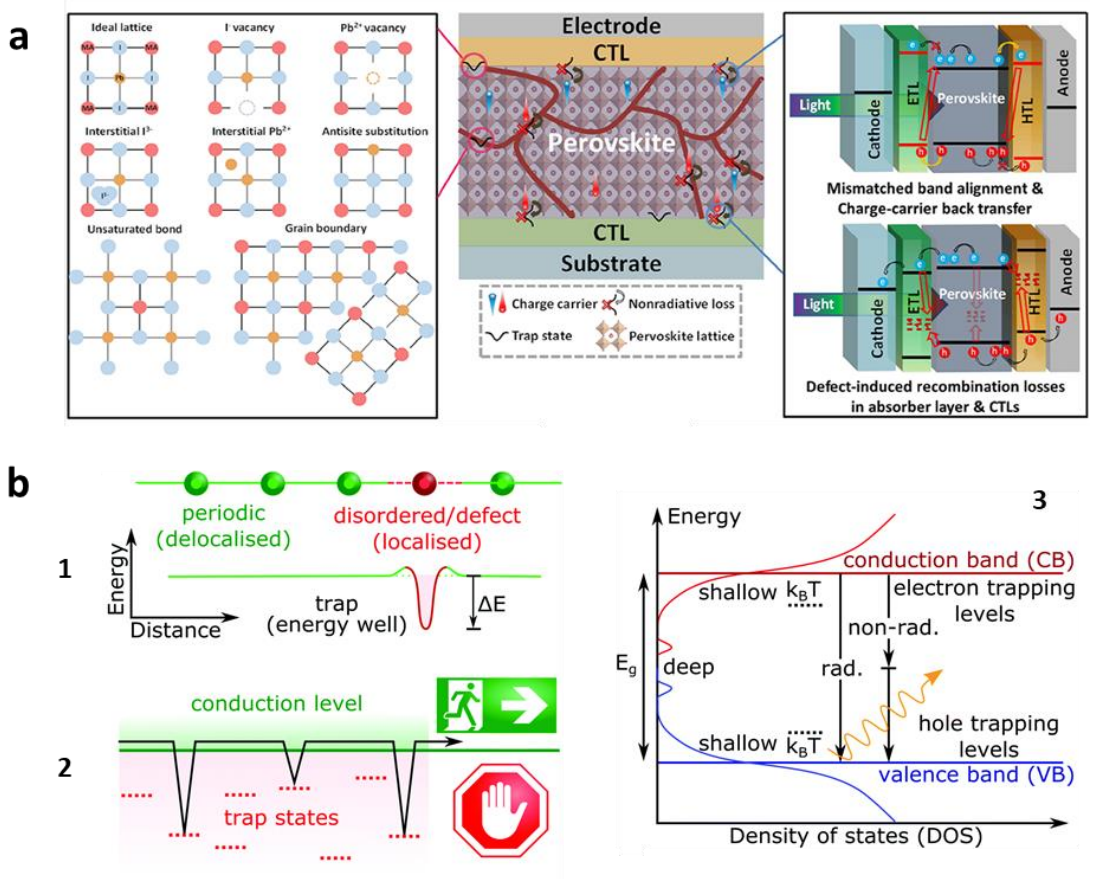

Figure 3.1. (a) Illustration of the main defects in perovskite and the induced interfacial non-radiative recombination losses. Reproduced from Niu et *al.*, J. Phys. Chem. Lett. 12 (2021). Copyright © 2021 American Chemical Society. (b) Scheme representing defects from an energetic point of view: (1) new energetic level introduced by a localized defect. (2) charge trapping kinetics. (3) defects induced recombination in a band diagram. Adapted from Jin *et al.*, Mater. Horiz. 7 (2020). Copyright © 2020 Royal Society of Chemistry.

The perovskite defects are generally grouped as extrinsic or intrinsic. Extrinsic defects are those related to interactions with the environment or the adjacent layers: they are generally caused by undercoordinated atoms at the surface and grain boundaries[115] and they are considered the main source of non-radiative recombination losses in PSCs.[116,117] The discussion in the experimental part of this dissertation will mainly deal with these kinds of defects. Intrinsic (or native) point defects are crystallographic defects: they arise from lattice imperfections and they are typically divided into vacancies, anti-site and interstitials. Vacancies are created when an atom is missing from its lattice site, while an atom occupying a wrong site is called anti-site. Interstitials arise, instead, from atoms residing in between sites. In the exemplary case of $MAPbI_3$, it is possible to identify 12 native point defects, specifically MA, Pb, and I vacancies and interstitials, together with the anti-site occupations MA_{Pb}, MA_I, Pb_{MA}, Pb_I, I_{MA}, and I_{Pb}.[24] An overview of the different defects and related non-radiative recombination losses is sketched in Figure 3.1a.

Defects have energy levels different from those of the conduction band and valence band edges. If their energy places them outside the bandgap they do not pose a problem. Indeed, it would not be favourable for the charges to occupy those states. However, if the energy levels of the defects are lower/higher than the conduction band/valence band edge, than the free carriers can energetically fall into them and get trapped, as represented in Figure 3.1b.[32,114] At this point, it becomes important

how deep within the bandgap is the defect located. If the defect is shallow, i.e. with energy close to that of the band edges, the trapped charge can escape with an additional energy (activation energy), which can be given thermally or through optical absorption. In this case, the effect of the defects is merely to slow down the movement of the free carriers through trapping-detrapping processes, reducing the effective mobility of the carriers. On the other hand, if the defect is deep within the bandgap, a trapped charge carrier will likely recombine. Indeed, in this case, the probability of re-emission is low compared to the probability of recombination. These electrons/holes are likely to recombine with a hole/electron emitting a phonon instead of a photon. Such non-radiative recombination process is called Shockley-Read-Hall (SRH) or trap-assisted and it is considered an important loss mechanism in all semiconductor applications, including solar cells[118–120]. Other relevant recombination mechanisms are band-to-band (generally radiative) and Auger recombination. SRH, band-to-band and Auger recombination are generally described in a simplified way through the following rate equation:

$$\frac{dn}{dt} = -k_1 n - k_2 n^2 - k_3 n^3 \qquad 3.1$$

where *dn/dt* describes the rate at which carriers decay, *n* the charge carriers density and k_1, k_2 and k_3 are the rate constants for the three kinds of recombination processes, respectively. However, at the surface we have to consider an additional recombination path given by dangling bonds and crystal imperfections. These defects are mostly positively or negatively charged and thus they attract electron and holes, making the surface site of particularly high recombination. The surface recombination is generally a type of SRH recombination and therefore it contributes, together with the bulk recombination, to the first order recombination, linearly dependent on the charge carriers density *n*. The surface recombination is characterized by a parameter called *surface recombination velocity* (*S*, in units cm/s), which represents the movements of the free carriers towards the surface. For this recombination to happen the carries need to diffuse to the surface, therefore the recombination rate depends also on diffusivity (*D*) and thickness (*d*). Specifically, the surface recombination coefficient (k_S) can be expressed as:

$$k_S = \left(\frac{4d^2}{\pi^2 D} + \frac{d}{S}\right)^{-1} \qquad 3.2$$

Where the first term accounts for the time needed to diffuse to the surface and the second for the actual recombination. In thin-film solar cells the surface recombination is considered to be dominant with respect to the bulk and the main source of recombination. A common technique to overcome losses due to surface recombination is surface passivation, which will be discussed later in Section 3.3.

3.1.2 Ion migration

It is well known that perovskites, being an ionic crystal, exhibit ion migration.[25,121] Ions constituting the material can migrate across it because of bias or light, leaving defects behind and accumulating at the interfaces.[122,123] In general, one can distinguish between bias-driven ion migration and diffusion induced by a gradient in vacancy concentration. In practice, it is difficult to separate the two phenomena, therefore in this dissertation the term "ion migration" will refer to both field-induced migration and diffusion.

A lot of research has been devoted to the understanding and characterization of ion migration: even if the calculated activation energies differ from study to study, it is commonly recognized that iodides, thanks to their low activation energy, constitute the largest fraction of the mobile ion density. On the other hand, Pb^{2+} ions possess very high activation energy and therefore tend to reside stably at their sites.[124] MA^+ ions have relatively high activation energy as well, but it has been shown that they can migrate, albeit comparably slowly.[125] MA^+ defects do not introduce deep traps, therefore they are not particularly harmful. However, the removal of MA^+ from the unit cell can modify the crystal structure and eventually lead to degradation.[126]

When bias is applied or when perovskite is stimulated by light, the mobile ions tend to move and migrate across the material. As a direct consequence, the migrated ions leave behind vacancies or other defects that are typically charged and become recombination centres. Moreover, they tend to accumulate at the interfaces with the CTLs, resulting in a partial screening of the built-in electric field, negatively impacting carrier collection. This further enhances recombination and it is one of the main causes of hysteresis in JV curves.[121,127] Interestingly, Domanski *et al.* showed that the losses related to ion migration can be recovered if the devices are let in dark for a comparably short amount of time, i.e. overnight.[71] This is a very important result since, in real-world applications, devices undergo a natural day/night cycle, which would then allow PSCs to recover these losses during the night and restart "fresh" in the morning.

3.1.3 Hysteresis

The term *hysteresis* represents a difference between reverse and forward scans in JV curves, where reverse scan goes from V_{oc} to 0 V and forward scan from 0 V to V_{oc}. In presence of hysteresis the second scan that is performed has often reduced efficiency, mainly related to a reduction in FF and sometimes V_{oc}.[26] This phenomenon has been brought to attention in the perovskite field by Snaith *et al*. in 2014.[128] In that report the authors also highlight how hysteresis depends on factors such as scan rate and device architecture. This dependence on measurement conditions and device structure makes it particularly problematic to compare devices coming from different laboratories. In order to obtain

reliable results, it is therefore always strongly suggested to accompany results from JV curves with stabilized power outputs.[77,128] For example, maximum power point (MPP) tracking measures the devices efficiency variation on a longer time scale (typically at least 100-200 s) in order to take into account any transient effects due to ion migration.

Ion migration (in particular halides ions migration[129]) is currently considered the main cause of hysteresis.[26,129,130] Initially the presence of a large defect density in the perovskite and its ferroelectric properties were also proposed,[128] but soon discarded by further measurements.[129,131] As described in the previous section, under bias or light ions moves across the perovskite absorber and tend to accumulate at the interfaces with the CTLs layers forming thin charged layer called *Debye layers*.[129,132] The Debye layers generate an additional electric field, which, if it works against the built-in electric field, leads to inefficient charge transfer. In particular, hysteresis happens because the migrated ions have a slow response and cannot redistribute fast enough. This is also the reason of the hysteresis dependence from scan rate: at slow scan rate the ions are fast enough to redistribute without causing hysteresis, at high scan rate ions basically do not have time to react and therefore can cause only small damage. However, at intermediate scan rates, we incur in the situation described above and JV curves exhibit noticeable hysteresis.[133]

The relation between ion migration and hysteresis has been proven by many theoretical works,[26,121,134] but it is challenging to obtain experimental evidence of the mechanism itself, although techniques like Kelvin probe force microscopy, impedance spectroscopy and galvanostatic measurements have proven useful to investigate ion migration.[121] Some studies associate hysteresis, at least partly, to accumulation of charges at the interfaces, claiming an interplay between this phenomenon and ion migration.[135,136] Therefore, the understanding of the processes behind hysteresis is not trivial and requires more investigation.

In any case, it is clear from all the studies that hysteresis is strongly connected to interfaces and a bad junction results in inefficient charge transport. This can be mitigated by any treatment that helps to increase charge carriers extraction, for example larger grains and passivation.[137,138] Another possibility is, instead, to tune the properties of the surrounding CTLs.[133] The interfaces with the adjacent layers are indeed of paramount importance for the functionality of PSCs.[139]

3.2 Interaction of perovskite with adjacent layers

So far we have discussed the characteristics of the perovskite material and especially its surface, which, in a device, corresponds to the interface with the adjacent layer. Regardless of the structure, the perovskite film is generally sandwiched between two CTLs and two electrodes. The properties of these materials and their relation are fundamental for the functionality of devices, indeed they determine charge transport and extraction of the photogenerated carriers. It is possible to summarize the most relevant features for a CTL in a few points:

a. *Good optical transmittance* in order to minimize optical losses and maximize absorption in the perovskite layer.
b. *High electrical conductivity* to optimize charge transport.
c. *Absence of pinholes*, which would cause current leakage and shunts.
d. *Well-matched energy level alignment (ELA)* for minimal energy loss and efficient charge transport and extraction.

Among these points, ELA is particularly related to interfaces and it will be the focus of this dissertation. ELA indeed plays an important role in charge transfer and it is strictly connected to recombination, but it also stands out as particularly challenging to obtain and evaluate.[12,79,140]

As already introduced in Section 2.6.2, the different layers are ideally energetically disposed as a "staircase", where electrons can flow towards lower energies along CBM/LUMO levels and holes can flow towards higher energies along VBM/HOMO levels. In this regard, there are mainly two barriers that can be an obstacle to charge transfer: extraction and injection barriers. We speak of *extraction barrier* when there is a misalignment between perovskite and CTL impeding the flow of majority charges between the two layers, for example if the perovskite VBM lies energetically higher than the HTL HOMO level. In this case devices would show loss of current around V_{oc} and reduced FF. An *injection barrier* is instead present in case of a large offset between perovskite and CTL, with for example the HTL HOMO level much higher than the perovskite VBM. This would limit the quasi-Fermi level splitting and thus cause a V_{oc} loss.[141] Therefore, it is important to have well-matched energy levels with appropriate offsets for efficient charge transfer.

Before going deeper into a discussion of ELA, it is noteworthy to highlight that for every material within a stack there are two kind of interfaces: the buried (or bottom) interface and the top interface. The difference is relevant because the two interfaces undergo different formation processes and this results in different defect structure and electronic alignment. In particular, the buried interface depends on the substrate underneath, which acts as template for the material's growth. While the top interface is already formed when the next layer is deposited.[29,142] This interface is also the one responsible for eventual interactions with subsequent layers or with external agents (while exposed) and, as mentioned above, it can be rather complicated. Moreover, not all deposition methods are

suitable on perovskite, therefore special care need to be considered when choosing the CTL to be deposited on top. For these reasons, the top interface requires particular attention and optimization.

3.2.1 Energy level alignment and charge transport

The ELA at the interface between perovskite and the adjacent layers is one of the main sources of V_{oc} losses in PSCs. Indeed, V_{oc} should ideally correspond to the QFLS within the absorbing layer. This happens if the quasi-Fermi levels (QFLs) are able to expand from the perovskite to the contacts without encountering barriers. Because of the combination of interfacial recombination and the presence of a big offset at the interface for the transport of majority carriers, the QFL at that interface has to bend, introducing a mismatch between QFLS and V_{oc} and thus proportionally reducing the external V_{oc}. In particular this is observed when the offset is bigger than 200 meV, in the case of smaller offsets the QFLs can remain flat and avoid V_{oc} loss.[34,143] An example is illustrated in Figure 3.2a for the case of a p-i-n device with offset between the perovskite VBM and the HTL (poly(triaryl)amine – PTAA - specifically) HOMO level. Simulations and experiments were performed with different common perovskite compositions and lead to the same conclusion: a QFLS-V_{oc} mismatch is present in case of offset between energy levels. Misalignment between energy levels is also a source of non-radiative recombination: energy level offsets exponentially increase the charge carrier density in the CTLs, i.e. exponentially increase the interfacial recombination.[36,144] Thus, since V_{oc} depends logarithmically on the recombination rate, this means that an offset is directly proportional to a V_{oc} loss.

Therefore, CTLs induce additional non-radiative recombination and causes V_{oc} losses, severely detrimental for devices. By characterizing top and bottom perovskite interfaces, and comparing QFLS and V_{oc} measurements for both n-i-p and p-i-n stacks, it was found that the most relevant energy losses happen at the top perovskite interface.[34] To represent the situation at V_{oc} from the point of view of recombination losses, it is useful to make a comparison with a bucket filled with water (Figure 3.2b).[145] The photo-generated current is the stream of water and the water level in the bucket is the achievable V_{oc}. Some of it is lost through the holes, i.e. bulk or surface recombination and other mechanisms. The losses will be dominated by the biggest hole, which, for well-performing devices, correspond to the interface of the perovskite with the transport layer on top. The condition of the device is important for the relevance of this conclusion, indeed, if for example the perovskite is highly defective, than the high recombination within the material would dominate. Thus, it is of great importance to determine the predominant loss channel before drawing any conclusion on the reasons for an eventual improvement in devices performance upon modifications.

This discussion is focused on the role of ELA in the determination of V_{oc}, however there are other factors affecting this parameter. Especially, as also commented in Section 3.1.1, defects play an

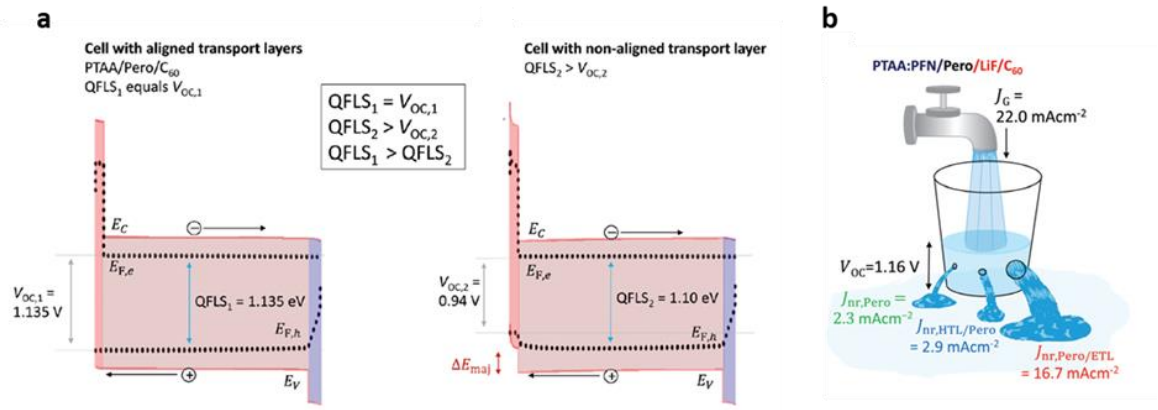

Figure 3.2. (a) Drift-diffusion simulations of QFLS and V_{oc} in a p-i-n device with aligned (left) and misaligned (right) CTLs. A reduction in V_{oc} and QFLS-V_{oc} mismatch due to an energy offset (ΔE_{maj}) between the perovskite and the HTL is evident in the second case. $E_{F,e/h}$ are the QFLs, E_c and E_V are conduction and valence band. (b) Representation of recombination losses at V_{oc} in an inverted perovskite solar cell. The water stream is the generated current density from the sun, the level of the water is the V_{oc} and the holes represent the different bulk or interfacial recombination losses. Any hole causes a reduction of the water level and thus of V_{oc}. Reproduced from Stolterfoht *et al*., Energy Environ. Sci. 12 (2019). Copyright © 2019 Royal Society of Chemistry.

important role: defect recombination in the bulk or at interfaces are often also a cause for V_{oc} losses.[115,117,146–149] In light of this, in order to optimize interfaces and extract the maximum V_{oc} it is important to combine different strategies. In particular, special attention should be put in (i) obtaining properly matched energy levels, (ii) optimize the perovskite material itself and (iii) reduce interfacial recombination losses through passivation.

3.2.2 Determination of PSCs energetics

Considering the importance of ELA for devices, the determination of the energy levels of the different layers and their respective alignment is an important task. The most common techniques to measure the energetics of a material are ultraviolet photoelectron spectroscopy (UPS), inverse photoemission spectroscopy (IPES), Kelvin probe (KP), Kelvin probe force microscopy (KPFM) and cyclic voltammetry (CV). The first two can give the most detailed and precise information regarding the energy levels of the analysed material and they are the generally the technique of choice for works focused on the characterization of the perovskite electronic structure. However, this kind of measurement requires ultra-high vacuum condition and a careful handling of the samples in order to avoid contamination. With UPS being a very surface sensitive technique, the presence of impurities can easily result in misleading results. Moreover, the measurement is performed with a high energy UV source, which could affect the results. KP, KPFM and CV, together with photoemission spectroscopy at ambient pressure (APS), are instead non-intrusive methods that require milder conditions. The latter techniques will be discussed in more detail in the methods section.

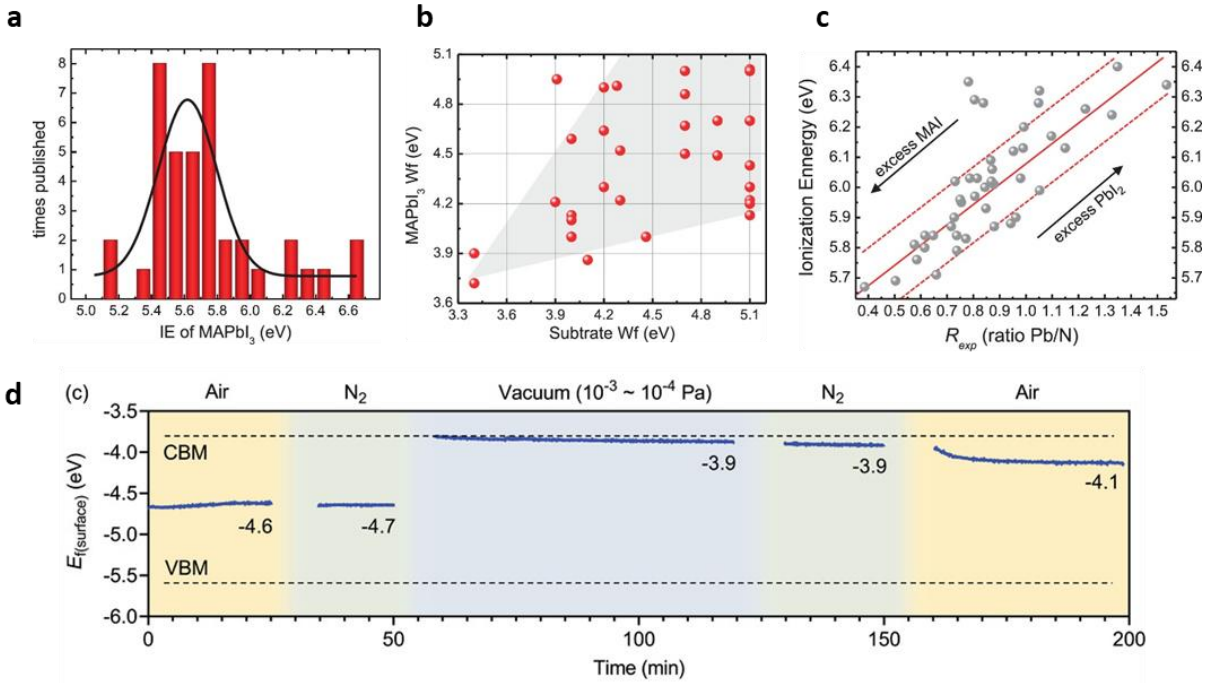

Figure 3.3. Variations on perovskite energetics. (a) Statistics on the different IE values for $MAPbI_3$ found in literature. (b) Variation of $MAPbI_3$ work function (Wf) depending on the substrate. (c) Dependence of IE on $MAPbI_3$ composition. (d) Shift of Fermi level for a cycle of measurements in different atmospheres (Air→N_2→vacuum→N_2→Air) (a-c) Reproduced from Olthof *et al.*, APL Mater. 4 (2016). Copyright © 2016 APL Materials.). (d) Reproduced from Hu *et al.*, Adv. Energy Mat. 10 (2020). Copyright © 2020 Wiley.

The experimental measurement of energy levels in PSCs and their alignment is quite challenging, as a consequence the results are varied and sometimes contradictive. Figure 3.3a, for example, reports different values found in literature for the ionization energy of $MAPbI_3$ films, showing a variation that covers more than 1 eV. The reason behind these discrepancies lies in the relatively high number of factors that can influence the results or the measurement itself. The energy levels can indeed be affected by internal and external factors. Internal factors can be considered for example substrate, perovskite composition, ion migration or the presence of dipoles. External factors are instead related to the measurement conditions and technique, as well as to the data analysis approach.

Dependence on the substrate

A dependence of the perovskite WF on the substrate and its doping level was soon discovered for thin layers by Miller *et al.*[150] in 2014, and shortly after confirmed by Schulz *et al.*[151] for thick $MAPbI_3$ layers (350-400 nm). Both groups report similar findings, in particular it seems like the perovskite is almost intrinsic if deposited on a p-type substrate (i.e. high WF), while E_F shifts close to the CB in case of an n-type substrate (i.e. low WF). The peculiar doping behaviour was further analysed by Caputo *et al.*,[152] suggesting an interaction with the substrate as driving mechanism. This seems to indicate that the WF of the substrate dictates the perovskite ELA. Indeed, since there is no evidence of changes in structural and optical properties, the modification of the perovskite doping character is likely due to the bottom interface rather than the bulk. This is particularly interesting in the case of thick perovskite layers, indeed, since the measurements on these studies were performed via UPS on top of the perovskite

film, it means that the change in E_F is propagated throughout the whole film. A correlation between WF of substrate and perovskite can be found also by comparing the results from other research groups (Figure 3.3b), although from this graph it is also evident that, even when using the same substrate, different works report quite different perovskite WF values. This therefore stress again the scattering of results due to the aforementioned reasons.

Light and atmosphere influence

More recently, some studies highlighted the effect of the measurement environment and light exposure on the experimental results. In particular, Hellmann *et al*.[153] performed photoelectron spectroscopy on vacuum deposited $MAPbI_3$-based devices both in dark and in light. Interestingly, the measurements in dark show that the absorber layer is n-type independently from the substrate, in contrast with the works mentioned above. The measurements in light reveal a shift of the Fermi level towards mid-gap in case of p-type substrates and no shift for n-type substrates. The authors therefore suggest to pay particular attention to unintentional illumination during the experiments, indeed even a small amount of light could affect the measurement and lead to a wrong data interpretation. The impact of atmosphere on the energetics of different kind of halide perovskites was instead explored by Hu *et al*.[154] (Figure 3.3d). What stands out from this study is the effect of vacuum on the energy levels. Indeed, while measuring in air or N_2 does not seem to affect E_F, going to high vacuum induce a shift of E_F towards the CB. The doping is then maintained even with a return to normal pressure, but it can be recovered by heating the substrates. The doping effect is ascribed to a passivation due to air exposure and a subsequent desorption of these molecules in vacuum.

These results rise some doubts on the substrate-dependent ELA discussed in the beginning, which could then be related to the condition of the measurement rather than a real substrates-induced shift. Further studies are needed, but it is clear that particular attention is needed when measuring the perovskite energetics.

Composition and stoichiometry variations

As discussed before, the perovskite layer has a complex composition. This is one of the advantages of PSCs since it allows an easy tuning of the bandgap. Obviously, it also means that the energy levels will be different depending on the composition (see Figure 2.6b from Section 2.6.1) and therefore the possible combinations for ELA are many. Most of the studies that performed a detailed determination of energetics are focused on the most common perovskite compositions, especially $MAPbI_3$.[79,140,153,155] There is also a very complete work from Tao *et al*.[13], where a wide range of Pb- and Sn-based perovskites are energetically characterized. However, for example, it is rare to find an accurate determination of the energy levels of the so-called “triple cation perovskite”, which is maybe the most used composition nowadays.[156] This underlines the complexity of the energetic landscape in the field of PSCs and the need for more characterization studies. Nevertheless, it is possible to make some

common observations. For example, it has been shown that switching halides from I to Br and Cl leads to a progressive increase of the bandgap[13] mainly related to a downshift of the VB.[140,157] On the other hand, metal-substitution leads instead to a shift of the CB,[158,159] although mixed-metal compositions showed variation in both CB and VB.[159] In general passing from Pb to Sn decreases the bandgap.[13]

A complex composition is also reflected in a complex stoichiometry. Variations in the precursors mixing ratios and/or the fabrication process can lead to (voluntary or not) non-stoichiometric films and consequent change in energetics. For example $MAPbI_3$ was shown to change from n-type to p-type depending on the PbI_2/MAI ratios[160] and to have a VBM dependant from the MAI concentration.[161] A representation of the variation on the IE of $MAPbI_3$ depending on MAI and PbI_2 excess is reported in Figure 3.3c.[155] Additionally, the presence of defects, interfacial dipoles and phenomena like ion migration can also affect the energy levels by changing the offset at the interface. In the case of presence of defects or ion migration the charge accumulation causes bend bending, which can be advantageous or not depending on the bending direction and stack configuration.[162,163] The effect of interfacial dipoles will be described in details in Section 3.3.4.

Insight into good practice for the study of energy level alignment

Some comments can be made in light of the wide range of variation and interpretation on ELA that can follow from all above described factors affecting the measurements. It is clear that the precise determination of the energetic values characterizing the perovskite material is quite challenging. It is of course of the utmost importance to pay particular attention (within the confines of the respective equipment and/or lab limitations) to the samples handling and to external factors, such as atmosphere and light exposure, keeping the same condition throughout the experiment. Nevertheless, this will anyhow likely lead to different results from one research group to another, even if only for differences in the setups and the possibility of controlling the measurement environment. Therefore, a comparison among the values obtained with the different measurements in the same set of experiments is more important than absolute numbers. Indeed, absolute numbers might be imprecise, however the difference between them would not be affected if the factors causing the error influence all the measurements in a similar way. Although of course some factors might have unknown different effects depending on the properties of the material, as in the case described above, where light affects or not the measurement depending on the doping of the substrate. Continuous new studies are needed in order to characterize all the possible parameters affecting a measurement, so that it is possible to take them into account during an experiment. Moreover, it is also important to state in a clear and detailed way the condition of the measurements, so that other research groups can effectively reproduce and/or compare results. This should be mandatory in good scientific practice, but it is especially relevant in the perovskite solar cells field.

Is energy level alignment actually relevant?

So far it has been discussed why a good ELA is important for obtaining efficient PSC, and many theoretical and experimental works support this interpretation.[140,164–169] Nevertheless, there are also several papers showing experimental evidence of little to no correlation between V_{oc} and energy levels.[170–174] The importance of ELA is currently a heavily debated topic and it is not possible to give a straight answer. However, there are several factors to take into account when debating energetics and their relation, which could help justifying the discrepancies among the results.

First of all, there is the problem of the precise determination of energy levels discussed in above. Due to the difficulties of such measurements, most of the times the values used for discussing ELA are taken from literature or from the pristine materials, not in the actual stack. Thus, they do not necessarily reflect the actual specific situation in a device. In the cases where the energetics are actually experimentally determined, the measurements can be affected by factors like the illumination source, atmosphere or characteristics of the setup, possibly leading to a misinterpretation of the real alignment. Moreover, often the energetics of every layer are estimated separately and according to vacuum level alignment. This is the standard and a generally accepted procedure, but it not always gives a true picture of what happens in the complete device, where Fermi level alignment occurs. Regarding this, a measurement of the different layers in the actual stack used in devices would be always preferable. In addition, the exact relation between the energy levels at the surface and in the bulk is not always clear. This is relevant considering that generally techniques for the measurement of energetics are surface sensitive. Last but not least, QFLS and consequently V_{oc} can be limited by other components of the cell, for example the perovskite bulk or an interface different from the one under analysis. In this case, that specific examined offset might actually not dominate, hence its effect is minor.

In conclusion, there could be situations where the ELA is less important than other aspects limiting the performance of the device and it is furthermore possible that the independence of the results from energetic offset is due to factors affecting the measurement or imprecision in the values used for the comparison. In general, the prospect exists that sometimes single energy levels do not play a central role, however obtaining ELA throughout the device is fundamental for its functionality.

Unfortunately, it is currently unavoidable to encounter the above-mentioned obstacles, and it is difficult to disentangle the different effects and draw actual conclusions. However, it is important to take these factors into consideration when discussing ELA in PSCs.

3.3 Functionalization as strategy

As described in the previous section, the perovskite layer is a polycrystalline film that contain a high number of different kinds of defects in the surface or in the bulk. These imperfections are generally detrimental for the devices` functionality, leading for example to recombination or ions migration, and in general hindering not only their efficiency, but also their stability. The most dangerous kinds of defects are those with energy deep within the bandgap, since they cause non-radiative recombination. Shallow defects are instead generally considered harmless, however they can easily migrate across the layers, causing unfavourable charge accumulation or hysteresis. For these reasons, it is of paramount importance to eliminate these imperfections and mitigate ion migration. The most common approach to achieve this purpose is the passivation of these defects by molecules that can interact with them.[175] An overview of the most common perovskite imperfections and related passivation techniques is represented in Figure 3.4.

Due to the ionic nature of perovskite, the defects are generally positively or negatively charged. To deactivate such defects it is possible to exploit passivation methods such as conversion, ionic bonding or coordinate bonding.[33] Conversion consists in chemically transforming surface and grain boundaries to a material with wider bandgap, thus eliminating the defects and obtaining a more favourable ELA. In case of ionic bonding, instead, there is the complete transfer of one or more valence electrons from one atom to the other, therefore anions and cations can serve as passivators for ions on the perovskite surface. Here we will focus more on last, but maybe more common, case: coordinate bonding.[176] This kind of passivation involves sharing two electrons coming from the same atom and thus forming what is called a Lewis adduct.[177]

3.3.1 Coordinate bonding: Lewis acids and Lewis bases

As a general definition, a Lewis base is a molecule with an electron pair not involved in bonding and which thus can be donated to another molecule (a Lewis acid) to form a dative bond, the result is generally referred to as Lewis adduct. On the other hand, a Lewis acid is a molecule with an empty orbital, which can accept an electron pair from another molecule (a Lewis base), again forming a Lewis adduct. At the perovskite surface the crystal structure is abruptly interrupted, leaving many unpaired electron or holes forming dangling bonds. For example, it is possible to find halide ions with free negative charge or Pb^{2+} ions with positive charge. As a consequence, passivating these imperfection with Lewis acids or Lewis bases has proven to be a successful technique.[33]

Functionalization via Lewis bases is particularly used, mainly because of the wide range of molecules which are compatible with the passivation of Pb^{2+}.[178–183] For instance good Lewis bases are molecules with functional groups containing nitrogen or sulphur, but also oxygen or phosphorus, since they all possess a lone pair of electrons to share with the Pb^{2+} ions. This approach was first introduced in the PSCs field by Noel *et al.*,[178] who treated the perovskite surface with thiophene and pyridine, and further developed with derivatives of these molecules.[184,185] A molecule that showed to be particularly

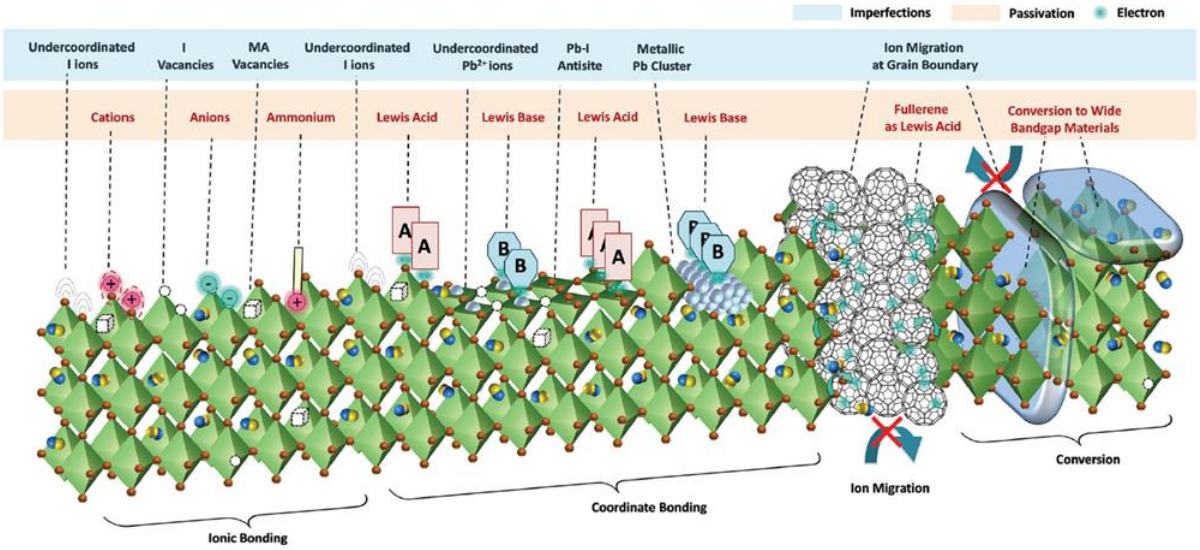

Figure 3.4. Different kind of imperfections in the perovskite layer and possible passivation techniques. Reproduced from Chen *et al.*, Chem. Soc. Rev. 48 (2019). Copyright © Royal Society of Chemistry 2019.

successful in reducing recombination is trioctylphosphine oxide (TOPO),[186–188] which highlights the positive effect of passivation with oxygen and phosphorus, although the application of this specific molecule in devices might not be ideal because of the long insulating aliphatic chains.

Lewis acids are instead employed for the passivation of halide ions. However, in the case of perovskite functionalization, it would be more correct to talk about molecules that *behave* like Lewis acids. Indeed, the interaction is not due to the presence of an empty orbital, but to the electron accepting capability of these molecules because of their specific features. For example, commonly used and very effective "Lewis acids" are fullerenes, which attract electron density from the halide ions thanks to particular aromatic properties related to their spherical shape.[189] Another example is given by molecules capable of halogen bonding, which possess a narrow area of positive electrostatic potential that can interact with the halide ions on the perovskite surface. This kind of bond is particularly important for this dissertation, therefore it will be described in detail in the next section.

3.3.2 Halogen Bonding

Halogen bonding (XB) is a kind of non-covalent interaction that is gaining more and more interest in the scientific community and it is particularly useful to construct supramolecular assemblies. The first XB complexes were prepared already a couple of centuries ago,[190] but it took decades of research to reach a good understanding of the nature of this interaction and even more to unify and rationalize all the findings.[191] Finally, a consensus was reached in 2013 leading to an official IUPAC definition: "*A halogen bond occurs when there is evidence of a net attractive interaction between an electrophilic region associated with a halogen atom in a molecular entity and a nucleophilic region in another, or the same, molecular entity*".[192]

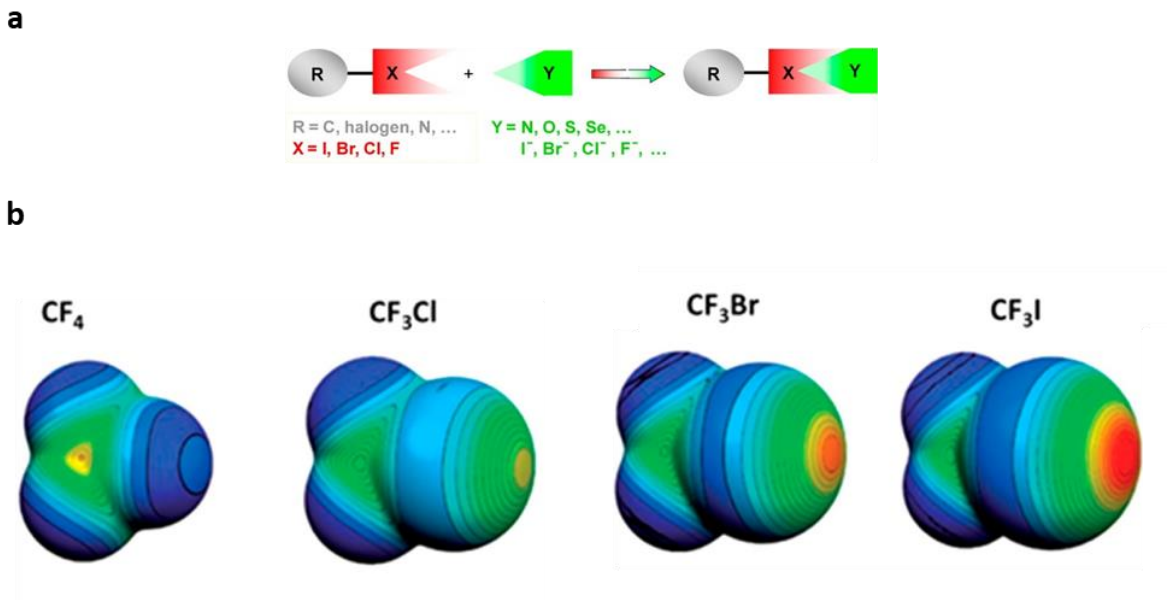

Figure 3.5. (a) Schematic representation of halogen bond (XB), where X is the electrophilic region and Y the nucleophilic region. (b) Electrostatic potential distribution for XB donors with different halogens, blue and red are areas of negative and positive potential respectively (specifically the colour ranges are: red, greater than 27 kcal/mol; yellow, between 20 and 14 kcal/mol; green, between 12 and 6 kcal/mol; blue, negative). Reproduced from Cavallo *et al.*, Chem. Rev. 116 (2016). Copyright © 2016 American Chemical Society.

Before discussing the application of XB as functionalization strategy, it is useful to describe characteristics and properties of this interaction in order to clarify its advantages.

Definition and properties

Halogens are highly electronegative atoms, thus they are considered sites of high electron density. This allow them to form attractive interactions as electron donors (nucleophiles). However, when an halogen (X) is covalently bonded to another or more atoms (R) the electron density distribute anisotropically: the more negative electron density due to the three pairs of unshared electrons form a belt around the central part of X and orthogonal to the bond, while the outermost region of X possesses lower electron density and is named *σ-hole*.[193,194] This region can form attractive interactions with electron-rich sites, therefore bonded X atoms act as electrophiles. The situation is schematized in Figure 3.5a, where R—X is a molecule with a halogen atom X (electrophile) and Y is an electron-rich entity (nucleophile). The σ-hole is centred on the R—X axis and it corresponds to the yellow/red areas (areas of positive potential) in Figure 3.5b. The intensity of the attraction depends on the electronegativity and polarizability of the X atom, specifically it increases with polarizability and decreases with the electronegativity, therefore it scales with the order Cl < Br < I. Generally, F, despite being an halogen, is not considered an XB donor as it does not form a σ-hole. It's interactions with electron rich entities possess slightly different features and are generally referred to as *fluorine bonds*.[195]

Qualitatively XB is similar to the well-known hydrogen bond (HB), however it is more selective and directional. In general, XB possesses the following features: directionality, strength tunability, hydrophobicity and donor atom dimensions.[196,197]

Directionality

Directionality is directly related to the position and size of the σ-hole. This region is indeed narrow and confined on the elongation of the R—X covalent bond (see Figure 3.5b). Therefore, the area of interaction is very limited and, when upon interaction the nucleophile Y enters the σ-hole, the R—X···Y bond is forcibly around 180°. The directionality also depends on the strength of the bond: short and strong bonds are more directional than long and weak ones. In general the bond angle decreases with reduction of polarizability, for example for C—X···N systems it is around 170° if X is I and 155° if X is Cl.[196] Directionality is one of the most important features of XB, indeed it promotes the formation of ordered and homogeneous molecular layers.

Strength tunability

The XB interaction strength depends on the different character of the σ-hole, i.e. on the XB donor and its features. In general, it increases with the polarizability of the X atom and the electron withdrawing ability of the moiety it is connected to, thus the bond strength follow the Cl < Br < I order. This is clearly visible in Figure 3.5b, where the compound with I has the strongest positive electrostatic potential, highlighting a well-defined σ-hole. Therefore, one strategy to tune the XB strength is changing the X atom. Another way to affect the σ-hole magnitude and thus the bond strength is to modify the hybridization of the C atom bound to the XB donor: the electron withdrawing ability increases with the s component is sp-hybridized orbitals, therefore the bond strength depends on the hybridization according to the order [C(sp)—X] > [C(sp^2)—X] > [C(sp^3)—X].[198] In general, any modification of the electron withdrawing ability of R will affect the bond strength, which therefore can be tuned by choosing moieties with desired characteristics. For example, the partial or total substitution of H with F in aromatic rings is a common method to increase the electron withdrawing ability and thus obtain a highly positive σ-hole.[199]

To summarize, the XB strength can be tuned by (i) single atom mutation, (ii) changing the sp-hybridization of the C atom bound to the XB donor and (iii) modifying the electron withdrawing ability of the moiety X is bonded to. This feature makes of XB a particularly versatile tool, moreover the strength of the bond is high compared to other non-covalent interactions.

Hydrophobicity

The presence of X atoms lead to hydrophobicity and lipophilicity in molecules, especially in case of perfluorocarbons compounds. This is very relevant in terms of applications, for example lipophilicity is particularly important in drug design since it controls the transport and absorption of the drug.[200] On the other hand, and more relevant to this dissertation, the hydrophobic nature of molecules with XB ability allows the formation of layers that can also protect the material they are deposited on from possibly degrading factors such as moisture.

Donor atom dimension

Halogen atoms possess bigger Van der Waals radii than hydrogen (1.47, 1.75, 1.85 and 1.98 Å for F, Cl, Br and I respectively compared to 1.20 Å for H). For this reason XB is more sensitive to steric hindrance, which can affect the stability of a system,[201] therefore this feature can be exploited to promote stable bonds.

These properties of XB are now well known and they have been thoroughly characterized.[196] The σ-hole concept is commonly used and it can mostly explain the behaviour and properties of halogens as electrophiles. However, there is a longstanding debate on the nature of XB, for which theoretical investigations play a major role.[202] Initially, the attractive interaction was ascribed to charge transfer phenomena, particularly in studies employing strong XB donors where there was a net electron density transfer.[203,204] Later on, electrostatic attraction became the predominant interpretation because of the analogies between XB and HB.[205,206] In reality, the answer likely sits in the middle and the interaction is the results of a combination of different elements. For example, a decomposition of the interaction energy was possible thanks to a method based on symmetry-adapted perturbation theory (SAPT) and density functional theory (DFT): the results revealed a mixed electrostatic-dispersion energy for XB complexes.[207] Overall, it is likely that XB attractive interaction is due to several different components, of which the dominant one might depend on the system, the interacting partners and the environment.[202]

Applications

Thanks to the above described properties XB has been widely exploited in the field of functional materials and crystal engineering.[208] For example hydrophobicity proved useful for aiding the transport of small ions,[209] while thanks to the large size of halogen atoms it was possible to design efficient all-inorganic light-emitting crystals[210] and the tunability allowed the study of light-responsive polymers.[211]

In the field of PSCs, XB can be particularly useful for the formation of ordered interlayers. Indeed XB donors can interact with the iodide ions present on the perovskite surface. Thanks to the directionality and strength of the XB interaction, the resulting layer will be ordered and homogenous, promoting a neat interface and adjusting the material structure.

Halogen bonding started to attract attention in the PSCs field a few years ago, after Abate *et al.* functionalized the perovskite surface with an XB donor, iodopentafluorobenzene (IPFB), promoting charge transfer and reducing recombination thanks to the screening effect of the molecule on the charge of the iodide ions.[212] These results inspired Zhang *et al.* to study the effect of this molecule and XB functionalization in PSCs from a theoretical point of view.[213] Their work clearly shows that IPFB preferably bind to the I^- ions on the surface, where it resides stably and it reduces charge trapping. Moreover, the calculations reveal that the relative position of the perovskite atoms is modified upon adsorption, improving the material structure. An experimental evidence of the improvement in crystallization in presence of XB is provided by Bi *et al.*[214], where XB donors are used as additives to

the perovskite solution. The presence of XB interactions lead to improved crystallinity and enhanced stability in devices. In PSCs the improvement in stability is generally accompanied by an increase in V_{oc} when XB donors are used as interlayers.[215,216]

Because of its features, it is particularly challenging to experimentally identify XB in solid state materials and especially in perovskite. Several techniques, including vibrational spectroscopy and UV-Vis, have been reported for the detection of XB in solution,[217] however the data interpretation is difficult and it can lead to misinterpretations. The most widely used technique to measure XB is nuclear magnetic resonance (NMR), both in solid state and solution, monitoring mainly ^{13}C and ^{19}F chemical shifts.[216,218] In particular, Ruiz-Preciado *et al*. performed a thorough investigation of 1,2,4,5-tetrafluoro-3,6-diiodobenzene on perovskite using the more versatile 2D NMR.[216] NMR can be an effective technique to detect XB, however a careful sample preparation is necessary, for example by functionalizing nanoparticles of perovskite. Considering the challenges of experimentally determining XB, the measurements are often accompanied or substituted by density functional theory (DFT) simulations[215,216] or first principle studies.[213]

The application of XB in PSCs is still relatively new and it is possible to find only a few related works. Nevertheless, it is possible to identify some common and reproducible advantages among these studies. Specifically, the presence of XB donors, either as additives or interlayers, seems to lead to an improvement in the crystal structure, together with enhanced V_{oc} and stability in devices. These results make of XB a particularly promising interaction for the improvement of PSCs and it is likely that its use will soon spread in the field.

3.3.3 Self-assembled monolayers

Self-assembled monolayers (SAMs) are a particularly interesting case among the different interface engineering techniques.[219,220] A SAM is defined as a molecular assembly that spontaneously form on a substrate by adsorption. It is typically composed of an anchoring group, a linker and a functional group. Thanks to the anchoring group, the molecules interact with the surface and assume an ordered distribution, which is one of the advantages of using SAMs for functionalization. The linker is generally an aliphatic chain and controls the supramolecular structure via Van der Waals interactions. The functional group plays also an important role since it has the capability of changing the surface properties. These kinds of layers can be deposited through different techniques.[219] Among the most common we can identify (i) liquid-phase deposition, where the substrates are immersed in a solution of the molecule to deposit, (ii) spin coating, where the film is deposited exploiting centrifugal force, and (iii) vapor deposition, in which the substrate is exposed to an environment saturated with the molecule.

In the PSCs field, SAMs are mainly used on top of the metal oxide layer, because the smooth surface makes the formation of an ordered layer easy and effective.[221–224] The roughness of the perovskite poses some challenges in this regard, however it is still possible to achieve the formation of SAMs on the perovskite layer and it has been proven to be beneficial for devices.[168,215] Thanks to the different kind of dangling bonds, the perovskite surface is indeed a good platform for the formation of SAMs with different features and the above described functionalization strategies can all potentially lead to the formation of SAMs. Nevertheless, the characterization of monolayers in perovskite remains challenging and it requires sophisticated techniques, for example x-rays reflectometry or transmission electron and scanning electron microscopy.

It is also important to point out that it seems like SAMs formed via XB functionalize the surface but do not "passivate" it, at least not with the characteristics that this term generally imply, i.e. they do not change the optoelectronic properties of the perovskite.[215,216] It has been proposed that in presence of an interfacial dipole, which is also present in case of XB, the passivation effect is given by the anchored molecules that electrostatically screen the charge from the ions they are interacting with.[212,225]

Overall, SAMs are particularly interesting because of their stability and ordered distribution. They can reduce the non-radiative recombination by binding to the surface defects, but also positively affect morphology and crystal structure.[226,227] Moreover, SAMs can form dipole moments at the interface, thus affecting the energy level alignment.[168,228,229]

3.3.4 Dipolar molecules and their effect on energy level alignment

The presence of dipolar molecules at an interface can deeply affect its electronic properties and it is therefore a useful tool for tuning ELA and charge transfer in devices.[230] As represented in Figure 3.6a, an interfacial dipole layer creates an abrupt drop in electrostatic potential from the negative charge to the positive charge side. The vacuum level (E_{VAC}) is therefore shifted, changing the energetics (i.e. WF, IE and EA) of the material at the interface. Specifically E_{VAC} will shift upwards, leading to higher WF, if the dipole points to the surface of the functionalized material (with the dipole defined as from negative to positive). While E_{VAC} will shift downwards, leading to lower WF, if the dipole points towards outside.[229,231] The shift is proportional to the dipole moment per area and, in an ideal case, can be expressed by the following formula:[232]

$$\Delta E_{VAC} = -\frac{q_e \mu}{\varepsilon_0 \varepsilon_{eff} A} \qquad 3.3$$

Where q_e is the charge on an electron, μ the dipole moment of an isolated molecule, A is the area, ε_0 the vacuum permittivity and ε_{eff} is the effective dielectric constant introduced for compensating the

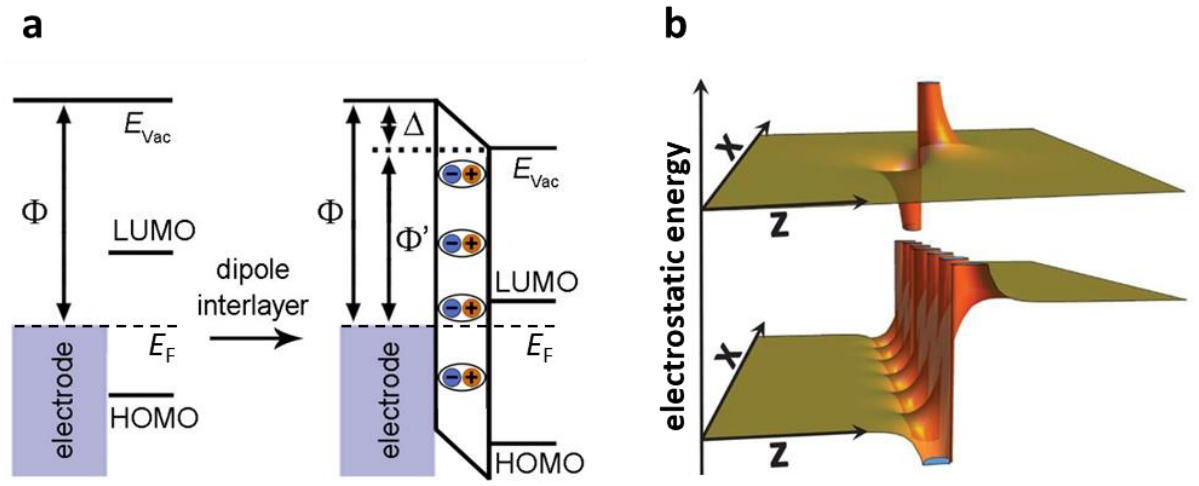

Figure 3.6. (a) Representation of the vacuum level (E_{Vac}) shift induced by the insertion of a dipolar layer at the interface between an electrode and a semiconductor. E_F is the Fermi level, Φ is the work function, Δ is the E_{Vac} step. Adapted from Chen *et al*., Am. Chem. Soc. 43 (2020). Copyright © 2020 American Chemical Society. (b) Change in electrostatic energy induce by a point dipole (top) and a compact array of dipoles (bottom). Adapted from Zojer *et al*., Adv. Mat. Int. 6 (2019). Copyright © 2019 Wiley.

effect of depolarization, i.e. the reduction of the net dipole of a molecule due to the electric field originating from the surrounding molecules.

As a consequence the WF also shift linearly with the dipole, indeed, in presence of a dipolar layer and ignoring an eventual band bending, the interfacial WF (WF^I) is given by:

$$WF^I = WF_{sub} + \Delta E_{Vac} \qquad 3.4$$

However, when talking about interfacial dipole due to surface functionalization with specific molecules[6], we have to consider that the net dipole is given by different components. Specifically, we have to take into account the intrinsic dipole of the molecules and the dipole related to the interaction.[233,234] The total dipole is simply given by the sum of the different components. The intrinsic dipole of a molecule is generally known or it can be fairly easily calculated. It can also be tuned by adding moieties or substituting part of the molecule, for example aromatic rings can increase polarizability. On the other hand, the interaction part is not trivial to determine, as different factors comes into play and contribute to a charge exchange phenomena. For example, there is a repulsion between the electron clouds of substrate and adsorbed molecule, generally referred to as *Pauli pushback*. Moreover, in case of covalent bond, a charge rearrangement takes place, while for coordinate bonding the hybrid orbitals are strongly localized either at the molecule or at the substrate and a net fractional number of electrons is transferred.[232,234]

Other important considerations to make related to the actual E_{VAC} shift caused by dipolar layers regard the orientation of the molecules and their packing. First of all, it is important to remember that only

[6] Interfacial dipoles are also formed naturally, for example because of charged defects or charge accumulation.[43] However, this is beyond the scope of this section, which focuses on surface functionalization via molecules and the effect of such treatments.

the part of the dipole which is perpendicular to the surface contribute to the shift. Therefore, μ in equation 3.3 is actually better expressed as:

$$\mu = \mu_0 \cos\theta \qquad 3.5$$

Where μ_0 is the intrinsic dipole and θ is the angle between the molecular axis and the surface (i.e. θ = 0° means perpendicular orientation). As a consequence, a strong intrinsic dipole does not always results in a strong WF shift. This also directly relate to the second consideration: the packing of the layer and the coverage play an important role in determining the effective change in energetics.[232–234] As visible in Figure 3.6b (top), if we consider a single point dipole the electrostatic potential is strongly perturbed in the vicinity of the molecule, but the effect fades away rapidly and it is not relevant on a bigger scale. The situation is different, instead, in presence of a packed array of dipoles (Figure 3.6b – bottom): in this case there is a superposition of the potential of the different molecules, which results in a definite step in electrostatic potential, i.e. different E_{VAC} left and right of the molecules layer. Therefore, an ordered and compact layer of molecules stacked perpendicularly to the surface is fundamental for obtaining the maximum E_{VAC} shift. Moreover, a compact layer allows the molecules to maintain more easily an up-right position and thus having a bigger part of their dipole contributing to the total shift. Although the effect of a compact dipolar layer will be eventually limited by the depolarization due to the dipole-dipole interaction.[235,236]

The discussion so far assumed ideal infinite layers, which is obviously different from actual cases, where for example there will likely be potential "leaks" due to defective layers and inhomogeneities. Moreover, it is particularly challenging to characterize the actual energetics shift induced by the dipoles. Energy levels characterization is generally performed through surface sensitive techniques, thus measuring directly on the functionalized substrates. However, in devices other layers will be deposited on top and a possible interaction with the subsequent layer can change the overall effect of the dipoles. Directly measuring the real interface within the device is difficult because it is now buried, nevertheless there are some approaches that allow such an investigation, for example delamination of the top layers or cross sectional measurements via KPFM.[237,238] These specifics sample preparation techniques are, however, particularly invasive, thus the characterization might not be accurate.

4 METHODS

This chapter presents the most relevant preparation and characterization methods used for the experiments described in the next chapters. In particular, the preparation of samples and devices will be presented, together with their performance, energetic and optical characterization. The purpose is to give a general overview of the processes and a qualitative idea of the working principles and possible characterizations with the different techniques. For a more detailed description of the specific measurements the reader is referred to the Appendix.

4.1 Samples and devices preparation

The films for either samples characterization or devices preparation were prepared through solution-based processes, with the exception of the deposition of the metal contact in devices (Au), which was thermally evaporated on the substrates.

The general layout of the devices corresponds to that described in section 2.6.2 for the n-i-p architecture. Specifically, TiO_2 was used as ETL. First a compact layer was deposited on FTO through spray-pyrolysis,[239] followed by a mesoporous layer, spin-coated and annealed. Doped 2,2',7,7'-Tetrakis[N,N-di(4-methoxyphenyl)amino]-9,9'-spirobifluorene (spiro-OMeTAD) was spin-coated on top of the perovskite layer as HTL, except in Chapter 7, where two novel HTMs are introduced. Finally, Au was evaporated as top contact. For the optical characterization via ultraviolet-visible spectroscopy (UV-Vis) and photoluminescence spectroscopy (PL) the perovskite films and the other layers of interest were directly deposited on glass. The energetic characterization, instead, requires a conductive substrates, thus the films were either deposited on ITO or prepared as devices up to the required layer. All the steps were performed in N_2 filled gloveboxes, except for the ETL deposition.

The perovskite film was prepared through the standard spin-coating one step process with anti-solvent treatment[101] and annealed for 30 min or 1h depending on the composition. The perovskite mainly used for the experiments in this dissertation was the so-called “triple cation”, with composition $Cs_{0.05}(FA_{0.85}MA_{0.15})_{0.95}Pb(I_{0.85}Br_{0.15})_3$, except for Chapter 6, where also $MAPbBr_3$ was employed. The two compositions required different spin-coating programs and anti-solvent drop moments.

Additional molecular assemblies were employed in this dissertation with the aim of functionalizing the perovskite surface. These molecules were deposited as monolayers between the perovskite and the subsequent layer. Special deposition techniques are required in order to obtain such monolayers and thus will be described in details in the following subsection.

All samples and devices analysed in this dissertation were prepared by the author.

4.1.1 SAMs deposition

Chapters 5 and Chapter 6 discuss the tuning of the perovskite energetics through SAMs of dipolar molecules. Among the different techniques for obtaining such layers mentioned in Section 3.3.3, it has been chosen to use liquid-phase deposition. For this purpose, specific beakers able to vertically hold several substrates were employed. Moreover, the beakers could also be sealed with a cap in order to avoid solvent evaporation during the deposition. The perovskite coated samples were placed in the beakers right after the annealing step, paying attention not to expose the films to air. This is of utmost importance for the purpose of functionalizing perovskite, indeed air can interact with the surface through the dangling bonds and thus cancelling or at least affecting the outcome of the SAM deposition. The beakers with the samples were then filled with a solution of the molecule to be deposited and let rest in the dark for a defined period of time (generally 20 min), after which the samples were extracted one by one and rinsed with the solvent in order to wash away eventual agglomerates and residuals.

Through this technique it is possible to achieve ordered monolayers of molecules, although in the case of perovskite it is challenging to obtain direct experimental evidence of the characteristic of the layer. Indeed the roughness of the surface poses a problem for the detection of such thin films, and it is necessary to rely on indirect characterization.

Another possibility is the direct spin coating of the molecules solution with appropriate concentration and spinning speed. However, by comparing samples prepared with these two methods, it seems like the former gives more reproducible and stable results. This is probably because dipping the substrates in the solution allows for a slow deposition, where the molecules orderly bind to the perovskite's undercoordinated ions, thus forming a more homogeneous layer.

In light of this, the "dipping method" has been the technique of choice for the experiments discussed in this dissertation, with the exception of the second part of Chapter 6, i.e. the deposition of urea on $MAPbBr_3$. In that case the molecules were deposited through spin-coating. The choice was due to the difficulty of finding a solvent dissolving urea but not the perovskite layer (important requirement for

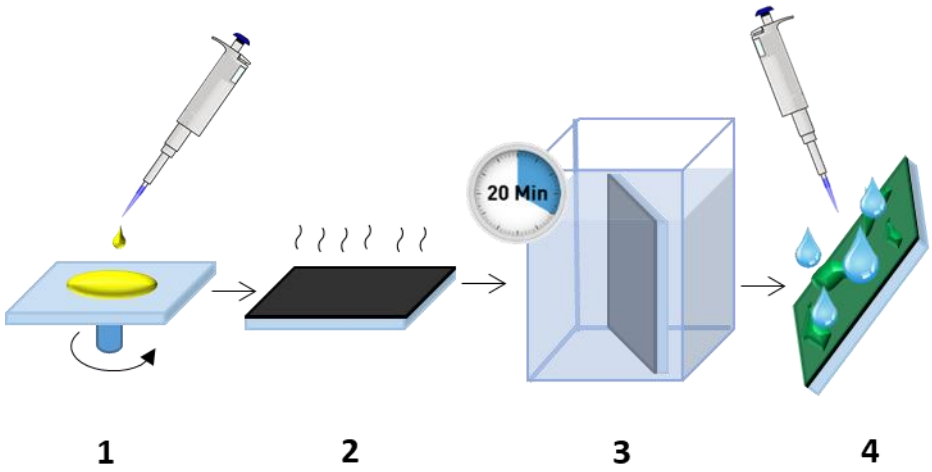

Figure 4.1. Description of the procedure for SAM deposition via "dipping method": the perovskite is spin coated (1) and annealed (2), then the substrate is dipped for 20 min in a solution of the desired molecule at a specific concentration (3) and finally rinsed with the solvent for removing agglomerates and residues (4).

the dipping method). In this case, a technique like spin-coating allows the solvent and the perovskite to be in contact for just a short period of time, allowing the deposition to happen with a limited damage to the surface.

4.2 Devices characterization

As mentioned in Section 2.5, the most common way to characterize the behaviour of solar cells is through the analysis of the JV curve. In most of the cases JV curves are not recorded under real sun, but using devices able to simulate the AM1.5 solar spectrum. This allows to compare the results among different labs and to obtain measurements independent from the location and weather conditions. The sun simulator used in this dissertation was a Wavelabs Sinus-70 LED class AAA. The light intensity was calibrated with a Silicon reference cell from Fraunhofer ISE and JV scans were performed in air with a Keithley 2400 SMU, controlled by a measurement control program written in LabView. The sample holder was also connected to a so-called pixel switch allowing the individual measurement of up to six solar cells (pixels) on the same sample.

The routine measurements consists of a first JV scan in light, followed by MPP-tracking of the best pixel, JV scan in dark and finally a second JV scan in light in order to check for possible light soaking effect.[240] The MPP-tracking is particularly important because it records the power output variation over a certain amount of time, thus giving a stabilized efficiency. This is more reliable than the PCE from the JV scan, which can be affected by transient phenomena, like ion migration. The technique used to measure MPP-tracking is called "perturb and observe" method[241] and consist in applying a certain voltage based on the previous JV scan, then increasing/decreasing this voltage by a small value: if the power output increases than the voltage will be increased/decreased again, otherwise it will

change to the opposite direction. Typically at least 120 s of MPP-tracking are advisable to obtain a reliable stabilized power output, but it depends on the device characteristics and can vary from case to case.[242]

MPP-tracking is also important because it helps evaluating the operational stability of the device. This can be assessed through specific systems, generally called "ageing setups", which perform MPP-tracking for long periods of time.[243] In addition to the MPP-tracking these instruments can also control the atmosphere (for example switching between air and N_2) and the temperature. Moreover, it is possible to filter out some parts of the solar spectrum, for example UV-light is detrimental for TiO_2 and if not filtered could "hide" the degradation mechanism of interest coming from other layers. Although the addition of a UV-blocking filter can lower the irradiance to approximately 800 W/m^2 because of the UV cut-off and the diffusion properties of the filter. Assessing the operational stability of devices is particularly in the prospect of real-world applications.

The stability measurement showed in Chapter 7 were measured in N_2 atmosphere and with UV-blocking filter in a custom-built high-throughput ageing setup.

The devices characterization was performed by the author, except for the ageing measurements.

4.3 Optical characterization

Optical characterization can give important information about the material quality, losses and electronic properties, for example it is possible to infer the recombination mechanisms and dynamics or the absorbed light and bandgap. Moreover, optical characterization techniques are not destructive. The next subsections will describe two of the main optical characterization methods that have been employed in the experiments of this dissertation: ultraviolet-visible (UV-Vis) and photoluminescence (PL) spectroscopies. These two techniques are complementary, indeed UV-Vis is based on the transition from ground state to excited state (absorption), while PL analyses the transition from excited state to ground state (photoluminescence). A comprehensive description of techniques for the perovskite characterization is given by a book edited by Pazoki, Hagfeldt and Edvinsson, but with contributions from many experts of the field, and it includes also optical characterization.[244]

4.3.1 UV-Vis spectroscopy

In UV-Vis spectroscopy the light absorption of the sample is recorded for different wavelengths (λ), from ultraviolet to the visible range and sometimes to the near infrared (UV-Vis-NIR in this case). When light is shone on the sample, part of it is absorbed and the rest is either reflected or transmitted. The absorption is given by the Beer-Lambert law:[245]

$$A = \log_{10}\left(\frac{I}{I_0}\right) \quad 4.1$$

where A is the absorbance, I_0 is the intensity of the incident light and I is the transmitted or reflected intensity. When measuring the transmitted light, I/I_0 is the *transmittance* (*T*) and is generally given in %. When measuring the reflected, light I/I_0 is the *reflectance* (*R*) and it represents the light reflected from the sample in comparison to the light reflected from a reference sample (that gives I_0). Perovskite samples show significant reflection and scattering due to the polycrystalline nature of the material and this can lead to distorted results. In order to account for all reflected and scattered light it is thus advisable to use an integrating sphere.

From UV-Vis measurements it is also possible to calculate the bandgap E_G. A rough estimation can be done by looking at the wavelength corresponding to the slope in transmission measurements and to the peak in reflection measurements. Indeed Planck's Law says:

$$E = \frac{hc}{\lambda} \quad 4.2$$

with *h* being the Planck's constant, *c* the speed of light and *λ* the wavelength. *E* in this case corresponds to the bandgap energy. However, it is more precise to estimate E_G from the so-called *Tauc's plot*.

This method requires the calculation of the *absorption coefficient α* from the absorbance data according to the formula:[246]

$$\alpha = \frac{2.303\ A}{d} \quad 4.3$$

with *A* the absorbance an *d* the sample thickness. The absorption coefficient is also given by the following expression:

$$\alpha = \frac{A\left(h\nu - E_g\right)^n}{h\nu} \quad 4.4$$

$$(\alpha h\nu)^{1/n} = A^{1/n}\, h\nu - A^{1/n}\, E_g \qquad 4.5$$

Where $n = ½$ for direct bandgap semiconductors. Therefore it is possible to obtain E_G from the intercept of the fit of the linear part of the slope obtained by plotting $(\alpha h\nu)^{1/n}$ against $h\nu$.

In this dissertation UV-Vis measurements, both in reflection and transmission mode, were used in Chapter 7 to evaluate the degradation of the materials upon solvent exposure. The setups used were a Perkin Elmer LAMBDA 1050 UV-VIS spectrometer for the reflectance measurement and a Cary 5000 UV-Vis-NIR spectrophotometer for the transmission measurement. The measurements were performed by collaborators with the assistance of the author.

4.3.2 Photoluminescence spectroscopy

When a material is illuminated with light, it absorbs the photons with energy bigger than its bandgap. Thanks to this energy electrons are excited from the VBM to the CBM and, if they are not extracted or if they do not recombine non-radiatively, they will radiatively recombine with a hole and emit a photon. This phenomenon is called photoluminescence (PL) and the re-emitted photons for the different wavelengths create the PL spectrum. Like for UV-Vis measurements, an integrating sphere is generally used to collect the emitted photons. According to Equation 4.2, the λ of the peak in the PL spectrum correspond to E_G.

The ratio between the emitted and absorbed photons (Φ_E and Φ_A respectively) define the PL quantum yield (PLQY) and it is a measure of the recombination in the material. Indeed the PLQY can be expressed in terms of recombination current as follow:

$$PLQY = \frac{\phi_E}{\phi_A} = \frac{J_{rad}}{J_G} = \frac{J_{rad}}{J_R} = \frac{J_{rad}}{J_{rad} + J_{non-rad}} \qquad 4.6$$

where J_G is the generation current and J_R is the total recombination current expressed as combination of radiative (J_{rad}) and non-radiative ($J_{non\text{-}rad}$) recombination currents. At V_{oc} there is no net current flowing and thus $J_G = J_R$. Therefore the higher the PLQY the lower the non-radiative component is. As described in Section 3.1.1, non-radiative recombination is caused by defects with deep energy that trap the charges and thus prevent them from recombining radiatively. High PLQY, so low non-radiative recombination, is sign of a good quality material with a low density of deep traps. More information regarding the evaluation of charge recombination and charge collection can be obtained through time resolved PL measurements (TRPL), which monitor the emission of the material over time after a short laser pulse.

From the PLQY it is also possible to calculate the QFLS. Indeed the QFLS can be expressed as:[35]

$$QFLS = QFLS_{rad} + K_B T \cdot \ln(PLQY) \quad 4.7$$

where $QFLS_{rad}$ is the radiative limit for the QFLS of the material. This sets the maximum V_{oc} achievable and corresponds to the situation of PLQY = 1, i.e. zero non-radiative recombination. This is a very useful relation, since it allows to explore the relationship between V_{oc} and QFLS.

Overall, PL measurements contain much useful information. Here the description has been limited to the analysis directly employed in this dissertation, where PL has been mainly used for the derivation of the QFLS and for monitoring the recombination processes (Chapter 7). The measurements were performed by collaborators.

4.4 Energetic characterization

As discussed in Section 3.2.2, the accurate determination of the energy levels of a semiconductor, and particularly of perovskite, is not an easy task. Techniques used for this purpose are surface sensitive methods such as photoemission spectroscopy (PES), Kelvin probe (KP), Kelvin probe force microscopy (KPFM) and cyclic voltammetry (CV). The most widely used PES techniques for energetic characterization are ultra-violet photoemission spectroscopy (UPS) and inverse photo-emission spectroscopy (IPES).[247] The former is based on the measurement of the kinetic energy of electrons emitted from the material upon absorption of UV light and it can determine the ionization energy and WF. The latter consist in directing a collimated electron beam at the sample and measure the emitted photons giving the energetic position of the CBM. The two methods are complementary and together allow a detailed and complete analysis of the energetics of the material, however they generally require ultra-high vacuum conditions, which is not optimal for analysis involving molecular monolayers, as in the case of this dissertation. Therefore the energetic characterization for the experiments described in the next chapters has been conducted through less invasive techniques, in particular KP, KPFM, CV and ambient pressure PES (APS), which will be introduced in this section.

4.4.1 Kelvin probe

The KP method[248] measures the difference in WF between two materials forming the two sides of a parallel plate capacitor. The KP working principle in the case of two different metals is schematically

represented in Figure 4.2. Specifically, Figure 4.2a shows the two materials when still separated: they are electrically neutral and the E_{VAC} is common. When connected through an external circuit (Figure 4.2b), the charges will flow from the material with lower WF to the one with higher until equilibrium is reached and E_F is aligned.

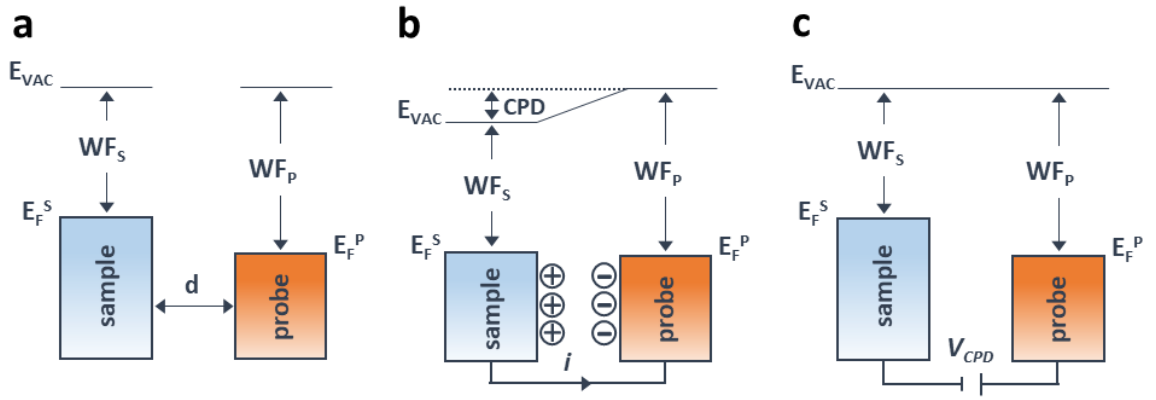

Figure 4.2. Representation of the working principle of the Kelvin probe. (a) Electronic energy levels of sample and probe before contact. E_F^S and E_F^P are the Fermi levels of sample and probe, WF_S and WF_P are the respective work functions, E_{VAC} is the local vacuum level and d is the distance between the materials. (b) After sample and probe are short-circuited a current *i* flows from the sample (lower WF) to the probe (higher WF) until equilibrium ($E_F^S = E_F^P$). An electric field, i.e. a drop in E_{VAC}, is present in the gap due to the accumulation of charges and it is called contact potential difference (CPD). (c) An external bias equal and opposite to the CPD is applied and cancels out the potential difference.

As a result an electric filed is present in the gap between the materials causing a drop in E_{VAC}, which is referred to as contact potential difference (CPD) and it corresponds to the difference between the WFs of the metals. The value of the CPD would be easy to calculate if capacitance C and stored charge Q were known, indeed for parallel plate capacitors Q = C·V, where V in our case is the CPD. However, the precise value of Q is difficult to estimate. The problem of the determination of the CPD was solved by Lord Kelvin,[249] who proposed to apply an external bias (V_{CPD}) to the system (Figure 4.2c). If the applied voltage is equal and opposite to the CPD, then the capacitor is discharged, E_{VAC} is aligned and the difference between the WF of the materials corresponds to V_{CPD}. At this point, considering that WF_P is known, it is straightforward to calculate WF_S, indeed:

$$V_{CPD} = \frac{\Delta_{WF}}{e} = \frac{WF_S - WF_P}{e} \qquad 4.8$$

In practice, V_{CPD} is identified by inducing a periodical vibration to the probe.[250] This way the capacitance between the materials is varied, changing the charge in the capacitor and creating a current flow. When the applied voltage is exactly V_{CPD} the capacitor is discharged and the current flow is zero. Currently the most common technique to induce the probe vibration is to connect the electrode to a piezoelectric ceramic.[251]

It is of course important to ensure that WF_P remains constant during the measurement, for this reason it is common practice to use inert materials as reference, like for example Au. Using a metal probe is also particularly reliable because the WF of metals does not change with light. This feature is

furthermore interesting when measuring a semiconductor. The KP method is indeed also applicable when the sample is a semiconductor and not a metal, as in the exemplary case used for the explanation. The working principle is exactly the same, but the interface possibly presents band bending. Thanks to the inert nature of the probe, it is possible to use KP to measure the variation of the semiconductor's WF with light, since in this case the light-induced WF shift comes only from the semiconductor. The variation of CPD for a semiconductor under illumination is called surface photovoltage (SPV).

KP has been the main tool used in this dissertation for the characterization of the energy levels shifts discussed in Chapter 5, Chapter 6 and Chapter 7. The setup was a custom-built KP consisting of a vibrating gold mesh driven by a piezo electric crystal (Kelvin probe and CPD controller by Besocke Delta Phi). The samples were measured in N_2, but it was necessary to mount them in air, thus a short air exposure was unavoidable. All the measurements with Kelvin probe were performed by the author. In order to obtain more reliable results, most of the relevant measurements were then repeated by collaborators using a KPFM mounted inside a N_2 filled glovebox.

4.4.2 Kelvin probe force microscopy

The Kelvin probe force microscopy (KPFM) is based on the same working principle of the KP method, but it uses a modified version of the atomic force microscope (AFM).[252,253] The AFM can measure the topography of a sample by probing the surface with a conductive tip, whose movement is monitored by studying the optical deflection of a laser shining on the tip itself. The tip is kept vibrating with constant amplitude (or frequency) and this amplitude is affected by any tip-sample interaction. A feedback circuit modifies the tip-surface distance so that the vibration amplitude is kept constant, recording this way the surface morphology. If tip and sample are electrically connected there is a potential between them and the force acting on the tip is defined as:

$$F = -\frac{d}{dz}\left(\frac{1}{2}CV^2\right) = -\frac{V^2}{2}\frac{dC}{dz} \qquad 4.9$$

where C is the capacitance, V the voltage and z the tip-sample distance. Similarly to the KP case, the variation of C is difficult to estimate, but the CPD can be inferred by applying an external voltage. However, in this case the applied voltage will nullify the force in the tip-sample capacitor, instead of the current. In KPFM we have two voltages applied to the tip with two feedback loops: an alternating voltage produces the electrostatic vibrations and a direct voltage compensate the oscillations due to the tip-sample potential difference until the force between them is cancelled out. The two voltages operates at different frequencies, thus topography and electrical characterization can be conducted simultaneously.

4.4.3 Ambient pressure photoemission spectroscopy

Ambient pressure photoemission spectroscopy (APS)[247,254] is a technique that operates similarly to the standard PES methods described in the introduction of this section, but without the need for ultra-high vacuum. APS, like UPS, exploits the photoelectric effect, measuring the number of photoelectrons emitted by the sample upon illumination with a monochromatic UV light. Since photoelectrons are emitted only if the energy of the incident photon is bigger than that of the VBM, it is possible to determine the ionization energy IE by measuring the produced photocurrent and comparing it with the excitation photon energy. In standard PES measurements the ultra-high vacuum enables the collection of the photoelectrons. At ambient pressure, instead, they are scattered by the much bigger O_2, N_2 and H_2O molecules and they cannot reach the detector. To circumvent this problem, in APS the ions created by the scattering of electrons and molecules are recorded, instead of the electrons themselves. Indeed the ions can migrate for a much longer path and reach the detector, which in this case is a positively biased KP tip. The inclusion of a KP probe in the setup is a convenient feature, since it allows the quasi-simultaneous measurement of WF (from KP) and IE (from APS), for this reason this technique is often also called KP-APS.

In this dissertation a KP-APS measurement tool provided by KP Technology Ltd. has been employed in Chapter 5 to show that a dipole induced WF shift also corresponds to a comparable IE shift. The measurements were performed by collaborators.

4.4.4 Cyclic voltammetry

Cyclic voltammetry (CV)[255] is a technique from the electrochemistry field that is often used to estimate the energy levels of a material. It is performed in an electrochemical cell filled with an electrolyte and which includes three electrodes: working, reference and counter electrode (WE, RE and CE respectively). WE is the electrode in which the reaction of interest occurs, therefore it is the material of which the energy levels are to be determined. RE has a stable and well-known potential, and it is thus used as reference. CE is generally made of an inert material and its purpose is to close the circuit with the WE, so that current can flow.

The CV technique consists in linearly scanning the potential of the working electrode between two chosen values, during the voltage sweep a potentiostat measures the current resulting from

electrochemical reactions occurring at the electrode interface. The WE will undergo an oxidation or a reduction reaction depending on the direction of the sweep. In semiconductors, the HOMO level corresponds to the energy necessary to extract an electron from a molecule, thus it is an oxidation reaction. The LUMO level is instead the energy needed to "inject" an electron in a molecule, which is a reduction reaction. Therefore, measuring the redox potentials (reduction and oxidation potential) of the semiconductor and adding the value of the respective redox potentials of RE can give the values of LUMO and HOMO levels.[256]

In Chapter 5, CV has been used to determine the HOMO level of functionalized and bare perovskite, which were the WE. The electrolyte was a 0.1M solution of Bu_4NPF_6 in dichloromethane, a platinum wire was the CE and an Ag/AgCl in saturated KCl was the RE. A partial degradation of the layer was observed during the reverse scan and therefore it was not possible to calculate the LUMO level. The measurements were performed by collaborators.

PART II

RESULTS

5 TUNING HALIDE PEROVSKITE ENERGY LEVELS

This chapter is based on the peer-reviewed article "Canil, L. et al., *Tuning Halide Perovskite Energy Levels*, Energy Environ. Sci., **2021**, 14, 1429-1438".[168]

The ability to control the energy levels in semiconductors is compelling for optoelectronic applications. In this chapter, the energy levels of halide perovskite semiconductors are tuned by using self-assembling monolayers of small molecules to induce stable dipoles at the surface. The direction and intensity of the surface dipoles rely on specific molecule-to-surface interactions. Electron acceptor or donor molecules result in a positive or negative energy level shift up to several hundreds of meV. This approach provides a versatile tool to control the energy levels of halide perovskite and adjust their alignment at the interface with charge transport materials in perovskite-based optoelectronics.

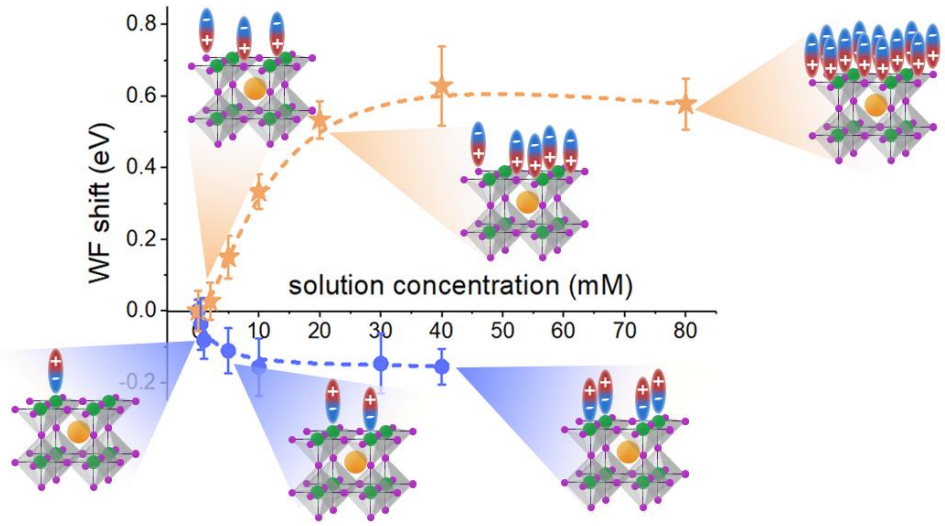

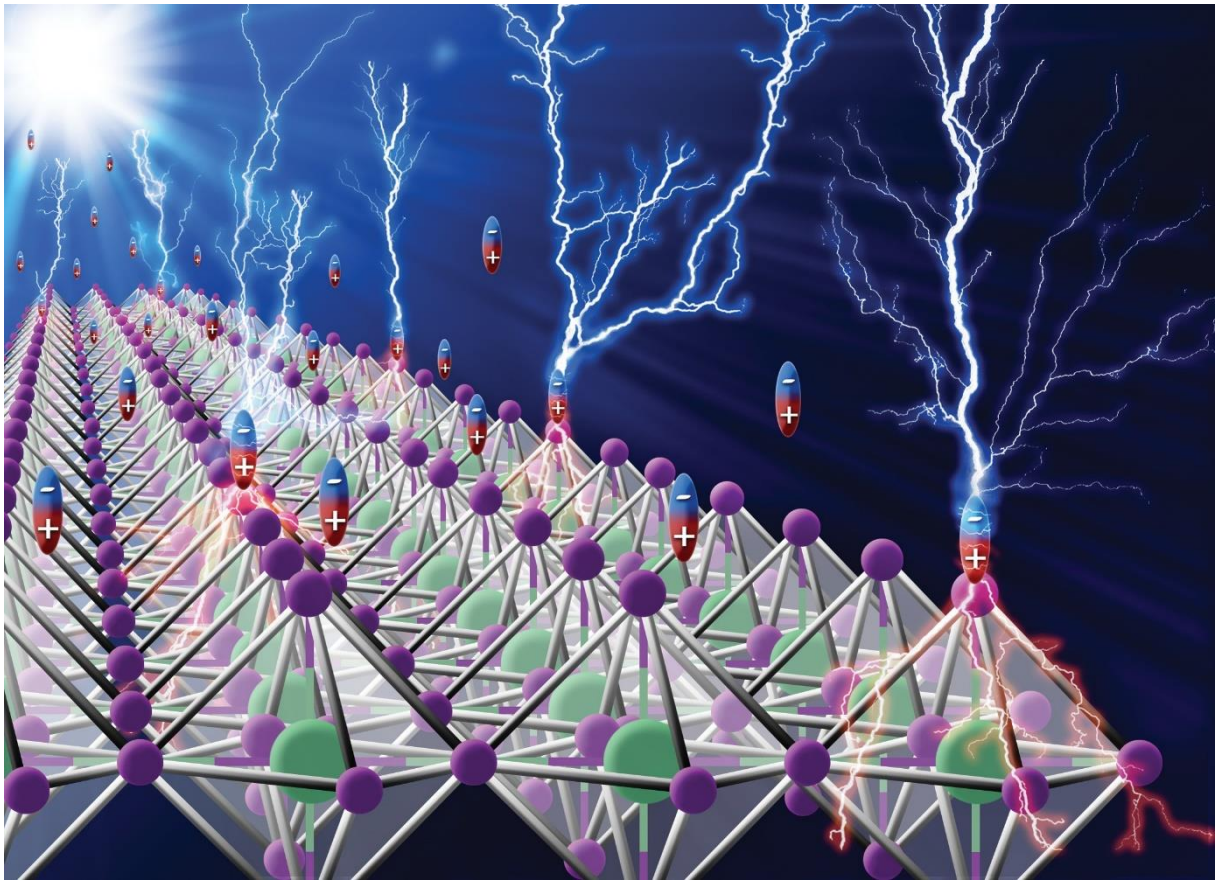

Cover by L. Canil

Showcasing research from Professor Antonio Abate's laboratory, Innovation Lab HySPRINT, Helmholtz-Zentrum Berlin für Materialen und Energie, Berlin, Germany.

Tuning halide perovskite energy levels

Perovskite solar cells are attracting great attention in the field of renewable energies. The possibility of combining different materials and compositions in these devices brings to significant advantages, but it also requires a careful optimization of the interfaces between the materials, including their energy level alignment. In this work, we show how to tune the energy levels of halide perovskite by controlling the deposition of dipolar self-assembled monolayers, providing a toolbox to simplify the application of halide perovskites in optoelectronic devices.

As featured in:

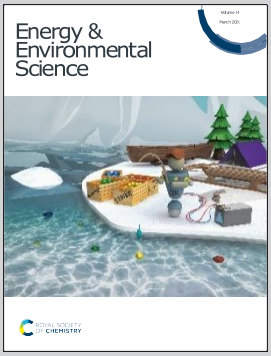

See Antonio Abate *et al.*, *Energy Environ. Sci.*, 2021, 14, 1429

ROYAL SOCIETY OF CHEMISTRY

rsc.li/ees

Registered charity number: 207890

5.1 Introduction

The position of the energy levels of a material is of crucial importance in optoelectronics, from detectors[257] to LEDs[258] to solar cells[140,259], mainly because of the energy level alignment (ELA) at interfaces between different materials comprised in these devices.

As discussed in Section 3.2.1, the ELA of the perovskite at the interface with the other materials comprising the device is essential for the efficiency of the charge separation and thus the PSC's performance. The importance of controlling the interface energetics is furthermore stressed by the high number of related reports that is possible to find in literature, mainly applied to electrode materials or charge selective layers, as shown for example in a helpful review from Kim *et al*.[233].

Probably the most common method for tuning the ELA between two materials is with the introduction of a dipolar interlayer, for example, by functionalizing the surface through specific molecules.[232,260–263] In particular, in the photovoltaic field, this concept has been intensively applied to change the work function (WF) of transparent conductive oxides and with that the position of the oxide Fermi level with regard to the charge transporting levels (CTLs) of the semiconductor on top. For instance, Zhang *et al*.[264] functionalized ZnO with dipolar molecules for organic solar cells. Yang *et al*.[265] inserted an interlayer between TiO_2 and perovskite, improving the charge extraction, similarly to Liu *et al*.[266], who instead modified the interface between SnO_2 and perovskite. A few cases can also be found related to WF tuning of the perovskite layer. Agresti *et al*.[267] engineered the perovskite/hole transport layer (HTL) interface with Titanium-carbide MXenes. At the same time, Wu *et al*.[268] developed a PSC with a moisture-resistant carbon electrode and functionalized the perovskite surface with PEO (poly(ethylene oxide)) to reduce the mismatch of the energy levels at the perovskite/carbon interface. Similarly, Dong *et al*.[269] used conjugated aniline PPEA (3-phenyl-2-propen-1-amine) at the interface between perovskite and PCBM (Phenyl-C61-butyric acid methyl ester), achieving a better ELA and, therefore, performance.

Among the different kinds of interlayers, self-assembled monolayers (SAMs) are of particular interest because of their stability and ordered distribution. Since the work of Campbell *et al*.[228,229], it is known that interfacial SAMs with a dipole can tune the WF of a material by changing the vacuum level position. This technique has been widely used on flat surfaces to, for example, manipulate the Schottky energy barrier between a metal electrode and an organic material.[221,222,270] Lange *et al*.[223] demonstrated that it is possible to use SAMs-modified ZnO as either HTL or ETL (electron transport layer), depending on the dipole of the molecules used for the functionalization, and recently the same group also showed how SAMs surface treatments and UV light soaking could influence the hole

injection properties of thin ZnO films.[224] Kong *et al*.[271], instead, proposed an HTL-free PSC where the energy level mismatch between ITO and perovskite was adjusted by introducing a monolayer to increase the ITO WF. At the same time, Zhang *et al*.[272] functionalized the TiO_2 surface, improving the charge extraction in PSCs.

Functionalizing surfaces with dipolar SAMs is proven to be a reliable and effective method to optimize the ELA. Nevertheless, SAMs have been rarely used directly on the perovskite surface. Controlling the formation of SAMs on halide perovskite films is difficult due to the relatively high surface roughness and uncontrolled surface chemistry. Sadhu *et al*.[273] elucidated, indeed, how molecules can self-assemble on the surface in different ways depending on the substrate and how the interaction influences the surface potential, highlighting the challenges of SAMs deposition on perovskite. There are so far no standard guidelines that would allow researchers to use this method systematically. Therefore, this chapter aims at answering the question: *Is it possible to systematically tune the perovskite energy levels?*

This study shows how to shift the perovskite WF through assemblies of dipolar molecules, and how to control the magnitude of the shift, without using necessarily different molecules. Moreover, it is also demonstrated that the change in WF corresponds to a change in band edges, therefore overall the dipolar molecules induce a shift in all the perovskite energy levels. By controlling the surface coverage through the concentration of the solution used for the deposition, it is possible to obtain an energetic shift up to several hundreds of meV. This finding distinguishes this work from others regarding perovskite energy levels tuning. Indeed, once a molecule with the desired binding mode and dipole direction is selected, this method allows the shifting of the energy levels only by changing the deposition parameters. Additionally, density functional theory (DFT) calculations demonstrate a correlation between surface coverage and energy levels shift, supporting the strategy presented here. The impact of this method on perovskite solar cells (PSCs) will be explored in Chapter 6.

The aim of this chapter is to provide a tool which could allow to directly select which molecule and deposition conditions are needed to obtain a specific energy level shift. This tool would provide more flexibility in the choice of the combination of materials, i.e. perovskite compositions and contact layers, to be used for any perovskite-based optoelectronic device. For example, in PSCs research it would be possible to ease the requirements for HTLs or ETLs, allowing researchers to focus on finding or synthesizing materials with good conductivity and excellent stability rather than a proper ELA.

5.2 How to tune the direction of the energy levels shift

Specific molecule-to-substrate interactions were used to self-assemble small molecules on the perovskite surface.[212,274] The combination of the intrinsic dipole of these molecules and the dipole created by the interaction between the molecules and the surface causes a shift in the perovskite energetics. For the sake of simplicity, from now on only the combined effect of these dipoles will be taken into account, calling "positive dipole" the case where the total dipole is pointing towards the perovskite surface and "negative dipole" the case in which the total dipole points outside with respect to the perovskite surface.

Figure 5.1a and Figure 5.1b shows the effect of a dipole on the perovskite vacuum level (E_{VAC}), and thus the WF. A negative dipole (Figure 5.1a) will shift the E_{VAC} downwards and therefore decrease the WF of the material. Specifically, in this chapter the results of the perovskite functionalized with amyl sulfide (csc5 - Figure 5.1c) will be discussed. This molecule is a Lewis base and can bind to the Pb^{2+} ions on the perovskite surface by donating its lone pair.[177]

On the other hand, a positive dipole will shift E_{VAC} upwards (Figure 5.1b), causing an increase in the WF of the functionalized material. In this case, the molecule of choice has been perfluorodecyl iodide (IPFC10 - Figure 5.1d) as an example of the described behaviour. IPFC10 is already known in the literature for being able to form SAMs and enhance the efficiency and stability of perovskite solar cells.[215,274] In this molecule, the iodine on the head remains slightly positive thanks to the electrons withdrawing effect of the fluorinated chain, which allows the molecule to behave like a Lewis acid and form halogen bond (XB)[196] with the halogen ions on the perovskite surface. It is worth noting that IPFC10, and in general molecules involving perfluorinated alkyl chains, form an XB interaction that is weak compared to other XB donors (for example haloarenes or haloalkynes).[196] However, it is important to be able to form a compact layer in order to obtain an interfacial dipole, and fluorinated chains are an optimal candidate for this purpose.[275] Thus this kind of molecule is more suitable for the goal of this work.

The selective absorption of Lewis bases and Lewis acids makes them perfect candidates for generating a negative or positive dipole and, in the case exposed here, the main component of the total dipole seems to come from their interaction with the surface (see agreement between simulations and experimentally measured shifts, later in the text). The chemical structures of the molecules employed in this chapter are reported in Appendix A1.

To demonstrate the scenario as mentioned above, various experimental and theoretical analyses were carried out. WF and bands edges' position were characterized making use of several techniques. Bare perovskite was used as reference and perovskite functionalized with 10 mM solutions of the two molecules as exemplary cases for the functionalization. The composition of the perovskite precursor solution employed in this chapter is $Cs_{0.05}(FA_{0.85}MA_{0.15})_{0.95}Pb(I_{0.85}Br_{0.15})_3$, which for simplicity will be referred to as *triple cation perovskite*.

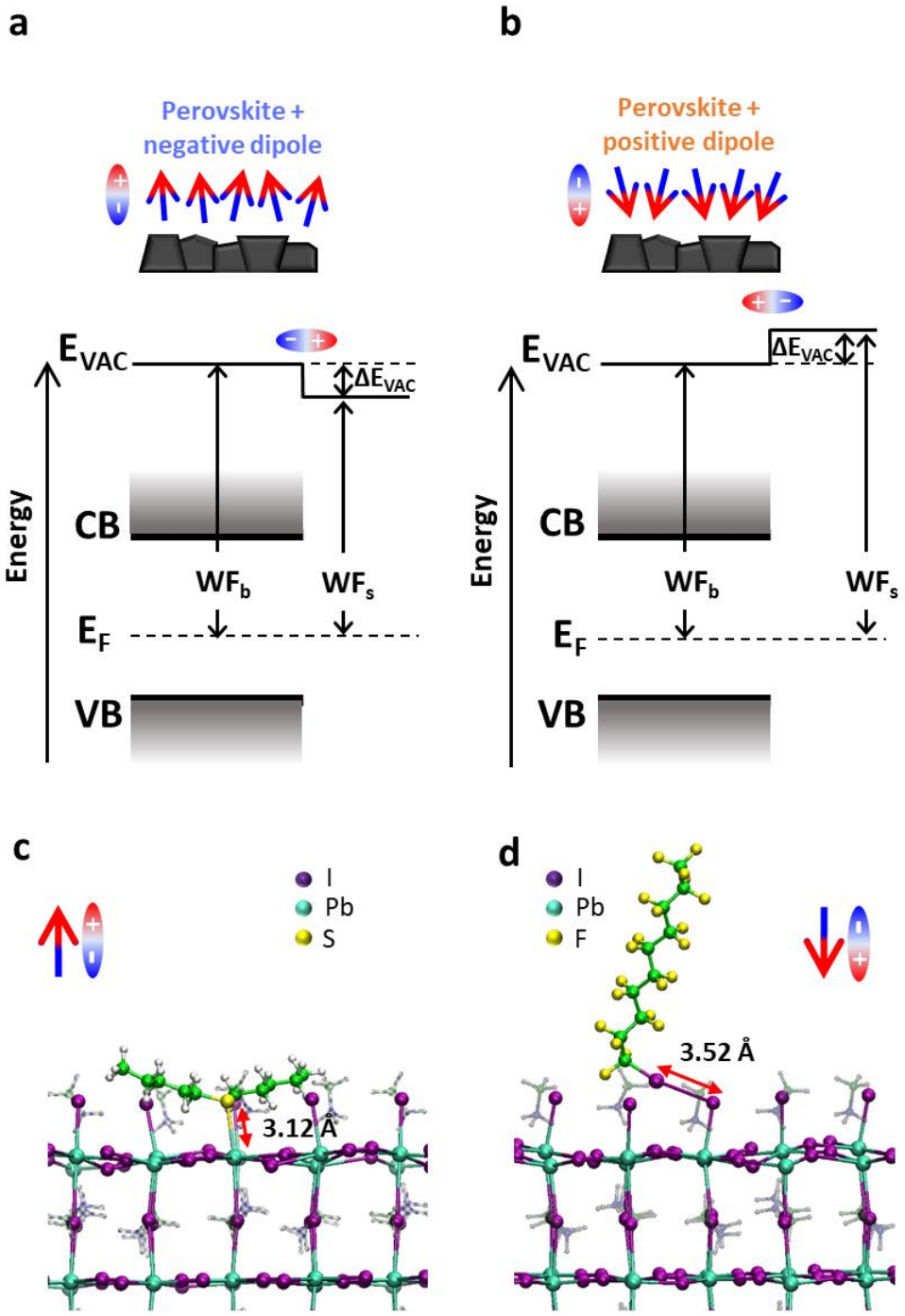

Figure 5.1. (a-b) Representation of the effect of the presence of a surface dipole on the perovskite band diagram for negative (a) and positive (b) dipoles. E_{VAC} is the local vacuum level, ΔE_{VAC} is the vacuum level shift induced by the dipolar monolayers, E_F is the Fermi level energy, CB and VB are conduction and valence band, WF_b is the bulk WF and WF_s is the surface WF. (c-d) Representation of the coupling of the two main molecules employed in this work in the case of a 50%-MAI terminated/50% PbI_2-terminated $MaPbI_3$ perovskite, where MAI is methylammonium iodide. Specifically, in (c) amyl sulfide (csc5), binding to Pb^{2+} ions of the surface and so representative of the negative dipole case. In (d) perfluorodecyl iodide (IPFC10), binding to the I^- ions on the surface and representative of the positive dipole case.

Measurements performed with different UPS setups gave repeatedly not reliable results, leading to the conclusion that the molecules might tend to detach in an ultra-high vacuum, making it challenging to draw actual conclusions from measurements in such conditions. For this reason, the characterization was performed with other techniques working at atmospheric pressure, such as Kelvin probe (KP), Kelvin probe force microscopy (KPFM), Ambient Pressure Photoemission Spectroscopy (APS) and cyclic voltammetry (CV). The obtained results were then compared to ensure their reliability.

The WF shift was evaluated through KP[248,276] measurements in different conditions (Figure 5.2a): in one case the experiment was entirely done in air (dashed lines), in the other case the samples were quickly mounted in air, but the investigation was carried out in N_2 atmosphere (solid lines). It is evident how the conditions of the measurement can influence the magnitude of the shift. In both cases, samples treated with positive dipoles present an increase of the WF compared to the bare perovskite reference, while samples treated with negative dipoles show a WF decrease.

To have a better idea of the real magnitude of the WF shift induced by the functionalization, KPFM[252,277] measurements were performed on not-air-exposed samples. Figure 5.2b displays the voltage maps of the WF shift for bare and functionalized perovskite together with the respective distributions. The results confirm the direction of the change already proven by KP and show a WF shift of about 150 meV for the negative dipole case and 300 meV for the positive dipole case. It is possible to notice that the distribution for the negative dipole functionalization is broader and less symmetric than the others, this might be an indication that at 10 mM concentration the surface is already saturated and in some areas, the molecules are packing in multilayers. This topic will be explored further in the following sections.

The maps also suggest that the shift is not homogeneous on the surface and the result is, therefore, an average of local WF variations. This behaviour is most likely due to the perovskite roughness and the presence of grains. In every map, the presence of small regions with a higher WF is indeed evident. Considering that our molecules functionalize the surface by binding to lead or halide ions, these regions probably indicate areas with a higher concentration of defects and thus higher concentration of molecules. According to the work of Gallet *et al*.[278], these regions might correspond to different facets of the crystalline structure. The local variation offers interesting data for further investigation. Nevertheless, it does not affect the results presented here, since the average gives the relevant quantity on a larger scale.

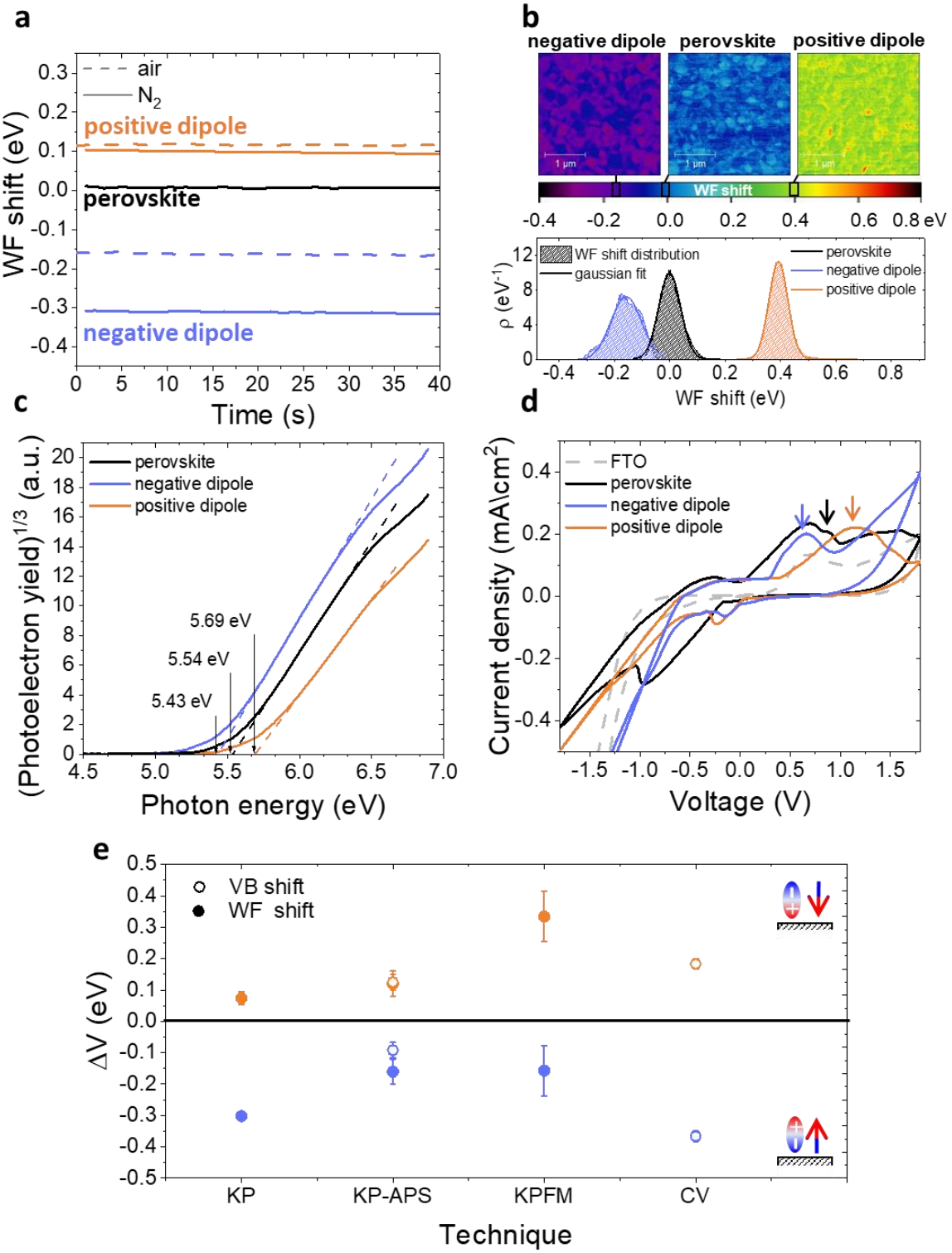

Figure 5.2. (a) WF shift due to the presence of interfacial dipoles measured with Kelvin probe (KP) in the dark in different environments: in one case (solid lines) the samples were measured in N_2 but shortly exposed to air while mounting them on the setup, in the second case (dashed lines) the samples were mounted and measured in air. (b) Kelvin probe force microscopy (KPFM) WF shift maps in the case of bare perovskite and perovskite functionalized with positive and negative dipoles with corresponding distribution (ρ) plots. (c) Ambient Photoelectron yield spectroscopy plots (APS) of ITO/perovskite (black), ITO/perovskite/IPFC10 (orange), ITO/perovskite/csc5 (blue). Measurements performed in air. (d) Cyclic voltammetry (CV) of bare FTO (grey), FTO/perovskite (black), FTO/perovskite/IPFC10 (orange), FTO/perovskite/csc5 (blue). (e) Comparison of the WF shift and VB shift related to perovskite obtained with different techniques for the cases of a positive and negative dipole.

The KP setup operated in air is combined with an APS tool (KP-APS)[276] in view to respectively determine the WF and the ionization energy (IE), i.e. the valence band maximum (VBM) relative to the local vacuum level on the same position over the sample. With the absolute WF and IE data measured, the KP-APS combination offers the possibility to determine the VBM shift and compare it with the WF shift under the same conditions. Figure 5.2c shows the IE as determined from photoelectron yield spectroscopy plots in APS measurements performed: as shown in Figure 5.2e, the shifts of VBM and WF match in direction and magnitude for the different cases. This result is significant because it shows that both WF and VBM are shifting equally, and thus it allows to exclude the possibility that the detected WF shifts are due to doping of the perovskite layer. Therefore, this provides evidence that the surface dipole affects all the surface energy levels of the perovskite.

Complementarily, the VB shift was monitored by performing CV on functionalized and bare perovskite on FTO (Figure 5.2d), respectively. From the first distinguishable oxidation peaks of the different CV scans, it is possible to calculate the VBM position by adding the redox potential of the Ag/AgCl electrode (4.65 eV)[255] for the different cases. It is possible to observe that the negative(positive) dipoles trigger a VBM shift downwards(upwards) in relation to the VBM of the reference perovskite on FTO. Both cases are comparable in direction and magnitude of VBM shifts to those measured with the other techniques. The position of the reduction peaks in the range of the negative bias is instead not reliable because some partial perovskite degradation during the reverse scan was noted. Therefore, a calculation of the conduction band minimum (CBM) position is not possible in this case.

Nevertheless, the bandgap was estimated from UV-Vis and EQE measurements (Figure A3.1). The obtained value is of approximately 1.64 eV and it is independent of the functionalization. It follows that the CBM is shifting in parallel with the VBM and WF.

Figure 5.2e summarizes the results. For all measurements conditions, it was possible to observe an increase(decrease) in WF and VBM in the case of a positive(negative) dipole functionalization. Differences in absolute numbers are a consequence of varied measurement conditions inherent to the respective setups. Moreover, these results show that, as expected, the dipoles affect both WF and band edges. Therefore, it is important to stress that, when talking about WF shift, a shift of VB and CB is also considered (generalized as energy levels shift).

5.3 How to tune the magnitude of the energy levels shift

Having established that the dipolar molecules can control the positive and negative shift of the perovskite WF, the focus shifted on achieving control over the magnitude of the change. The concentration of the solution used for the deposition was varied to control the distribution of the molecules on the perovskite surface and, consequently, the magnitude of the WF shift.

The change in WF was measured for the different solution concentrations through KP and KPFM, obtaining similar trends with both methods (Figure A3.3).

Figure 5.3a and Figure 5.2b show how the perovskite WF is changing depending on the solution concentration in the case of positive (Figure 5.2a) and negative (Figure 5.2b) dipole. In the positive dipole case (Figure 5.2a), the work function is increasing with the increasing of the solution concentration until reaching saturation at about 40 mM. The two molecules (perfluorodecyl and perfluorododecyl iodide – IPFC10 and IPFC12) differ only in the chain length. Therefore, the difference in the magnitude of the shift is due to the difference in the strength of the dipole, where the latter has a smaller dipole due to the higher molecular length.

A similar trend is obtained in the case of a negative dipole (Figure 5.2b), but with the WF decreasing compared to the perovskite one and reaching saturation already for a concentration of about 10 mM. In this case, the two molecules are different both in structure and binding group (amyl sulfide -csc5- and trioctylphosphine oxide -TOPO-), therefore it is possible to state that it is the dipole type, not the specific molecule, which defines the direction of the shift.

It is worth noting that TOPO-functionalized perovskite shows an extreme WF shift. Moreover, it was not possible to collect data for more than 10 mM concentration because for higher molarities the solution was damaging the perovskite film, presumably by dissolving the lead cations[279] (Figure A3.2). This seems to suggest that TOPO might be a tricky molecule to use in devices, despite its excellent passivation properties reported by several papers[186–188].

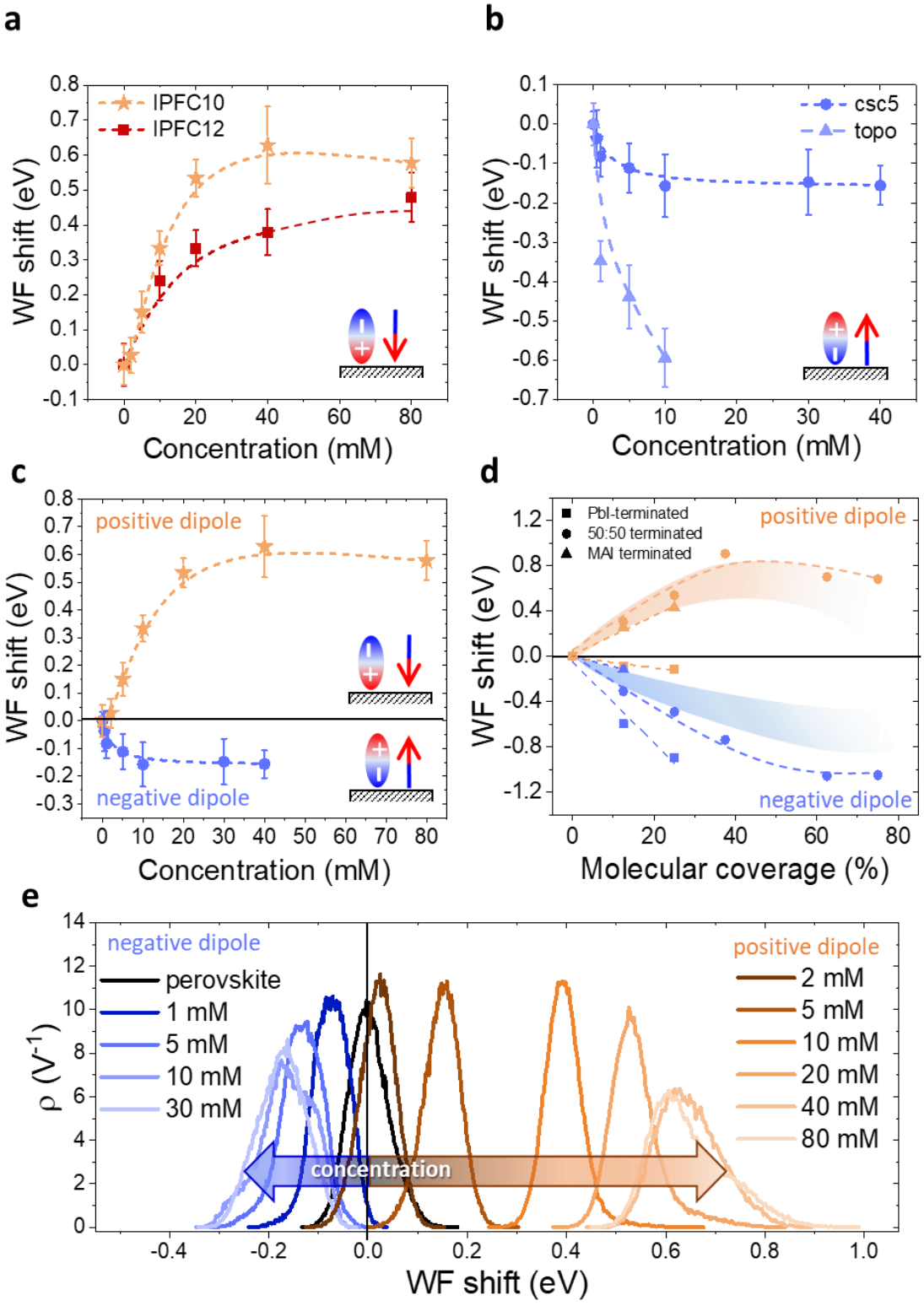

Figure 5.3. KPFM measurements showing the WF changing depending on the solution concentration when the perovskite is functionalized with a positive (a) and negative (b) dipole. In this specific case, the molecules creating a positive dipole were IPFC10 and IPFC12, and the ones making a negative dipole were csc5 and TOPO. (c) Comparison of the WF trends for the positive (orange) and negative (blue) dipole. (d) DFT simulations of the relation between WF shift and coverage for different surface terminations of $MAPbI_3$, the shaded stripes represent the probable condition of the samples experimentally measured. (e) Distribution (ρ) of the WF shifts from KPFM measurements for different concentrations of negative and positive dipoles. The curves in (a),(b),(c) and (d) are spline fitting of the data.

The above results show that by changing the solution concentration, it is possible to tune the magnitude of the WF shift up to several hundreds of meV. It is known that polar monolayers properties are determined not only by the type of molecules and bonding configuration to the substrate but also by size, (dis-)order and adsorption patterns within the monolayer[280,281]. Therefore, the trends showed in Figure 5.2 can be explained by considering the deposition kinetics and it is likely related to the coverage. At first, all defect sites (i.e. Pb^{2+} and halide ions) are free, consequently, as soon as the samples are immersed in the solution, the molecules start to bind to them. However, with low solution concentration, not all the defect sites can be occupied by a molecule, therefore the surface is not fully functionalized. With the increase of the concentration the functionalization level increases as well, until reaching a point where (ideally) every surface defect is occupied by a molecule, therefore the curves reach a plateau, and the condition for maximum WF shift is achieved.

To be noted that a similar process would happen if the solution concentration were kept constant and the dipping time varied (see Figure A3.4), for this reason, it is crucial to keep one of these parameters fixed. In this case, it was chosen to settle the dipping time and vary the concentration, but it is important to note that changing the dipping time would give the same results, since the process is related to the deposition kinetics of the molecules.

Another exciting feature is visible by comparing the trends for the positive and negative dipoles (Figure 5.2c): the concentration at which the WF starts to saturate is different for the two cases. This behaviour may indicate a specific ratio of defects at the perovskite surface, in particular the ratio between halides and Pb vacancies. Indeed, in these experiments, the positive dipole is given by a Lewis acid, which is binding to the halides on the surface, while the negative dipole is provided by a Lewis base, which is binding to the Pb ions. Therefore, the fact that the negative dipole functionalization curve saturates at lower concentrations than the positive dipole curve suggests that there are less Pb ions on the surface compared to halide ions, i.e. there are more Pb vacancies. This result is in agreement with the work of Philippe *et al*.[282], where the I/Pb ratio at the surface for triple-cation perovskite is said to be around 3. Moreover, it is also essential to consider the geometry and the steric hindrance of the two molecules. Indeed, while IPFC10 consist of a straight-comparably rigid-chain which allows the molecules to form a compact vertical layer, csc5 has two aliphatic chains that most likely limits the number of molecules which can bind to the surface, thus leading earlier to saturation.

The difference in behaviour is also highlighted by the WF distribution curves in Figure 5.2e (respective contact potential difference (CPD) maps in Figure A3.5 and Figure A3.6). The negative dipole curve stops shifting and therefore reaches saturation for lower concentrations than the positive dipole one. Moreover, it is interesting to see how both curves start to broaden and lose symmetry while approaching saturation. This shows that initially (i.e. for low concentrations) the molecules are nicely depositing and forming an ordered homogeneous monolayer. In contrast, with increasing concentration, the deposition seems to become less uniform, probably forming some agglomerates, especially when saturation is reached. It cannot be excluded that the observed change in WF is also dependent by different factors, such as the possible formation of multilayers and their effect on the molecules arrangement. Indeed, it was not possible to experimentally assess if the deposited

molecules formed a monolayer, as expected, or multilayers. The presence of multilayers could in principle contribute to the potential drop associated with the dipoles,[232] however, in order for this to happen, the additional layers should be ordered, which is unlikely considering the weak interactions foreseeable among the molecules. Therefore it is more likely that the observed trend are indeed related to the coverage and the molecules' arrangement rather than an increase in thickness.

To support the experiments, DFT simulations performed by collaborators were used to investigate the interaction of csc5 and IPFC10 with the $MAPbI_3$ surface, here considered as the prototype lead halide perovskite. Molecule adsorption has been modelled on the (001) surface, which is the simplest model of a tetragonal slab, for three different terminations: (i) PbI_2-terminated, (ii) 50%-MAI and 50% PbI_2-terminated (half terminated), (iii) MAI-terminated, where MAI is methylammonium iodide.

The results confirm that overall, under all considered adsorption situations, csc5 provides a WF reduction while IPFC10 leads to a WF increase. The simulations evaluated the WF shift for the two molecules for different values of surface coverage. Figure 5.2d shows the predicted WF variation for different levels of coverage for the three examined terminations. In particular, the half-terminated case was extended to higher levels of coverage until reaching a saturation of the energetic shift.

As visible in Figure 5.2d, in all the three cases, the WF initially shifts almost linearly with the coverage. Then saturation of the WF shift is observed for coverage higher than 40-50%, in excellent agreement with the experimentally measured trends. Considering that the measurements were performed on triple-cation perovskite, the experimental results would be comparable with a situation in between half-terminated surface and MAI-terminated surface (see shaded stripes in Figure 5.2d).

By comparing the experimental trends in Figure 5.2c with the simulation trends in Figure 5.2d for the half-terminated case, it can be noticed how, in both cases, the WF shift has a higher magnitude for IPFC10. The slight decrease of WF for IPFC10 in Figure 5.2d is ascribed to the formation of IPFC10-Pb bonds on the saturated surface, which partially decreases the WF. The numbers suggest that experimentally saturation is reached for a coverage of about 20% in the case of IPFC10 and 10% for csc5. As previously pointed out, this difference is most likely related to a smaller amount of Pb ions on the surface combined with a bigger steric hindrance of csc5. Naturally, variations between simulations and experiments can arise due to the different thermodynamics on the other surface of the grains and the presence of defects. Moreover, it is important to keep in mind that the simulations were performed on an ideal $MAPbI_3$ flat surface.

Overall, the simulations support the correlation between surface coverage and WF shift and prove the validity of this method to tune the perovskite work function in a controlled way.

5.4 Conclusions

In short, the answer to the initial question "*Is it possible to systematically tune the perovskite energy levels?*" is *yes*. This chapter shows how to control the deposition of dipolar self-assembled monolayers on halide perovskite and obtain this way a controlled shift of perovskite work function, valence and conduction bands. The direction of the shift can be controlled with the direction of the surface dipoles and the magnitude of the shift can be controlled by tuning the density of the surface dipoles, obtaining an energetic shift up to several hundreds of meV. The work presented here shows that tuning the energy levels of semiconductors through surface functionalization with dipolar molecules, which is a well known method in organic and inorganic semiconductor physics, can be extended to hybrid organic-inorganic perovskite semiconductors. This provides a new toolbox to enhance further the flexibility of applying halide perovskites in optoelectronics. The application of this method in devices is examined in the next chapter.

6 THE EFFECT OF ENERGY LEVEL TUNING IN DEVICES

Section 6.2 of this chapter is based on the peer-reviewed article "Canil, L. et al., *Tuning Halide Perovskite Energy Levels*, Energy Environ. Sci., **2021**, 14, 1429-1438".[168]

The previous chapter introduced a method for tuning the perovskite energy levels through assemblies of dipolar molecules. This strategy has great potential for the improvements of energy level alignment in perovskite solar cells. However, the step from measuring a change in energetics to seeing its effect in devices is not straightforward. In this chapter, the perovskite energy level tuning method is applied to different systems, namely devices with triple cation (CsMAFA) perovskite and devices with $MAPbBr_3$. The perovskite layer is functionalized with different concentrations of dipolar molecules, which were chosen based on the energy level alignment of the system in order to reduce the energetic offset with the subsequent layer. The impact on perovskite solar cells is reported and discussed in detail for both cases. The results show a significant improvement in V_{oc} of about 60 meV for the case of $MAPbBr_3$ devices. Triple cation devices present the same trend, but with less evident enhancement. These results attest the validity of the energy level tuning method presented in Chapter 5. Moreover, they highlight how the effectiveness of such tuning depends on the relevance of the energetic offset among the sources of losses in the device. Indeed, applying the energy level tuning method is particularly useful in presence of big offsets at the functionalized interface (as for $MAPbBr_3$ devices), while it results in limited improvement for already optimized systems (as for triple cation devices). A special section is dedicated to comments on the features of the $MAPbBr_3$ reference devices and their optimization.

6.1 Introduction

The tunable properties of the perovskite material[21] give the possibility to prepare devices with different characteristics. For example, the bandgap of Pb-based perovskites can be tuned from 1.5 eV to 3 eV.[13] This directly results in devices with different requirements in terms of energy level alignment (ELA). The importance of ELA has been already thoroughly discussed in Section 3.2, clarifying its fundamental role for an efficient charge transport, reduction of recombination and enhancement of the quasi-fermi level splitting (QFLS).[34]

Most of the commonly used charge transport layers (CTLs) have energy levels which fit the valence band maximum (VBM) and conduction band minimum (CBM) of the perovskites possessing a bandgap of around 1.6 eV, which corresponds to the compositions giving the most efficient devices.[19,47] However, these CTLs might not be suitable for perovskites with different bandgaps. In these cases, it is necessary to find or synthesize new materials with suitable energy levels, so that there is a small offset between the CTL's HOMO/LUMO and the perovskite VBM/CBM. As alternative to this approach, or in combination with it, it is possible to directly adjust the energy levels at the required interface. Chapter 5 presented a possible method to tune the energetics of the perovskite layer. The results clearly showed that it is possible to shift the perovskite work function (WF) up to several hundreds of meV through monolayers of dipolar molecules. The shift in WF correspond to an equal shift in the energy of the bands edges, thus the method allows a tuning of all the energy levels. The direction and magnitude of the shift can be tuned by controlling direction of the dipoles and the deposition conditions.

Nevertheless, the measurement are performed on exposed surfaces, while in the device the same surface is buried. Therefore, the energetics might be different and it is not straightforward to pass from the measurement to the actual effect within a device.[283] This chapter explores the application of the energy level tuning method in devices with perovskites of different compositions, which therefore require different conditions for the ELA. The chapter is divided into two main sections: a first part is devoted to the study of energy level tuning in one of the standard state-of-the-art perovskites, i.e. the so-called triple cation perovskite. The second part focuses on a less commonly used in devices, hence also less "optimized" stack: wide-bandgap PSCs, exemplified by $MAPbBr_3$. In this case, some insights on the development of such devices and their behaviour are also presented.

The main objective of this chapter is to answer the important question: *Is the energy level tuning method presented in Chapter 5 working when applied in devices?* Which is also directly connected to the more general question posed in Section 3.2.1 : *Is energy level alignment actually relevant?*

The results presented here indicate that tuning the perovskite energy levels via functionalization with dipolar molecules positively affects the performance of the devices, mainly through an improvement in V_{oc}, which is likely due to a combined effect of passivation and adjustment of the ELA. Moreover, the comparison of the results for devices with triple cation and $MAPbBr_3$ shows that the effectiveness of the method depends on the system. Specifically, the improvement will not be particularly relevant if the ELA of the device is already optimized even without any functionalization, i.e. if the offset between perovskite and CTLs is already relatively small, like in the case of triple cation perovskite. While it will be evident in systems experiencing a relevant misalignment of the energy levels, such as in the case of wide-bandgap solar cells. $MAPbBr_3$ devices functionalized with a tailored dipolar molecule show a V_{oc} enhancement of about 60 meV and an increase in performance of more than 1 %.

6.2 Triple cation perovskite solar cells

Triple cation perovskite is the common name of a Pb-based mixed halides perovskite (I and Br) containing three cations, namely methylammonium (MA^+), formamidinium (FA^+) and cesium (Cs^+). The perovskite composition used for the first perovskite devices was "simple" $MAPbI_3$:[17] it became the archetypical perovskite and it has been extensively used over the years. In 2014 the introduction of a novel composition containing MA and FA further improved PSCs,[101] leading to an established protocol for high efficiency devices. Finally Saliba *et al*.[284] demonstrated that adding small alkali metal cations (like Rb or Cs) can enhance both stability and efficiency of the devices. Since then, triple cation perovskite has been the composition of choice for obtaining reproducible high efficiency perovskite solar cells (PSCs).[19]

The number of reported values for the different photovoltaic parameters shown in the statistics of Figure 6.1a is evidence of the widespread use of triple cation perovskite in PSCs. Devices with this composition can deliver solar cells with efficiency over 20 %, characterized by V_{oc} around 1.15 eV, FF of 70-80 % and J_{sc} over 20 mA/cm^2. The success of this composition is due, beside to its stability, to a bandgap of 1.6 eV, which allows good absorption in the visible spectrum. Another important role is played by the CTLs, indeed most of the commonly used were optimized for the energetically similar $MAPbI_3$, thus they have a good ELA with the triple cation perovskite absorber.

Overall, triple cation perovskite represents the composition of reference for state-of-the-art PSCs, for this reason it has been chosen for testing the application of the energy level tuning method described in Chapter 5. In n-i-p devices with stack FTO/TiO_2/triple-cation/spiro-OMeTAD/Au[7], the perovskite/HTL offset is of about 300 meV,[156] as schematically represented in Figure 6.1b. Therefore, in order to reduce it, it is necessary to decrease the perovskite energy levels, paying attention not to shift them excessively, since this would lead to an unfavourable ELA with the perovskite VBM higher than the spiro-OMeTAD HOMO. In Chapter 5 two molecules with the ability of decreasing the energy levels were presented and their effect on triple cation perovskite characterized: amyl sulfide (csc5) and trioctylphosphine oxide (TOPO)[8]. The latter can shift the perovskite WF of more than 300 meV even for very low solution concentrations. This is excessive for the purpose of reducing the perovskite/HTL offset in the case of triple cation devices. On the other hand, the relatively small shift induced by csc5 (max 160 meV – Figure 5.3) seems optimal for the purpose of this experiment. To note that, as shown in Chapter 5, a shift in the WF correspond to an equivalent shift of the band edges. Therefore, the treatment affects all the perovskite energy levels.

[7] FTO is fluorine-doped tin oxide, spiro-OMeTAD is 2,2',7,7'-Tetrakis[N,N-di(4-methoxyphenyl)amino]-9,9'-spirobifluorene.
[8] Chemical structures are reported in Appendix A1.

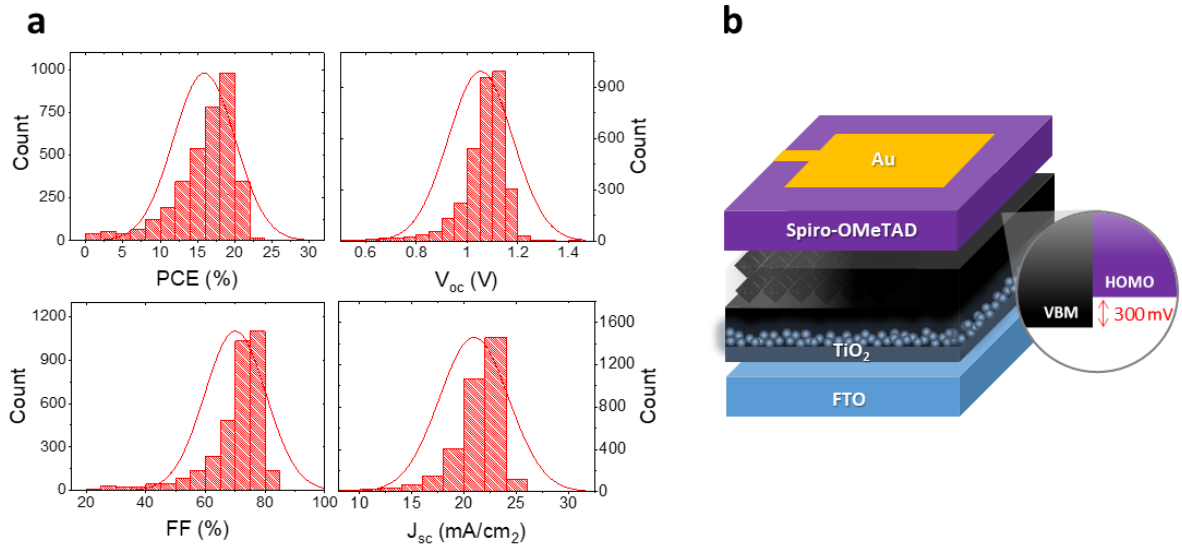

Figure 6.1. (a) Statistics on the photovoltaics parameters' literature values for devices with triple-cation perovskite. Plotted from data collected in the perovskite database.[285] Database accessed on 1.08.2021 (b) Standard stack for n-i-p triple-cation devices, highlighting the offset between the perovskite absorber and the HTL.

6.2.1 Energy level tuning of triple-cation devices

Standard n-i-p devices with stack FTO/TiO_2/triple-cation/csc5/spiro-OMeTAD/Au were prepared, details on the preparation protocol are reported in Appendix A2, the triple cation composition is $Cs_{0.05}(FA_{0.85}MA_{0.15})_{0.95}Pb(I_{0.85}Br_{0.15})_3$. The perovskite was functionalized with different concentrations of csc5 to create a negative dipole at the interface and modify in this way the ELA. The expected effect of the dipolar functionalization is to reduce the approximately 300 meV offset between the perovskite VBM and the spiro-OMeTAD HOMO.

Specifically, the effect of functionalization was explored for a low concentration of the molecule's solution (0.5 mM), meaning a WF shift of about 40 meV, and for high concentration (10 mM), which represents already a situation of surface saturation and gives a WF shift of approximately 160 meV (see Figure 5.3).

Figure 6.2 shows how the photovoltaic (PV) parameters such as open-circuit voltage (V_{oc}), short-circuit current (J_{sc}), fill factor (FF), and photovoltaic conversion efficiency (PCE) are changing. It is possible to notice that the V_{oc} is increasing with increasing concentration, while the FF remains constant after the initial improvement and the J_{sc} does not change significantly.

When the perovskite surface is functionalized with dipolar molecules, there are different factors that can affect the devices' PV parameters. The dipoles induce a change in ELA, but at the same time, there is evidence that the produced electrical field can screen charges, obtaining an effect similar to passivation.[225] Moreover, the molecules are binding to defects on the perovskite surface, reducing in

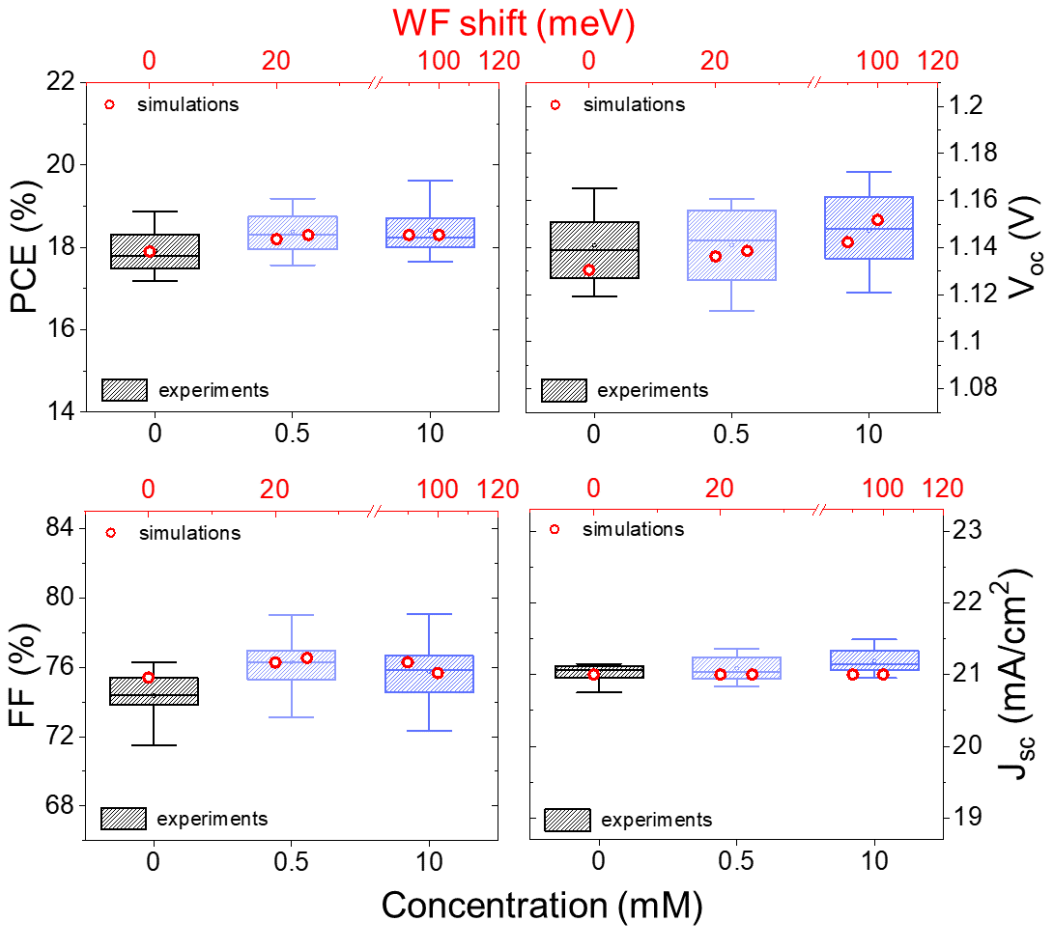

Figure 6.2. PCE, V_{oc}, FF and J_{sc} of n-i-p devices with structure FTO/TiO_2/triple-cation/csc5/spiro-OMeTAD/Au for different molecule's solution concentrations and simulated values of negative WF shift. The box charts are the values obtained experimentally from JV curves measured at 0.01 V/s. The statistics are estimated from 8 , 11, and 13 pixels for 0 mM, 0.5 mM, and 10 mM, respectively. A pixel is a single solar cell. The red circles represent how the photovoltaic parameters change depending on the WF shift according to drift-diffusion simulations.

this way the trap states. It is therefore difficult to disentangle the effect of the different factors, especially in this case, where the changes are relatively small. Thus, drift-diffusion simulations were performed to gain a better insight.

In the simulations, one of the JV curves from the control devices, carefully chosen as representative of their average behaviour, was set as a reference. Then only the perovskite energetics and the recombination time were varied to simulate the presence of a negative dipole at the interface between perovskite and spiro-OMeTAD. The results are represented by the red circles in Figure 6.2.

The simulations show that the experimental trend is reproducible considering smaller WF shifts than those measured with KPFM and increasing the recombination time constant at the interface from $1.6e^{-10}$ s to $2.84e^{-10}$ s. In particular, the simulations predict a WF shift of about 25 meV for devices functionalized with a 0.5 mM solution and 100 meV for the 10 mM case. This seems to indicate that part of the deposited molecules are lost in the devices making process, leading to a smaller WF shift and, therefore, also to just a slight reduction on the perovskite/spiro-OMeTAD offset. Additionally, it is difficult to predict the effect of the deposition of a layer on top of the molecules (spiro-OMeTAD in

this case), thus this could also lead to interfacial changes resulting in a reduced "real" energy level shift compared to that measured on the exposed perovskite surface.

Both experimental data and simulations show an initial increase in FF, in average from 74 % to 77 %, and a progressive, albeit limited, V_{oc} enhancement (~10 meV). These results are consistent with a reduced perovskite/spiro-OMeTAD offset and with suppression of recombination. It is also worth highlighting the consistency of this behaviour with the results from a previous work employing IPFC10 at the interface between perovskite and C60 in n-i-p PSCs,[215] where a similar V_{oc} trend was observed.

It is also possible to notice that the simulations do not predict a change in J_{sc}, while experimentally, a small variation is observed. Nevertheless, it is quite common in perovskite solar cells to have J_{sc} fluctuation of about ± 0.5 mA/cm^2 even for identical devices. Therefore, this change is not to be considered significant.

Overall, the simulations show the effect of interfacial dipoles and the WF shifts on PSCs and highlight that the behaviour observed experimentally can be justified by considering only the influence of the dipoles. It is also worth noting that the actual WF shift in the device seems to be reduced compared to the nominal value measured on the exposed surface, which is a factor to take into consideration for future experiments.

These results suggest that the presence of a dipolar layer at the interface between perovskite and CTLs can influence and, if the conditions are appropriately chosen, improve ELA in PSCs. In the case described in this section, the ELA of the system (i.e. devices with triple cation perovskite) was already optimized even without any functionalization, thus it is not surprising that the overall changes are limited. Therefore, in order to explore the real potential of the energy levels tuning method, it is interesting to apply it to a system that, at the state-of-the-art, still requires optimization and presents big offsets between the different layers. This could be the case, for instance, of devices still comprising triple cation perovskite, but with different (maybe even very stable and conductive, but less energetically optimized) CTLs. Alternatively, solar cells comprising the so-called wide-bandgap perovskite are another good example of such a system. In this case, the ability to adjust the ELA by tuning the energy levels of the perovskite is an advantage, because it eases the requirement of finding new CTLs with suitable energetics.

6.3 Wide-bandgap perovskite solar cells

As introduced in Section 2.6.1, the Pb-based perovskite bandgap can be tuned approximately from 1.5 to 3 eV by changing the ABX_3 composition. A bandgap of 1.6 eV, as in the case of the triple cation perovskite,[156] at the centre of the previous section, is optimal for single junction devices because it absorbs most of the visible part of the solar spectrum. The bandgap can be enlarged, for example, by increasing the amount of Br. The archetypical wide-bandgap perovskite is $MAPbBr_3$ with a bandgap of 2.3 eV.[286] $MAPbBr_3$ can be employed in multi-junction solar cells for the absorption of high-energy photons.[287–289] Moreover, it is particularly stable compared to the standard $MAPbI_3$ composition[290] and it can easily form large single crystal that can be employed in devices.[291] However, despite these advantages, not many studies have focused on $MAPbBr_3$-based devices. This is evident by comparing the statistics of Figure 6.3a with those showed in Figure 6.1a related to triple cation solar cells, there is indeed an outstanding difference in the number of reported values for the two cases: 3600 for triple cation compared to 300 for $MAPbBr_3$.[285] The lack of research on the topic is also stressed by the spread of the histograms, symptom of scarce reproducibility among the results from different labs.

The challenge of these kinds of devices arises mainly from the quality of the film and the energetic alignment with the CTLs. It is indeed thermodynamically favourable for $MAPbBr_3$ to crystallize rapidly,[292,293] this however often hinders the formation of a smooth and compact film because of the formation of structural and electronic defects. Hence, a lot of the research performed on devices with this composition has been devoted to the improvement of the crystallization process, for example through solvent[292,294] and precursor solution[295] engineering or via novel deposition methods.[164,296,297] On the other hand, obtaining a uniform and compact film is not enough for achieving high-performing devices. Defects with energy levels deep within the bandgap are still an important source of non-radiative recombination,[298] thus passivation routes have also been explored.[292,299] However, reportedly the main bottleneck for $MAPbBr_3$ devices lies in the energetic misalignment.[292] Indeed, the big bandgap results in a significantly deeper VBM for $MAPbBr_3$ compared to the commonly used compositions. Often the "standard" HTLs (like spiro-OMeTAD or PTAA) are still employed, although they are not well suited for this case because of their relatively shallow HOMO level. For example, Figure 6.3b shows the energy levels at the interface between the perovskite and spiro-OMeTAD, highlighting an offset of around 800 mV[140] that greatly reduces the possible voltage output. To alleviate the misalignment several CTLs have been explored or developed,[169,300–302] allowing for the achievement of a record V_{oc} of 1.653 mV with efficiency around 10%.[301] However, the radiative V_{oc} limit for a bandgap of 2.3 eV is 1.97 eV,[117] thus the V_{oc} loss of this perovskite composition is still enormous (> 300 meV). Especially compared with triple cation devices, which can reach a V_{oc} around 1.2 eV with a radiative limit of 1.33 eV,[117] therefore displaying a three times lower V_{oc} loss.

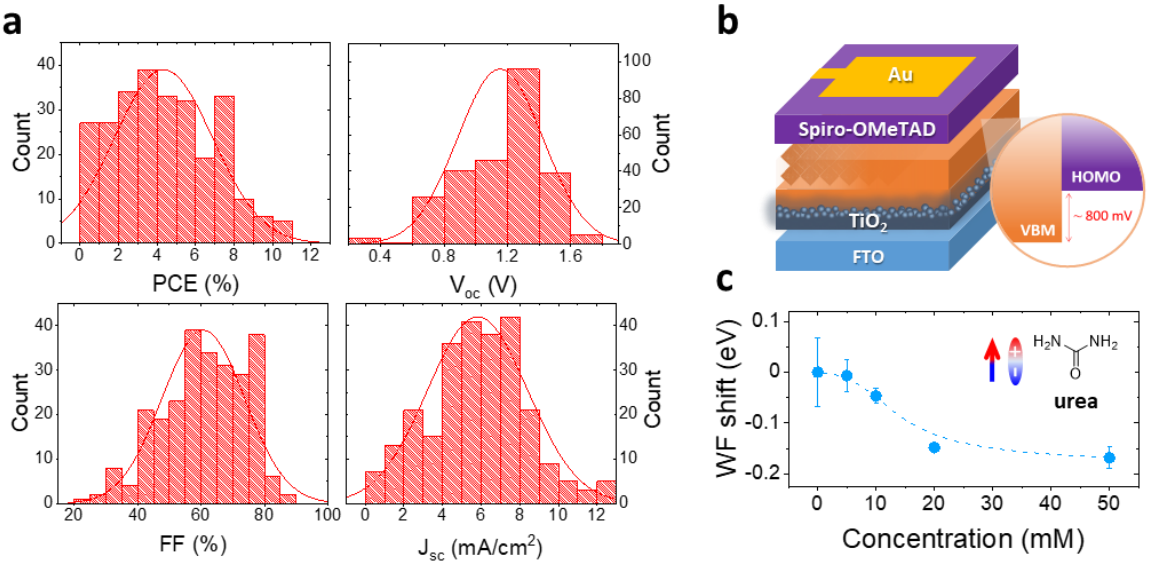

Figure 6.3. (a) Statistics on the photovoltaics parameters' literature values for devices with $MAPbBr_3$ perovskite. Plotted from data collected in the perovskite database.[285] Database accessed on 1.08.2021 (b) Standard stack for n-i-p $MAPbBr_3$ devices, highlighting the offset between the perovskite absorber and the HTL. (c) Kelvin probe measurement of FTO/TiO_2/$MAPbBr_3$ samples functionalized with different concentrations of urea, showing the decrease of WF due to the interfacial dipole. Measurement performed in N_2 after a short exposure to air.

It is therefore clear that $MAPbBr_3$ devices constitute a system that still needs optimization on different aspects, including film quality improvement, defects reduction and considerable ELA adjustment. For this reason, it is a suitable candidate for evaluating the effect of the functionalization with dipolar molecules presented in Chapter 5 when applied to devices. Moreover, $MAPbBr_3$ is a material with a lot of potential, with the ability of delivering stable devices with high voltage output. Therefore, reducing the voltage loss of $MAPbBr_3$ solar cells, without the need of finding new energetically well-matched HTLs, is a step forward towards the full exploitation of the advantages of this kind of device.

6.3.1 Urea functionalization

In the case of $MAPbBr_3$ devices the purpose is to reduce the perovskite/HTL offset, hence it is necessary to functionalize the surface with a negative dipole, which will decrease the perovskite WF and energetic bands. Among the molecules studied in Chapter 5, TOPO would be an ideal candidate because of its large induced WF shift towards lower values. However, the three long aliphatic chains might be an issue in devices, indeed they could form an insulating layer or they could be an obstacle to the formation of a compact homogeneous layer. Hence, it has been chosen to switch to a molecule of smaller dimensions, but which retains the important characteristic of having a large negative dipole. A molecule possessing these features is for example urea, a Lewis base with a dipole moment of about 4.5 D (structure in the inset of Figure 6.3c).[303] Urea can bind to the perovskite surface via coordinate

bonding between the oxygen in the molecule and the Pb ions on the perovskite surface, thus creating a negative dipole.

Kelvin probe measurements (Figure 6.3c) confirm that the passivation of perovskite with urea leads to a decrease in WF, with the magnitude of the shift increasing with the concentration, as characteristic of molecules that interact with the substrate. However, it is also possible to note that the trend visible in Figure 6.3c appears different from those observed in Chapter 5 in the case of functionalization with Lewis bases (Figure 5.3): here the shift saturates at higher concentrations and there seem to be no effect for the lowest concentration, i.e. 5 mM. The reason is probably a combination of factors. First of all urea is particularly small compared to any of the molecules explored in Chapter 5**.** Therefore, a higher urea solution concentration is needed to saturate the surface and thus achieve the maximum WF shift. Additionally, while all the molecules in Chapter 5 were deposited dipping the substrates in a solution of the molecule of interest, urea was instead spin-coated on the substrates. This necessarily leads to a change in the deposition dynamics and, thus, possibly on the molecules distribution.

As explained in the methods section, the decision of using spin-coating arises from the solvent used for preparing the urea solution, i.e. isopropanol (IPA). Indeed, a degradation of the perovskite was observed after more than a few seconds of solvent exposure, thus making it impossible to use the dipping method. IPA was chosen after unsuccessfully testing several other solvents. The challenge of finding a suitable solvent is related to the polar nature of urea, indeed the molecule dissolves mainly in polar solvents, for example water, ethanol, methanol or acetonitrile. However, these solvents affects also the organic part of perovskite, i.e. the polar cations. Several other common solvents have been tested to find an alternative that could dissolve urea but not dissolve perovskite. For instance common antisolvents such as toluene, chlorobenzene, ethyl acetate, diethyl ether, and dibuthyl ether. The tests showed that ethyl acetate could dissolve urea at low concentrations by keeping the solution at around 60°C. However, once the solution was dropped on the substrate it was quickly cooling down and recrystallizing. The other solvents did not dissolve urea at any tested condition, i.e. different concentrations, and temperatures up to 80°C. IPA, instead, could successfully dissolve urea with a few minutes of heating at 60°C in a thermoshaker. As a consequence, IPA resulted the best solution, since it can be spin coated on perovskite without particular damage.

Another observation that rises from Figure 6.3 is that the magnitude of the shift is relatively small considering the significant intrinsic dipole of the molecule. This could be related to possible hydrogen bonding interaction between urea and halide anions on the perovskite, which would counteract the effect of the negative dipole created from the O---Pb^{2+} interaction. Moreover, it is also possible that the big dipole of urea create repulsion with surrounding molecules, thus leading to the formation of less compact layer. However, it might be misleading to focus on the absolute numbers of this measurement. Indeed, because of the specific features of the setup, it was necessary to expose the samples to air while mounting them. Thus, the results include an effect from air exposure that it is challenging to account for. Moreover, the tests on solar cells with functionalized perovskite (both in this and the next chapter) seem to indicate that the actual offset reduction in devices is smaller than the predicted induced energy level shift. Based on these factors, it has little meaning to try to

accurately characterize the WF shift value of a single molecule. An assessment of the magnitude of the shift makes sense in terms of comparison with other molecules deposited with the same conditions and method, as in the previous chapter. However, this detailed characterization is beyond the scope of this chapter. Here the relevant result is the direction of the shift, while the magnitude is merely an indication of the potential actual shift.

6.3.2 Energy level tuning of $MAPbBr_3$ devices

Devices with n-i-p structure have been prepared in order to investigate the effect of the absorber functionalization with dipolar molecules in the case of PSCs with a large offset at the perovskite/HTL interface. The devices stack is FTO/TiO_2/$MAPbBr_3$/urea/spiro-OMeTAD/Au. The devices preparation protocol is commented in Section 6.3.3 and reported in details in Appendix A2. As mentioned above, it has been shown that PSCs with $MAPbBr_3$ as absorber can reach higher efficiency with HTLs possessing a deeper HOMO than spiro-OMeTAD. Nevertheless, the purpose of this study is not obtaining a record device, but investigating the effect of the induced energy level shift. Hence, keeping spiro-OMeTAD as HTL has the twofold advantage of resulting in a situation with a big offset at the absorber/HTL interface and allowing a direct comparison with Section 6.2, since the same stack is used.

$MAPbBr_3$ was functionalized by spin-coating solutions of urea with different concentrations, specifically from 5 mM to 50 mM. Figure 6.4 shows the evolution of power conversion efficiency (PCE), open circuit voltage (V_{oc}), fill factor (FF), and short circuit current (J_{sc}), with increasing solution concentration. The case of 0 mM corresponds to devices without treatment and, thus, it is the reference. The box charts display both reverse and forward scans. The two scans are especially distinguishable in the FF graph, where the higher values are the reverse scans and the lower the forward scans. A relevant hysteresis is immediately evident, indicating accumulation of ions and charges at the interfaces. This is consistent with previous works[292,300] and it is likely directly connected to the big perovskite/HTL offset, which facilitates the accumulation of charges at that interface. The FF and PCE statistics show that the hysteresis is particularly big for the reference devices, and it decreases upon functionalization, indicating a positive effect of the urea treatment. The hysteresis reduction is probably due to a combination of the effects from the energy level shift and the passivation, which are difficult to disentangle. Indeed a reduction of the offset decreases the probability of charges accumulation at the interface and a reduction of trap density decreases the amount of mobile ions.

Moreover, from Figure 6.4 it is possible to notice a trend in V_{oc} that is reflected in the performance. However, drawing conclusions solely from the analysis of the box charts might be misleading. Indeed the values of the different PV parameters from the reverse scan of the JV curves (often used for the determination of PSCs performance) does not reflect the real (stabilized) values because of the pronounced hysteresis. Therefore, in order to make an accurate analysis of the effects of the

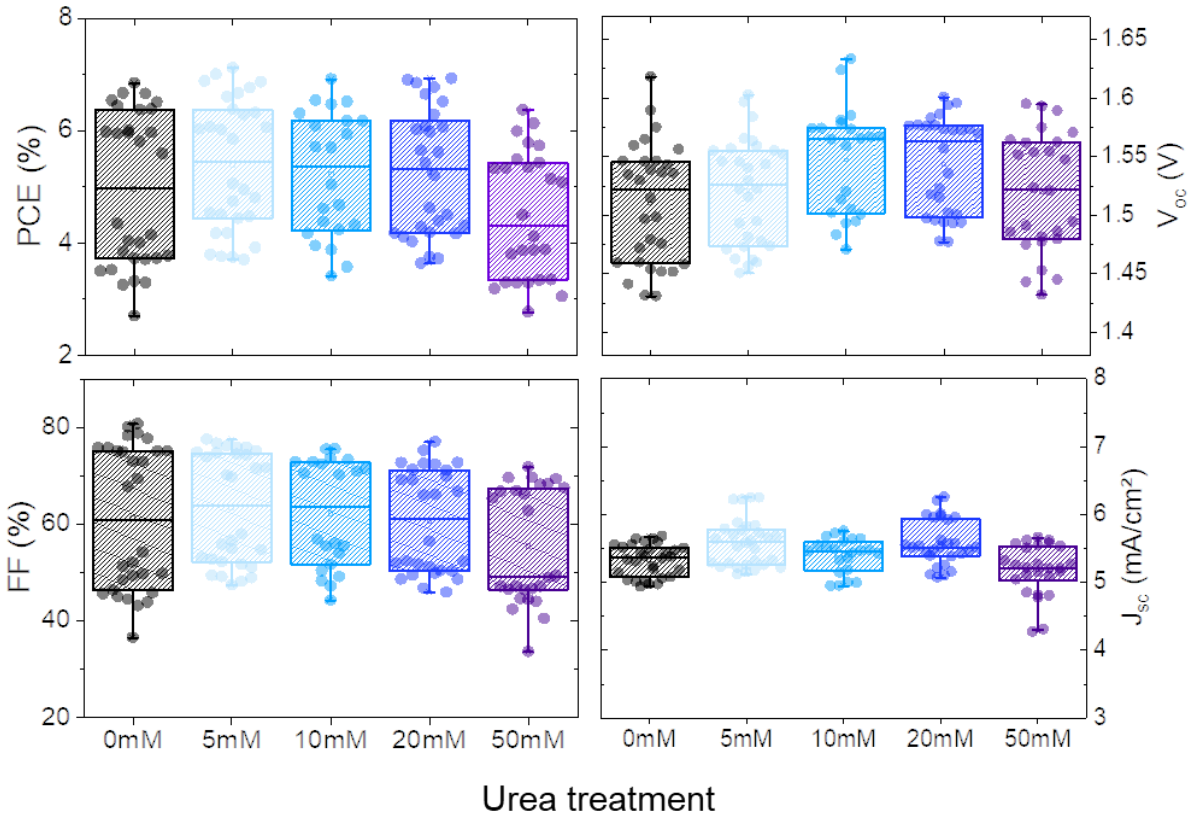

Figure 6.4. PCE, V_{oc}, FF and J_{sc} of devices with structure FTO/TiO_2/$MAPbBr_3$/urea/spiro-OMeTAD/Au for different concentrations of urea. Measurements performed in a N_2 filled glovebox with shadow masks limiting the area to 0.1 cm^2. 18 pixels (i.e. single solar cells) per condition, reverse and forward scans. Pixels showing unusual behaviours were excluded from the statistic.

functionalization, MPP- and V_{oc}-tracking have been performed. The outcome of these measurements can be considered a reliable evaluation of the actual PCE and V_{oc} of the devices, since the values are recorded over a certain amount of time (in this case ~120 s), thus without being biased by transient phenomena.

The results are displayed in Figure 6.5, where the top row shows the MPP (left) and V_{oc} (right) tracks of the best pixels and the bottom row shows the average values calculated from all the MPP (left) and V_{oc} (right) tracks measured, with the error expressed through standard deviation. The average were calculated from the values at the end of the tracks, i.e. at 120 s.

The trends for the best pixels and the average values are very similar: the devices show improved V_{oc} and PCE in presence of urea, reaching the best values for a concentration of 20 mM. The V_{oc} enhancement is of 60 mV between the average values of untreated devices and devices with 20 mM urea. Specifically the reference devices have an average V_{oc} of 1.49 eV and the 20 mM functionalized devices of 1.55 eV. The highest stabilized V_{oc} for samples with 20 mM urea corresponds to 1.58 eV, while for the best reference device gives a maximum V_{oc} of 1.54 eV. The PCE improvement from the MPP track is overall more than 1 %, while from the data in Figure 6.4 it is only around 0.5 %. This is related to the reduced hysteresis of the functionalized devices, and it highlights the importance of basing the data evaluation on stabilized values, especially in presence of a relevant hysteresis.

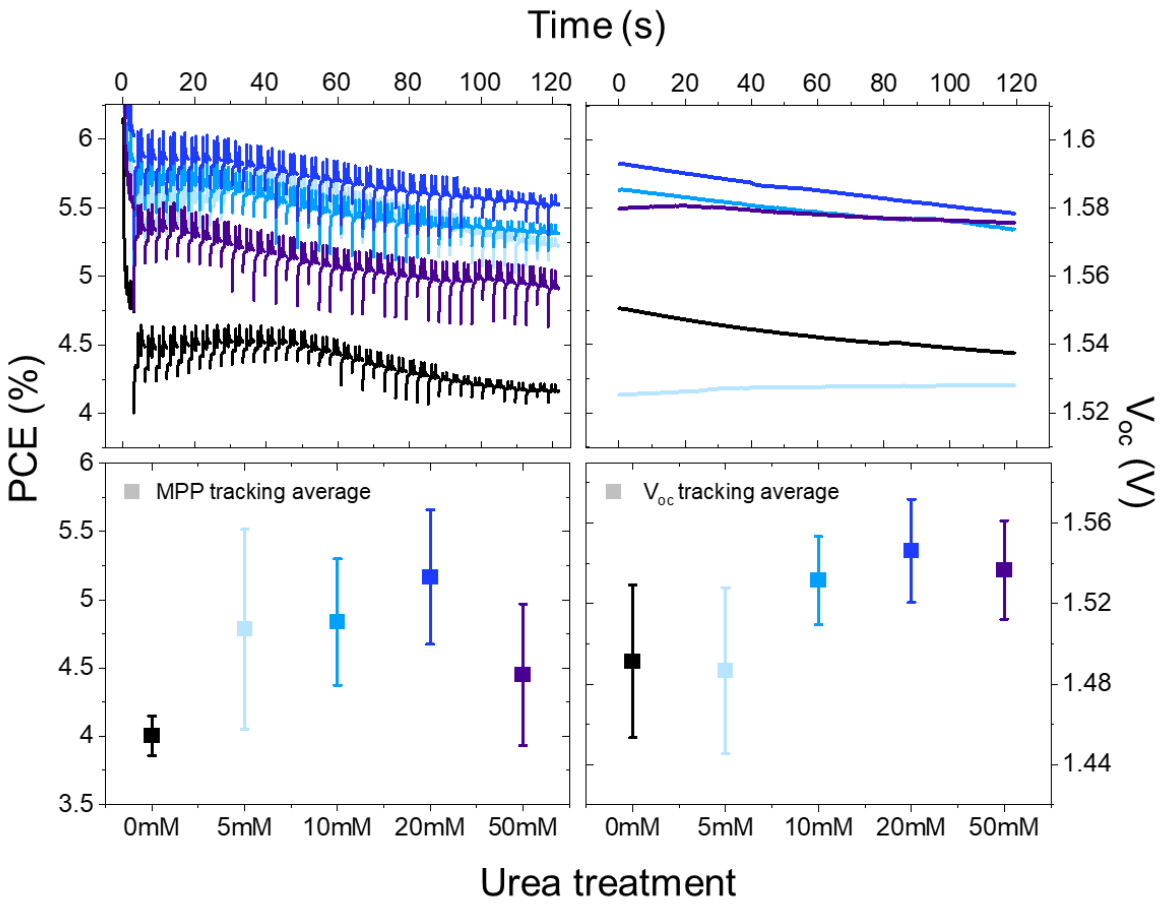

Figure 6.5. Top row: MPP- and V_{oc}-tracking (left and right respectively) of the best pixels of FTO/TiO_2/$MAPbBr_3$/urea/spiro-OMeTAD/Au devices for passivation with different concentrations of urea. Bottom row: average and respective standard deviation of the last values from the MPP (left) and Voc (right) tracks of FTO/TiO_2/$MAPbBr_3$/urea/spiro-OMeTAD/Au devices, 3-10 values per condition.

The V_{oc} seems to follow the same trend of the WF shift displayed in Figure 6.3c, i.e. no relevant change for low concentrations and then progressing increase until stabilization. This is evidence of a correlation between the two measurement and thus, based on the results from Chapter 5, of a dependence of V_{oc} from the coverage. The slight performance decrease experienced in the case of 50 mM concentration can be interpreted, similarly to the case of TOPO exposed in Chapter 5, as a possible damage induced by high concentration of urea on perovskite due to the strength of the base and its interaction with the Pb ions.[279] Alternatively, it is also possible that already at that concentration urea cannot completely dissolve in IPA, thus bringing imperfections to the film.

It is also interesting to note that for the case of 5 mM functionalization we observe a PCE improvement, but not a corresponding V_{oc} change. Therefore this enhancement is likely related to the (expected) passivating effect of urea, reflected especially in a reduction of the hysteresis and related average FF increase (Figure 6.4). For the higher concentrations, the improvement is instead probably due to a combination of the positive effects of passivation and ELA adjustment, which are generally both present when functionalizing a surface with dipolar molecules. Disentangling the two effects could be possible through a very thorough analysis with different techniques,[167] but it would be difficult to

make reliable conclusions. Nevertheless, in this case, the strong correlation between the trends in V_{oc} and WF shift supports the significant contribution of the change in ELA to the V_{oc} enhancement.

To sum up, the functionalization of $MAPbBr_3$ with a dipolar molecule able to decrease the energy levels (urea) leads to a definite V_{oc} improvement of 60 mV and a PCE enhancement of more than 1%. The result is likely related to the combined effect of passivation and ELA adjustment. However, a direct correlation between the trends in WF shift and V_{oc} is noted, pointing to the energetic tuning as main cause for the V_{oc} enhancement. As in the case of devices with triple-cation, the V_{oc} improvement is smaller than the potential offset reduction that is possible to predict on the base of the WF shift measurement. However, the improvement is considerable and the effect of the functionalization reduced the voltage loss typical of $MAPbBr_3$ devices and main bottleneck for their application.

6.3.3 Comments on the preparation and analysis of $MAPbBr_3$ devices

In contrast to triple-cation devices, whose protocol has been thoroughly optimized and it is widely used in our lab, there was no established procedure for the preparation of $MAPbBr_3$ devices. The protocol was developed on the basis of studies performed on the optimization of the deposition parameters for $MAPbBr_3$ and other perovskite compositions.[304] According to this work it is possible to obtain a smooth film without pin-holes by spin coating 80 µl of precursor solution[9] for 60 s at 4000 rpm, with 150 µl toluene drop after 10 s. However, this method leads to a film thickness of about 300 nm (Figure A4.1), which is too thin for a good solar cell, since it would be hindering the absorption and thus the current generation.[305,306] Therefore, optimization studies were performed in order to increase the thickness, specifically the spinning speed and the moment of the antisolvent drop were varied. The thickness and morphology variations were monitored via scanning electron microscopy (SEM): the results for the different conditions are reported in detail in

Figure A4.1, while Figure 6.6 display some exemplary cases. By changing these two parameters it is possible to tune the perovskite thickness up to more than 1 µm (Figure 6.6). However, as evident from Figure 6.6, with increasing thickness significant holes start to form between the $MAPbBr_3$ and the TiO_2 layers. Therefore, the optimal condition for the reparation of devices seems to be 60 s of spinning at 2000 rpm, with antisolvent drop after 15 s, resulting in a compact film of almost 500 nm, without pinholes.

The devices shown in this chapter were prepared following this protocol and it is noteworthy to point out the relevance of the obtained V_{oc} values without any functionalization. Indeed the reference devices, as those corresponding to 0 mM in Figure 6.4, show stabilized V_{oc} up to 1.54 eV. This is a particularly good result considering that the highest reported V_{oc} for $MAPbBr_3$ devices with spiro-

[9] MABr:$PbBr_2$ 1:1, 1.2 M, in DMF:DMSO 4:1

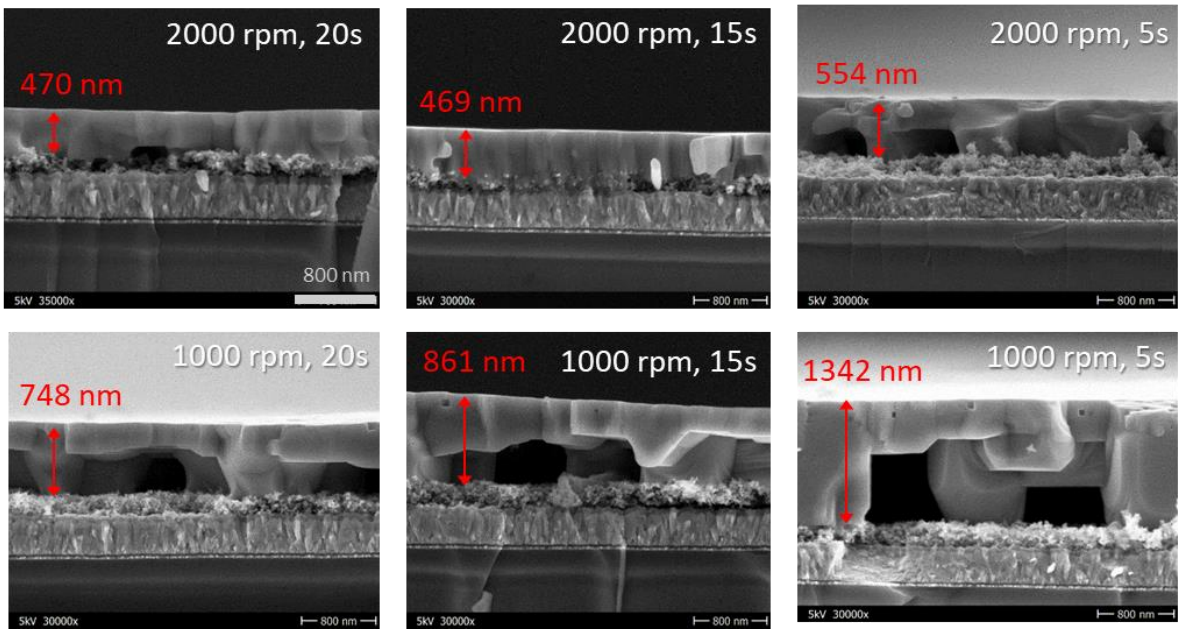

Figure 6.6. SEM pictures of FTO/TiO_2/$MAPbBr_3$ samples with different deposition reported in the single pictures as spinning time, antisolvent drop time.

OMeTAD and TiO_2 as CTLs is 1.49 eV,[300] with values obtained from JV curve, thus not stabilized. Therefore, devices with $MAPbBr_3$ prepared according to the developed protocol have great potential for achieving a new record V_{oc}, if the stack will be optimized with well aligned CTLs and proper perovskite functionalization. At the same time, further optimization is needed to achieve higher J_{sc}. The J_{sc} is, indeed, currently hindering the efficiency, in spite of the optimal V_{oc}. A J_{sc} of ~7-8 mA/cm^2 would be required to achieve the performance of the most efficient $MAPbBr_3$ devices.[164,295,301] External quantum efficiency (EQE) measurement (Figure A4.2) revealed a loss for wavelengths higher than 370 nm, which is likely the cause of the low J_{sc} and might indicate that the perovskite layer is not thick enough. In this case the preparation protocol will need to be further optimized to increase the thickness without developing the holes noticed in Figure 6.6.

Overall, the reliable characterization of $MAPbBr_3$ solar cells is not trivial. The big hysteresis and variation of the parameters (for example the V_{oc} can change over a range of 200 mV, 5-10 times higher than the variation for triple cation PSCs) makes it difficult to understand the real behaviour of the devices. For this reason it is advisable to collect a lot of data and repeated measurements in order to perform a careful statistical analysis of the results before drawing any conclusion.

6.4 Conclusions

This chapter investigates the application in devices of the energy level tuning method presented in Chapter 5. In particular, dipolar molecules are used to functionalize the perovskite surface and decrease its WF, in order to reduce the energetic offset with the HTL. This strategy is applied to PSCs with two different compositions, namely triple cation perovskite and $MAPbBr_3$. These two systems are exemplary cases of solar cells with good ELA on one side (triple cation devices) and with a bad ELA, i.e. large energetic offsets, on the other ($MAPbBr_3$ devices). After tailored functionalization, the devices showed improvement in both cases, in particular in the form of V_{oc} enhancement. For triple cation solar cells the change is limited, however drift-diffusion simulations supports its relation to a variation in ELA. On the other hand, $MAPbBr_3$ devices show a definite stabilised V_{oc} improvement of 60 meV upon functionalization using a 20 mM solution of urea, together with an increase of more than 1% in PCE. The results are obtained from stabilized PCE and V_{oc} measurements, which is particularly relevant considering the considerable hysteresis in these devices. Functionalized $MAPbBr_3$ devices also display reduction of hysteresis, compatible with a passivating effect of urea and a reduction of the offset at the interface. The V_{oc} of devices prepared with different urea concentrations follow the same trend of the WF shift measured via Kelvin probe, thus highlighting a correlation between the change in ELA and in V_{oc}.

It is therefore now possible to answer the questions posed in the introduction: *Is the energy level tuning method presented in Chapter 5 working when applied in devices? Is energy level alignment actually relevant?* Overall, the devices characterizations suggests that tuning the perovskite energetics through a layer of dipolar molecules is an effective method for adjusting the ELA and thus improving devices. Therefore, the answer to the first question is *yes*. Or better: *yes, but*. *But* it is important to consider the conditions of the system and what are the main sources of losses. Indeed, the results also stress that the effectiveness of such strategy depends on the system. Specifically the improvement will be limited if the ELA is already close to optimal, as in the case of triple-cation devices. Instead, in presence of a large energetic mismatch, as for $MAPbBr_3$ devices, the effect will be significant. And this answers also the second question: ELA *is* relevant in general, *but* it depends on the conditions of the system, and in particular on the main sources of losses. If the system presents misaligned energy levels and big offsets, than tuning the perovskite energy levels through dipolar molecules will improve the devices. On the other hand, if the system has already well-matched energy levels, than the same strategy will be less effective.

7 A HALO-FUNCTIONAL HOLE-TRANSPORT MATERIAL

This chapter is based on the peer-reviewed article "Canil, L. et al., *Halogen-Bonded Hole-Transport Material Suppresses Charge Recombination and Enhances Stability of Perovskite Solar Cells*, Adv. Energy Mater., **2021**, 2101553".[307]

Interfaces play a crucial role in determining perovskite solar cells (PSCs) performance and stability. It is therefore of great importance to constantly work towards improving their design. The study presented in this chapter shows the advantages of using a hole-transport material (HTM) that can anchor to the perovskite surface through halogen bonding (XB). A halo-functional HTM (PFI) is compared to a reference HTM (PF), identical in optoelectronic properties and chemical structure but lacking the ability to form XB. The interaction between PFI and perovskite is supported by simulations and experiments. XB allows the HTM to create an ordered and homogenous layer on the perovskite surface, thus improving the perovskite/HTM interface. Thanks to the compact and ordered interface, PFI displays increased resistance to solvent exposure compared to its not-interacting counterpart. Moreover, PFI devices show suppressed non-radiative recombination and reduced hysteresis, with a V_{oc} enhancement ≥ 20 meV and a remarkable stability, retaining more than 90% efficiency after 550 hrs of continuous maximum power point tracking. This chapter combines the improvements related to the perovskite functionalization with dipolar molecules presented in the previous chapters with the advantages of XB. The results highlight the potential that XB can bring to the context of PSCs, paving the way for a new halo-functional design strategy for charge-transport layers, which tackles the challenges of charge transport and interface improvement simultaneously.

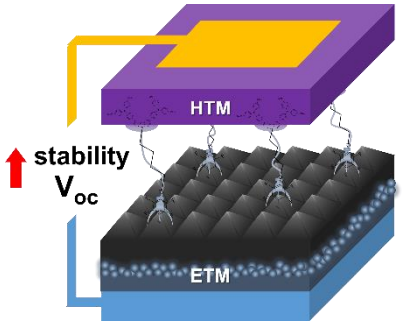

7.1 Introduction

Perovskite solar cells (PSCs) are undoubtedly one of the leading actors in the field of solar energy conversion, however, before their wide-scale use in real-world applications, several challenges still need to be addressed to improve their performance and especially their stability.[10,308] The best state-of-the-art devices possess complex stoichiometry, which leads to different perovskite surface terminations and the consequent related interactions.[33] For this reason, interfaces play a critical role in the devices' functionality, and their improvement is one of the main challenges that need to be tackled.[29,36] One of the most common approaches to optimize interfaces between different layers in PSCs is introducing an interlayer that functionalizes the perovskite surface.[33,309,310] Chapter 5 and Chapter 6 showed that this method can be used to systematically tune the perovskite energy levels and reduce interfacial recombination. Now the questions are: *Is it possible to further develop this strategy by incorporating the functionalization and energy level tuning ability directly in the subsequent charge transport layer (CTL)? And what is a good perovskite/CTL interaction for this purpose?*

Recently, some works started to integrate the functionalization feature in the CTL above the perovskite to combine (i) interaction with the perovskite surface and (ii) charge transport and extraction within one material, thus removing one additional interface.[311–315] All these works have in common the functionalization of perovskite with molecules that bind to the undercoordinated Pb^{2+} ions and focus on the passivating effect. Instead little attention is posed to the energy level alignment (ELA) and no reports exist on exploiting non-covalent interactions between CTLs and the iodide ions on the perovskite surface, of which halogen bonding[196] is a fascinating case.

As detailed in Section 3.3.2, Halogen bonding (XB) is a non-covalent electrostatically driven interaction between an electrophilic region in a molecule and a nucleophilic region in another, or the same, molecule.[192] The electrophilic region is commonly associated with a polarizable halogen atom substituted in an electron-withdrawing environment. The substitution creates a region of positive electrostatic potential within the molecule called "σ-hole".[193] The σ-hole can interact with electron-rich sites in other molecules, thus forming halogen bonding. XB is of particular interest because of its directionality, tunable interaction strength and often hydrophobicity.[192,196] Thanks to these unique features, XB has been widely exploited in the context of soft functional materials and crystal engineering,[208] for example, for the design of supramolecular gels[316] and liquid crystals[317] or the development of light-responsive polymers.[318]

Halogen bonding was first introduced to the PSCs field in 2014 by Abate *et al*.[212]. They functionalized the perovskite surface with iodopentafluorobenzene (IPFB), achieving suppressed recombination and

improved charge extraction due to the screening effect of the molecule on the electrostatic charge of the iodide ions. Later on, various works have highlighted the positive impact of XB on the perovskite crystallographic structure, thus leading to a more symmetric surface.[213,214,216] Moreover, XB allows the formation of ordered and structured layers, and several studies have reported improved stability and performance in devices.[215,216,319] Based on these findings, XB appears as an optimal supramolecular strategy to improve interfaces and, consequently, performance and stability in PSCs. However there is no report on XB being used in combination with materials with charge-transport properties to obtain CTLs that directly interact with the perovskite surface. Developing such material could enable forming an ordered and neat interface promoting stability and performance in devices without introducing an interlayer between perovskite and CTL.

This chapter presents a carbazole-based material ($C_{62}H_5F_4IN_3O_5$ - named PFI, Figure 7.1a) with good hole selectivity, stability, and energy levels position, which is capable of anchoring to the perovskite surface through XB thanks to a σ-hole generated by the presence of an iodine atom within the molecule.[196,212] The material was designed by collaborators from the *University of Tampere* in the frame of the *SolarWAVE project* (see Appendix A6). The results were compared with PF ($C_{62}H_5F_5N_3O_5$, Figure 7.1b), a material with the same structure and properties except for the absence of the iodine atom and therefore lacking the ability to form XB. The findings presented in this chapter show that the XB-donating material interacts strongly with the perovskite layer, enhancing the samples' resilience to solvent exposure, improving the energy level alignment (ELA) in devices and suppressing non-radiative recombination. The employment of PFI as hole-transport material (HTM) in PSCs results in an open-circuit voltage (V_{oc}) enhancement of about 20 meV compared to PF, together with a reduced hysteresis and significantly enhanced stability, maintaining more than 90% of the post burn-in efficiency after 550 hrs of continuous maximum power point (MPP) tracking and with a projected T_{S80} of ~2600 hrs. These results are ascribed to XB between perovskite and the HTM, which allows the formation of an ordered interfacial layer. Moreover, the findings are coherent with a study from Dai *et al.*[10],[320] where an I-terminated SAM was employed at the interface between SnO_2 and perovskite, resulting in increased adhesion toughness at the interface and leading to devices with reduced hysteresis, enhanced V_{oc}, and improved operational stability.

The results reported in this chapter suggest that designing materials that can interact with the perovskite surface via specific supramolecular interactions while simultaneously acting as CTLs is crucial for tackling the challenges related to interfaces in PSCs and can bring significant improvement to devices. This chapter highlights the advantages of XB as the supramolecular interaction of choice in HTM design for PSCs, proposing a new approach to develop tailored charge transport materials for PSCs.

[10] The study was published around the time the manuscript on which this chapter is based was submitted.

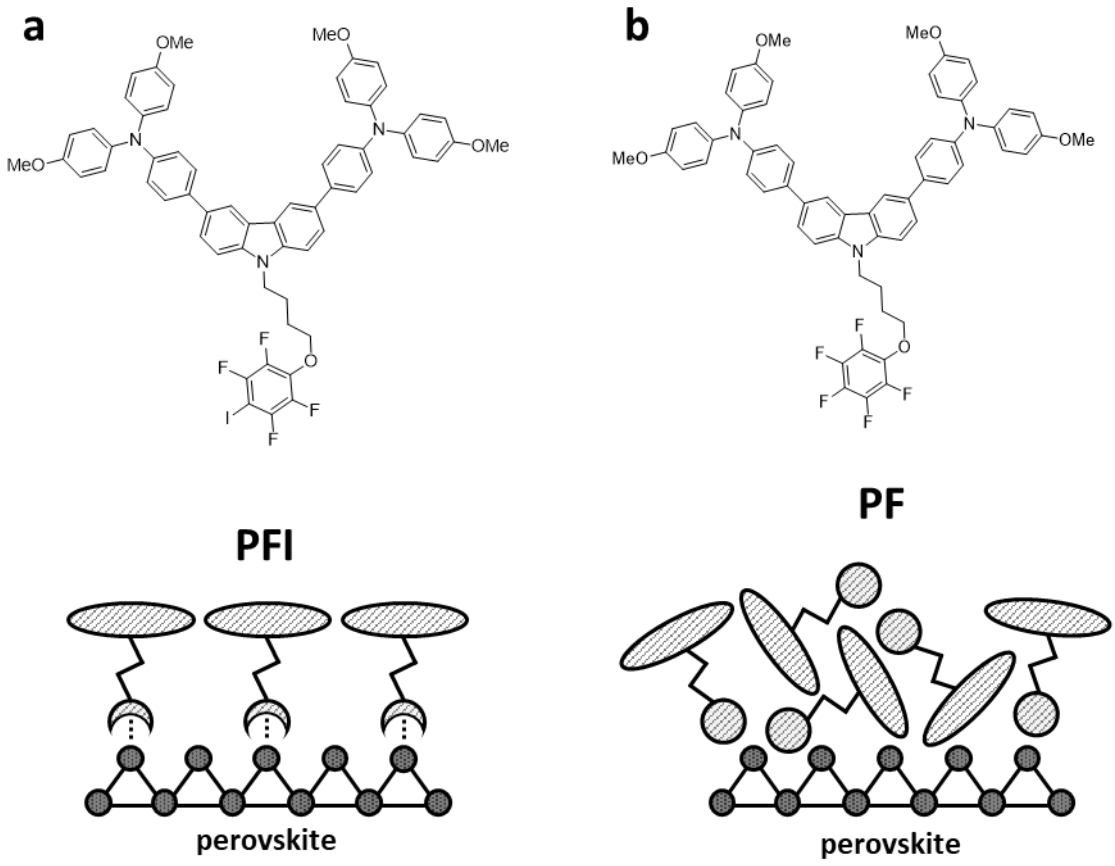

Figure 7.1. Molecular structures and respective hypothesized arrangement on the perovskite surface for PFI (a) and PF (b).

7.2 Understanding the interaction of PFI and PF with the perovskite surface

Figure 7.1 shows the molecular structure of the two materials and the respective expected arrangement on the perovskite surface. As mentioned above, the presence of σ-hole in PFI allows the material to form XB with the halides on the perovskite. At the same time, the pentafluoro moiety in PF is unable to interact via XB and does not form specific chemical interactions. Therefore, PF can act as a reference to explore the effects of PFI's XB with perovskite.

It is possible to think of these materials as a composition of two parts serving distinct functions: the carbazole-based core, responsible for the energy levels and hole-transport properties, and the fluorinated ring, connected to the core through an alkyl chain, responsible for interactions with the perovskite surface. As represented in Figure 7.1a, PFI can be simplistically depicted as an HTM with a clawed arm, which allows the material to anchor to the surface via XB and form an ordered layer. On the contrary, PF molecules will most likely assume a random distribution on the perovskite, as

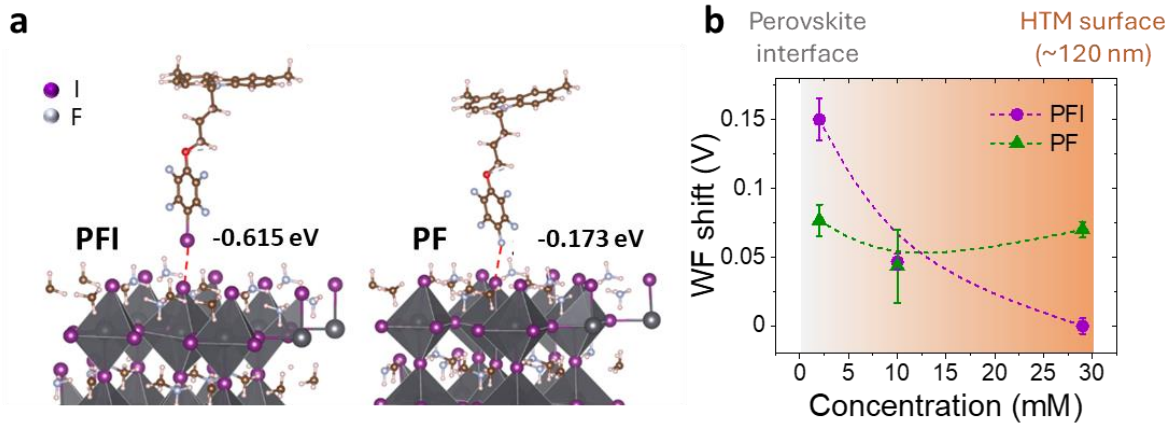

Figure 7.2. (a) DFT simulations of the adsorption of PFI (left) and PF (right) on $MAPbI_3$ perovskite exemplified for the case of MAI terminated surface with an indication of the respective adsorption energies (Pb-terminated surface in Appendix A5). (b) Kelvin Probe measurements showing how the work function (WF) of PFI and PF changes for different solution concentrations compared to the WF of PFI at 29 mM (i.e. the concentration used for all HTMs in devices), which is set as 0. Measurements performed in air on FTO/TiO_2/perovskite/HTM samples.

schematized in Figure 7.1. The hypothesis presented here is that the improved interface with PFI can promote stability and prevent ion accumulation, thereby bringing several advantages to the devices.

The moiety which is responsible for XB in PFI was already proven to form such bond with perovskite by Abate *et al*.[212] and later further investigated by Zhang *et al*.[213]. However, additional theoretical and experimental analyses were performed in order to understand the interaction of the molecules with the surface and to find evidence of the anchoring properties of PFI.

First, the interaction of PFI and PF with the perovskite surface was simulated using $MAPbI_3$ as the prototype lead halide perovskite. The adsorption of the molecules has been modelled on the (001) surface of tetragonal $MAPbI_3$ for MAI-terminated and PbI_2-terminated surfaces,[168,321,322] where MAI is methylammonium iodide.

As highlighted by the absorption energy values reported in Figure 7.2, the simulations reveal that PFI consistently exhibits adsorption energy 2-3 times higher than that for PF, evidence of a much stronger interaction of the former with the perovskite surface. This is irrespectively of the molecule-slab orientation and the termination of the perovskite surface (the different cases are reported in

Figure A5.1 and Table A5.1). Although the adsorption of PFI is favoured in a parallel adsorption mode, i.e. with the phenyl ring placed parallel to the perovskite surface (see Figure A5.2), the $I\cdots I^-$ interaction is instead maximized when the molecule is placed in perpendicular configuration (see Figure 7.2a), showing an almost linear interaction angle. This trend is expected from the directional nature of XB due to the narrow positive area corresponding to the σ-hole[196]. In contrast, the low adsorption energy of PF suggests that there is no preferred interaction for this molecule, and its distribution and orientation probably depends on weak intermolecular interactions within adsorbed molecules. The simulations thus indicate the presence of XB between PFI and the perovskite layer. Moreover, the strength of the PFI-perovskite interaction compared to the PF-perovskite interaction supports our interpretation that PFI can anchor itself to the perovskite, likely providing a well-defined layer at the

interface. In contrast, PF molecules will probably assume random orientations and, therefore, a less uniform and compact distribution. These results are coherent with the first-principles analysis performed by Zhang *et al*.[213] on the adsorption of IPFB, which correspond to the part of PFI capable of interaction. In that study, the authors show that IPFB adsorption positively affects the structure and orientation of perovskite at the interface. The molecule resides stably at its position on the surface, with adsorption energy comparable to that calculated here for PFI.

Experimental evidence that PFI, in contrast to PF, interacts with the perovskite surface is given in Figure 7.2b. Here Kelvin Probe (KP) was used to measure the work function (WF) of doped PFI and PF spin-coated with different concentrations on the perovskite layer. The perovskite used was triple cation perovskite with precursor solution composition $Cs_{0.05}(FA_{0.85}MA_{0.15})_{0.95}Pb(I_{0.85}Br_{0.15})_3$. Low concentrations correspond to a situation were there are only one or few monolayers of PFI and PF, thus allowing to observe the energetics at the perovskite interface. High concentrations (i.e. 29 mM) correspond to a layer of around 120 nm, which is the condition used in devices. At this concentration the measured WF is the one of the material itself. The results show that the WF of PF remain constant for the different concentrations, while PFI varies. This suggests that PF does not bind to anything specific. The molecules distribute randomly on the perovskite surface, thus what we measure is always the WF of PF, at all concentrations, without any additional effect due to interfacial interactions. The altered WF of PFI at the perovskite interface compared to its value at 29 mM can instead be ascribed to the XB interaction and it is coherent with the shift that such a dipole induce.[232,260] Therefore this measurement experimentally support the interaction between PFI and the perovskite. This specific result not only support the claim of an interaction between PFI and perovskite, but it further validates the statements of Chapter 5.

7.3 Resilience to solvent exposure

The resilience of perovskite/HTMs samples to solvent exposure was tested in order to further demonstrate the presence of an interaction between PFI and perovskite. The samples were immersed for 15 s in ethanol (a solvent that can slowly dissolve the materials) and, immediately after, UV-Vis absorption spectra were recorded to assess any possible change in the films, which can be detected through changes in the optical properties. The measurements were done in reflection mode to be more surface sensitive and focus on the HTM layers rather than the perovskite bulk. The procedure was repeated several times up to 60 s of solvent exposure to monitor the dissolution process of PFI and PF.

Figure 7.3a shows how the reflection spectra for PFI (right) and PF (left) change for different dipping time intervals. The peaks at ~ 400 nm (A in Figure 7.3) are characteristic of the two HTMs (see UV-Vis of the pure materials in Figure A5.4), while the peaks at ~ 800 nm (B in Figure 7.3) are associated with

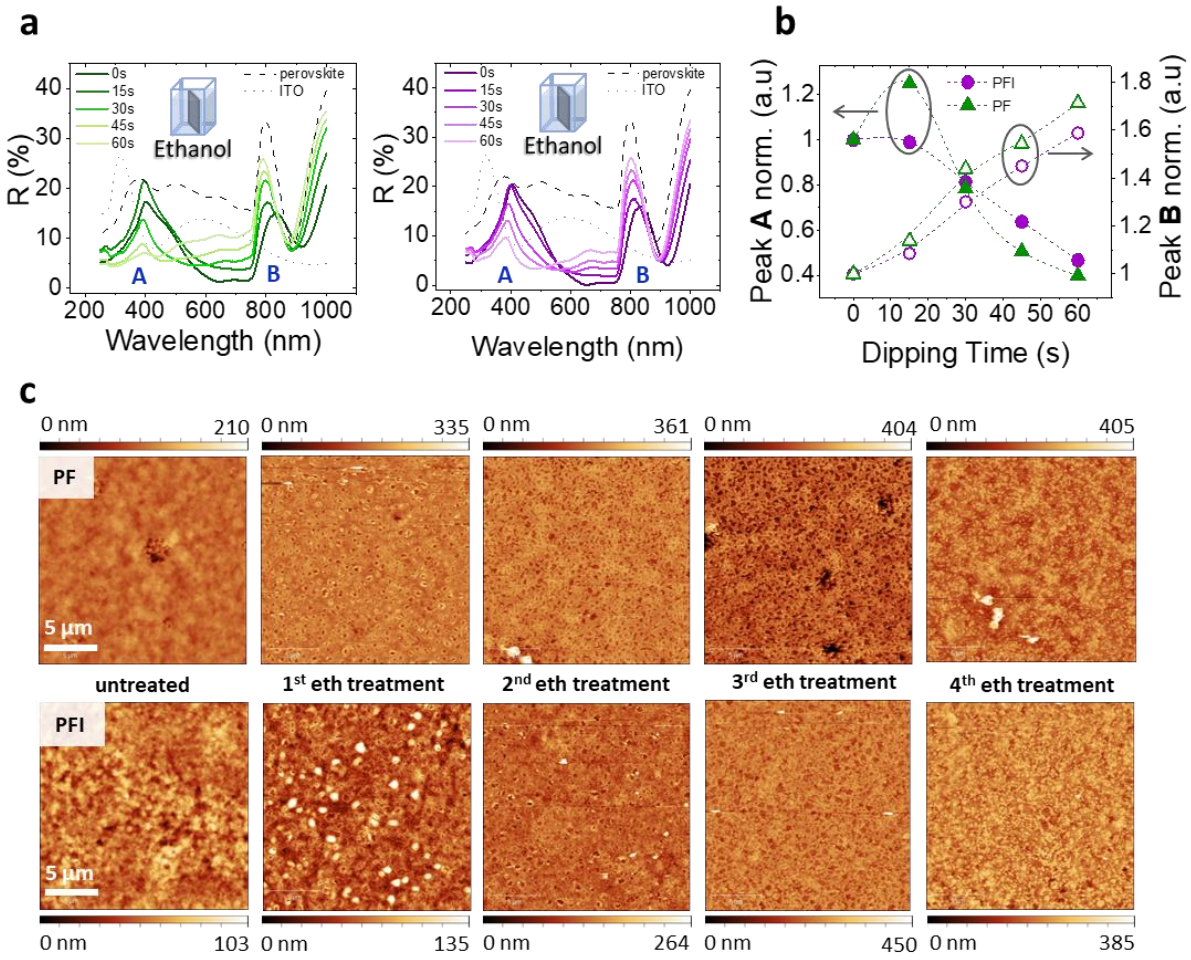

Figure 7.3. (a) UV-Vis reflection spectra of ITO/perovskite/PFI (left) and ITO/perovskite/PF (right) samples after immersion in ethanol for different time intervals. (b) Comparison of the change in intensity of the peak at A and B for PFI and PF depending on the dipping time. (c) AFM topography maps of PF (top) and PFI (bottom) deposited on glass/perovskite with 29 mM concentration. The different maps, ordered orizontally, represent the effect of subsequent ethanol treatments on the morphology for the two materials.

the perovskite layer detected through the HTMs. As a reference, the figures also show the signals for the ITO substrate and the bare perovskite layer. With this in mind, it is possible to compare the two materials and observe as a general trend that A decreases with dipping time while B increases. This means that the signal coming from the HTMs is decreasing in intensity with dipping time, while that related to the perovskite is increasing, which matches the idea that the two materials are dissolving and "exposing" more the underneath layer, i.e. the perovskite. Figure 7.3b highlights the behaviour of the two materials by showing A and B normalized at the initial condition, i.e. before exposure to ethanol. The results after the first 15 s in ethanol are particularly interesting. We can observe how for PFI, the intensity of the A peak remains stable, while for PF, we can see an increase in the signal. The latter can be interpreted as due to the formation of agglomerates of PF at the surface. After exposing the sample to the solvent for a further 15 s, the signal decreases to under the initial value and keeps this trend for the following dipping sessions. Therefore, it seems that PF clusters are initially formed due to the material desorption and are afterwards washed away while the film is slowly dissolving.

On the other hand, the fact that PFI remains stable during the first 15 s of solvent exposure indicates that the material is more resilient to dissolution. This can be ascribed to XB between PFI and the halide ions at the perovskite surface, which makes more difficult to detach molecules and increases the hydrophobicity of PFI thanks to the formation of a more ordered layer, making it more resistant to polar solvents. The increase in hydrophobicity is furthermore supported by water contact angle measurements, showing a contact angle of more than 92° in the case of PFI and 89° for PF (Figure A5.5).

It is also relevant to note that, after the initial 15 s of ethanol dipping, the A peak for PF starts to decrease at a faster rate than for PFI, indeed indicating a different resistance to re-solubility for the two materials. Similar observations can be done for the evolution of peak B: the stronger it becomes, the more it is possible to "see" the perovskite layer, i.e. the thinner the HTM. As highlighted in Figure 7.3b, the B peak for PF increases its intensity faster than PFI, especially during the first 30 s.

To further support the results, the test was repeated while measuring UV-Vis in transmission mode (Figure A5.6). In this case, since most of the signal comes from the perovskite layer, it is more difficult to draw conclusions. Nevertheless, it is possible to notice that, except for an initial shift after the first dipping interval, the PFI spectrum remains almost unchanged, while the PF one becomes more and more similar to the perovskite reference, indicating likely an increased dissolution of the material.

An additional characterization via atomic force microscopy (AFM) was performed as complementary measurement to UV-Vis and in order to strengthen the claim stated above. PFI/PF-coated films were exposed to the solvent and the change in topography was monitored. The results are reported in Figure 7.3c and are coherent with the trend observed through UV-Vis. Specifically, it is possible to notice that, upon solvent exposure, holes start to form on the surfaces and their density increase after every treatment. However, while PF displays a high density of holes directly after the first exposure to ethanol, PF seems to remain more stable, with the apparent formation of agglomerates, but not evident damage. Overall, it appears that PF degrades faster than PFI upon ethanol treatment.

Together with allowing a further monitoring of the dissolution process, AFM images of two different untreated PFI and PF films (Figure A5.7) show features that could be evidence of diverse stacking for the two materials. In particular, PF present some imperfections displaying holes in a circular pattern, which are instead absent in PFI films. This might suggest that the ordered interfacial monolayer formed in the case of the halogen-bonded PFI molecules can help the growth of more compact and uniform upper layers compared to PF. Therefore, it can be speculated that the patterns of holes visible for the latter could be related to a less compact stacking.

Overall, the findings from UV-Vis and AFM support the beneficial effects of XB and clearly show how the capability of an HTM of interacting with the underneath layer, in this case perovskite, can positively affect its hydrophobicity and resilience to dissolution, resulting in improved stability of the whole system.

Table 7.1. Optoelectronic properties of PFI, PF, and spiro-OMeTAD. λ_{abs} is the absorption wavelength, E_G is the bandgap, μ is the hole mobility. Energy levels measured in solution and without dopants. Measurements details in Appendix A5.2.

HTM	λ_{abs} (nm)		HOMO (eV)	LUMO (eV)	E_G (eV)	μ ($cm^2V^{-1}s^{-1}$)	
	liquid	*solid*				*undoped*	*doped*
PFI	336	337	4.96	1.86	3.1	$2.0x10^{-5}$	$2.2x10^{-4}$
PF	336	337	4.97	1.87	3.1	$2.5x10^{-5}$	$2.0x10^{-4}$
Spiro-OMeTAD			4.82			$6.0x10^{-5}$	$7.2x10^{-4}$

7.4 Application in devices

The results until now brought evidence that PFI can anchor to the halides on the perovskite surface through XB, promoting the formation of an ordered and stable interfacial layer compared to the reference PF. To evaluate the applicability of these materials in devices and assess the related effects, their optical properties, energy levels and hole mobility were tested. The relevant results are highlighted in Table 7.1, while further details are reported in the Appendix A5.2. UV-Vis absorption measurements in liquid and solid-state show negligible absorbance in the visible range, thus excluding an interference between HTMs and perovskite absorption. The energy levels of undoped materials reported in Table 7.1 were determined through differential pulse voltammetry, while the WF of the doped HTMs were compared with that of spiro-OMeTAD through KP measurements (as previously discussed and shown in Figure 7.2b). Moreover, the space-charge-limited-current method[324] was employed to measure the mobilities, both with and without dopants. The two materials exhibit comparable values, just slightly lower than those measured for spiro-OMeTAD as reference.

7.4.1 Devices performance

The above presented results suggest that the HTMs are suitable for perovskite-based devices. Hence, n-i-p devices with doped PFI and PF as hole transport layers were prepared and the respective performances tested. Statistics on the resulting photovoltaic parameters are reported in Figure 7.4a and Table 7.2, together with the values for the best pixels. Furthermore, Table 7.2 also shows the results for devices with spiro-OMeTAD as HTM (fabricated in identical conditions) to highlight that PFI- and PF-based solar cells can reach the same efficiency as those with the state-of-art HTM spiro-OMeTAD. It is worth noting that spiro-OMeTAD was chosen as reference because of its wide use,

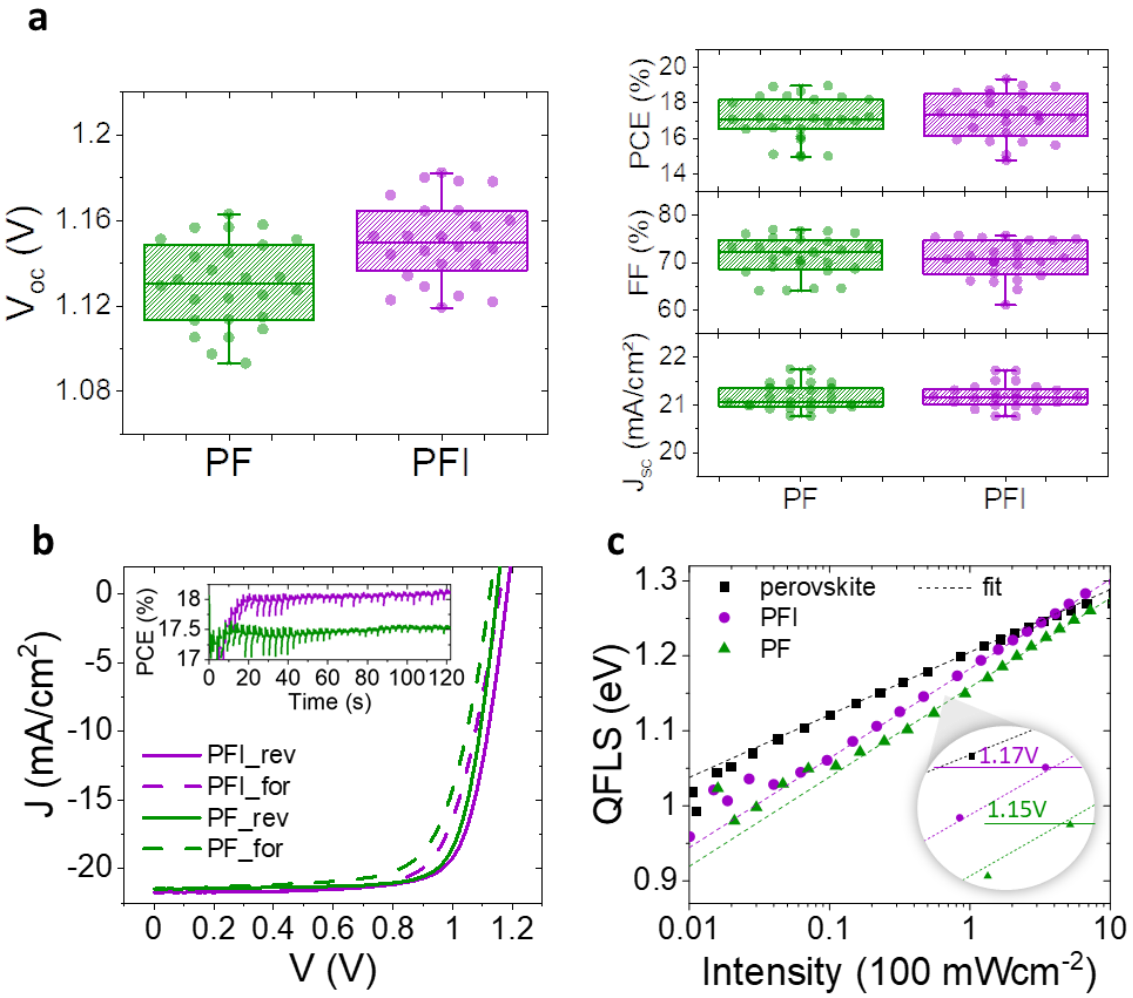

Figure 7.4. (a) Photovoltaic parameters of n-i-p devices with structure FTO/TiO_2/perovskite/HTMs/Au, box charts from 12 and 13 pixels (i.e. single solar cells) for PFI and PF respectively, reverse and forward scans. (b) *JV*-curves of the best pixels recorded at 100 mV/s scanning speed in the inset MPP-tracking of the reported pixels. (c) Absolute steady-state PL measurements for different light intensities showing the QFLS for glass/perovskite and glass/perovskite/HTMs (doped), with a highlight on the difference in values between PF and PFI. Measurements performed on the film side.

however other HTMs enabled reaching high efficiency, sometimes even without the use of dopants.[325–330] It is foreseeable that the concept of halo-functional HTM introduced here could be further developed to achieve even higher efficiencies, ideally without the need of doping. Therefore this work aims at showing the advantages of this kind of HTM, hoping to pave the way to a new set of halo-functional materials leading to high efficiency and stable devices.

The results presented in Figure 7.4 show that employing PFI over PF as HTM has positive effects on devices, especially in terms of reduction of interfacial charge recombination and ion density. As reported in the literature, the XB functionalization does not change the optoelectronic properties of the substrates,[215,216] therefore, it is essential to point out that its advantages instead come from the ordered and homogeneous distribution of the molecules at the interface. FF and J_{sc} remain similar in the two cases, while there is a definite V_{oc} improvement in devices comprising PFI. This leads to an increase in PCE, especially visible from the stabilized power output in the inset in Figure 7.4b. Specifically, an average V_{oc} enhancement of about 20 meV (increased to more than 30 meV for the

Table 7.2. Photovoltaic parameters and hysteresis index (H-index) of devices with PFI, PF and spiro-OMeTAD for the best pixels and the average (avg.) of 12, 13 and 14 pixels, respectively. The stabilized power output corresponding to the best pixels for 120 s MPP-tracking is also reported. H-index is calculated as PCE_{rev}/PCE_{for}, where rev and for are reverse and forward scan, respectively

HTM	PCE (%)			V_{oc} (mV)		FF (%)		J_{sc} (mA/cm²)		H-index	
	$Best_{JV}$	$Best_{stabilized}$	Avg.	Best	Avg.	Best	Avg.	Best	Avg.	Best	Avg.
PFI	19.3	18.1	17.3	1182	1150	75	72	21.7	21.3	1.08	1.07
PF	19.0	17.5	17.1	1148	1130	77	71	21.5	21.2	1.18	1.12
Spiro-OMeTAD	19.5	19.3	18.0	1181	1154	75	72	22.2	21.0	1.05	1.07

best pixels) is observed, which suggests that PFI suppresses the charges' capability of recombining at the perovskite/HTM interface. This behaviour is confirmed by the data shown in Figure 7.4c. Photoluminescence (PL) measurements were performed on perovskite/HTM stacks (with doped HTMs) and on the neat perovskite layer at different light intensities to extract the internal voltage of the partial cell stack, i.e. the quasi-fermi level splitting (QFLS). Considering that the QFLS of the perovskite/HTM stack is almost identical to the neat layer at one sun, this measurement highlights that PFI nearly overcomes the interfacial recombination loss typically caused by the deposition of an HTM on top of perovskite. This scenario is particularly relevant since it is one of the leading causes of V_{oc} loss in PSCs.[34,36,331] Moreover, the difference between the QFLS of PFI and PF at one sun is around 20 mV, matching perfectly with the V_{oc} enhancement obtained from the devices. This measurement, therefore, highlights the ability of PFI to suppress recombination and confirms that the increase in V_{oc} is related to the difference between PFI and PF, i.e. the ability of PFI of forming XB and thus a neat interface.

The positive effect of PFI in suppressing the recombination is also supported by a reduction of the hysteresis in the *JV* curves, as evident in Figure 7.4b and stressed by the hysteresis indexes (H-indexes) calculated in Table 7.2. It is indeed known from the literature that hysteresis mainly arises from the absorber material and that interfaces and CTLs are fundamental for its reduction.[128,135] Specifically, hysteresis is often correlated to the detrimental effect of mobile ions.[26,129,133] In this case, PFI is likely to limit their migration by anchoring itself to the halide ions on the perovskite, promoting the formation of a better-terminated surface compared to PF.

7.4.2 Operational stability

The advantages of using a halo-functional HTM in perovskite-based devices are evident in the photovoltaic performance of the devices and their stability under working conditions. Two different batches of devices were tested using a custom-made ageing setup and keeping identical conditions in both cases. The tests were performed according to ISOS-L-1I.[77] All pixels were tested in a controlled environment under continuous MPP-tracking at one sun illumination to assess their long-term stability. a reports the results of one of the tests as an example, while the other one is shown in Figure A5.10. In the case presented in Figure 7.5a, the devices were aged for approximately 550 hrs, and the displayed MPP tracks are the average of 7 pixels and 4 pixels for PFI- and PF-based devices, respectively. Pixels showing significantly different performances were removed from the average. The data were normalized to the value at ~ 10 hrs, after the so-called "burn-in",[332] and plotted in logarithmic scale from that point, with error bars giving the standard deviation. A plot in linear scale and from 0 h is displayed in Figure A5.9.

Both PF- and PFI-based devices retain more than 90% of their initial efficiency during the measurement, evidence of excellent stability. Devices with PFI as HTM show enhanced stability compared to devices with PF. Although the difference is not large, it is significant considering that the trends represent the averages of several devices. This result is of particular importance because, in real-world applications, a long term stable energy output is more relevant than the efficiency obtained from JV-curves. As an approximation, their stability trend were linearly projected to identify the probable T_{S80},[77,332] i.e. the time at which the efficiency has reached 80% of the value after burn-in. PFI-based devices deliver a remarkable projected T_{S80} of ~2600 hrs, more than double of that extrapolated for PF-based devices.

It is also significant to note that the number of devices that remained operational after the ageing test is higher for PFI. Indeed, as represented in Figure 7.5b, if all the tested devices (6 devices per HTM with a total of 36 pixels per HTM) are taken into account, less than half of the pixels using PF as HTM survived the ageing test, in contrast to devices with PFI which show more than 80% of working pixels. Note that these statistics count as "non-operational" devices that do not show power output after the test and devices that displayed particularly unusual behaviours during the test.

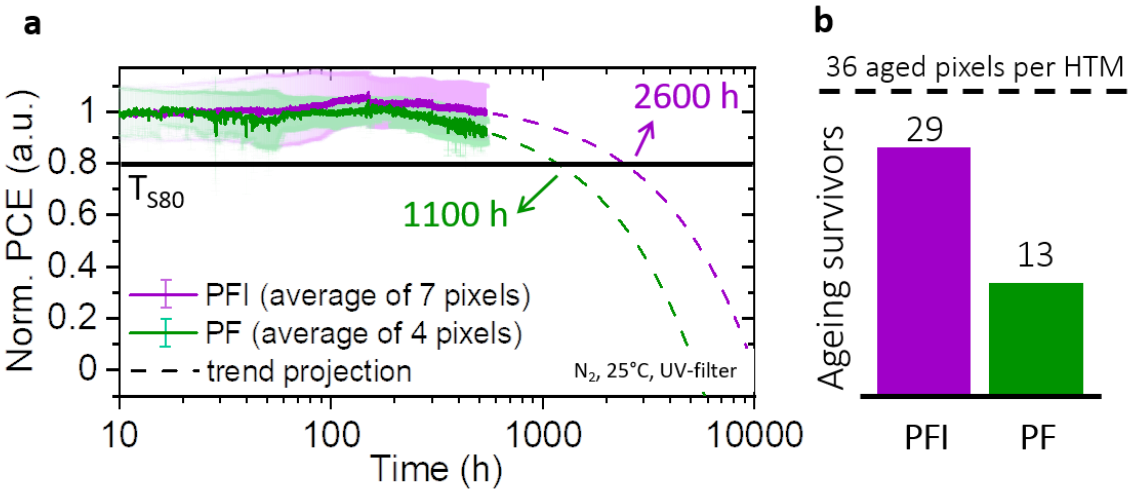

Figure 7.5. (a) Normalized PCE of FTO/TiO_2/perovskite/HTMs/Au devices for ~ 550 h of continuous MPP-tracking under 1 sun illumination. The measurements were performed through a custom-made ageing setup in an N_2 atmosphere with a UV-blocking filter. The device temperature was actively kept at 25°C. Average of 7 pixels for PFI and 4 pixels for PF, corresponding to one measured batch. Another batch was tested, leading to the same trends (Figure A5.10). Pixels showing significantly different performances were removed from the average. Data are plotted in log scale, with error bars (standard deviation) and were normalized to the value at 10 hrs, corresponding to the end of the so-called "burn-in".[332] Dashed lines represent the linear projection of the stability trend to identify the time at which 80% of the efficiency from the end of burn-in is reached (T_{S80}[77]). (b) Statistics displaying the pixels that still showed power output after the test and did not show any unusual behaviour during the test ("ageing survivors") compared to the total number of aged pixels in the course of two tests. A pixel is a single solar cell in a device.

PSCs' operational stability can be affected by different external and internal elements.[28] Considering that the ageing tests were performed in an N_2 atmosphere and at controlled temperature, the observed difference in stability is likely connected to intrinsic factors. In particular, as already mentioned before, the ability of PFI to anchor to the halide ions on the perovskite can prevent them from moving under light and bias. It is believed that ion migration is one of the primary sources for PCSs' intrinsic degradation.[71,121] Indeed, this phenomenon leads to vacancies and other defects, therefore increasing the number of recombination centres. Moreover, ions can accumulate at interfaces and create unfavourable electric fields. For these reasons, the interaction between PFI and the I^- ions likely plays an essential role in limiting ion migration, reducing hysteresis and improving the long-term operational stability of the devices, which is a result of high importance considering that stability is one of the main problems associated with PSCs.

7.5 Conclusions

This chapter presents a halo-functional material (PFI) that can act both as HTM and anchor to the perovskite surface through halogen bonding (XB), forming a well-ordered interface. The results for PFI were compared with a reference material (PF) identical in structure except for the iodine atom enabling the interaction. Theoretical and experimental evidence suggests that PFI has a strong and directional interaction with the perovskite surface that makes the samples more resilient to degradation than PF. Moreover, the presence of XB leads to suppression of recombination and ion migration. This is reflected in a ≥ 20 mV V_{oc} improvement, reduction in the JV hysteresis and operational stability enhancement in the corresponding devices. Solar cells with PFI as HTM display excellent stability after 500 hrs under continuous MPP-tracking and with a projected T_{S80} of ~ 2600 hrs, which is more than double than what was obtained for devices with PF. Therefore, to answer the questions posed in the introduction, *it is indeed possible to further develop the energy level tuning strategy by incorporating the functionalization ability directly in the subsequent CTL,* and *XB is an optimal perovskite/CTL interaction for this purpose*. Indeed, the results clearly highlight the benefits of XB and prove it to be a successful concept in the context of PSCs.

In conclusion, this chapter shows that, by combining charge transport capability and the ability to interact with the iodides on the perovskite surface into one material, it is possible to create an HTM that can orderly anchor to the perovskite layer, thus promoting a well-defined interface, which is critical for obtaining efficient and, most importantly, stable perovskite solar cells.

8 CONCLUSION AND OUTLOOK

Perovskite solar cells (PSCs) are complex devices that require the combination of several layers and their properties in order to work. The number of factors to take into account is enormous, each layer needs to satisfy specific chemical and physical requirements not only to serve its own purpose, but also in relation to the other layers. As a consequence, the interface between the different materials is one of the most significant weak points in these kinds of devices. It can hinder the charge carriers' transport and be a source of significant non-radiative recombination.

This dissertation deals with the challenges associated with such interfaces, especially the interface between the perovskite and the subsequent layer, which is considered one of the main sources of losses in PSCs.[34] In particular, the work here presented focuses on the energy level alignment (ELA) between the absorber (perovskite) and the hole-transport layer (HTL), and on the improvement of stability at that interface. The relevance of ELA is a heavily debated topic in the scientific community. On the other hand, it is generally accepted that aligned energy levels among the different layers are beneficial for an efficient charge transport and extraction with low recombination at the interfaces. In order to achieve this condition, the charge transport layers (CTLs) need to be chosen making sure that their energetic bands satisfy a proper ELA with the respective adjacent layers. However, this requirement can be eased by possessing the ability of directly modifying the position of the energy levels within the device.

The work in this dissertation introduces and discusses a method to *improve the interface of the perovskite with the adjacent layer*, with a focus on *ELA adjustment*, *reduction of non-radiative recombination,* and *stability enhancement*. Specifically, molecular assemblies are used to functionalize the perovskite surface and induce an energy level shift together with a saturation of the dangling bonds. To achieve this result, the molecules need to possess specific properties. In particular, they need to have a dipole and they need to be able to interact with the perovskite. The range of molecules that have these characteristics is broad. Some of them are explored throughout this dissertation, specifically Lewis acids and Lewis bases able to interact with the different ions on the perovskite surface. The results highlight a particular category: molecules with the ability to form halogen bonding (XB) with the perovskite. XB-driven assemblies show the ability to create an ordered and homogenous layer, thus improving and stabilizing the perovskite/HTL interface.

Overall, Chapter 5 introduces a method for tuning the perovskite energy levels. This method was already known in semiconductors physics, but it was not yet shown to work on PSCs. Chapter 6

demonstrates and comments the application of this method on different kinds of devices, namely PSCs with different perovskite compositions (triple cation and $MAPbBr_3$). Chapter 7 further develops the concept by incorporating the functionalization and energy level tuning strategy in a novel hole-transport material that can interact with the perovskite via XB. In particular, this chapter shows the advantages that such interaction can bring to PSCs, especially in terms of stability.

The method introduced in Chapter 5 consists in exploiting the effect of interfacial dipoles induced by dipolar molecules. A layer of dipoles generates a shift in the local vacuum level, thus decreasing or increasing the work function, ionization energy, and electron affinity of a material. The direction of the shift depends on the direction of the collective dipole: a dipole pointing towards the surface (with the dipole defined as "-" to "+") shifts the vacuum level upwards, while a dipole pointing towards outside shift the vacuum level downwards. The interfacial dipole can be achieved through molecules that possess an intrinsic dipole and/or generate an "interaction dipole" when binding to the surface. Therefore, functionalizing a surface with a layer of dipolar molecules induces a shift of the material's energy levels. This strategy is commonly used to adjust the energy levels of materials with a flat and homogeneous surface, such as transparent conductive oxide layers. However, the task is more challenging on the rough and chemically varied perovskite surface.

The results from Chapter 5 demonstrates that it is possible to functionalize the perovskite surface with dipolar molecules and thus tune its energy levels. Moreover, it is shown how to control direction and magnitude of the change. The direction of the shift depends on the direction of the dipole, hence it is important to choose the molecule to use taking into consideration if the desired effect is an increase or a decrease of the energetics. As a general rule, the interaction of the perovskite with Lewis bases decreases the energetics, while the interaction with Lewis acids increases them. However, both intrinsic dipole and interaction dipole are to be considered and the final effect will depend on the direction of the total dipole. The magnitude of the shift depends on the concentration of the solution used for the deposition. This is likely related to the deposition kinetics and correlated to the surface coverage of the molecules. With high concentration of the molecules' solution the perovskite surface is fully functionalized and thus the maximum achievable energy levels shift is reached, however, with low solution concentration the surface is not fully functionalized and so the induced shift is smaller. Therefore, it is possible to adjust the magnitude of the shift without changing the molecule. On the other hand, the dipole of the molecule affects the magnitude of the shift as well, hence the final results depend on the combination of the two parameters. With these considerations in mind, it is possible to perform a tailored tuning of the perovskite energy levels. The molecules employed in Chapter 5 showed the possibility to obtain a shift up to several hundreds of meV in both directions. This method, when applied to devices, allows an adjustment of the ELA and thus it can ease the energetic requirements for the adjacent layer.

The characterization of the energy level shifts gives also the possibility to gain further insights and make some considerations on the molecules' behaviours. For example, the energetic shift induced by the molecules binding to Pb^{2+} ions reaches saturation at lower solution concentrations than that caused by the molecules binding to the I^- ions. This can give indications about the distribution of the

molecules. First of all, it might be related to the fact that the perovskite composition employed in these experiments has approximately a 1:3 Pb:I proportion, thus a higher concentration of molecules will be required to saturate the halides surface defects. Secondly, an important role is played by the dimension of the molecules and/or their tendency to stay up-right. Molecules with two or three aliphatic chains, like the Lewis bases used in the experiments of Chapter 5, occupy more space and have a bigger steric hindrance than the presented Lewis acids, whose fluorinated chains allow them to form a compact layer. Therefore, from this point of view, if the molecules are large, a lower concentration will be needed to saturate the surface. This is furthermore supported by the energy levels shift trend of urea shown in Chapter 6. Indeed urea is still a Lewis base, but, in this case, the saturation condition is reached for a higher concentration than the Lewis bases in Chapter 5, and this is probably due to the significantly lower dimension of the molecule. Overall, the dimension of the molecules is something to keep in mind when choosing which solution concentrations to explore during the planning of a new experiment.

In short, Chapter 5 shows how to tune the perovskite energy levels with control over direction and magnitude of the shift, together with leading to some considerations to take into account when choosing the appropriate molecule and condition for an experiment. This concept is further developed in Chapter 6.

In Chapter 6 the energy level tuning method is applied to two representative systems: triple cation PSCs, exemplifying a situation with already optimized ELA, and $MAPbBr_3$ wide-bandgap PSCs, exemplifying a situation with a relevant offset at the perovskite/HTL interface.

In the first case, the perovskite is functionalized with two different concentrations of csc5, one of the Lewis bases explored in Chapter 5, which was proven to lower the triple cation energy levels of up to 160 mV. When employed in n-i-p devices with TiO_2 and spiro-OMeTAD as CTLs, the functionalization leads to a progressive, albeit small, increase in V_{oc} and FF, which can be ascribed to a combination of passivation and ELA adjustment. This is furthermore supported by drift-diffusion simulations indicating the same trend can be obtained by changing only the ELA at the interface and the recombination time.

For $MAPbBr_3$ devices, the perovskite is functionalized with different concentrations of urea. This molecule was chosen for its large dipole and small dimensions, thus optimal for inducing a relevant change in energy levels towards lower values, as required by the misalignment of this system. In this case the effect on the overall performance is significant, increasing the V_{oc} up to 60 meV and the efficiency of more than 1 %. Considering the substantial hysteresis of these kinds of devices, the mentioned values were calculated from a statistical analysis of data obtained from MPP- and V_{oc}-tracking. The V_{oc} trend follows the energy level shift trend measured with the Kelvin probe technique, indicating a correlation, and thus a dependence of the V_{oc} enhancement on the improved ELA.

The results from the experiments on the two above-presented systems confirm that tuning the perovskite energy levels according to the method described in Chapter 5 successfully leads to a performance improvement, increasing in particular the V_{oc}. This technique is mostly effective when applied to systems where a large energetic offset at the treated interface is one of the main sources

of losses, while it shows little effect on devices that possess well-matched energy levels. This observation gives an experimental insight on the heavily debated topic of the importance (or not) of ELA. Indeed, the different behaviours observed for the triple cation and $MAPbBr_3$ systems indicate that large energetic offsets are a source of losses and ELA play a relevant role in obtaining efficient devices. However, at the same time, it is important to consider which the other sources of losses are. If the energetic offset is less detrimental than other factors, than tuning will not lead to significant advantages. Therefore, the experimental results suggest that, in agreement with other studies,[34] ELA matters, but how much it matters depends on the overall condition (specifically the different losses) of the system.

Moreover, the devices results show that, for both triple cation and $MAPbBr_3$ PSCs, the V_{oc} improvement is smaller compared to the expected value based on the measured energy level shift. This implies that part of the potential shift that the dipoles could induce is lost when a new layer is deposited on top of the perovskite and it is a factor to take into account when planning an adjustment of the energy levels through this method.

Chapter 7 is based on the same concepts introduced in the previous chapters, however in this case the functionalization does not happen through an interlayer of selected molecules, but by incorporating a moiety that is able to interact with the perovskite in a novel hole-transport material (HTM). Hence, the material has the double role of efficiently transporting charge carriers and interacting with the dangling bonds on the surface. Thanks to this feature, the additional interface related to the insertion of an interlayer for the functionalization is removed.

In particular, the novel HTM (named PFI) can interact with the perovskite surface via XB. This specific interaction was chosen because of the interesting properties characteristic of XB and described in Section 3.3.2. Specifically, its (i) directionality, (ii) tuneable interaction strength and (iii) hydrophobicity. Indeed these features facilitate the formation of an ordered and compact layer, that improves the perovskite/HTL interface.

In Chapter 7 the interaction of PFI with perovskite is analysed from different aspects and compared to that of PF, a material that can act as reference since it has the same chemical structure and optoelectronic properties, except for the iodine atom which allows PFI to interact with the I^- ions on the perovskite surface through XB. Moreover, the effect of employing such a material in devices is explored. Simulations highlight a stronger interaction with the perovskite layer for PFI than for PF and indicate directionality, with a bond angle of approximately 180° for the I --- I^- interaction. These results serve as supporting evidence of the XB ability of PFI, while a detailed experimental characterization of the bond for the moiety responsible for the interaction was conducted in previous works, specifically dedicated to the purpose.[212] Indeed, the direct experimental characterization of XB as interaction is a challenging task. However, it is possible to obtain indirect evidence of such interaction from the energetic characterization through Kelvin probe: the measurement shows the energy levels of PFI shifting with the solution concentration, while the shift of PF's energy levels is constant for the

different concentrations. This specific result evidences that PFI has an interaction with the perovskite, while PF does not.

The behaviour of the HTMs is also analysed from the point of view of stability to external factors, such as solvent exposure. Samples with perovskite coated with the two HTMs are repeatedly exposed to ethanol, a solvent that can slowly dissolve them, and they are characterized after each treatment with techniques able to evaluate changes in the optical properties and morphology, specifically UV-Vis (both in reflection and transmission mode) and AFM. The results from both methods indicate an increased resilience to dissolution for PFI compared to PF. This behaviour can be associated with the anchoring capability of PFI and its directionality, due to XB. As a consequence, a more compact and ordered interfacial layer is formed, enhancing the stability of the sample.

Further advantages are observed when PFI was employed as hole-transport layer (HTL) in n-i-p devices and compared with PF. The analysis of the photovoltaic parameters shows a reduction in non-radiative recombination for PFI-based devices, which is reflected in a V_{oc} enhancement of about 20 meV on average. This is further supported by quasi-Fermi level splitting (QFLS) measurements, stressing how this improvement is related to the difference between the two materials, thus the ability to form XB. Moreover, the little difference between the QFLS of bare perovskite and PFI-coated perovskite indicates that the interfacial recombination losses typically induced by the deposition of a layer on top of perovskite are particularly small in this case. Additionally, devices with PFI display reduced hysteresis, a symptom of lowered ion migration, probably related to the interaction between the I^- ions on the perovskite and the HTM, which limits their possibility to move. This affects also the operational stability of the solar cells, leading to devices with PFI being more than two times more stable than those with PF under continuous MPP-tracking.

Therefore, the results presented in Chapter 7 on one side further support the possibility of tuning the perovskite energy levels through interfacial dipoles and the related improvements in devices. On the other, they highlight the advantages that functionalization via XB can bring to PSCs, especially when integrated directly within the CTL.

Overall, the results exposed in this dissertation convey the following messages:

(i) The perovskite functionalization via monolayers of dipolar molecules can be an effective and versatile tool to tune interfacial energetics and charge transfer properties in perovskite solar cells.

(ii) The effectiveness of the method depends on several factors that is important to take into consideration. Including, but not limited to, the characteristic of molecules and related dipoles, the features and losses of the different layers comprising the device and their interaction, and the (currently unclear) relation between the measured energetic values and the respective actual values within the device.

(iii) Halogen bonding is a particularly interesting interaction that can simultaneously improve the perovskite/charge-transport layer interface, enhancing stability, and tune the

interfacial energetics, reducing the non-radiative recombination and enhancing the device performance.

Moreover, the different experiments and related results stress the challenges of surface functionalization and energy level tuning on perovskite. In this regard, it is possible to make some considerations that can be used as guidelines when planning to adjust the energy levels of PSCs.

Most of the following considerations are directly connected to the peculiarity of the perovskite material and its features. As a starting point, it is important to keep in mind that the properties of the perovskite surface are affected by *air exposure*, therefore this should be avoided or the related effects should be evaluated. Moreover, a relevant aspect is the *roughness of the perovskite layer*, including the *variations of facets and terminations* of the exposed surface. This complicates the formation and characterization of ordered monolayers, however it is also a key point for the versatility of this method. A pinpointed tailoring of the interface properties would be possible if the systematic control of the exposed facets and defects ratios were feasible. Nevertheless, the simultaneous presence of surface defects with opposite charges brings to advantages in terms of functionalization flexibility. Indeed, it allows the use of molecules able to bind to either kind of defects, and consequently the range of possible induced changes is wide.

Thanks to this feature, it is in theory possible to employ an extensive number of different molecules. However, as it became clear during the development of the work for this dissertation, the molecules need to satisfy some stringent requirements in order to be employed in PSCs and have a positive effect. In particular, it is important to consider the *dimension of the molecule* and the *strength of the interaction*. The dimension of the molecule is relevant because on that depends the condition (i.e. the solution concentration) that gives the maximum achievable energy level shift and consequently allows the identification of the range in which is possible to tune the energetics. Moreover, too big molecules could have drawbacks, such as being partially insulating or limiting the number of defects that it is possible to functionalize. A molecule that interacts strongly with the ions on the perovskite is in principle an advantage, since this generally means strong interfacial dipole and thus potentially a big range for energy level shift. However, a very strong interaction can damage the perovskite, presumably by dissolving some of the ions, as in the case of TOPO seen in Chapter 5. Therefore, it is important to find the right balance, identifying molecules that interact strongly with the perovskite (if needed) but without damaging it. The same care should be placed in the choice of the *solvent*. Moreover, ideally the molecules should have dimension and features that allows them to form a compact layer. These limitations in the choices of molecules makes it even more important to have the ability to obtain energy level shifts of different intensities from the same molecule, as in the method exposed in this dissertation. In this way, once a molecule with good features is selected, different ELA adjustments can be performed, without the need to change the molecule.

Of course, an important condition, depending on the desired effect, is the direction of the dipole. In this case, the possibilities are only two: dipole towards the surface, i.e. increasing the energetics, or dipole pointing outside, i.e. decreasing the energetics. Nevertheless, it might not be straightforward

to know the *direction of the total dipole*. Indeed, this depends on the combination of the intrinsic dipole of the molecule and the dipole of the interaction, and it is not clear which one is predominant. The answer might depend on the situation, the DFT simulations shown in Chapter 5 seem to indicate that the interaction dipole is more relevant than the intrinsic dipole, however a strong intrinsic dipole might become dominant combined with a weak interaction. It is therefore advisable to evaluate both the dipoles via simulations before proceeding with an experiment, especially if they point to opposite directions.

The results coming from the applications in devices stressed a particularly relevant factor: *the actual V_{oc} enhancement is significantly lower than the potential energy levels shift* measured during the characterization of functionalized samples. This is particularly important to keep in mind when planning an experiment. The effect was observed consistently, but the mismatch was different depending on the case. Once the (functionalized) perovskite surface is "buried" under another layer, the surrounding conditions change. For example, charges rearrangements and interactions between the materials might happen and, additionally, new defects are generally induced.[34] Therefore, the real problem is that it is actually unknown how the surface's properties change after the deposition of the subsequent layer and which is the actual energetic situation at the interface within the device. Moreover, in a complete device, every bulk and interface play a role and affect the overall performance and stability. Therefore, it is also possible that the potential improvement brought by functionalization and energy level tuning strategies is limited by other losses in the solar cells. This became particularly clear over the course of different experiments devoted to the attempt of showing the usefulness of tuning the perovskite energy levels. Indeed, several batches of devices were prepared using triple cation as perovskite and novel materials prepared by collaborators as HTLs: these materials had energy levels not well suited for applications in PSCs and thus leading to a potentially optimal situation for obtaining an improvement through energy level tuning. Nevertheless, the results did not show relevant changes, in principle pointing to a failure of the method. However, it was also noted that devices with these HTLs showed a particularly bad photovoltaic behaviour, with large hysteresis and low efficiency. Thus, the absence of a change in performance after the treatment might be related to other intrinsic losses more relevant than the ELA at the perovskite/HTM interface. Based on this it became clear that, to actually evaluate the effectiveness of the energy level tuning method, it was necessary to shift to systems where it is known that one of the main sources of losses is the perovskite/HTL offset.

This leads to a general comment that I believe it is relevant to make: *"failed" experiments are the backbone of scientific progress.* Experimental research, for everybody and in every field, passes through countless experiments that are categorized as "failed" and not reported or even mentioned. Within the frame of this dissertation, tens of molecules were explored, in addition to solvents, HTMs, and experimental conditions in general. Overall around 1300 devices were prepared, without counting the samples for characterization. Needless to say that only a small fraction of these made it to this dissertation, however it is on the knowledge gained from those experiments that the actual results

were obtained. “Failures” are the root of research, and reporting them might actually help other researchers not to repeat attempts that were already explored.

Overall, if the guidelines exposed above are followed, the perovskite functionalization through assemblies of dipolar molecules can be a powerful tool to adjust the interfacial properties of PSCs, and in particular the ELA. This dissertation explores the application of this method on two systems, devices with triple cation and devices with $MAPbBr_3$. For the first system, a detailed study is additionally performed in order to show the advantages of the incorporation of such a functionalization in the HTL, identifying XB as particularly useful interaction for the functionalization. These findings allow for more flexibility in the requirements between the different layers, and in the choice of materials, paving the way to the possibility of applying a systematic tuning of the perovskite interfacial properties in different stacks. Indeed, the method here exposed can be expanded to all kinds of perovskite-based devices and this gives interesting prospects. For example, it would be possible to use the energy level tuning method to improve the performance and stability of PSCs employing CTLs that are energetically non-ideal, but possess good stability and high mobility. On the other hand, as in the case of $MAPbBr_3$, perovskites with different bandgaps could be used without the need to develop new CTLs with well-matched energy levels. For example, this method could be used to tune the energy levels in Sn-based or inorganic perovskites. Moreover, in addition to the flexibility given by the ELA tuning ability, it is important to exploit the stability enhancement that arises from XB-driven assemblies. Therefore, functionalizing the perovskite with molecules able to form XB should be generalized as a stabilization strategy, even when ELA adjustment is not required. As a general perspective, it would be useful to shift the research for the development of new CTLs towards materials that can both efficiently transport charges and functionalize the perovskite surface, paying particular attention to the kind of functionalization, so that ELA can be simultaneously adjusted depending on the requirements.

On the other hand, in spite of the interesting perspectives, there are still many aspects regarding interfaces and their possible functionalization with molecules that are unclear and limit the full potential of the strategy proposed in this dissertation. In order to be able to actually use molecular assemblies to control the interfacial dynamics, fine-tune the energetics, and further reduce detrimental losses in PSCs, it is necessary to gain a better understanding of the features of perovskite/CTL interface within the device and of the deposition mechanisms of molecules on perovskite.

Regarding the latter, it would useful for example to establish *how molecular layers actually look like on perovskite*, *how do molecules distribute depending on the surface features*, *what are the deposition dynamics*. Simulations can give precious insights on this regard, but giving an answer from the experimental point of view is a quite challenging task, especially because the roughness of the perovskite layer limits the efficacy of an evaluation based on the determination of the thickness of the molecular layer. It could be possible to gain some understanding by combining different high-resolution surface sensitive techniques, possible methods span from surface imaging with atomic-scale resolution to ultra-fast spectroscopy techniques. However, in most of these cases, the measurement itself often damages the surface, biasing the results. In addition to these in-depth characterizations, in

order to gain a better understanding of the deposition dynamics, it would be of particular interest to perform in-situ measurements during the molecules' deposition process.

Similar suggestions can be made concerning the features of the interfaces, especially from the point of view of the determination of energetics and losses. Detailed studies on the identification of the main sources of interfacial losses have been performed through photoluminescence-based techniques giving helpful insights on the topic.[36] Regarding the characterization of the energy levels of a material, established high-resolution methods, such as UPS, are commonly used. However, the determination of the *real* energy levels within a device is still a major obstacle due to the difficulties of measuring the energetics of buried interfaces. Some results have been obtained by preparing full devices and then removing the top layers until exposure of the surface of interest[283,333] or by measuring tapered cross-sections,[334] however these are still invasive methods and do not necessarily reveal the actual energetics. A possible strategy could be to focus on in-situ measurements during the deposition of each layer using standard non-invasive characterization techniques, such as Kelvin probe or ambient pressure photoemission spectroscopy. However, performing such measurements in practice might be challenging. Therefore the main questions remain: *what is the real energy level alignment within the device? What it the real energy level shift induced by a layer of dipolar molecules?* The answer to these questions is fundamental to design tailored energy level tuning and functionalization strategies.

In conclusion, the work in this dissertation shows how to improve interfaces and especially ELA in PSCs by functionalizing the perovskite surface with dipolar molecules possessing specific features. Molecules able to form halogen bonding seem a particularly interesting option for this purpose, moreover the integration of such functionalization ability within the charge-transport layer reduces the number of interfaces in the device, thus removing a source of losses. In order to fully exploit the potential of this method and being able to systematically apply it to perovskite-based devices, it is necessary to gain a deeper understanding of molecules deposition dynamics and the real energetic features of the perovskite/CTL interface. In general, this strategy can lead to efficient and stable PSCs, even for structures that are currently not completely exploited because of unsuitable ELA. Ideally, it will be possible to tune the properties of PSCs depending on the requirements, thus broadening the possibilities of application for PSCs towards wide-scale commercialization.

9 Bibliography

[1] https://www.tgcom24.mediaset.it/cronaca/veneto/acqua-alta-a-venezia-due-morti-fino-a-venerd-sar-emergenza_11071952-201902a.shtml.

[2] Centro previsioni e segnalazioni maree Venezia (https://www.comune.venezia.it/it/content/distribuzione-decennale-delle-alte-maree-110-cm). (Accessed: 08/2021).

[3] Tosi L., Teatini P., Strozzi T., *Natural Versus Anthropogenic Subsidence Of Venice*, Sci. Rep., **2013**, 3, 1–9.

[4] Carbognin L. et al., *Global Change And Relative Sea Level Rise At Venice: What Impact In Term Of Flooding*, Clim. Dyn., **2010**, 35, 1055–1063.

[5] Reimann L. et al., *Mediterranean UNESCO World Heritage At Risk From Coastal Flooding And Erosion Due To Sea-Level Rise*, Nat. Commun., **2018**, 9, 1–11.

[6] IPCC, *Climate Change 2021: The Physical Science Basis - Summary For Policymakers*, **2021**.

[7] United Nations Framework Convention on Climate Change - The Paris agreement (https://unfccc.int/sites/default/files/english_paris_agreement.pdf).

[8] IRENA, *World Energy Transitions Outlook: 1.5°C Pathway*, **2021**.

[9] Fraunhofer ISE: Photovoltaics Report (updated: 27 July 2021).

[10] Correa-Baena J.-P. et al., *Promises And Challenges Of Perovskite Solar Cells*, Science, **2017**, 358, 739–744.

[11] Goldschmidt V.M., *Die Gesetze Der Krystallochemie*, Naturwissenschaften, **1926**, 14, 477–485.

[12] Olthof S., *Research Update: The Electronic Structure Of Hybrid Perovskite Layers And Their Energetic Alignment In Devices*, APL Mater., **2016**, 4, 1–10.

[13] Tao S. et al., *Absolute Energy Level Positions In Tin- And Lead-Based Halide Perovskites*, Nat. Commun., **2019**, 10, 1–10.

[14] Manser J.S., Christians J.A., Kamat P. V., *Intriguing Optoelectronic Properties Of Metal Halide Perovskites*, Chem. Rev., **2016**, 116, 12956–13008.

[15] Kojima A. et al., *Organometal Halide Perovskites As Visible-Light Sensitizers For Photovoltaic Cells*, J. Am. Chem. Soc., **2009**, 131, 6050–1.

[16] Kim H.S. et al., *Lead Iodide Perovskite Sensitized All-Solid-State Submicron Thin Film Mesoscopic Solar Cell With Efficiency Exceeding 9%*, Sci. Rep., **2012**, 2, 1–7.

[17] Lee M.M.. et al., *Efficient Hybrid Solar Cells Based On Meso-Superstructured Organometal Halide Perovskites*, Science, **2012**, 338, 643–648.

[18] Best Research-Cell Efficiency Chart | Photovoltaic Research | NREL https://www.nrel.gov/pv/cell-efficiency.html (accessed: July 2021).

[19] Saliba M. et al., *How To Make Over 20% Efficient Perovskite Solar Cells In Regular (N-I-P) And Inverted (P-I-N) Architectures*, Chem. Mater., **2018**, 30, 4193–4201.

[20] Jena A.K., Kulkarni A., Miyasaka T., *Halide Perovskite Photovoltaics: Background, Status, And Future Prospects*, Chem. Rev., **2019**, 119, 3036–3103.

[21] Correa-Baena J.P. et al., *The Rapid Evolution Of Highly Efficient Perovskite Solar Cells*, Energy Environ. Sci., **2017**, 10, 710–727.

[22] Egger D.A. et al., *What Remains Unexplained About The Properties Of Halide Perovskites?*, Adv. Mater., **2018**, 1800691, 1–11.

[23] Yin W.J., Shi T., Yan Y., *Superior Photovoltaic Properties Of Lead Halide Perovskites: Insights From First-Principles Theory*, J. Phys. Chem. C, **2015**, 119, 5253–5264.

[24] Ball J.M., Petrozza A., *Defects In Perovskite-Halides And Their Effects In Solar Cells*, Nat. Energy, **2016**, 1, 1–13.

[25] Eames C. et al., *Ionic Transport In Hybrid Lead Iodide Perovskite Solar Cells*, Nat. Commun., **2015**, 6, 2–9.

[26] Tress W., *Metal Halide Perovskites As Mixed Electronic-Ionic Conductors: Challenges And Opportunities - From*

Hysteresis To Memristivity, J. Phys. Chem. Lett., **2017**, 8, 3106–3114.

[27] Jošt M. et al., *Monolithic Perovskite Tandem Solar Cells: A Review Of The Present Status And Advanced Characterization Methods Toward 30% Efficiency*, Adv. Energy Mater., **2020**, 10, 1–43.

[28] Domanski K. et al., *Systematic Investigation Of The Impact Of Operation Conditions On The Degradation Behaviour Of Perovskite Solar Cells*, Nat. Energy, **2018**, 3, 61–67.

[29] Schulz P., Cahen D., Kahn A., *Halide Perovskites: Is It All About The Interfaces?*, Chem. Rev., **2019**, 119, 3349–3417.

[30] Kroemer H., *Heterostructure Devices: A Device Physicist Looks At Interfaces*, Surf. Sci., **1983**, 132, 543–576.

[31] Castro-Méndez A. et al., *The Role Of Grain Boundaries In Perovskite Solar Cells*, Adv. Energy Mater., **2019**, 9, 1–10.

[32] Jin H. et al., *It's A Trap! On The Nature Of Localised States And Charge Trapping In Lead Halide Perovskites*, Mater. Horizons, **2020**, 7, 397–410.

[33] Chen B. et al., *Imperfections And Their Passivation In Halide Perovskite Solar Cells*, Chem. Soc. Rev., **2019**, 48, 3842--3867.

[34] Stolterfoht M. et al., *The Impact Of Energy Alignment And Interfacial Recombination On The Internal And External Open-Circuit Voltage Of Perovskite Solar Cells*, Energy Environ. Sci., **2019**, 12, 2778–2788.

[35] Caprioglio P. et al., *On The Relation Between The Open-Circuit Voltage And Quasi-Fermi Level Splitting In Efficient Perovskite Solar Cells*, Adv. Energy Mater., **2019**, 9, 1–10.

[36] Wolff C.M. et al., *Nonradiative Recombination In Perovskite Solar Cells: The Role Of Interfaces*, Adv. Mater., **2019**, 31, 1–20.

[37] Sze S.M., *Physics of Semiconductor Devices*, Wiley, **1981**.

[38] Wurfel P., *Physics of solar cells*, Wiley, **2009**.

[39] Bisquert J., *The physics of solar cells*, Taylor and Francis, **2018**.

[40] Mönch W., *Semiconductor Surfaces and Interfaces*, Springer, **1993**.

[41] Rana F., Chapter 2: Semiconductor Heterostructures. In *Semiconductor Optoelectronics*; 2011; 1–29.

[42] Tress W., *Organic Solar Cells: Theory, Experiment, and Device Simulation*, Springer, **2014**.

[43] Kahn A., *Fermi Level, Work Function And Vacuum Level*, Mater. Horizons, **2016**, 3, 7–10.

[44] Cahen D., Kahn A., *Electron Energetics At Surfaces And Interfaces: Concepts And Experiments*, Adv. Mater., **2003**, 15, 271–277.

[45] Ishii H. et al., *Energy Level Alignment And Interfacial Electronic Structures At Organic Metal And Organic Organic Interfaces*, Adv. Mater., **1999**, 11.

[46] NREL Reference Solar Spectral Irradiance. https://rredc.nrel.gov/solar//spectra/ (accessed: 07/2021).

[47] Shockley W., Queisser H.J., *Detailed Balance Limit Of Efficiency Of P-N Junction Solar Cells*, J. Appl. Phys., **1961**, 32, 510–519.

[48] Kagan C.R., Mitzi D.B., Dimitrakopoulos C.D., *Organic-Inorganic Hybrid Materials As Semiconducting Channels In Thin-Film Field-Effect Transistors*, Science, **1999**, 286, 945–947.

[49] Wang Z. et al., *Two-Dimensional Eclipsed Arrangement Hybrid Perovskites For Tunable Energy Level Alignments And Photovoltaics*, J. Mater. Chem. C, **2019**, 7, 5139–5147.

[50] Ishihara T., Takahashi J., Goto T., *Optical Properties Due To Electronic Transitions In Two-Dimensional Semiconductors (CnH2n+1NH3)2PbI4*, Phys. Rev. B, **1990**, 42, 11099–11107.

[51] R. J. H. Voorhoeve et al., *Perovskite Oxides: Materials Science In Catalysis*, Science, **1977**, 195, 827–833.

[52] Moniruddin M. et al., *Recent Progress On Perovskite Materials In Photovoltaic And Water Splitting Applications*, Mater. Today Energy, **2018**, 7, 246–259.

[53] Veldhuis S.A. et al., *Perovskite Materials For Light-Emitting Diodes And Lasers*, Adv. Mater., **2016**, 28, 6804–6834.

[54] Rose G., *Beschreibung Einiger Neuen Mineralien Des Urals*, Ann. Phys., **1840**, 126, 652–656.

[55] Akkerman Q.A., Manna L., *What Defines A Halide Perovskite?*, ACS Energy Lett., **2020**, 604–610.

[56] Poglitsch A., Weber D., *Dynamic Disorder In Methylammoniumtrihalogenoplumbates (II) Observed By Millimeter-Wave Spectroscopy*, J. Chem. Phys., **1987**, 87, 6373–6378.

[57] N. Onoda-Yamamuro et al., *P-T Phase Relations Og CH3NH3PbX3 (X = Cl, Br, I) Crystals*, J. Phys. Chem. Solids, **1992**, 53, 277–281.

[58] Brivio F. et al., *Lattice Dynamics And Vibrational Spectra Of The Orthorhombic, Tetragonal, And Cubic Phases Of Methylammonium Lead Iodide*, Phys. Rev. B - Condens. Matter Mater. Phys., **2015**, 92, 1–8.

[59] Noel N.K. et al., *Lead-Free Organic-Inorganic Tin Halide Perovskites For Photovoltaic Applications*, Energy Environ. Sci., **2014**, 7, 3061–3068.

[60] Li J. et al., *Biological Impact Of Lead From Halide Perovskites Reveals The Risk Of Introducing A Safe Threshold*, Nat. Commun., **2020**, 11, 1–5.

[61] Nasti G., Abate A., *Tin Halide Perovskite (ASnX3) Solar Cells: A Comprehensive Guide Toward The Highest Power Conversion Efficiency*, Adv. Energy Mater., **2020**, 10, 1–16.

[62] Unger E.L. et al., *Roadmap And Roadblocks For The Band Gap Tunability Of Metal Halide Perovskites*, J. Mater. Chem. A, **2017**, 5, 11401–11409.

[63] Umebayashi T. et al., *Electronic Structures Of Lead Iodide Based Low-Dimensional Crystals*, Phys. Rev. B - Condens. Matter Mater. Phys., **2003**, 67, 2–7.

[64] Gholipour S. et al., *Globularity-Selected Large Molecules For A New Generation Of Multication Perovskites*, Adv. Mater., **2017**, 29, 1–9.

[65] Yamada Y. et al., *Near-Band-Edge Optical Responses Of Solution-Processed Organic-Inorganic Hybrid Perovskite CH3NH3PbI3 On Mesoporous TiO2 Electrodes*, Appl. Phys. Express, **2014**, 7, 5–9.

[66] Phillips L.J. et al., *Solar Energy Materials & Solar Cells Maximizing The Optical Performance Of Planar CH3NH3 PbI3 Hybrid Perovskite Heterojunction Stacks*, Sol. Energy Mater. Sol. Cells, **2016**, 147, 327–333.

[67] Stranks S.D. et al., *Electron-Hole Diffusion Lengths Exceeding 1 Micrometer In An Organometal Trihalide Perovskite Absorber*, Science, **2013**, 342, 341–344.

[68] Dong Q. et al., *Electron-Hole Diffusion Length >175 Mm In Solution-Grown CH3NH3PbI3 Single Crystals*, Sci. express, **2015**, 43210, 1–8.

[69] Sharenko A., Toney M.F., *Relationships Between Lead Halide Perovskite Thin-Film Fabrication, Morphology, And Performance In Solar Cells*, J. Am. Chem. Soc., **2016**, 138, 463–470.

[70] Kim H.S., Seo J.Y., Park N.G., *Material And Device Stability In Perovskite Solar Cells*, ChemSusChem, **2016**, 9, 2528–2540.

[71] Domanski K. et al., *Migration Of Cations Induces Reversible Performance Losses Over Day/Night Cycling In Perovskite Solar Cells*, Energy Environ. Sci., **2017**, 10, 604–613.

[72] Song Z. et al., *Perovskite Solar Cell Stability In Humid Air: Partially Reversible Phase Transitions In The PbI2-CH3NH3I-H2O System*, Adv. Energy Mater., **2016**, 6, 1–7.

[73] Malinauskas T. et al., *Enhancing Thermal Stability And Lifetime Of Solid-State Dye-Sensitized Solar Cells Via Molecular Engineering Of The Hole-Transporting Material Spiro-OMeTAD*, ACS Appl. Mater. Interfaces, **2015**, 7, 11107–11116.

[74] Jena A.K., Ikegami M., Miyasaka T., *Severe Morphological Deformation Of Spiro-OMeTAD In (CH3NH3)PbI3 Solar Cells At High Temperature*, ACS Energy Lett., **2017**, 2, 1760–1761.

[75] Domanski K. et al., *Not All That Glitters Is Gold: Metal-Migration-Induced Degradation In Perovskite Solar Cells*, ACS Nano, **2016**, 10, 6306–6314.

[76] Pathak S.K. et al., *Performance And Stability Enhancement Of Dye-Sensitized And Perovskite Solar Cells By Al Doping Of TiO2*, Adv. Funct. Mater., **2014**, 24, 6046–6055.

[77] Khenkin M. V et al., *Consensus Statement For Stability Assessment And Reporting For Perovskite Photovoltaics Based On ISOS Procedures*, Nat. Energy, **2020**, 5, 35–49.

[78] Saliba M. et al., *Measuring Aging Stability Of Perovskite Solar Cells*, Joule, **2018**, 80, 1–6.

[79] Wang S. et al., *Energy Level Alignment At Interfaces In Metal Halide Perovskite Solar Cells*, Adv. Mater. Interfaces, **2018**, 1800260, 1–30.

[80] Mahesh S. et al., *Revealing The Origin Of Voltage Loss In Mixed-Halide Perovskite Solar Cells*, Energy Environ. Sci., **2020**, 13, 258–267.

[81] Jaysankar M. et al., *Minimizing Voltage Loss In Wide-Bandgap Perovskites For Tandem Solar Cells*, ACS Energy Lett., **2019**, 4, 259–264.

[82] Calió L. et al., *Hole-Transport Materials For Perovskite Solar Cells*, Angew. Chemie - Int. Ed., **2016**, 55, 14522–14545.

[83] Li S. et al., *A Brief Review Of Hole Transporting Materials Commonly Used In Perovskite Solar Cells*, Rare Met., **2021**, 40, 2712–2729.

[84] Vivo P., Salunke J.K., Priimagi A., *Hole-Transporting Materials For Printable Perovskite Solar Cells*, Materials, **2017**, 10, 1–44.

[85] Salunke J. et al., *Phenothiazine-Based Hole-Transporting Materials Toward Eco-Friendly Perovskite Solar Cells*, ACS Appl. Energy Mater., **2019**, 2, 3021–3027.

[86] Valadi K. et al., *Metal Oxide Electron Transport Materials For Perovskite Solar Cells: A Review*, Environ. Chem. Lett., **2021**, 19, 2185–2207.

[87] Lin L. et al., *Inorganic Electron Transport Materials In Perovskite Solar Cells*, Adv. Funct. Mater., **2021**, 31, 1–24.

[88] Said A.A., Xie J., Zhang Q., *Recent Progress In Organic Electron Transport Materials In Inverted Perovskite Solar Cells*, Small, **2019**, 15, 1–23.

[89] Zhou Z., Pang S., *Highly Efficient Inverted Hole-Transport-Layer-Free Perovskite Solar Cells*, J. Mater. Chem. A, **2020**, 8, 503–512.

[90] Chen H., Yang S., *Methods And Strategies For Achieving High-Performance Carbon-Based Perovskite Solar Cells Without Hole Transport Materials*, J. Mater. Chem. A, **2019**, 7, 15476–15490.

[91] Huang L. et al., *Efficient Electron Transport Layer-Free Perovskite Solar Cells Enabled By Discontinuous Polar Molecular Films: A Story Of New Materials And Old Ideas?*, ACS Sustain. Chem. Eng., **2021**, 9, 936–943.

[92] Huang L., Ge Z., *Simple, Robust, And Going More Efficient: Recent Advance On Electron Transport Layer-Free Perovskite Solar Cells*, Adv. Energy Mater., **2019**, 9, 1–31.

[93] Braun F., *Über Die Stromleitung Durch Schwefel-Metalle*, Pogg. Ann., **1874**, 153, 556–563.

[94] Williams R.H., *Interfaces In Semiconductor Structures And Devices*, Phys. J., **1989**, 45, 219–223.

[95] Ono L.K., Qi Y., *Surface And Interface Aspects Of Organometal Halide Perovskite Materials And Solar Cells*, J. Phys. Chem. Lett., **2016**, 7, 4764–4794.

[96] Song T. Bin et al., *Perovskite Solar Cells: Film Formation And Properties*, J. Mater. Chem. A, **2015**, 3, 9032–9050.

[97] Salim T. et al., *Perovskite-Based Solar Cells: Impact Of Morphology And Device Architecture On Device Performance*, J. Mater. Chem. A, **2015**, 3, 8943–8969.

[98] Deng W. et al., *Molecular Interlayers In Hybrid Perovskite Solar Cells*, Adv. Energy Mater., **2018**, 8, 1–20.

[99] Zhou Y. et al., *Microstructures Of Organometal Trihalide Perovskites For Solar Cells: Their Evolution From Solutions And Characterization*, J. Phys. Chem. Lett., **2015**, 6, 4827–4839.

[100] Dubey A. et al., *A Strategic Review On Processing Routes Towards Highly Efficient Perovskite Solar Cells*, J. Mater. Chem. A, **2018**, 6, 2406–2431.

[101] Jeon N.J. et al., *Solvent Engineering For High-Performance Inorganic-Organic Hybrid Perovskite Solar Cells*, Nat. Mater., **2014**, 13, 897–903.

[102] Yin Y. et al., *Vacuum-Drying Processed Micrometer-Thick Stable CsPbBr3 Perovskite Films With Efficient Blue-To-Green Photoconversion*, Small, **2019**, 15, 1–6.

[103] Liao K. et al., *Hot-Casting Large-Grain Perovskite Film For Efficient Solar Cells: Film Formation And Device Performance*, Nano-Micro Lett., **2020**, 12, 1–22.

[104] Roß M. et al., *Co-Evaporated P-I-N Perovskite Solar Cells Beyond 20% Efficiency: Impact Of Substrate Temperature And Hole-Transport Layer*, ACS Appl. Mater. Interfaces, **2020**, 12, 39261–39272.

[105] Liu M., Johnston M.B., Snaith H.J., *Efficient Planar Heterojunction Perovskite Solar Cells By Vapour Deposition*, Nature, **2013**, 501, 395–398.

[106] Cotella G. et al., *One-Step Deposition By Slot-Die Coating Of Mixed Lead Halide Perovskite For Photovoltaic Applications*, Sol. Energy Mater. Sol. Cells, **2017**, 159, 362–369.

[107] Mathies F. et al., *Inkjet-Printed Triple Cation Perovskite Solar Cells*, ACS Appl. Energy Mater., **2018**, 1, 1834–1839.

[108] Haruyama J. et al., *Termination Dependence Of Tetragonal CH3NH3PbI 3 Surfaces For Perovskite Solar Cells*, J. Phys. Chem. Lett., **2014**, 5, 2903–2909.

[109] Wang Y. et al., *Density Functional Studies Of Stoichiometric Surfaces Of Orthorhombic Hybrid Perovskite CH3NH3PbI3*, J. Phys. Chem. C, **2015**, 119, 1136–1145.

[110] Paquin F. et al., *Multi-Phase Semicrystalline Microstructures Drive Exciton Dissociation In Neat Plastic Semiconductors*, J. Mater. Chem. C, **2015**, 3, 10715–10722.

[111] Hieulle J. et al., *Scanning Probe Microscopy Applied To Organic–Inorganic Halide Perovskite Materials And Solar Cells*, Small Methods, **2018**, 2, 1–17.

[112] Moia D., Maier J., *Ion Transport, Defect Chemistry, And The Device Physics Of Hybrid Perovskite Solar Cells*, ACS Energy Lett., **2021**, 6, 1566–1576.

[113] Steirer K.X. et al., *Defect Tolerance In Methylammonium Lead Triiodide Perovskite*, ACS Energy Lett., **2016**, 1, 360–366.

[114] Queisser H.J., Haller E.E., *Defects In Semiconductors: Some Fatal, Some Vital*, Science, **1998**, 281, 945–950.

[115] Sherkar T.S. et al., *Recombination In Perovskite Solar Cells: Significance Of Grain Boundaries, Interface Traps, And Defect Ions*, ACS Energy Lett., **2017**, 2, 1214–1222.

[116] Luo D. et al., *Minimizing Non-Radiative Recombination Losses In Perovskite Solar Cells*, Nat. Rev. Mater., **2020**, 5, 44–60.

[117] Tress W., *Perovskite Solar Cells On The Way To Their Radiative Efficiency Limit – Insights Into A Success Story Of High Open-Circuit Voltage And Low Recombination*, Adv. Energy Mater., **2017**, 7, 1–18.

[118] Shockley W., Read W.T., *Statistics Of The Recombinations Of Holes And Electrons*, Phys. Rev., **1952**, 87, 835–842.

[119] Hall R.N., *Electron-Hole Recombination In Germanium*, Phys. Rev., **1952**, 87, 387.

[120] Johnston M.B., Herz L.M., *Hybrid Perovskites For Photovoltaics: Charge-Carrier Recombination, Diffusion, And Radiative Efficiencies*, Acc. Chem. Res., **2016**, 49, 146–154.

[121] Zhao Y. et al., *Effects Of Ion Migration And Improvement Strategies For The Operational Stability Of Perovskite Solar Cells*, Phys. Chem. Chem. Phys., **2021**, 23, 94–106.

[122] Lee H. et al., *Direct Experimental Evidence Of Halide Ionic Migration Under Bias In CH3NH3PbI3-XClx-Based Perovskite Solar Cells Using GD-OES Analysis*, ACS Energy Lett., **2017**, 2, 943–949.

[123] DeQuilettes D.W. et al., *Photo-Induced Halide Redistribution In Organic-Inorganic Perovskite Films*, Nat. Commun., **2016**, 7, 1–9.

[124] Azpiroz J.M. et al., *Defect Migration In Methylammonium Lead Iodide And Its Role In Perovskite Solar Cell Operation*, Energy Environ. Sci., **2015**, 8, 2118–2127.

[125] Senocrate A. et al., *Slow CH3NH3+ Diffusion In CH3NH3PbI3 Under Light Measured By Solid-State NMR And Tracer Diffusion*, J. Phys. Chem. C, **2018**, 122, 21803–21806.

[126] Merdasa A. et al., *Super-Resolution Luminescence Microspectroscopy Reveals The Mechanism Of Photoinduced Degradation In CH3NH3PbI3 Perovskite Nanocrystals*, J. Phys. Chem. C, **2016**, 120, 10711–10719.

[127] Tong C.J. et al., *Synergy Between Ion Migration And Charge Carrier Recombination In Metal-Halide Perovskites*, J. Am. Chem. Soc., **2020**, 142, 3060–3068.

[128] Snaith H.J. et al., *Anomalous Hysteresis In Perovskite Solar Cells*, J. Phys. Chem. Lett., **2014**, 5, 1511–1515.

[129] Richardson G. et al., *Can Slow-Moving Ions Explain Hysteresis In The Current-Voltage Curves Of Perovskite Solar Cells?*, Energy Environ. Sci., **2016**, 9, 1476–1485.

[130] Lan D., *The Physics Of Ion Migration In Perovskite Solar Cells: Insights Into Hysteresis, Device Performance, And Characterization*, Prog. Photovoltaics Res. Appl., **2020**, 28, 533–537.

[131] Beilsten-Edmands J. et al., *Non-Ferroelectric Nature Of The Conductance Hysteresis In CH3NH3PbI3 Perovskite-Based Photovoltaic Devices*, Appl. Phys. Lett., **2015**, 106, 1–6.

[132] Helmholtz H., *Studien Über Electrische Grenzschichten*, Ann. der Phys. und Chemie, **1879**, 7, 22.

[133] Courtier N.E. et al., *How Transport Layer Properties Affect Perovskite Solar Cell Performance : Insights From A Coupled Charge Transport / Ion Migration Model*, Energy Environ. Sci., **2019**, 12, 396–409.

[134] Chen T. et al., *Correlating Hysteresis Phenomena With Interfacial Charge Accumulation In Perovskite Solar Cells*, Phys. Chem. Chem. Phys., **2019**, 22, 245–251.

[135] Weber S.A.L. et al., *How The Formation Of Interfacial Charge Causes Hysteresis In Perovskite Solar Cells*, Energy Environ. Sci., **2018**, 11, 2404–2413.

[136] Calado P. et al., *Evidence For Ion Migration In Hybrid Perovskite Solar Cells With Minimal Hysteresis*, Nat. Commun., **2016**, 7, 1–10.

[137] Shao Y. et al., *Origin And Elimination Of Photocurrent Hysteresis By Fullerene Passivation In CH3NH3PbI3 Planar Heterojunction Solar Cells*, Nat. Commun., **2014**, 5, 1–7.

[138] Correa-Baena J.P. et al., *Unbroken Perovskite: Interplay Of Morphology, Electro-Optical Properties, And Ionic Movement*, Adv. Mater., **2016**, 28, 5031–5037.

[139] Fakharuddin A. et al., *Interfaces In Perovskite Solar Cells*, Adv. Energy Mater., **2017**, 7, 1–44.

[140] Schulz P. et al., *Interface Energetics In Organo-Metal Halide Perovskite-Based Photovoltaic Cells*, Energy Environ. Sci., **2014**, 7, 1377–1381.

[141] Tress W., Leo K., Riede M., *Influence Of Hole-Transport Layers And Donor Materials On Open-Circuit Voltage And Shape Of I-V Curves Of Organic Solar Cells*, Adv. Funct. Mater., **2011**, 21, 2140–2149.

[142] Climent-Pascual E. et al., *Influence Of The Substrate On The Bulk Properties Of Hybrid Lead Halide Perovskite Films*, J. Mater. Chem. A, **2016**, 4, 18153–18163.

[143] Tessler N., Vaynzof Y., *Insights From Device Modeling Of Perovskite Solar Cells*, ACS Energy Lett., **2020**, 5, 1260–1270.

[144] Wu N. et al., *Identifying The Cause Of Voltage And Fill Factor Losses In Perovskite Solar Cells By Using Luminescence Measurements*, Energy Technol., **2017**, 5, 1827–1835.

[145] Yablonovitch E., *Lecture Series: Stanford University For EE 237 Solar Energy Conversion By Dr. Aneesh Nainani*, Lect. Ser. Stanford Univ. EE 237 Sol. Energy Convers., **2013**.

[146] Yang W.S. et al., *Iodide Management In Formamidinium-Lead-Halide-Based Perovskite Layers For Efficient Solar Cells*, Science, **2017**, 356, 1376–1379.

[147] Tress W. et al., *Interpretation And Evolution Of Open-Circuit Voltage, Recombination, Ideality Factor And Subgap Defect States During Reversible Light-Soaking And Irreversible Degradation Of Perovskite Solar Cells*, Energy Environ. Sci., **2018**, 11, 151–165.

[148] Leijtens T. et al., *Carrier Trapping And Recombination: The Role Of Defect Physics In Enhancing The Open Circuit Voltage Of Metal Halide Perovskite Solar Cells*, Energy Environ. Sci., **2016**, 9, 3472–3481.

[149] Bi D. et al., *Polymer-Templated Nucleation And Crystal Growth Of Perovskite Films For Solar Cells With Efficiency Greater Than 21%*, Nat. Energy, **2016**, 1, 1–5.

[150] Miller E.M. et al., *Substrate-Controlled Band Positions In CH3NH3PbI3 Perovskite Films*, Phys. Chem. Chem. Phys., **2014**, 16, 22122–22130.

[151] Schulz P. et al., *Electronic Level Alignment In Inverted Organometal Perovskite Solar Cells*, Adv. Mater. Interfaces, **2015**, 2, 1–5.

[152] Caputo M. et al., *Electronic Structure Of MAPbI3 And MAPbCl3: Importance Of Band Alignment*, Sci. Rep., **2019**, 9, 1–11.

[153] Hellmann T. et al., *The Electronic Structure Of MAPI-Based Perovskite Solar Cells: Detailed Band Diagram Determination By Photoemission Spectroscopy Comparing Classical And Inverted Device Stacks*, Adv. Energy Mater., **2020**, 10, 1–11.

[154] Hu Z. et al., *The Impact Of Atmosphere On Energetics Of Lead Halide Perovskites*, Adv. Energy Mater., **2020**, 10, 1–11.

[155] Emara J. et al., *Impact Of Film Stoichiometry On The Ionization Energy And Electronic Structure Of CH3NH3PbI3 Perovskites*, Adv. Mater., **2016**, 28, 553–559.

[156] Prochowicz D. et al., *Influence Of A-Site Cations On The Open-Circuit Voltage Of Efficient Perovskite Solar Cells: A Case Of Rubidium And Guanidinium Additives*, J. Mater. Chem. A, **2019**, 7, 8218–8225.

[157] Li C. et al., *Halide-Substituted Electronic Properties Of Organometal Halide Perovskite Films: Direct And Inverse Photoemission Studies*, ACS Appl. Mater. Interfaces, **2016**, 8, 11526–11531.

[158] Walsh A., *Principles Of Chemical Bonding And Band Gap Engineering In Hybrid Organic-Inorganic Halide Perovskites*, J. Phys. Chem. C, **2015**, 119, 5755–5760.

[159] Hao F. et al., *Anomalous Band Gap Behavior In Mixed Sn And Pb Perovskites Enables Broadening Of Absorption Spectrum In Solar Cells*, J. Am. Chem. Soc., **2014**, 136, 8094–8099.

[160] Wang Q. et al., *Qualifying Composition Dependent P And N Self-Doping In CH3NH3PbI3*, Appl. Phys. Lett., **2014**, 105, 1–5.

[161] Shin D. et al., *Unraveling The Charge Extraction Mechanism Of Perovskite Solar Cells Fabricated With Two-Step Spin Coating: Interfacial Energetics Between Methylammonium Lead Iodide And C60*, J. Phys. Chem. Lett., **2017**, 8, 5423–5429.

[162] Heo S. et al., *Deep Level Trapped Defect Analysis In CH3NH3PbI3 Perovskite Solar Cells By Deep Level Transient Spectroscopy*, Energy Environ. Sci., **2017**, 10, 1128–1133.

[163] Li C. et al., *Iodine Migration And Its Effect On Hysteresis In Perovskite Solar Cells*, Adv. Mater., **2016**, 28, 2446–2454.

[164] Wu C.G., Chiang C.H., Chang S.H., *A Perovskite Cell With A Record-High-Voc Of 1.61 V Based On Solvent Annealed CH3NH3PbBr3/ICBA Active Layer*, Nanoscale, **2016**, 8, 4077–4085.

[165] Polander L.E. et al., *Hole-Transport Material Variation In Fully Vacuum Deposited Perovskite Solar Cells*, APL Mater., **2014**, 2, 1–6.

[166] Wolff C.M. et al., *Reduced Interface-Mediated Recombination For High Open-Circuit Voltages In CH3NH3PbI3 Solar Cells*, Adv. Mater., **2017**, 29, 1–8.

[167] Gelmetti I. et al., *Energy Alignment And Recombination In Perovskite Solar Cells: Weighted Influence On The Open Circuit Voltage*, Energy Environ. Sci., **2019**, 12, 1309–1316.

[168] Canil L. et al., *Tuning Halide Perovskite Energy Levels*, Energy Environ. Sci., **2021**, 14, 1429–1438.

[169] Ryu S. et al., *Voltage Output Of Efficient Perovskite Solar Cells With High Open-Circuit Voltage And Fill Factor*, Energy Environ. Sci., **2014**, 7, 2614–2618.

[170] Belisle R.A. et al., *Minimal Effect Of The Hole-Transport Material Ionization Potential On The Open-Circuit Voltage Of Perovskite Solar Cells*, ACS Energy Lett., **2016**, 1, 556–560.

[171] Park S.M. et al., *Processing Dependent Influence Of The Hole Transport Layer Ionization Energy On Methylammonium Lead Iodide Perovskite Photovoltaics*, ACS Appl. Mater. Interfaces, **2018**, 10, 15548–15557.

[172] Liang P.W. et al., *Roles Of Fullerene-Based Interlayers In Enhancing The Performance Of Organometal Perovskite Thin-Film Solar Cells*, Adv. Energy Mater., **2015**, 5, 1–7.

[173] Dänekamp B. et al., *Influence Of Hole Transport Material Ionization Energy On The Performance Of Perovskite Solar Cells*, J. Mater. Chem. C, **2019**, 7, 523–527.

[174] Jiménez-López J. et al., *Charge Injection, Carriers Recombination And HOMO Energy Level Relationship In Perovskite Solar Cells*, Sci. Rep., **2017**, 7, 1–10.

[175] Byranvand M.M.., Saliba M., *Defect Passivation Of Perovskite Films For Highly Efficient And Stable Solar Cells*, Sol. RRL, **2021**.

[176] Wang S. et al., *Lewis Acid/Base Approach For Efficacious Defect Passivation In Perovskite Solar Cells*, J. Mater. Chem. A, **2020**, 8, 12201–12225.

[177] Lewis G.N., *Valence and the Structure of Atoms and Molecules*, **1923**.

[178] Noel N.K. et al., *Enhanced Photoluminescence And Solar Cell Performance Via Lewis Base Passivation Of Organic-Inorganic Lead Halide Perovskites*, ACS Nano, **2014**, 8, 9815–9821.

[179] Wang J. et al., *Highly Efficient All-Inorganic Perovskite Solar Cells With Suppressed Non-Radiative Recombination By A Lewis Base*, Nat. Commun., **2020**, 11, 1–9.

[180] Lin Y. et al., *π-Conjugated Lewis Base: Efficient Trap-Passivation And Charge-Extraction For Hybrid Perovskite Solar Cells*, Adv. Mater., **2017**, 29, 1–6.

[181] Peng J. et al., *A Universal Double-Side Passivation For High Open-Circuit Voltage In Perovskite Solar Cells: Role Of Carbonyl Groups In Poly(Methyl Methacrylate)*, Adv. Energy Mater., **2018**, 8, 1–9.

[182] Li M.H. et al., *A Sulfur-Rich Small Molecule As A Bifunctional Interfacial Layer For Stable Perovskite Solar Cells With Efficiencies Exceeding 22%*, Nano Energy, **2021**, 79, 105462.

[183] Sutanto A.A. et al., *Phosphine Oxide Derivative As A Passivating Agent To Enhance The Performance Of Perovskite Solar Cells*, ACS Appl. Energy Mater., **2021**, 4, 1259–1268.

[184] Wen T.Y. et al., *Surface Electronic Modification Of Perovskite Thin Film With Water-Resistant Electron Delocalized Molecules For Stable And Efficient Photovoltaics*, Adv. Energy Mater., **2018**, 8, 1–7.

[185] Zeng Q. et al., *Polymer-Passivated Inorganic Cesium Lead Mixed-Halide Perovskites For Stable And Efficient Solar Cells With High Open-Circuit Voltage Over 1.3 V*, Adv. Mater., **2018**, 30, 1–9.

[186] Braly I.L. et al., *Hybrid Perovskite Films Approaching The Radiative Limit With Over 90% Photoluminescence Quantum Efficiency*, Nat. Photonics, **2018**, 12, 355–361.

[187] Dequilettes D.W. et al., *Photoluminescence Lifetimes Exceeding 8 Ms And Quantum Yields Exceeding 30% In Hybrid Perovskite Thin Films By Ligand Passivation*, ACS Energy Lett., **2016**, 1, 438–444.

[188] Belisle R.A. et al., *Impact Of Surfaces On Photoinduced Halide Segregation In Mixed-Halide Perovskites*, ACS Energy Lett., **2018**, 3, 2694–2700.

[189] Haddon R.C., *Chemistry Of The Fullerenes: The Manifestation Of Strain In A Class Of Continuous*, New Ser., **1993**, 261, 1545–1550.

[190] Colin M.M.., Gaultier de Claubry H., *Sur Le Combinaisons De L'iode Avec Les Substances Végétales Et Animales.*, Ann. Chim., **1814**, 90, 87–100.

[191] Metrangolo P., Resnati G., *Halogen Bonding: A Paradigm In Supramolecular Chemistry*, Chem. a Eur. J., **2001**, 7, 2511–2519.

[192] Desiraju G.R. et al., *Definition Of The Halogen Bond (IUPAC Recommendations 2013)**, pure appl. chem, **2013**, 85, 1711–1713.

[193] Clark T. et al., *Halogen Bonding: The σ-Hole: Proceedings Of "Modeling Interactions In Biomolecules II", Prague, September 5th-9th, 2005*, J. Mol. Model., **2006**, 13, 291–296.

[194] Metrangolo P., Resnati G., *Halogen Bonding: fundamentals and applications*, Springer, **2008**.

[195] Eskandari K., Lesani M., *Does Fluorine Participate In Halogen Bonding?*, Chem. - A Eur. J., **2015**, 21, 4739–4746.

[196] Cavallo G. et al., *The Halogen Bond*, Chem. Rev., **2016**, 116, 2478–2601.

[197] Priimagi A. et al., *The Halogen Bond In The Design Of Functional Supramolecular Materials: Recent Advances*, Acc. Chem. Res., **2013**, 46, 2686–2695.

[198] Metrangolo P. et al., *Halogen Bonding In Supramolecular Chemistry*, Angew. Chemie - Int. Ed., **2008**, 47, 6114–6127.

[199] Valerio G. et al., *Halogen Bonding In Fluoroalkylhalides: A Quantum Chemical Study Of Increasing Fluorine Substitution*, J. Phys. Chem. A, **2000**, 104, 10–13.

[200] Auffinger P. et al., *Halogen Bonds In Biological Molecules*, Proc. Natl. Acad. Sci. U. S. A., **2004**, 101, 16789–16794.

[201] Parker A.J. et al., *Halogen Bonding In DNA Base Pairs*, J. Am. Chem. Soc., **2012**, 134, 5165–5172.

[202] Costa P.J., *The Halogen Bond: Nature And Applications*, Phys. Sci. Rev., **2019**, 2, 1–16.

[203] Mulliken R.S., *Molecular Compounds And Their Spectra. III. The Interaction Of Electron Donors And Acceptors*, J. Phys. Chem., **1952**, 56, 801–822.

[204] Reiling S., Besnard M., Bopp P.A., *Theoretical Studies On The Pyridine - I2 Charge-Transfer Complex . 1. Ab-Initio Calculations On I2 And Pyridine - I2*, J. Phys. Chem. A, **1997**, 5639, 4409–4415.

[205] Corradi E. et al., *Halogen Bonding Versus Hydrogen Bonding In Driving Self-Assembly Processes*, Angew. Chemie - Int. Ed., **2000**, 39, 1782–1786.

[206] Metrangolo P., Resnati G., *Chemistry: Halogen Versus Hydrogen*, Science, **2008**, 321, 918–919.

[207] Riley K.E., Hobza P., *The Relative Roles Of Electrostatics And Dispersion In The Stabilization Of Halogen Bonds*, Phys. Chem. Chem. Phys., **2013**, 15, 17742–17751.

[208] Mukherjee A., Tothadi S., Desiraju G.R., *Halogen Bonds In Crystal Engineering: Like Hydrogen Bonds Yet Different*, Acc. Chem. Res., **2014**, 47, 2514–2524.

[209] Jentzsch A.V. et al., *Transmembrane Anion Transport Mediated By Halogen-Bond Donors*, Nat. Commun., **2012**, 3, 1–8.

[210] Bolton O. et al., *Activating Efficient Phosphorescence From Purely Organic Materials By Crystal Design*, Nat. Chem., **2011**, 3, 205–210.

[211] Priimagi A. et al., *Halogen Bonding Versus Hydrogen Bonding In Driving Self-Assembly And Performance Of Light-Responsive Supramolecular Polymers*, Adv. Funct. Mater., **2012**, 22, 2572–2579.

[212] Abate A. et al., *Supramolecular Halogen Bond Passivation Of Organic − Inorganic Halide Perovskite Solar Cells*, Nano Lett., **2014**, 14, 3247–3254.

[213] Zhang L. et al., *First-Principles Study Of Molecular Adsorption On Lead Iodide Perovskite Surface: A Case Study Of Halogen Bond Passivation For Solar Cell Application*, J. Phys. Chem. C, **2016**, 120, 23536–232541.

[214] Bi S. et al., *Halogen Bonding Reduces Intrinsic Traps And Enhances Charge Mobilities In Halide Perovskite Solar Cells*, J. Mater. Chem. A, **2019**, 7, 6840–6848.

[215] Wolff C.M. et al., *Perfluorinated Self-Assembled Monolayers Enhance The Stability And Efficiency Of Inverted Perovskite Solar Cells*, ACS Nano, **2020**, 14, 1445–1456.

[216] Ruiz-preciado M.A. et al., *Supramolecular Modulation Of Hybrid Perovskite Solar Cells Via Bifunctional Halogen*

Bonding Revealed By Two-Dimensional 19F Solid-State NMR Spectroscopy, J. Am. Chem. Soc., **2020**, 142, 1645–1654.

[217] Erdélyi M., *Halogen Bonding In Solution*, Chem. Soc. Rev., **2012**, 41, 3547–3557.

[218] Abate A. et al., *Supramolecular Halogen Bond Passivation Of Organic-Inorganic Halide Perovskite Solar Cells*, Nano Lett., **2014**, 14, 3247–3254.

[219] Love J.C. et al., *Self-Assembled Monolayers Of Thiolates On Metals As A Form Of Nanotechnology*, Chem. Rev., **2005**, 105, 1103–1169.

[220] Choi K. et al., *A Short Review On Interface Engineering Of Perovskite Solar Cells: A Self-Assembled Monolayer And Its Roles*, Sol. RRL, **2019**, 4, 1–20.

[221] Alloway D.M. et al., *Interface Dipoles Arising From Self-Assembled Monolayers On Gold: UV-Photoemission Studies Of Alkanethiols And Partially Fluorinated Alkanethiols*, J. Phys. Chem. B, **2003**, 107, 11690–11699.

[222] Ford W.E. et al., *Organic Dipole Layers For Ultralow Work Function Electrodes*, ACS Nano, **2014**, 8, 9173–9180.

[223] Lange I. et al., *Tuning The Work Function Of Polar Zinc Oxide Surfaces Using Modifi Ed Phosphonic Acid Self-Assembled Monolayers*, Adv. Energy Mater., **2014**, 1–11.

[224] Raoufi M., Neher D., *Simultaneous Effect Of UV-Radiation And Surface Modification On The Work Function And Hole Injection Properties Of ZnO Thin Films*, Phisica Status Solidi A, **2020**, 217, 1–6.

[225] Ansari F. et al., *Passivation Mechanism Exploiting Surface Dipoles Affords High-Performance Perovskite Solar Cells*, J. Am. Chem. Soc., **2020**, 142, 11428–11433.

[226] Will J. et al., *Evidence Of Tailoring The Interfacial Chemical Composition In Normal Structure Hybrid Organohalide Perovskites By A Self-Assembled Monolayer*, ACS Appl. Mater. Interfaces, **2018**, 10, 5511–5518.

[227] Liu K. et al., *Fullerene Derivative Anchored SnO2 For High-Performance Perovskite Solar Cells*, Energy Environ. Sci., **2018**, 11, 3463–3471.

[228] Campbell I.H. et al., *Controlling Charge Injection In Organic Electronic Devices Using Self-Assembled Monolayers*, Appl. Phys. Lett., **1997**, 71, 3528–3530.

[229] Campbell I. et al., *Controlling Schottky Energy Barriers In Organic Electronic Devices Using Self-Assembled Monolayers*, Phys. Rev. B, **1996**, 54, R14321–R14324.

[230] Chen L. et al., *Interfacial Dipole In Organic And Perovskite Solar Cells*, J. Am. Chem. Soc., **2020**, 142, 18281–18292.

[231] Schultz T. et al., *The Interlayer Method: A Universal Tool For Energy Level Alignment Tuning At Inorganic/Organic Semiconductor Heterojunctions*, Adv. Funct. Mater., **2020**, 2010174, 1–7.

[232] Zojer E., Taucher T.C., Hofmann O.T., *The Impact Of Dipolar Layers On The Electronic Properties Of Organic/Inorganic Hybrid Interfaces*, Adv. Mater. Interfaces, **2019**, 6.

[233] Lim K.-G., Ahn S., Lee T.-W., *Energy Level Alignment Of Dipolar Interface Layer In Organic And Hybrid Perovskite Solar Cells*, J. Mater. Chem. C, **2018**, 2915–2924.

[234] Vilan A., Cahen D., *Chemical Modification Of Semiconductor Surfaces For Molecular Electronics*, Chem. Rev., **2017**, 117, 4624–4666.

[235] Topping J., *On The Mutual Potential Energy Of A Plane Network Of Doublets*, Proc. R. Soc. London, **1926**, 116, 67–72.

[236] Taucher T.C., Zojer E., *The Potential Of X-Ray Photoelectron Spectroscopy For Determining Interface Dipoles Of Self-Assembled Monolayers*, Appl. Sci., **2020**, 10, 48–52.

[237] Chen Q. et al., *Quantitative Operando Visualization Of The Energy Band Depth Profile In Solar Cells*, Nat. Commun., **2015**, 6, 1–9.

[238] Wang J. et al., *Effect Of Metal/Bulk-Heterojunction Interfacial Properties On Organic Photovoltaic Device Performance*, J. Mater. Chem. A, **2014**, 2, 15288–15293.

[239] Möllmann A. et al., *Highly Compact TiO2 Films By Spray Pyrolysis And Application In Perovskite Solar Cells*, Adv. Eng. Mater., **2019**, 21, 1–8.

[240] Watts C.L. et al., *Light Soaking In Metal Halide Perovskites Studied Via Steady-State Microwave Conductivity*, Commun. Phys., **2020**, 3, 1–10.

[241] Cimaroli A.J. et al., *Tracking The Maximum Power Point Of Hysteretic Perovskite Solar Cells Using A Predictive Algorithm*, J. Mater. Chem. C, **2017**, 5, 10152–10157.

[242] Rakocevic L. et al., *Reliable Performance Comparison Of Perovskite Solar Cells Using Optimized Maximum Power Point Tracking*, Sol. RRL, **2019**, 3, 1–9.

[243] Köbler H. et al., High-Throughput Aging System for Perovskite Solar Cells (https://www.nanoge.org/proceedings/SCHP/5e9607f7ddcd936cbe82645a). Proceedings of HOPV19. 2019.

[244] Pazoki M., Hagfeldt A., Edvinsson T., *Characterization techniques for perovskite solar cell materials*, **2019**.

[245] Swinehart D.F., *The Beer-Lambert Law*, J. Chem. Educ., **1962**, 39, 333–335.

[246] Perkamus H.-H., *UV/Vis Spectroscopy and its Applications*, Springer, **1992**.

[247] Béchu S. et al., *Photoemission Spectroscopy Characterization Of Halide Perovskites*, Adv. Energy Mater., **2020**, 10, 1–25.

[248] Kronik L., Shapira Y., *Surface Photovoltage Phenomena: Theory , Experiment, And Applications*, Surf. Sci. Rep., **1999**, 37, 1–206.

[249] Kelvin, Lord, *Contact Electricity Of Metals*, Philos. Mag. Ser. 5, **1898**, 46, 82–120.

[250] Zisman W.A., *A New Method Of Measuring Contact Potential Differences In Metals*, Rev. Sci. Instrum., **1932**, 3, 367–370.

[251] Besocke K., Berger S., *Piezoelectric Driven Kelvin Probe For Contact Potential Difference Studies*, Rev. Sci. Instrum., **1976**, 47, 840–842.

[252] Nonnenmacher M. et al., *Kelvin Probe Force Microscopy*, Appl. Phys. Lett., **1991**, 2921, 2921–2923.

[253] Kang Z. et al., *Kelvin Probe Force Microscopy For Perovskite Solar Cells*, Sci. China Mater., **2019**, 1–14.

[254] Baikie I.D. et al., *Ambient Pressure Photoemission Spectroscopy Of Metal Surfaces*, Appl. Surf. Sci., **2014**, 323, 45–53.

[255] Bond A.M. et al., *Electroanalytical Methods Guide to Experiments and Applications 2nd, revised and extended edition*, **2009**.

[256] D'Andrade B.W. et al., *Relationship Between The Ionization And Oxidation Potentials Of Molecular Organic Semiconductors*, Org. Electron., **2005**, 6, 11–20.

[257] Ciavatti A. et al., *Boosting Direct X-Ray Detection In Organic Thin Films By Small Molecules Tailoring*, Adv. Funct. Mater., **2019**, 29, 1–8.

[258] Stössel M. et al., *Impact Of The Cathode Metal Work Function On The Performance Of Vacuum-Deposited Organic Light Emitting-Devices*, Appl. Phys. A, **1999**, 390, 387–390.

[259] Wang Y. et al., *Efficient α-CsPbI3Photovoltaics With Surface Terminated Organic Cations*, Joule, **2018**, 1–11.

[260] Yajima T. et al., *Controlling Band Alignments By Artificial Interface Dipoles At Perovskite Heterointerfaces*, Nat. Commun., **2015**, 6, 1–5.

[261] Ye M. et al., *Recent Advances In Interfacial Engineering Of Perovskite Solar Cells*, J. Phys. D. Appl. Phys., **2017**, 50.

[262] Zhao P., Kim B.J., Jung H.S., *Passivation In Perovskite Solar Cells: A Review*, Mater. Today Energy, **2018**, 7, 267–286.

[263] Boer B. De et al., *Tuning Of Metal Work Functions With Self-Assembled Monolayers*, Adv. Mater., **2005**, 17, 621–625.

[264] Zhang X. et al., *Facilitating Electron Collection Of Organic Photovoltaics By Passivating Trap States And Tailoring Work Function*, Sol. Energy, **2019**, 181, 9–16.

[265] Yang Y. et al., *Eliminating Charge Accumulation Via Interfacial Dipole For Efficient And Stable Perovskite Solar Cells*, ACS Appl. Mater. Interfaces, **2019**, 11, 34964–34972.

[266] Liu D. et al., *Vacancies Substitution Induced Interfacial Dipole Formation And Defect Passivation For Highly Stable Perovskite Solar Cells*, Chem. Eng. J., **2020**, 125010.

[267] Agresti A. et al., *Titanium-Carbide MXenes For Work Function And Interface Engineering In Perovskite Solar Cells*, Nat. Mater., **2019**, 18, 1228–1234.

[268] Wu Z. et al., *Highly Efficient And Stable Perovskite Solar Cells Via Modification Of Energy Levels At The Perovskite / Carbon Electrode Interface*, **2019**, 1804284, 1–7.

[269] Dong H. et al., *Conjugated Molecules "Bridge": Functional Ligand Toward Highly Efficient And Long-Term Stable Perovskite Solar Cell*, Adv. Funct. Mater., **2019**, 1808119, 1–11.

[270] Zenasni O., Jamison A.C., Lee T.R., *The Impact Of Fluorination On The Structure And Properties Of Self-Assembled Monolayer Films*, Soft Matter, **2013**, 9, 6356–6370.

[271] Kong W. et al., *Organic Monomolecular Layers Enable Energy-Level Matching For Efficient Hole Transporting Layer Free Inverted Perovskite Solar Cells*, ACS Nano, **2019**, 13, 1625–1634.

[272] Zhang R. et al., *Enhancing Perovskite Quality And Energy Level Alignment Of TiO2 Nanorod Arrays-Based Solar Cells Via Interfacial Modification*, Sol. Energy Mater. Sol. Cells, **2019**, 191, 183–189.

[273] Sadhu S. et al., *Unexpected Surface Interactions Between Fluorocarbons And Hybrid Organic Inorganic Perovskites Evidenced By PM-IRRAS And Their Application Towards Tuning The Surface Potential*, Mater. Horizons, **2019**, 6, 192–197.

[274] Abate A. et al., *Halogen-Bond Driven Self-Assembly Of Perfluorocarbon Monolayers On Silicon Nitride*, J. Mater. Chem. A, **2019**, 7, 24445–24453.

[275] Abate A. et al., *Anisotropic Ionic Conductivity In Fluorinated Ionic Liquid Crystals Suitable For Optoelectronic Applications*, J. Mater. Chem. A, **2013**, 1, 6572–6578.

[276] Harwell J.R. et al., *Probing The Energy Levels Of Perovskite Solar Cells: Via Kelvin Probe And UV Ambient Pressure Photoemission Spectroscopy*, Phys. Chem. Chem. Phys., **2016**, 18, 19738–19745.

[277] Reddy S.S. et al., *Lewis Acid-Base Adduct-Type Organic Hole Transport Material For High Performance And Air-Stable Perovskite*, Nano Energy, **2019**, 58, 284–292.

[278] Gallet T. et al., *Fermi-Level Pinning In Methylammonium Lead Iodide Perovskites*, Nanoscale, **2019**, 11, 16828–16836.

[279] Eperon G.E., Ginger D.S., *B-Site Metal Cation Exchange In Halide Perovskites*, ACS Energy Lett., **2017**, 2, 1190–1196.

[280] Gozlan N., Tisch U., Haick H., *Tailoring The Work Function Of Gold Surface By Controlling Coverage And Disorder Of Polar Molecular Monolayers*, **2008**, 12988–12992.

[281] Yang Y. et al., *Surface Dipoles And Electron Transfer At The Metal Oxide-Metal Interface: A 2PPE Study Of Size-Selected Metal Oxide Clusters Supported On Cu(111)*, J. Phys. Chem. C, **2014**, 118, 13697–13706.

[282] Philippe B. et al., *Chemical Distribution Of Multiple Cation (Rb+, Cs+, MA+, And FA+) Perovskite Materials By Photoelectron Spectroscopy*, Chem. Mater., **2017**, 29, 3589–3596.

[283] Yang X. et al., *Buried Interfaces In Halide Perovskite Photovoltaics*, Adv. Mater., **2021**, 2006435, 1–10.

[284] Saliba M. et al., *Cesium-Containing Triple Cation Perovskite Solar Cells: Improved Stability, Reproducibility And High Efficiency*, Energy Environ. Sci., **2016**, 9, 1989–1997.

[285] Jacobsson J., *Releasing The Power Of The Crowd With FAIR Data Management By Introducing The Perovskite Database Project*, under Rev. Nat. Energy, **2021**.

[286] Edri E. et al., *High Open-Circuit Voltage Solar Cells Based On Organic-Inorganic Lead Bromide Perovskite*, J. Phys. Chem. Lett., **2013**, 4, 897–902.

[287] Hörantner M.T. et al., *The Potential Of Multijunction Perovskite Solar Cells*, ACS Energy Lett., **2017**, 2, 2506–2513.

[288] Heo J.H., Im S.H., *CH3NH3PbBr3–CH3NH3PbI3Perovskite–Perovskite Tandem Solar Cells With Exceeding 2.2 V Open Circuit Voltage*, Adv. Mater., **2016**, 28, 5121–5125.

[289] Sheng R. et al., *Four-Terminal Tandem Solar Cells Using CH3NH3PbBr3 By Spectrum Splitting*, J. Phys. Chem. Lett., **2015**, 6, 3931–3934.

[290] McGovern L. et al., *Understanding The Stability Of MAPbBr3versus MAPbI3: Suppression Of Methylammonium Migration And Reduction Of Halide Migration*, J. Phys. Chem. Lett., **2020**, 11, 7127–7132.

[291] Rao H.S. et al., *A Micron-Scale Laminar MAPbBr3 Single Crystal For An Efficient And Stable Perovskite Solar Cell*, Chem. Commun., **2017**, 53, 5163–5166.

[292] Noel N.K. et al., *Highly Crystalline Methylammonium Lead Tribromide Perovskite Films For Efficient Photovoltaic Devices*, ACS Energy Lett., **2018**, 3, 1233–1240.

[293] Rehermann C. et al., *Origin Of Ionic Inhomogeneity In MAPb(IxBr1-X)3Perovskite Thin Films Revealed By In-Situ Spectroscopy During Spin Coating And Annealing*, ACS Appl. Mater. Interfaces, **2020**, 12, 30343–30352.

[294] Singh S., Kabra D., *Influence Of Solvent Additive On The Chemical And Electronic Environment Of Wide Bandgap Perovskite Thin Films*, J. Mater. Chem. C, **2018**, 6, 12052–12061.

[295] Heo J.H., Song D.H., Im S.H., *Planar CH3NH3PbBr3 Hybrid Solar Cells With 10.4% Power Conversion Efficiency, Fabricated By Controlled Crystallization In The Spin-Coating Process*, Adv. Mater., **2014**, 26, 8179–8183.

[296] Zheng X. et al., *Room Temperature Fabrication Of CH3NH3PbBr3 By Anti-Solvent Assisted Crystallization Approach For Perovskite Solar Cells With Fast Response And Small J-V Hysteresis*, Nano Energy, **2015**, 17, 269–278.

[297] Chen H. et al., *An Amorphous Precursor Route To The Conformable Oriented Crystallization Of CH3NH3PbBr3 In Mesoporous Scaffolds: Toward Efficient And Thermally Stable Carbon-Based Perovskite Solar Cells*, J. Mater. Chem. A, **2016**, 4, 12897–12912.

[298] Levine I. et al., *Direct Probing Of Gap States And Their Passivation In Halide Perovskites By High-Sensitivity, Variable Energy Ultraviolet Photoelectron Spectroscopy*, J. Phys. Chem. C, **2021**, 125, 5217–5225.

[299] Ferdowsi P. et al., *Ultrathin Polymeric Films For Interfacial Passivation In Wide Band-Gap Perovskite Solar Cells*, Sci. Rep., **2020**, 10, 1–10.

[300] Carli S. et al., *A New 1,3,4-Oxadiazole-Based Hole-Transport Material For Efficient CH3NH3PbBr3 Perovskite Solar Cells*, ChemSusChem, **2016**, 9, 657–661.

[301] Hu X. et al., *Wide-Bandgap Perovskite Solar Cells With Large Open-Circuit Voltage Of 1653 MV Through Interfacial Engineering*, Sol. RRL, **2018**, 2, 1–10.

[302] Dar M.I. et al., *High Open Circuit Voltage For Perovskite Solar Cells With S,Si-Heteropentacene-Based Hole Conductors*, Eur. J. Inorg. Chem., **2018**, 2018, 4573–4578.

[303] Gilkerson W.R.., Srivastava K.K., *The Dipole Moment Of Urea*, J. Phys. Chem., **1960**, 64, 1485–1487.

[304] Rehermann C., *Exploring The Precursor-Process-Property Space In Metal Halide Perovskite Thin-Films*, Dissertation, **2020**.

[305] Rai M., Wong L.H., Etgar L., *Effect Of Perovskite Thickness On Electroluminescence And Solar Cell Conversion Efficiency*, J. Phys. Chem. Lett., **2020**, 11, 8189–8194.

[306] Qarony W. et al., *Optical Analysis In CH3NH3 PbI3 And CH3NH3PbI2Cl Based Thin-Film Perovskite Solar Cell*, Am. J. Energy Res., **2015**, 3, 19–24.

[307] Canil L. et al., *Halogen-Bonded Hole-Transport Material Suppresses Charge Recombination And Enhances Stability Of Perovskite Solar Cells*, Adv. Energy Mater., **2021**, 11, 1–9.

[308] Park N.G. et al., *Towards Stable And Commercially Available Perovskite Solar Cells*, Nat. Energy, **2016**, 1.

[309] Zhang H., Nazeeruddin M.K., Choy W.C.H., *Perovskite Photovoltaics: The Significant Role Of Ligands In Film Formation, Passivation, And Stability*, Adv. Mater., **2019**, 31, 1–29.

[310] Han T.H. et al., *Interface And Defect Engineering For Metal Halide Perovskite Optoelectronic Devices*, Adv. Mater., **2019**, 1803515, 1–35.

[311] Ding X. et al., *Passivation Functionalized Phenothiazine-Based Hole Transport Material For Highly Efficient Perovskite Solar Cell With Efficiency Exceeding 22%*, Chem. Eng. J., **2020**, 410, 1–8.

[312] Zhao B.X. et al., *A Hole-Transport Material That Also Passivates Perovskite Surface Defects For Solar Cells With Improved Efficiency And Stability*, Energy Environ. Sci., **2020**, 13, 4334–4343.

[313] Wang S.Y. et al., *Defect Passivation By Amide-Based Hole-Transporting Interfacial Layer Enhanced Perovskite Grain Growth For Efficient P-I-N Perovskite Solar Cells*, ACS Appl. Mater. Interfaces, **2019**, 11, 40050–40061.

[314] Qi F. et al., *A Dopant-Free Polymeric Hole-Transporting Material Enabled High Fill Factor Over 81% For Highly Efficient Perovskite Solar Cells*, Adv. Energy Mater., **2019**, 9, 1–7.

[315] Zhang J. et al., *Simultaneous Defect Passivation And Hole Mobility Enhancement Of Perovskite Solar Cells By Incorporating Anionic Metal-Organic Framework Into Hole Transport Materials*, Chem. Eng. J., **2021**, 408, 1–7.

[316] Meazza L. et al., *Halogen-Bonding-Triggered Supramolecular Gel Formation*, Nat. Chem., **2013**, 5, 42–47.

[317] Wang H. et al., *The Halogen Bond: An Emerging Supramolecular Tool In The Design Of Functional Mesomorphic Materials*, Chem. - A Eur. J., **2019**, 25, 1369–1378.

[318] Saccone M. et al., *Supramolecular Hierarchy Among Halogen And Hydrogen Bond Donors In Light-Induced Surface Patterning*, J. Mater. Chem. C, **2015**, 3, 759–768.

[319] Paek S. et al., *Molecular Design And Operational Stability: Toward Stable 3D/2D Perovskite Interlayers*, Adv. Sci., **2020**, 7, 1–11.

[320] Dai Z. et al., *Interfacial Toughening With Self-Assembled Monolayers Enhances Perovskite Solar Cell Reliability*, Science, **2021**, 372, 618–622.

[321] Mosconi E., Azpiroz J.M., Angelis F. De, *Ab Initio Molecular Dynamics Simulations Of Methylammonium Lead Iodide Perovskite Degradation By Water*, Chem. Mater., **2015**, 27, 4885–4892.

[322] Meggiolaro D. et al., *Energy Level Tuning At The MAPbI $_3$ Perovskite/Contact Interface Using Chemical Treatment*, ACS Energy Lett., **2019**, 2181–2184.

[323] Schölin R. et al., *Energy Level Shifts In Spiro-OMeTAD Molecular Thin Films When Adding Li-TFSI*, J. Phys. Chem. C, **2012**, 116, 26300–26305.

[324] Chu T.Y., Song O.K., *Hole Mobility Of N, N′ -Bis(Naphthalen-1-Yl)- N, N′ -Bis(Phenyl) Benzidine Investigated By Using Space-Charge-Limited Currents*, Appl. Phys. Lett., **2007**, 90, 1–4.

[325] Zhang F. et al., *Polymeric, Cost-Effective, Dopant-Free Hole Transport Materials For Efficient And Stable Perovskite Solar Cells*, J. Am. Chem. Soc., **2019**, 141, 19700–19707.

[326] Wang Y. et al., *Dopant-Free Small-Molecule Hole-Transporting Material For Inverted Perovskite Solar Cells With Efficiency Exceeding 21%*, Adv. Mater., **2019**, 31, 1–10.

[327] Niu T. et al., *D-A-π-A-D-Type Dopant-Free Hole Transport Material For Low-Cost, Efficient, And Stable Perovskite Solar Cells*, Joule, **2021**, 5, 249–269.

[328] Kim S.G. et al., *Capturing Mobile Lithium Ions In A Molecular Hole Transporter Enhances The Thermal Stability Of Perovskite Solar Cells*, Adv. Mater., **2021**, 33, 1–10.

[329] Fu Q. et al., *Multifunctional Two-Dimensional Conjugated Materials For Dopant-Free Perovskite Solar Cells With Efficiency Exceeding 22%*, ACS Energy Lett., **2021**, 1521–1532.

[330] Ge Q.Q. et al., *A Two-Dimensional Hole-Transporting Material For High-Performance Perovskite Solar Cells With 20 % Average Efficiency*, Angew. Chemie - Int. Ed., **2018**, 57, 10959–10965.

[331] Stolterfoht M. et al., *How To Quantify The Efficiency Potential Of Neat Perovskite Films: Perovskite Semiconductors With An Implied Efficiency Exceeding 28%*, Adv. Mater., **2020**, 32, 1–10.

[332] Roesch R. et al., *Procedures And Practices For Evaluating Thin-Film Solar Cell Stability*, Adv. Energy Mater., **2015**, 5, 1–24.

[333] Jeong J. et al., *Unveiling The Origin Of Performance Reduction In Perovskite Solar Cells With TiO2 Electron Transport Layer: Conduction Band Minimum Mismatches And Chemical Interactions At Buried Interface*, Appl. Surf. Sci., **2019**, 495, 1–10.

[334] Wussler M. et al., *Tapered Cross-Section Photoelectron Spectroscopy Of State-Of-The-Art Mixed Ion Perovskite Solar Cells: Band Bending Profile In The Dark, Photopotential Profile Under Open Circuit Illumination, And Band Diagram*, Adv. Funct. Mater., **2020**, 30, 1–12.

[335] Cramer T. et al., *Direct Imaging Of Defect Formation In Strained Organic Flexible Electronics By Scanning Kelvin Probe Microscopy*, Sci. Rep., **2016**, 6, 1–9.

[336] Raoui Y. et al., *Energy Level Engineering Of Charge Selective Contact And Halide Perovskite By Modulating Band Offset: Mechanistic Insights*, J. Energy Chem., **2021**, 54, 822–829.

[337] Das C. et al., *Surface, Interface, And Bulk Electronic And Chemical Properties Of Complete Perovskite Solar Cells: Tapered Cross-Section Photoelectron Spectroscopy, A Novel Solution*, ACS Appl. Mater. Interfaces, **2020**, 12, 40949–40957.

APPENDIX

A. APPENDIX

A1 Molecules

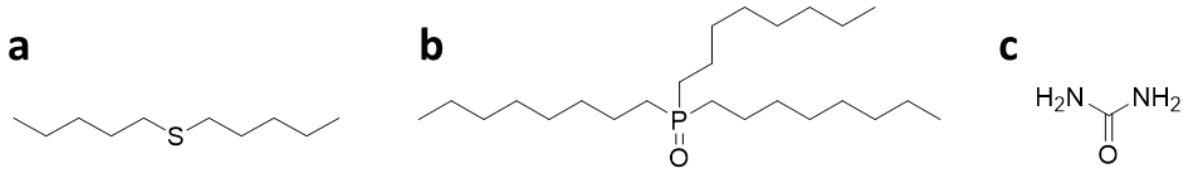

Figure A1.1. Lewis bases: (a) amyl sulfide – csc5, (b) Trioctylphosphine oxide – TOPO, (c) urea. Plotted with ChemDraw.

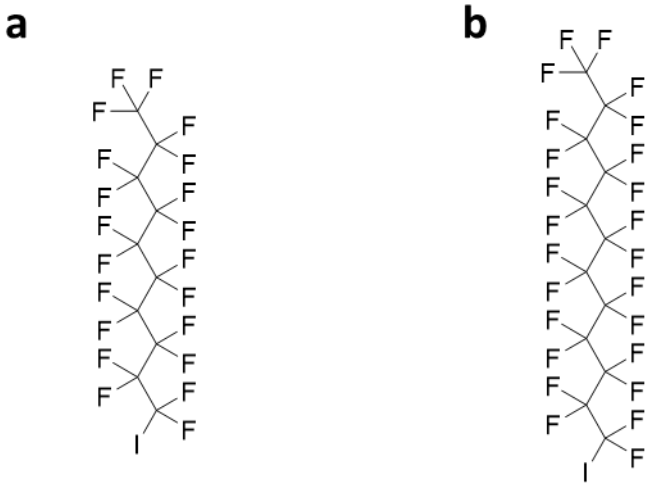

Figure A1.2. Lewis acids: (a) perfluorodecyl iodide – IPFC10, (b) perfluorododecyl iodide – IPFC12. Plotted with ChemDraw.

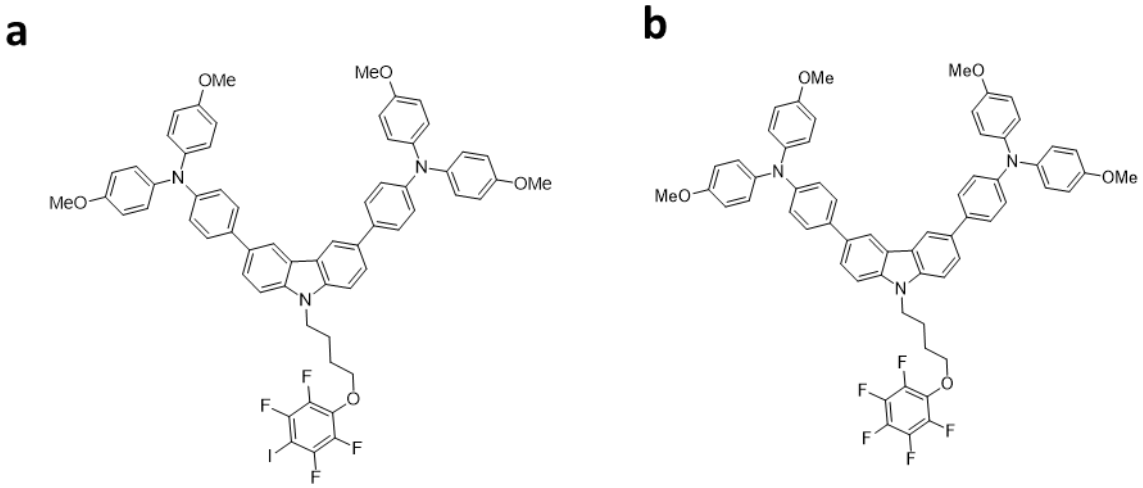

Figure A1.3. Hole-transport materials: (a) $C_{62}H_5F_4IN_3O_5$ – PFI, (b) $C_{62}H_5F_5N_3O_5$ – PF. Plotted by collaborators.

A2 Samples and devices preparation and characterization

The following description is an addition to the qualitative description of section 4.1 and contains details on materials and procedures for the preparation of the samples and devices used in Chapter 5, Chapter 6 and Chapter 7.

All chemicals without specifications were ordered from Sigma Aldrich and were used as received.

Devices were prepared on etched FTO substrates (TEC 15 from Ying Kou) with dimensions 2.5x2.5 cm^2. Before use all the substrates were washed by sonication for 15 min. with Mucasol solution 2% in water (Schülke), DI water (only 5 min.), isopropanol and acetone respectively.

The washing procedure was followed by 15 min of O_3&UV treatment, then the samples were placed on a high temperature hot plate (Gestigkeit PZ28-3TD) for the compact TiO_2 sintering. TiO_2 compact layer was deposited by aerosol spray pyrolysis using oxygen as a carrier gas. The precursor solution for deposition on 27 substrates is: 0.48 ml of Acetylacetone (Santa Cruz Biotechnology) and 0.72 ml of titanium diisopropoxide bis(acetylacetonate) stock solution (75% in 2-propanol) diluted in 10.8 ml of ethanol (12 ml in total). The substrates were heated to 450 °C and kept at this temperature for 15 min before and 30 min after the spray of the precursor solution. The whole solution was sprayed using oxygen as carrying gas at a distance of 20 cm with inclination of 45°, with at least 20 s of delay between each spraying cycle.

The mesoporous TiO_2 was prepared by a spin coating step followed by sintering. The solution is made of TiO_2 paste (30 nrd for triple cation devices, 18 nrd for $MAPbBr_3$, greatcellsolar) dissolved in ethanol (125 mg/ml). 80 µl of solution were spin coated at 4000 rpm for 10s, annealed for few minutes at 100 °C and then sintered in the same hotplate used for the compact TiO_2 at 450°C for 30 min (after ramping up to these values in about 40 min).

Finally, the substrates were treated with Li (LiTFSI in acetonitrile roughly 10 mg/ml) right before the perovskite spin coating. 80 µl of Li solution were spin coated at 3000 rpm for 10 s, annealed for few minutes at 100 °C and then sintered following the same procedure as for the mesoporous TiO_2. This step was skipped in the case of $MAPbBr_3$ devices.

All the steps mentioned so far were performed in air. All the following steps were performed in N_2-filled gloveboxes.

The perovskite solution was prepared as follow:

- Triple cation perovskite: stock solutions of PbI_2 (1.5 M, TCI) and $PbBr_2$ (1.5 M, TCI) in anhydrous DMF/DMSO = 4:1 (v:v) were previously prepared and heated again overnight at 60 °C in a thermoshaker before use. MABr and FAI powders (dyenamo) were weighed out in two

separate vials and then the proper volume of PbI_2 ($PbBr_2$) stock solutions was calculated and added to the vials containing the FAI (MABr) powder to get a stoichiometry of FAI:PbI_2 (MABr:$PbBr_2$) of 1:1.09. Before deposition, the solutions were mixed as follows: $FAPbI_3$:$MaPbBr_3$ = 85:15 (v:v). Further CsI (1.5 M) from a stock solution in DMSO was eventually added to the precursor solution to produce a final composition with the stoichiometry $Cs_{0.05}(FA_{0.85}MA_{0.15})_{0.95}Pb(I_{0.85}Br_{0.15})_3$

- MAPbBr$_3$ perovskite: a stock solution of and $PbBr_2$ (1.2 M, TCI) in anhydrous DMF/DMSO = 4:1 (v:v) was previously prepared and heated again overnight at 60°C in a thermoshaker before use. MABr powder (dyenamo) was weighed out in a vial and then the proper volume of $PbBr_2$ stock solution was calculated and added to the vials containing the MABr powder to get a stoichiometry of MABr:$PbBr_2$ of 1:1.

The samples were then taken to a N_2-filled glovebox for the perovskite spin coating. The spin-coating protocols are as follow:

- Triple cation perovskite: 80 µl of perovskite solution were drop-casted on the substrates and spin coated in a two-step program at 1000 rpm for 10 s and 6000 rpm for 20 s. 5 s prior to the end of the program, 100 µl of CBZ were poured on the spinning substrate. Afterwards, the samples were annealed at 100 °C for 1 h.
- MAPbBr$_3$ devices: 80 µl of perovskite solution were drop-casted on the substrates and spin coated at 2000 rpm for 60 s. 150 µl of toluene were poured on the spinning substrate after 15s from the start of the spinning. Afterwards, the samples were annealed at 100 °C for 30 min.

At this point for the experiments in Chapter 5 and Chapter 6 the molecules were deposited on the substrates following the procedure described in Section 4.1.1.

Next, the hole-transport material (HTM) was deposited. Spiro-OMeTAD, PFI or PF were spin coated on top of the samples, depending on the experiment. A 29 mM solution of the respective HTM in chlorobenzene with additives (4-tert-Butypyridine, LiTFSI and Co(III)TFSI) was prepared using stock solutions. The additives were added with the following molar ratio to the HTM: 3.2 for 4-tert-Butypyridine, 0.53 for LiTFSI and 0.1 for Co(III)TFSI. The solution was then dynamically spin coated on the substrates: the solution was drop casted on the substrates right after the acceleration step (1.8 s at 200 rpm), a spinning step of 30 s at 1800 s rpm followed. Samples with HTMs without dopants were also prepared for comparison following the same procedure and solutions parameters.

After storing inside a dry air box overnight, the samples were transferred into the thermal evaporator (Mbraun Pro Vap 3G) for the deposition of 100 nm Au. The active area resulting from the use of masks during the evaporation was 0.18 cm^2, area that was then, thanks to shadow masks, reduced to 0.1 cm^2 for the solar simulator testing.

The light JV of perovskite solar cells were recorded using a Wavelabs Sinus-70 LED class AAA solar simulator in air for triple cation devices, and an Oriel LCS-100 class ABB solar simulator in a nitrogen-

filled glovebox for $MAPbBr_3$ devices. The light intensity was calibrated with a Silicon reference cell from Fraunhofer ISE. JV scans were performed with a Keithley 2400 SMU, controlled by a measurement control program written in LabView. For triple-cation devices the voltage step was of 10 mV with an integration time of 50 ms per point and settling time of 50 ms after voltage application, corresponding to a scan rate of 100 mV/s. For $MAPbBr_3$ devices the voltage step was of 20 mV with an integration time of 40 ms per point and settling time of 40 ms after voltage application, corresponding to a scan rate of 200 mV/s.

A3 Supporting Information: *Chapter 5*

A3.1 Methods

Atomic Force Microscopy: AFM experiments were performed on a NX10 system from Park-Systems, Korea. The AFM was positioned in a Glove-Box containing dry nitrogen atmosphere. KPFM measurements were performed with PPP-NCST-Au probes (Nanosensors, k=7.4 N/m) or NSC36/CrAu-B (Mikromasch k=2 N/m) following measurement procedures as described in literature[335]. Measurements were performed in dark, straylight of the AFM-beam (830 nm) had no impact on measurements.

Kelvin Probe: The contact potential difference measurements (CPD) were performed with a Kelvin probe consisting of a vibrating gold mesh driven by a piezo electric crystal (Kelvin probe S and CPD controller by Besocke Delta Phi). The samples were opened in air and quickly mounted in the setup, which was subsequently closed and evacuated until a pressure of roughly 0.5 mbar. The vacuum chamber was then refilled with N_2 until a pressure of approximately 670 mbar and, at this point, the measurement was started.

Electrochemical measurements: Cyclic voltammetry of the perovskite thin films with and without the tailored molecules (e.g. IPFC10 or csc5) coating on FTO glasses was performed in a three-electrode electrochemical cell using a potentiostat (Ivium Technologies B.V., Compact Stat). Experiments were carried out in an electrolyte containing 0.1 M Bu_4NPF_6 in dichloromethane. The thin film sample, a platinum wire, and an Ag/AgCl in saturated KCl were employed as a working, counter and reference electrode, respectively. The area of the working electrode that was exposed to the electrolyte was 0.785 cm^2. The measurements were conducted with a scan rate of 100 mV s^{-1}. A continuous nitrogen bubbling was applied on the electrolyte during the measurement to minimize the influence of oxygen on the determination of the redox potential. All measured potentials were correlated with the redox potential of Ag/AgCl, converting to energy level (CB and VB) vs. vacuum level: 1) $E_{VB} = E_{ox} + 4.65$; 2) $E_{CB} = 4.65 + E_{re,}$ where E_{ox} is the oxidized potential and E_{re} is the reduced potential.

Table A3.1. Cyclic voltammetry results

	E_{ox}, V	E_{VB}, eV	E_{re}, V	E_{CB}, eV
FTO+perov	0,88	5,53	-0,91	3,74
FTO+perov+IC10	1,1	5,75	-0,25	4,37
FTO+perov+csc5	0,52	5,17	-0,14	4,51

KP-APS: The Kelvin probe (KP) and the Ambient Pressure Photoemission Spectroscopy (APS) techniques are combined in a single KP-APS measurement tool provided by KP Technology Ltd. to determine the work function (WF) and the ionization energy of materials which defines the WF in case of metals and the valence band edge in case of semiconductors[254]. The KP system employs a 2.0 mm diameter tip with a gold alloy coating which is calibrated on a gold reference sample. The KP is placed in a Faraday cage which screens the external electrical fields. The contact potential difference (CPD) between tip and reference is measured with a resolution of up to 3 mV. The APS system uses the same Kelvin probe to detect the photoemission currents as a function of incident photon energy. The light source comprises a deuterium (D_2) lamp coupled with a grating monochromator. The range of the incident photon energy is 3.6-6.9 eV. The sample is illuminated via a DUV optical fiber. The photoemission threshold is determined with a resolution of 30 meV.

A3.2 Additional data

Table A3.2. Results of the KP-APS measurement. APS (light blue) and Kelvin Probe (light yellow) data were collected during the same measurement in order to have an idea of the whole band diagram.

	CPD (± 2 mV)		**SPV (± 3 meV)**	**Work function (± 0.04 eV)**		**Ionization energy (IE) (± 0.03 eV)**	**E_F - E_{VBM} (± 0.05 eV)**	
	dark	illum.		dark	illum.		dark	illum.
perovskite	-5	135	140	4.96	5.10	5.54	0.58	0.44
csc5	-156	-30	126	4.80	4.92	5.43	0.64	0.51
IPFC10	124	203	79	5.08	5.16	5.69	0.61	0.53

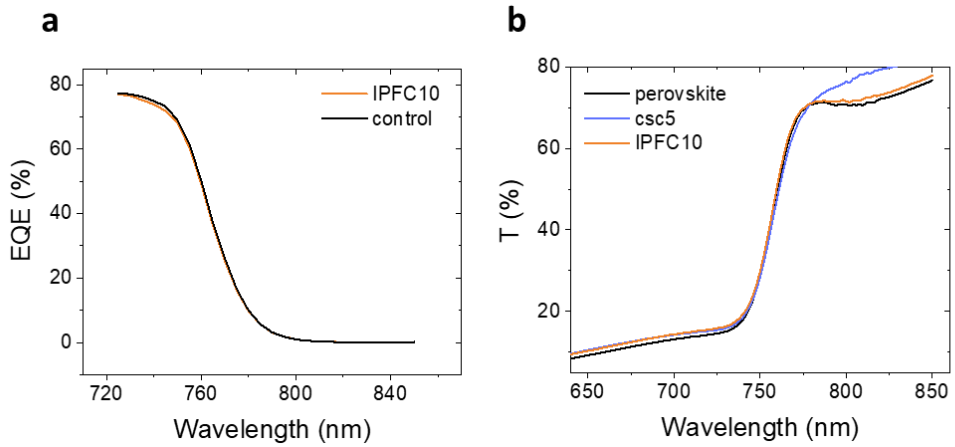

Figure A3.1. EQE (a) and UV-Vis (b) of bare and functionalized perovskite showing that the bandgap is not changing. EQE performed in N_2 atmosphere, UV-Vis performed in air.

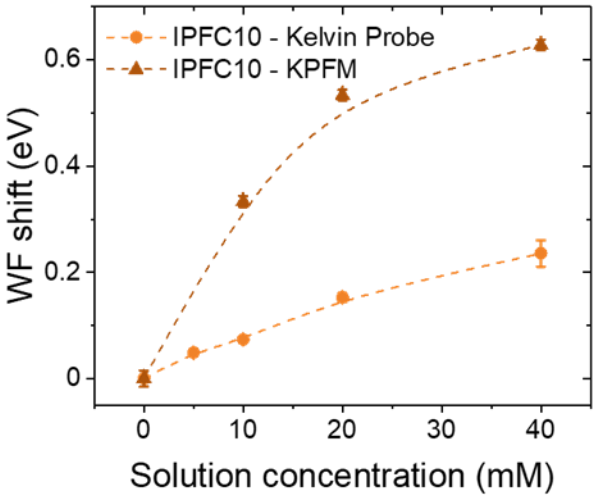

Figure A3.3. Comparison between Kelvin Probe and KPFM measurements proving that both measurements show the same trend. The magnitude of the shift is different because of the different measurement conditions, mainly the fact that Kelvin Probe was measured in air while KPFM in N_2.

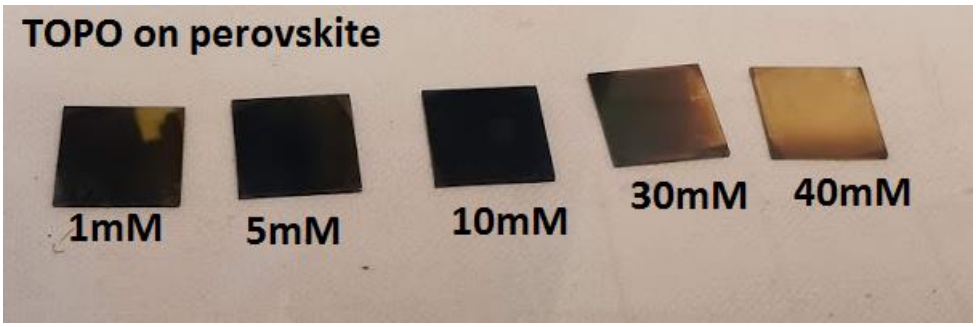

Figure A3.2. Effect of the deposition of TOPO on top of perovskite by dipping the substrates for 20min in TOPO solutions of different concentrations.

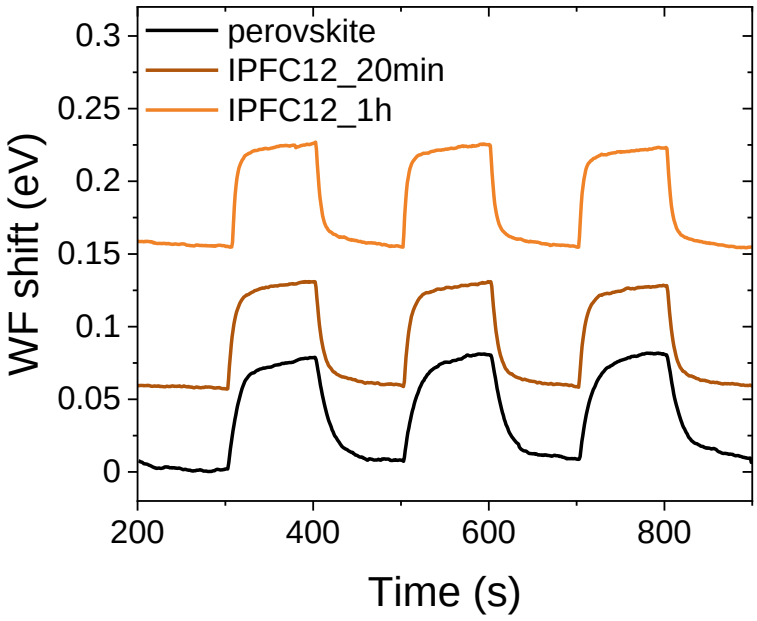

Figure A3.4. Kelvin probe WF shift measurement in dark and light of perovskite functionalized with IPFC12 for different dipping times.

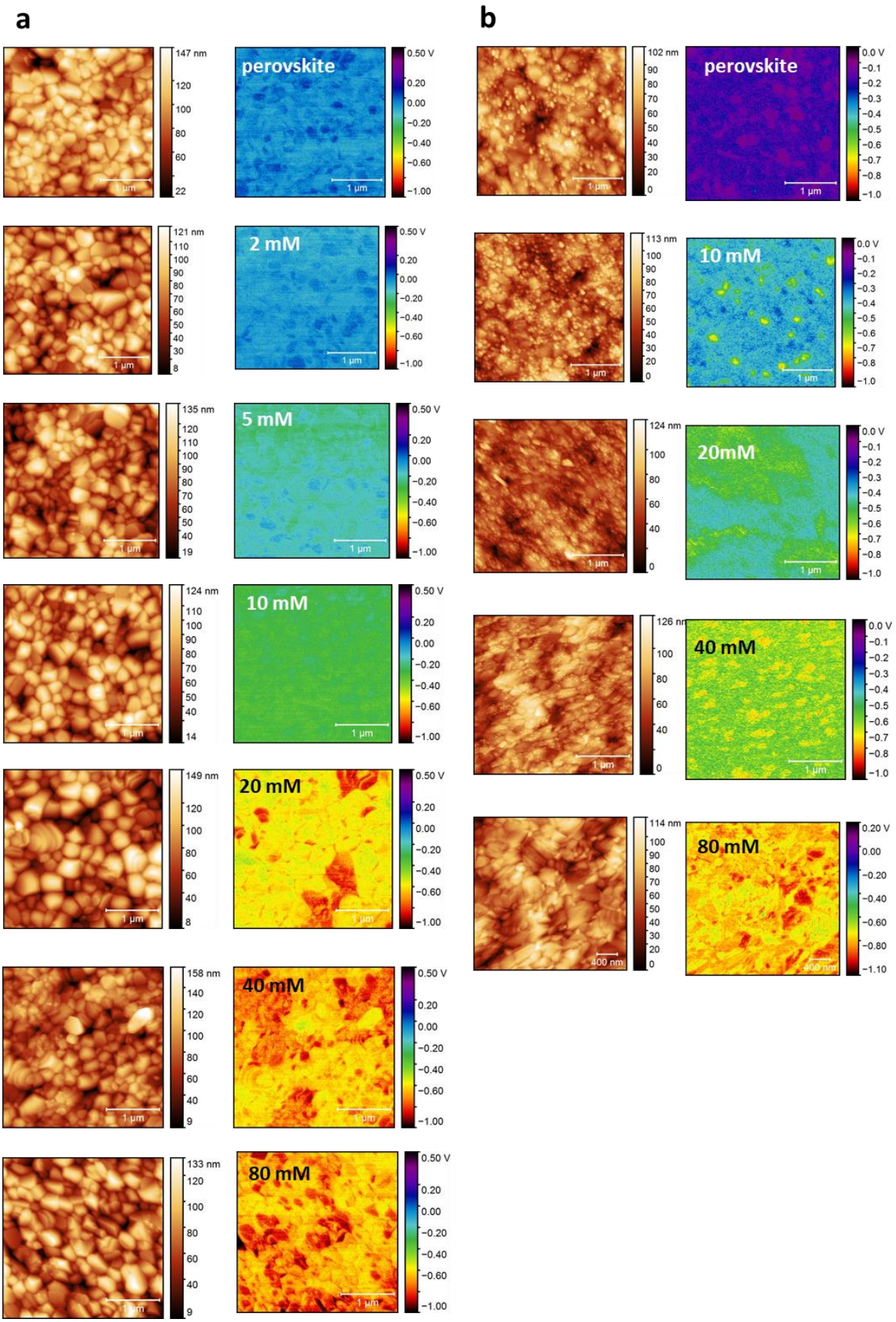

Figure A3.5. CPD and AFM maps for IPFC10 (a) and IPFC12 (b) at different concentrations.

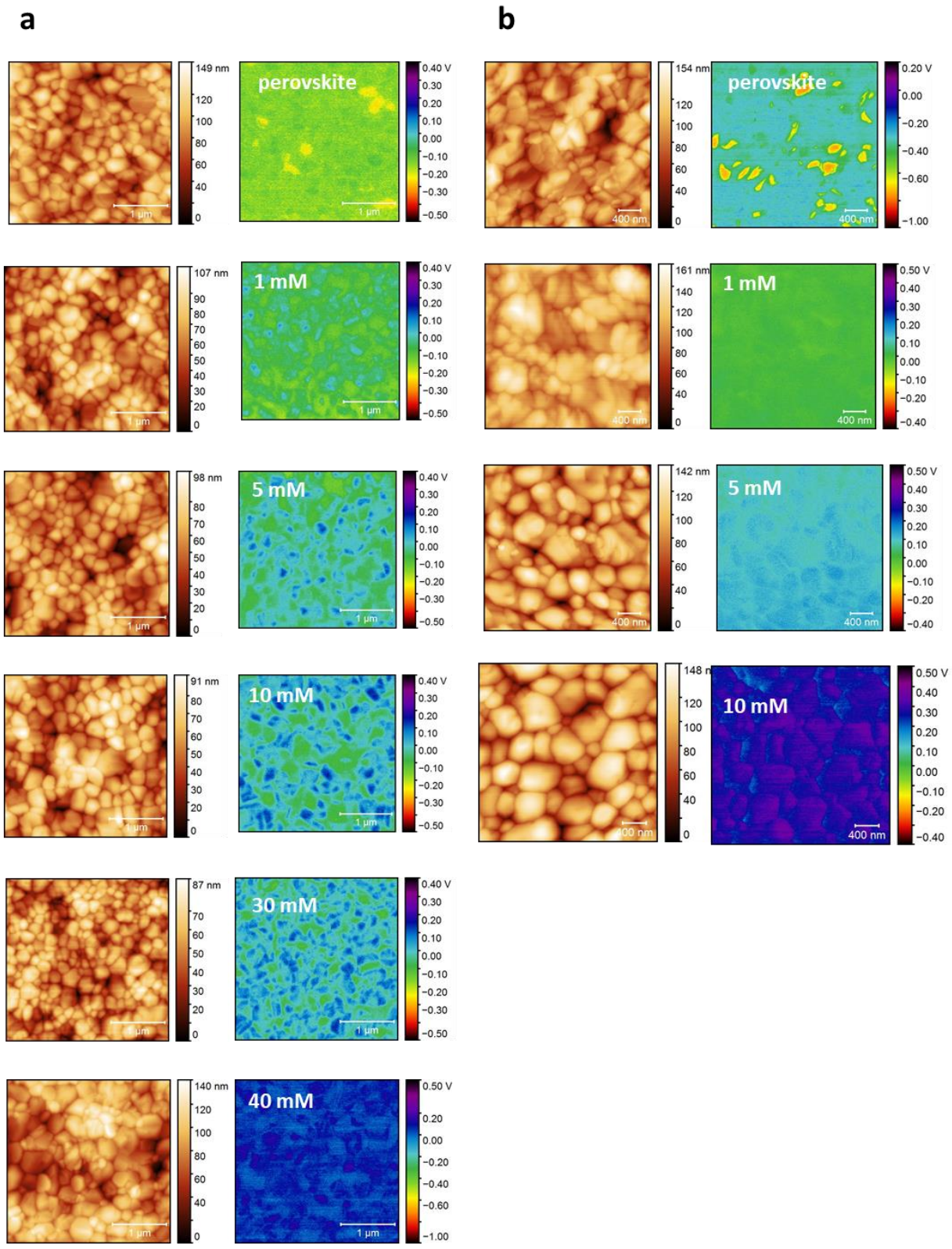

Figure A3.6.CPD and AFM maps for csc5 (a) and TOPO (b) at different concentrations.

A4 Supporting Information: *Chapter 6*

SEM characterization

SEM pictures were recorded with a Hitachi S 4100 Scanning Electron Microscope.

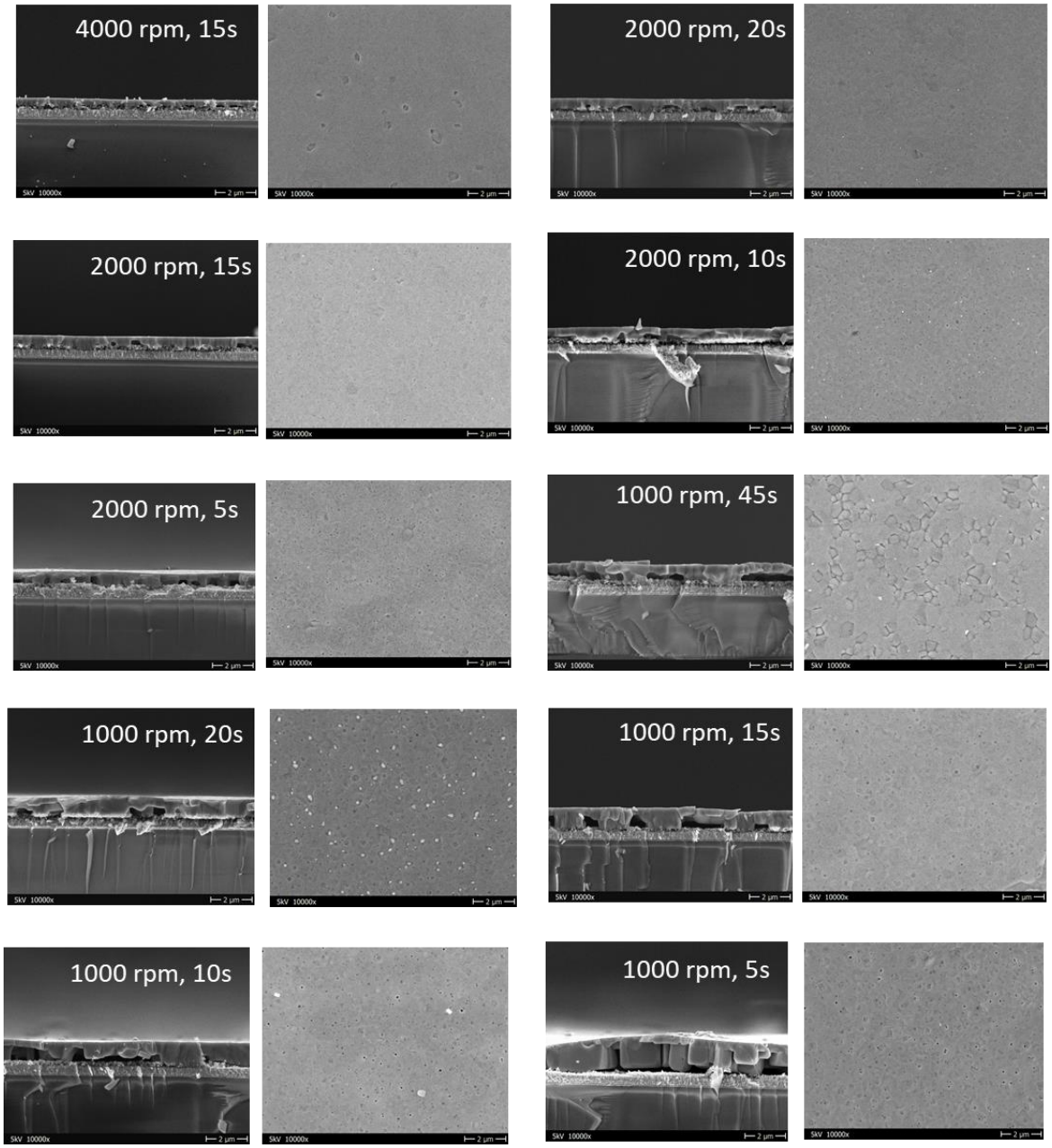

Figure A4.1. SEM pictures of FTO/TiO_2/$MAPbBr_3$ samples for different spin-coating parameters indicated in the figure (spinning rate, antisolvent drop time). For every condition cross-section (left) and top-view (right) are reported.

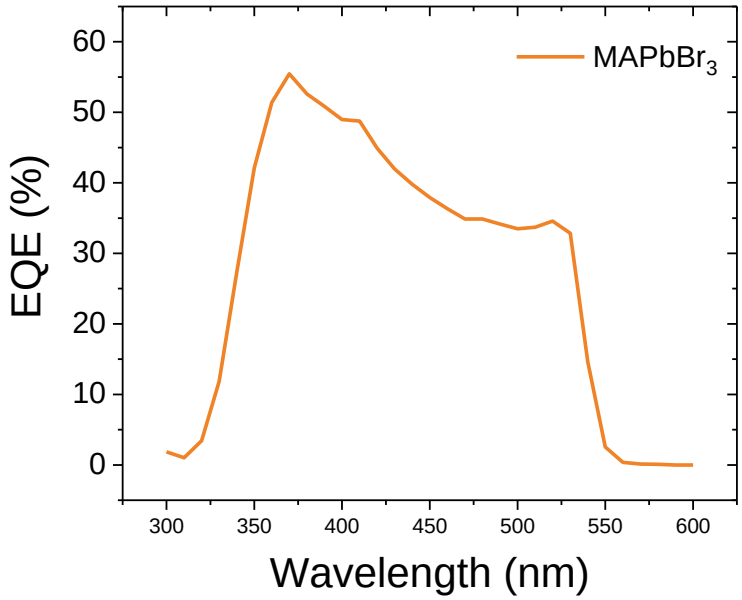

Figure A4.2 External Quantum Efficiency (EQE) measurement of FTO/TiO2/$MAPbBr_3$/Au devices.

A5 Supporting Information: *Chapter 7*

A5.1 DFT simulations

Density functional theory (DFT) simulations were performed by collaborators.

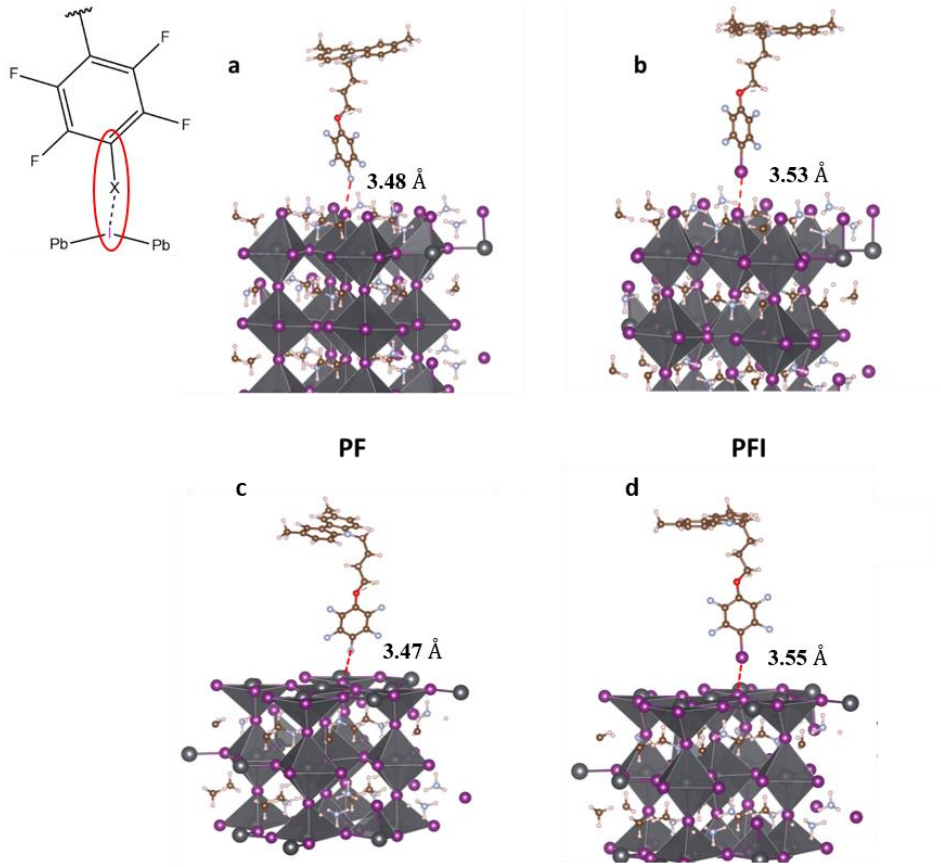

Figure A5.1. Optimized structures of PF (a,c) and PFI (b,d) anchored to a perovskite MAI-terminated (a,b) and PbI_2-terminated (c,d) surfaces with bond lengths in Å.

Table A5.1. Adsorption energies and interaction angles for PFI and PF in the case of MAI-terminated and PbI_2-terminated surfaces.

Termination - molecule	E_ads (eV)	Interaction Angle (degree)
MAI-PFI	-0.61	178.2
MAI-PF	-0.17	165.3
PbI_2-PFI	-0.64	176.5
PbI_2-PF	-0.26	163.4

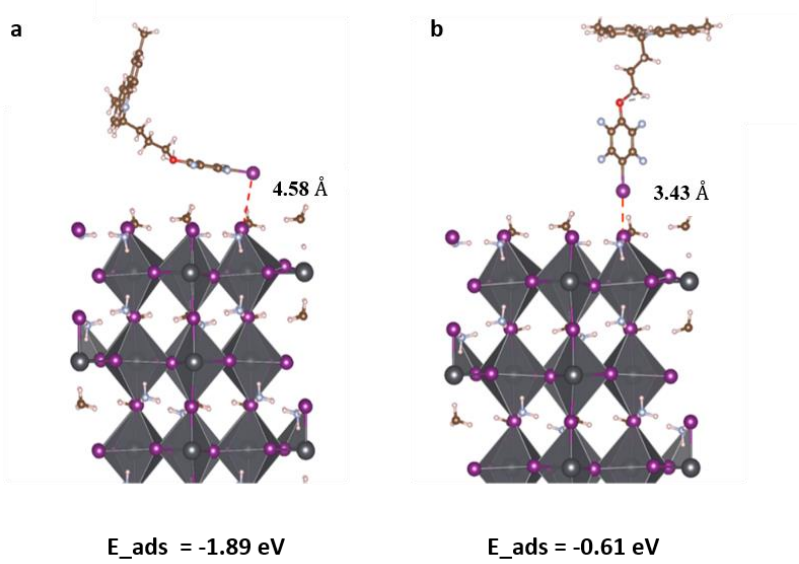

Figure A5.2. Study on the orientation of PFI with respect to a MAI-terminated perovskite surface without employing long-term dispersion correction. (a) parallel orientation. (b) perpendicular orientation.

Table A5.2. Dipole moments for PFI and PF on MAI-terminated and PbI_2-terminated surface for perpendicular and parallel disposition.

Dipole moment (Debye)	TOTAL	Z-Comp	E_ads(eV)		TOTAL	Z-Comp	E_ads(eV)
1) MAI_PFI_PERP	2.53	1.76	-0.62	**3) MAI_PFI_PARALL**	2.90	-0.91	-1.89
2) MAI_PF_PERP	3.02	2.44	-0.17	**4) MAI_PF_PARALL**	3.04	0.53	-0.81
5) PbI2_PFI_PERP	2.44	1.78	-0.64	**7) PbI2_PFI_PARALL**	2.90	-0.65	-2.26
6) PbI2_PF_PERP	3.02	2.42	-0.26	**8) PbI2_PF_PARALL**	3.19	-0.48	-2.26

A5.2 Methods and additional data

Kelvin Probe

The contact potential difference measurements (CPD) were performed with a Kelvin probe consisting of a vibrating gold mesh driven by a piezo electric crystal (Kelvin probe S and CPD controller by Besocke Delta Phi). The samples were measured in air.

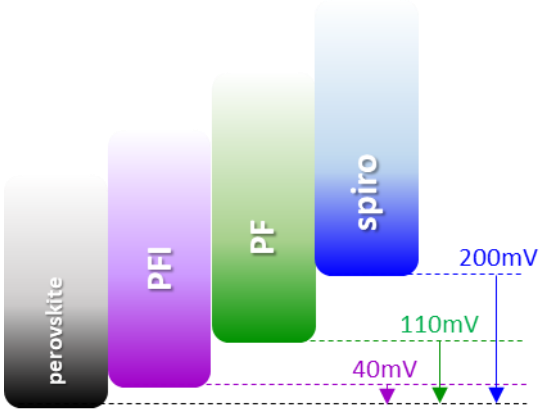

Figure A5.3. Schematic energy level alignment of the valence band maximum of perovskite with the different HTMs. The offset of 200mV for spiro-OMeTAD is taken from literature[336]. The offsets for PFI and PFI are estimated from the Kelvin Probe measurements.

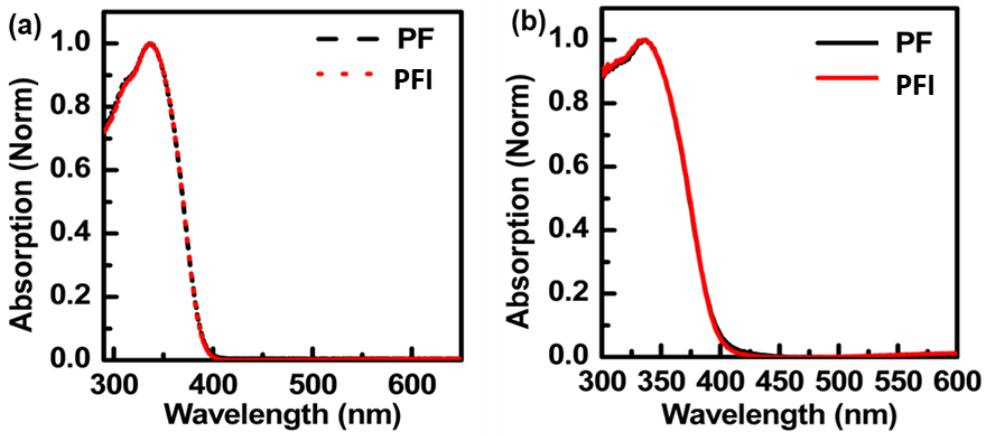

Figure A5.4. Normalized absorption of PF and PFI in chloroform (10^{-5}M) (a), and in solid state on glass films (b).

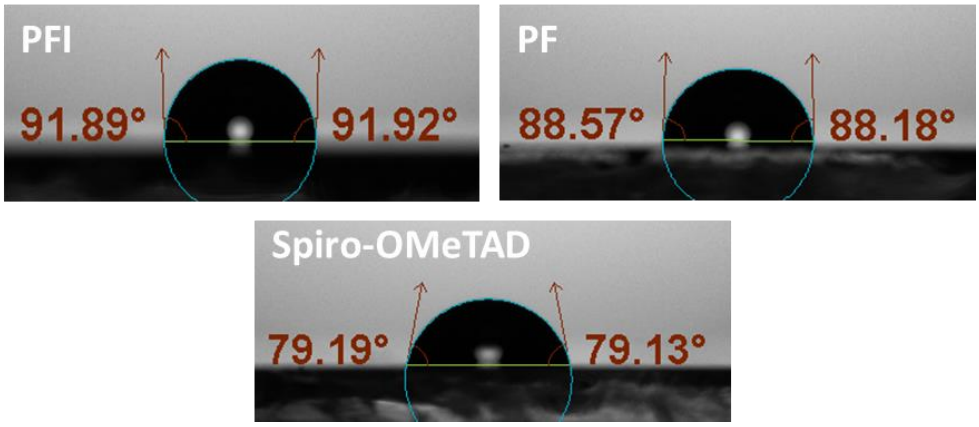

Figure A5.5. Water contact angle measurement for PFI, PF and Spiro-OMeTAD.

UV-Vis

Diffusion reflectance spectra of samples were performed with a Perkin Elmer LAMBDA 1050 UV/VIS spectrometer. Optical transmission measurements were carried out using a Cary 5000 UV-Vis-NIR spectrophotometer. The measurements were performed together with collaborators.

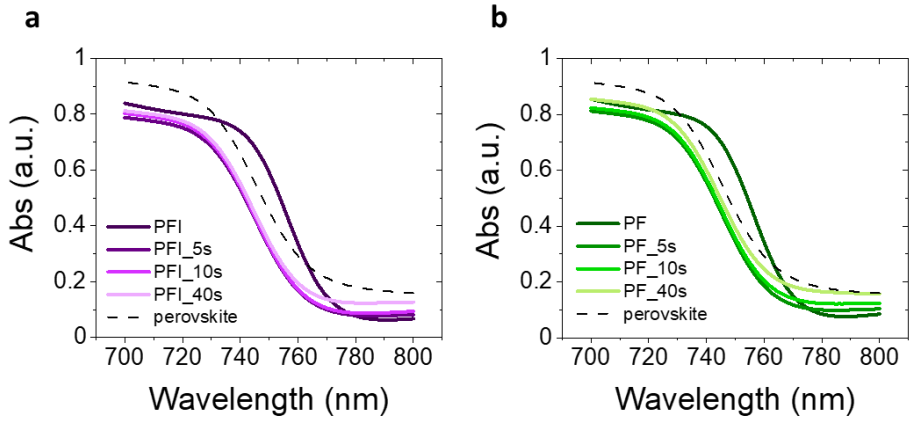

Figure A5.6. UV-Vis transmission spectra of glass/perovskite/PFI (a) and glass/perovskite/PF (b) samples after immersion in ethanol for different time intervals.

Atomic Force Microscopy

Atomic Force Microscopy (AFM) was performed on PFI and PF layers with 29 mM concentration in order to assess the morphology. A Multimode scanning force microscope (SFM, Bruker corp.) was operated in Tapping Mode using Mikromasch HQ:NSC15/AlBs cantilevers (nominal resonance frequency 325 kHz, typical spring constant 40 N/m).

The measurements were repeated after treating the samples with ethanol in order to support the findings of the UV-Vis measurements from Figure 7.3c. In this case it was not possible to dip the whole sample in ethanol because of the characteristics of the setup, therefore the treatment consisted in deposition of one drop of ethanol on 0.5x0.5cm^2 substrates, with removal of the solvent after 15s by means of substrate spinning. The measurements were performed together with a collaborator.

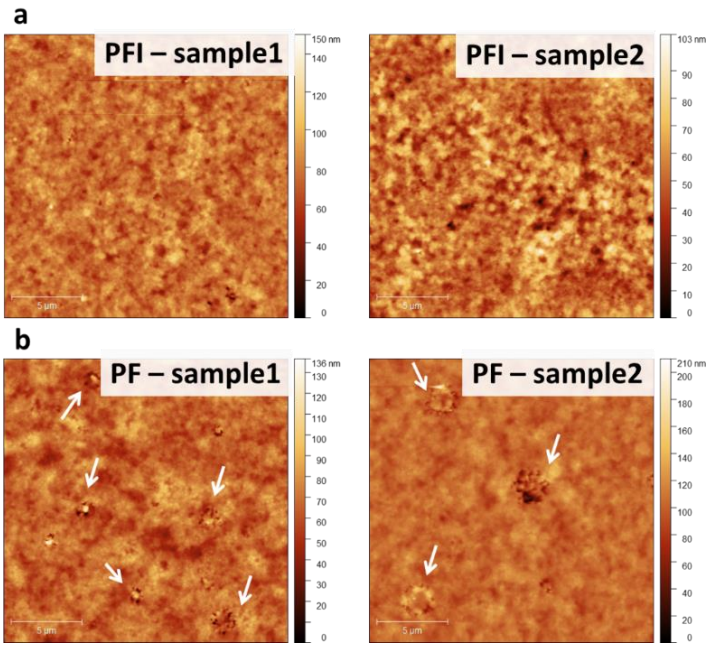

Figure A5.7. AFM topography maps of PFI (a) and PF (b) deposited on glass/perovskite with 29 mM concentration for two different samples. The white arrows in b indicate regular imperfections on the PF surface.

Space charge limited current mobility measurements

To evaluate their charge carrier transport ability, single-carrier devices were fabricated and characterized. The hole-only device had the following structure ITO/PEDOT:PSS/HTM/MoO_3/Au.

The hole-only device with PEDOT:PSS and MoO_3 buffer layer forms a quasi-Ohmic contact between organic layer and electrodes; thus, the hole mobility (μ) were extrapolated from the JV curves by space charge limited current (SCLC) method with an equation as follow:

$$J = \frac{9}{8}\varepsilon\varepsilon_0\mu\frac{V^2}{d^3}$$

Where J is the current density; ε_0 is the zero-field mobility, which is a constant 8.85×10^{-14} C/V cm; ε is the relative permittivity of the material, which is considered to be 3 for organic materials; V is the applied voltage; μ is the hole mobility; and d is the thickness of active layer.

The results are reported in Table 7.1 in the main text.

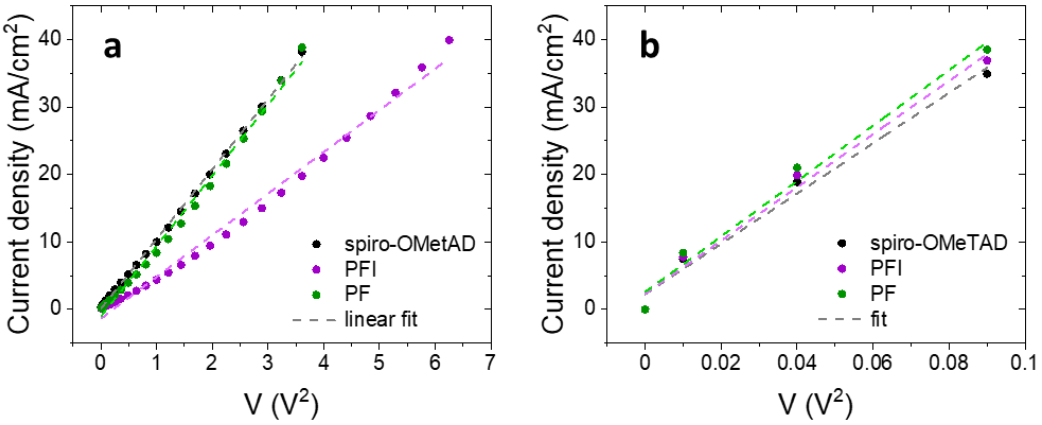

Figure A5.8. JV curves of single-carrier devices with structure ITO/PEDOT:PSS/HTM/MoO3/Au for undoped (a) and doped (b) HTMs

Ageing measurement

Solar cells were aged in a custom-built High-throughput Ageing Setup.[243] All cells were individually MPP-tracked using special electronics. To track the MPP, a perturb and observe algorithm[242] with a delay time of 1s and a voltage step-width of 0.01V was applied. PCE and MPP values were recorded every 2 min for all cells automatically. Devices were actively cooled with Peltier-elements and kept at 25 °C at all time with active areas touching a heatpad for direct thermal coupling. Ageing was performed under a continuous flow of nitrogen in a closed box, no additional encapsulation was used. Sunlight with 1000 W/m^2 intensity was provided by a metal-halide lamp using a H_2 filter. The light intensity was actively controlled with the help of a silicon irradiation-sensor. The UV-blocking foil „KFU15“ by Mitsui was used to block UV-light with wavelengths below 380 nm. Due to the UV cut-off and the diffusing properties of the filter, the irradiance reaching the tested solar cells was measured to be app. 800 W/m^2. The test is in accordance with the protocol ISOS-L-1I.[77]

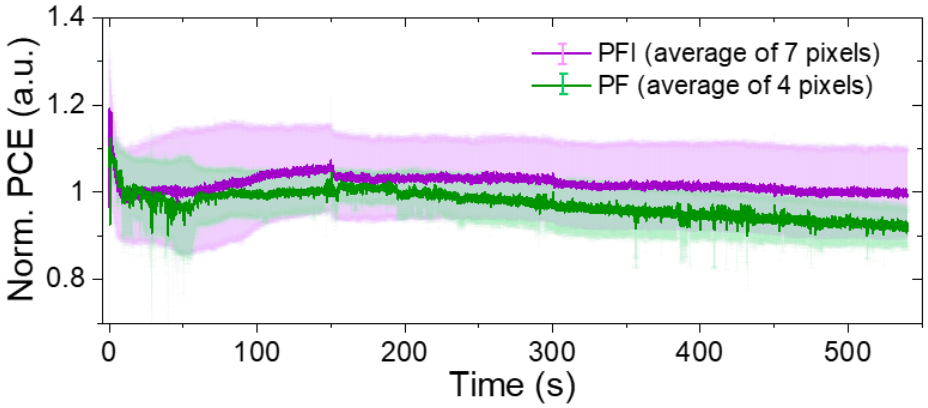

Figure A5.9. Normalized PCE of FTO/TiO_2/perovskite/HTMs/Au devices for ~550 hrs of continuous MPP-tracking under 1 sun illumination, measurement performed in N_2 atmosphere with UV-blocking filter, temperature was actively kept constant at 25°C. Average of 7 pixels for PFI and 4 pixels for PF. Data normalized after to the value after burn-in (~10 hrs) and plotted in linear scale with error bars (standard deviation).

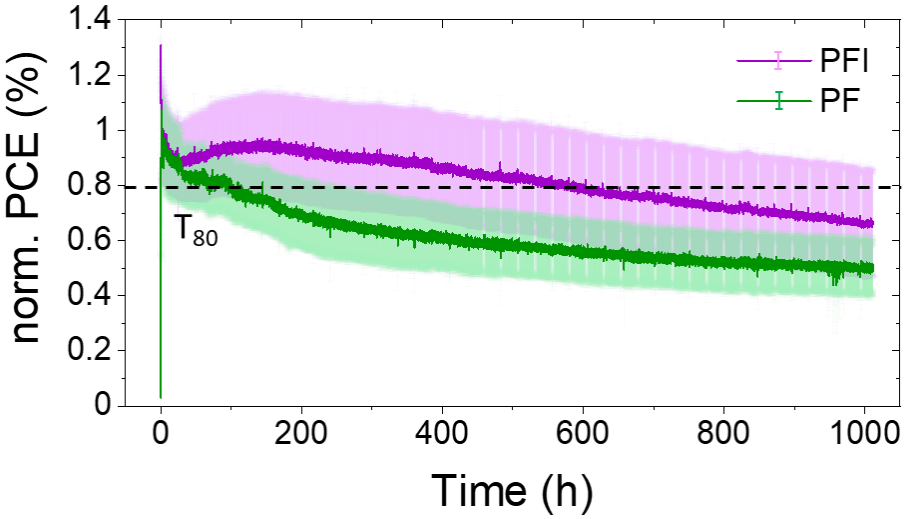

Figure A5.10. Normalized PCE of FTO/TiO2/perovskite/HTMs/Au devices for ~1000 hrs of continuous MPP-tracking under 1 sun illumination, measurement performed in N_2 atmosphere with UV-blocking filter, temperature was actively kept constant at 25°C. Average of 22 pixels for PFI and 9 pixels for PF. Data normalized at the peak efficiency and plotted in linear scale with error bars (standard deviation). To note that the devices tested here displayed worst PV parameters in JV measurements compared those shown in the main text. This justifies the quicker degradation over the measurement.

A6 SolarWAVE project

The solarWAVE project is a project developed by HZB and the Tampere University of Technology (TAU) with the aim of tackling the big challenge of perovskite solar cells (PSCs) stability by combining the development of new materials and surface passivation techniques. The final purpose is the development of a prototype of stable flexible module which can be integrated in industrial reel-to-reel production.

To achieve the goal HZB worked in synergy with the TAU and the Finnish-Chinese company Confidex, bringing together the respective expertise in order to develop new materials, exploring the concepts of halogen bonding and small molecules passivation, and finally bring all the results together to produce a prototype. Specifically, HZB provided deep knowhow in device making and a well-equipped lab for preparing and testing solar cells, together with expertise in small molecules passivation and halogen bond. TAU, instead, has researchers with a strong background in synthetic chemistry, who designed and synthesized the new materials to be tested for this project. Finally, Confidex was the fundamental link between academic research and industry and had an important role in adapting the devices so that they can be applied to a prototype. The author has been the main responsible for this project at HZB.

The approach followed to reach the scope of the project can be summarized in the following interim technical (TO), scientific (SO) and commercialization (CO) objectives and milestones (D):

- *TO1.* **Reproduce state-of-the-art power conversion efficiency**.
    - D1: Highly efficient PSCs
- *TO2.* **Design and build a custom-made accelerated ageing setup** for studying the effect of different passivation methods on the stability of PSCs.
    - D2: Ageing test device
- *SO1.* **Identify new and stable organic and inorganic compounds**, acting as selective contacts (hole- or electron-transporting materials) in the cell, and studying their relative degradation mechanisms.
    - *D3: small-area highly stable PSCs with new selective contacts.*
- *SO2.* **Implement new compounds to functionalize the perovskite surface** by making perovskite highly water repellent via linking it with perfluorinated molecules (hydrophobic in nature) and passivating it via supramolecular halogen bonding.
    - *D4: small-area highly stable PSCs with passivated surface.*
    - *D5: technology validated in real environment.*

- *SO3.* **Demonstrate prototype devices**.
    - *D6: Reel-to-reel printed large area PSCs modules.*
- *CO1.* **Prepare SolarWAVE prototype towards commercialization**.
    - *D7: IPR strategies*
    - *D8: Blueprint for smart labels*
    - *D9: Revised blueprint*
    - *D10: Pilot customer identification*
    - *D11: Final IPR disclosure*

HZB was mainly in charge of TO1, TO2, SO1, and SO2. In particular the work towards reaching SO2 was performed with materials provided by TAU. SO3 was developed in collaboration with Confidex, which also provided the commercialization objectives.

TO1 and TO2 were quickly reached, indeed the standard PSCs produced at HZB as "control" devices are state-of-the-art and thus meet the requirements of TO1 (see reference devices in Part II). The ageing setup used in Chapter 7 fulfilled, instead, TO2. The objectives from SO2 were reached through the results reported in Wolff *et al*.[215].

The main work has been on the development of SO1: *identify novel organic/inorganic selective contacts*. The main objective was incorporating the achievements from SO2 (perovskite functionalization via small molecules) in novel hole transport materials. The results from this part of the project constitute the content of Chapter 7. Additional hole transport materials able to bind to Pb^{2+} ions were tested, but with less successful results compared to PFI and PF. Therefore, in the final part of the solarWAVE project the work focused on the latter materials.

Regarding SO3, the aim was preparing a prototype to use for powering Bluetooth low energy (BLE) cards/labels for indoor usage. The prototype has been achieved by preparing flexible PSCs and connect the different pixels through manual connections (Figure A6.1). The current version can deliver around 1.3 V at low light intensity, however further experiments to improve it in order to achieve a minimum of 1.6 V are in progress.

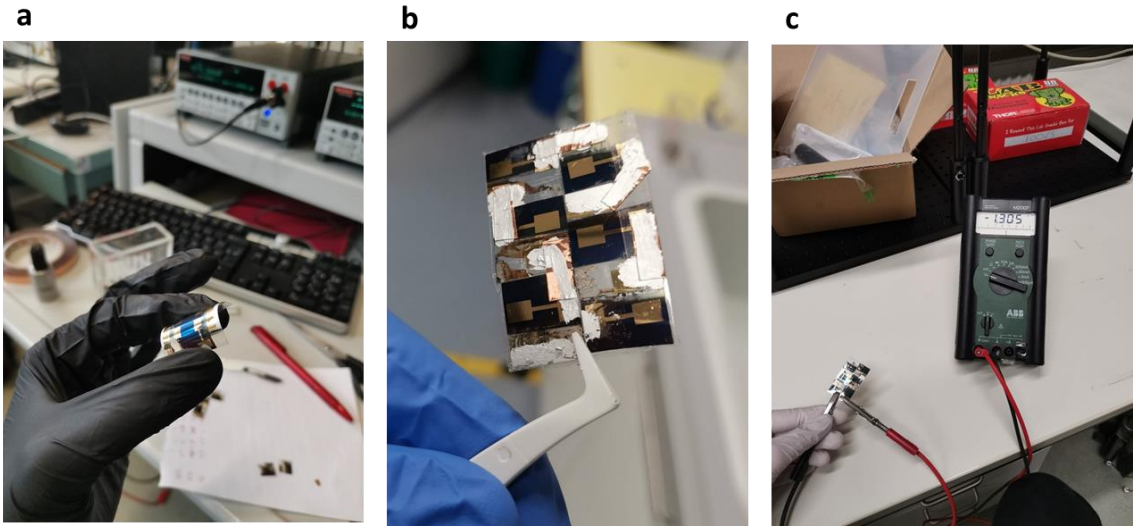

Figure A6.1. Development of the prototype module. (a) Flexible perovskite solar cell. (b) Module with manual connections made from the pixels of different flexible devices. (c) Voltage output of the module at low light intensity.

A7 Publications and Conference Contributions

Peer-reviewed publications

Tuning Halide Perovskite Energy Levels
L. Canil, T. Cramer, B. Fraboni, D. Ricciarelli, D. Meggiolaro, A. Singh, M. Liu, M. Rusu, C.M. Wolff, N. Phung, Q. Wang, D. Neher, T. Unold, P. Vivo, A. Gagliardi, F. De Angelis, A. Abate*
Energy Environ. Sci., **2021**, 14, 1429
https://doi.org/10.1039/D0EE02216K

Halogen-Bonded Hole-Transport Material Suppresses Charge Recombination and Enhances Stability of Perovskite Solar Cells
L. Canil, J. Salunke, Q. Wang, M. Liu, H. Köbler, M. Flatken, L. Gregori, D. Meggiolaro, D. Ricciarelli, F. De Angelis, M. Stolterfoht, D. Neher, A. Priimagi, P. Vivo*, A. Abate*
Adv. Energy Mater., **2021**, 2101553.
https://doi.org/10.1002/aenm.202101553

Perfluorinated Self-Assembled Monolayers Enhance the Stability and Efficiency of Inverted Perovskite Solar Cells
C. M. Wolff, L. Canil, C. Rehermann, N. Ngoc Linh, F. Zu, M. Ralaiarisoa, P. Caprioglio, L. Fiedler, M. Stolterfoht, S. Kogikoski, I. Bald, N. Koch, E. L. Unger, T. Dittrich, A. Abate*, D. Neher*
ACS Nano, **2020**, 14, 1445–1456
https://doi.org/10.1021/acsnano.9b03268

Structure-induced optoelectronic properties of phenothiazine-based materials
S. Revoju, A. Matuhina, L. Canil, H. Salonen, A. Hiltunen, A. Abate and P. Vivo*
J. Mater. Chem. C, **2020**, 8, 15486
https://doi.org/10.1039/D0TC03421E

Monitoring Charge Carrier Diffusion across a Perovskite Film with Transient Absorption Spectroscopy
H. P. Pasanen*, P. Vivo, L. Canil, H. Hempel, T. Unold, A. Abate, N. V. Tkachenko*
Phys. Chem. Lett., **2020**, 11, 2, 445–450
https://doi.org/10.1021/acs.jpclett.9b03427

Refractive index change dominates the transient absorption response of metal halide perovskite thin films in the near infrared
H. P. Pasanen*, P. Vivo, L. Canil, A. Abate, N. V. Tkachenko*
Phys. Chem. Chem. Phys., **2019**, 21, 14663-14670
https://doi.org/10.1039/C9CP02291K

Oral conference contributions

Hydrophobic self-assembling monolayers for stable perovskite solar cells
L. Canil, G. Chistiakova, O. Shargaieva, A. Abate
Materials Research Society (MRS) Fall Meeting 2018, Boston, USA, 11/2018

Perovskite Work Function Tuning through Self-Assembling Monolayers of Small Molecules
L. Canil, T. Dittrich, T. Cramer, M. Liu, A. Abate
Perovskite Solar Cells and Optoelectronics (PSCO) 2019, Lausanne, Switzerland, 09/2019

Perovskite Work Function Tuning through Self-Assembling Monolayers of Small Molecules
L. Canil, T. Dittrich, T. Cramer, M. Liu, A. Abate
NanoGe Fall Meeting 2019, Berlin, Germany, 11/2019

Poster conference contributions

Self-assembling monolayers at the interface in perovskite solar cells
L. Canil, D. di Girolamo, S. Sanchez Alonso, A. Abate
Perovskite Solar Cells and Optoelectronics (PSCO) 2018, Lausanne, Switzerland, 09/2018

Work Function Tuning through Self-Assembling Monolayers of Fluorinated Molecules
L. Canil, T. Dittrich, A. Abate
Interfaces in Organic and Hybrid Thin-Film Optoelectronics (nanoGe INFORM) 2019, Valencia, Spain, 03/2019

Work Function Tuning through Self-Assembling Monolayers of Fluorinated Molecules
L. Canil, T. Dittrich, A. Abate
Hybrid and Organic Photovoltaics (nanoGe HOPV) 2019, Rome, Italy, 05/2019

Other international contributions

Work Function Tuning through Self-Assembling Monolayers of Fluorinated Molecules
L. Canil, T. Dittrich, O. Shargaieva, A. Abate
Invited seminar at Universitat Jaume I – INAM, Castellón de la Plana, Spain, 03/2019

A8 Declaration of originality

I here declare that this dissertation is from the author's original works, except the parts which give rightful references to other people's works, and that this dissertation has not been submitted to any other university in Germany or abroad.

Potsdam, August 2021

Laura Canil

A9 Acknowledgements

This is the end of a long adventure, and the beginning of a new one. I can't really express how much these last years meant to me. I learnt a lot, I grew personally and professionally, I discovered new sides of myself, and I had a lot of fun. All of this would not have been possible without the people who shared this path with me.

First of all, I would like to thank my supervisor and mentor *Prof. Dr. Antonio Abate*. *Antonio*, you always believed in me and pushed me to recognize my value, thank you for guiding me in this journey and giving me the possibility to live so many wonderful experiences. I'm also extremely grateful to my supervisor at the University of Potsdam *Prof. Dr. Dieter Neher*: you have been constantly available for answering my questions, helping me with invaluable insights, thank you for your patience and support. Moreover, I would like to express my deepest appreciation to *Prof. Dr. Jovana Milić* for taking the time to critically evaluate my thesis.

A big thank goes to *Prof. Dr. Paola Vivo*. Our collaboration in the SolarWAVE project has been a great experience, thank you for hosting me in your group and for all the shared knowledge, discussions, and support. I cannot begin to express my gratitude for *Dr. Qiong Wang* and *Dr. Martin Stolterfoht*, your help, especially in the last months, has been invaluable. The many scientific discussions with you deeply improved my scientific knowledge and understanding. Additionally, I owe an important debt to *Dr. Thomas Dittrich*, your Kelvin probe setup has been a fundamental tool for my research, thank you for teaching me how to use it, and for always being available to let me measure and to discuss the results. I'm also particularly thankful to *Dr. Florian Ruske*, your feedbacks during the preparation of this thesis were really helpful, you are probably one of the few people who actually read it all.

I'm grateful for the possibility of working in the HySPRINT lab and participate in the HyPerCells graduate school. In particular, I would like to show my appreciation for all the work and help from the lab managers, *Prof. Dr. Steve Albrecht* and *Prof. Dr. Eva Unger*, the technicians, *Moni* and *Hagen*, and all the staff, especially *Carola Ferber*, *Carola Klimm*, *Andreas von Kozierowski*, *Thomas Lußsky*, and our awesome secretaries *Antonia Tallarek* and *Marion Krusche*. During these three and a half years of work at HZB I had the chance to meet many people and share with them the "excitement" of looking for a free evaporator slot, the frustration of failed experiments, but also the thrill of successful ones, and many fun moments inside and outside the lab. Special thanks goes of course to all the past and present members of the *InterActive group*, it was great to work with you. *Marion*, from Boston to Boßeln, from hiking to the beach-volleyball field, we certainly had fun together, my PhD would not have been the same without you. *Jorge*, thank you saving me (or trying to) from my chemistry ignorance, but most importantly thank you for all the after-work beers and for introducing me to "the family". *Nga*, you have always being there for me from the beginning and even after you left, I'm really grateful for your support, help and friendship. Looking forward to meeting you again, and let's try not to miss the flight this time ;P. *Hans*, I'm happy I had the chance to work with you (and your friend mpp-peter) and to get to know you as person, your chilled attitude is always an inspiration, I hope we will have many more "stories to tell". *Diego*, thank you for constantly bringing positive vibes, your jokes always make my day. Not-thank you for letting me here alone to take the blame for the coffee though ;). *Jeronimo*, looking forward to more Friday-day(s). *Valerio* and *Thomas*, the newbies (;P), I updated this

acknowledgement section after submitting only for you. You are great friends and scientists, I'm happy to have you around. And *Silver*, *Mahmoud*, *Maria, Guixiang, Meng, Nikos, Zafar, Zahra, Paola, Joel, Juanita, Raj, Ece, Varsha, Stephania, Weiwei*, *Junming*, and all the people that passed by our group: has been a pleasure to meet all of you. I'm also grateful to all the people from other groups than I had the chance to share some time with. *Silvia*, it's been short but intense, thank you for the lab singing (sorry to everybody else), the long talks seasoned with a lot of laughter, food and drinks, and for bringing some Veneto to the lab. I hope this is just the start of a great friendship. *Caro*, we went a long way from "oh you are the new girl!", thanks for all our wine/pizza evenings and for keeping an eye on me ;). And how could I not thank "the boys", *Lukas, Philipp, Marcel, Marko*, it was really fun to have you around these years. Another big shout-out goes to Aboma, thank you for being always there for me both at work and outside, I'm looking forward to many more nights-out, also because we have to get those steak tips again. *Christian*, Professor, I really appreciate all the support and suggestions you gave me. *Hannah*, my Lausanne-"shopping"-buddy, thanks for all the fun memories. *Igal*, your insights are always valuable, now I hope we'll finally manage to party together.

A very important thank you to all my international friends in Berlin, in Amsterdam, and beyond. Because without them all of this would have been much harder. Thanks to all *my rugby team*, you are like family. *Marta*, you probably hate all this cheesiness here, but I still want to thank you for always taking care of me and for the countless awesome party nights, loud singing, getting lost, random trips. In the end, we know that together we can take it to end of the line. *Torsten*, *Santi*, you are way more than coaches to me, in you I found some real friends. Thanks for all the support and the fun, can't wait for our next adventures together. *Helena*, my mediterranean friend, *Neli*, my absolutely-not-cute friend, I'm very happy our paths crossed, looking forward to a lot more Säschsczrwseghsc trips. There will be always a penthouse waiting for us. *Elli*, www.mipiacitu, do I need to say more? To a lot more karaoke nights! *Ina*, *Sini*, *Anna*, *Maggie*, it's always great to hangout with you. *Irene* (and *Sofi*), *Shayna*, *Cloe*, the most amazing group of "serious" people, I feel much more fun await us. Dear *Poco-girls*: *Leoni, Elena, Anaïs, Mel, Ginny*. I'm thankful for the few months we had together, it was enough to build unforgettable memories. *Silvia*, thanks for helping me balance between sport and spritz, although I'm still waiting for a bacaro tour together. A big hug to *Marco*, *Federica*, *Giorgio*, *Andrea*, *Ale*, *Dario*, *Eliane*, *Johannes*, *Lucie*, *Nasim* and all the people that made my time in Amsterdam unforgettable. Especially *Caro*, my pinky unicorn. You are one of the most important people in my life, a reference point. I don't know what I would do without you and there's not enough space here for all the things I'm grateful for, so, simply, thank you for everything.

Non può mancare un grande ringraziamento a tutti i miei amici in Italia. Grazie Fisici: *Lucia, Ludo, Isabella, Marin, Andrea, Pietro, Luca* (e consorti vari). Non penso sarebbe stato possibile superare 5 anni di fisica senza il vostro supporto e i gruppi studio, ma anche senza le nostre interminabili partite a carte, i mercoledì universitari, le feste di fisica, le feste di Marin, i bacaro tour e chi più ne ha più ne metta. Grazie *Jambo Mambo crew*, per avermi insegnato la vera essenza del viaggio. In particolare grazie *Enrica*, per stare sempre là ad ascoltarmi e per i consigli invariabilmente azzeccati. Ok, anche per il vino e il salame. Grazie *Menny, Kiwa* e in particolare *Vicky*, prosecco nel mio spritz, ma soprattutto insostituibile amica. Grazie *Vanessa* e *Marta*, amiche di sempre. E grazie *Claudia*, per avermi sempre seguito da vicino e accompagnato lungo il mio percorso.

Infine, il grazie più speciale va alla mia famiglia. Grazie *Gil, Anita, Francesco, Mauri, Fabi, Emma, Matteo* e *Olivia*, per farmi sempre sentire a casa. Grazie *Nonna Margherita*, per mostrarmi costantemente il

tuo amore e sostegno, ti voglio bene. Grazie *Marco* e *Sara*, per continuare a sopportarmi nonostante tutto. Grazie *Mamma* e *Papà* per aver sempre supportato le mie scelte e avermi dato la possibilità di seguire la mia strada. So che potrò sempre contare su tutti voi, Grazie.